

Topology optimisation of the divertor monoblock

A thesis submitted to the University of Manchester for the degree of
Doctor of Philosophy
in the Faculty of Science and Engineering

2023

Oliver Richard Marshall
Department of Mechanical, Aerospace and Civil Engineering

Contents

Contents	2
List of figures	7
List of tables	15
Abstract	17
Declaration of originality	18
Copyright statement	19
Acknowledgements	20
1 Introduction	21
1.1 Nuclear fusion	21
1.2 Tokamaks	22
1.3 ITER and future devices	23
1.4 Progress in tokamak performance	25
1.5 The divertor	26
1.5.1 The ITER divertor design	26
1.5.2 Alternative divertor concepts	29
1.5.3 Design considerations for high heat flux components	29
1.6 Fusion technology readiness and development	32
1.7 Topology optimisation for design	32
1.7.1 Interpolation and penalisation	34
1.7.2 Techniques for design control	35
1.7.3 The method of moving asymptotes	35
1.7.4 Interaction with fusion research	36
1.8 Monoblock design exploration	36
1.8.1 Previous studies on topology optimisation for fusion	37
1.9 Overview of topology optimisation workflow	39
1.10 Additive manufacturing and functional grading	45
1.11 Summary of context and motivation	47
1.12 Thesis structure	47
1.13 Statement of contributions	51
2 Paper 1 - A Review of Tokamak Divertor Design for Digital Engineering	52

2.1	Introduction	52
2.1.1	Tokamaks	53
2.1.2	The divertor	53
2.1.3	Digital modelling techniques	54
2.1.4	A vision for comprehensive fusion reactor modelling	54
2.1.5	Structure	54
2.1.6	The state of global fusion research	55
2.1.7	Previous reviews	56
2.2	Stakeholder decisions	59
2.2.1	Tokamak accident scenarios involving the divertor	60
2.3	The top-down approach to modelling the divertor	61
2.3.1	Commonly used systems codes	61
2.3.2	Divertor geometry and protection	64
2.3.3	Advanced divertor configurations	66
2.3.4	Power plant modelling	68
2.3.5	Uncertainty in divertor design	74
2.4	Divertor target modelling	75
2.4.1	Divertor armour modelling	75
2.4.2	Design codes	75
2.4.3	Armour geometries and concepts	77
2.4.4	Divertor target loading conditions	82
2.4.5	Deformation, damage and failure	84
2.4.6	Coolant fluid modelling	85
2.4.7	Fluid heat transfer modelling	86
2.4.8	Thermal-hydraulics	87
2.4.9	Cooling pipe geometries and design concepts	90
2.5	Summary of findings	94
2.6	Additional commentary on Chapter 2	95
3	Paper 2 - Thermal Testing of Additively Manufactured CuCrZr Samples for Application to Nuclear Fusion	97
3.1	Introduction	98
3.1.1	CuCrZr properties	98
3.1.2	The importance of process optimisation	100
3.2	Methodology	100
3.2.1	Material and preparation	100
3.2.2	Process optimisation	101
3.2.3	Build parameters	102
3.2.4	Machining	102
3.2.5	Method for obtaining coefficients of thermal expansion	103
3.2.6	Method for obtaining thermal diffusivity	105
3.3	Results	107
3.3.1	Dilatometry	107

3.3.2	Laser flash analysis	110
3.3.3	Thermal conductivity	113
3.4	Discussion	115
3.4.1	Uncertainty estimation	115
3.4.2	Comparison to conventional CuCrZr alloy	116
3.4.3	Thermal expansion	116
3.4.4	Relationship to laser build power	117
3.4.5	Experimental difficulties	117
3.4.6	Possible causes for sample phase change	117
3.5	Conclusions	119
3.6	Additional commentary on Chapter 3	119
4	Topology optimisation literature survey	121
4.1	Introduction	121
4.2	Additional background and context	122
4.2.1	Optimisation algorithms	122
4.2.2	Evolutionary Structural Optimisation	123
4.2.3	Genetic algorithms	123
4.2.4	Numerical instabilities	123
4.3	Thermal optimisation studies	124
4.3.1	Previous reviews	125
4.3.2	Conduction focused optimisation	125
4.3.3	Incorporating convection	129
4.4	Topology optimisation for fluids	130
4.4.1	The development of fluid topology optimisation methodology	130
4.4.2	Consideration of additional fluid flow scenarios	133
4.5	Thermo-fluid problems	135
4.6	Engineering applications	139
4.6.1	Optimisation for manufacturing	143
4.7	State of the field	143
4.8	Software evaluation	144
4.8.1	Commercial software	144
4.8.2	COMSOL Multiphysics	145
4.8.3	Educational tools	145
4.8.4	Large scale optimisation	147
4.8.5	Other codes	149
4.9	Conclusions and strategy for computational work	149
5	Paper 3 - Thermal Topology Optimisation of a Plasma Facing Component for use in Next-Generation Fusion Reactors	151
5.1	Introduction	152
5.2	Problem description	153
5.2.1	Modelling setup	153

5.3	Results	154
5.4	Conclusions	156
6	Paper 4 - Multi-Objective Topology Optimisation of a Tungsten Divertor Monoblock, With Consideration of Toroidal Beveling and Multiple Attachment Scenarios	157
6.1	Introduction	158
6.2	Concept and methodology	159
6.2.1	Finite element analysis	159
6.2.2	Geometries and loading conditions	160
6.2.3	Topology optimisation	161
6.2.4	Temperature constraints	161
6.2.5	Materials and manufacturing	162
6.2.6	Consideration of cost functions	163
6.2.7	Reducing the Cu-content of designs	164
6.3	Flat monoblock results	165
6.3.1	Suspended flat monoblock optimisation results	165
6.3.2	Extension of the design domain	167
6.3.3	Fixed flat monoblock optimisation results	167
6.3.4	The ductile to brittle transition temperature (DBTT) constraint	168
6.3.5	Reduced Cu content designs	169
6.4	Bevelled monoblock results	170
6.4.1	Suspended bevelled monoblock optimisation results	171
6.4.2	Identifying a design compromise	173
6.5	Discussion and conclusions	174
6.5.1	Multi-objective optimisation	174
6.5.2	Material temperature constraints	174
6.5.3	The case for an increased thermal conductance monoblock	175
6.5.4	Conclusions	175
6.6	Additional commentary on Chapters 5 and 6	176
7	Paper 5 - Conjugate Topology Optimisation of Turbulent Flow for the Design of Novel Plasma Facing Component Geometries	177
7.1	Introduction	178
7.1.1	Plasma-Facing Component (PFC) design	179
7.2	Methodology	179
7.2.1	Boundary conditions	179
7.2.2	Turbulence modelling	180
7.2.3	Computational cost	180
7.2.4	Topology optimisation formulation	181
7.2.5	Fluid optimisation	181
7.2.6	Material property interpolation	183
7.2.7	Consideration of objective functions	184

7.2.8	Thermal objectives in conjugate heat transfer topology optimisation . . .	184
7.3	Results	186
7.3.1	Laminar flow results	186
7.3.2	Turbulent flow results	187
7.4	Discussion	192
7.4.1	Topology optimisation challenges and limitations	193
7.5	Conclusion	194
8	Conclusions and commentary	195
8.1	Chapter 2 conclusions	195
8.1.1	Commentary and further work	196
8.2	Chapter 3 conclusions	196
8.2.1	Commentary and further work	197
8.3	Chapter 4 conclusions	197
8.3.1	Commentary and further work	198
8.4	Chapter 5 conclusions	198
8.4.1	Commentary and further work	198
8.5	Chapter 6 conclusions	198
8.5.1	Commentary and further work	199
8.6	Chapter 7 conclusions	199
8.6.1	Commentary and future work	200
9	Overall discussion	201
9.1	Overall project summary	201
9.2	Evolution of the project	201
9.3	The body of work	202
9.4	Further work and research impact	203
	References	205
	Appendices	255
A	IAEA net zero policy proposal	256

List of figures

1.1	Binding energy per nucleon, showing the transition between the regimes where nuclear fusion and nuclear fission are energetically favourable, reproduced from (Girtan <i>et al.</i> 2021).	22
1.2	Schematic of ITER with some of the main components labelled. Reproduced from (Dubus 2014).	24
1.3	Progress in fusion reactor performance compared to microprocessors and particle accelerators. Annotated with the names of the major devices in the respective industry. Reproduced from (Ikeda 2010).	25
1.4	Cross section of a single magnetic null divertor configuration, with important features labelled. Reproduced from (G. Federici, Biel, <i>et al.</i> 2017)	27
1.5	Sketch of ITER monoblock geometry reproduced from (Delaporte-Mathurin <i>et al.</i> 2020) which shows the inner CuCrZr cooling pipe set separated from the W monoblock by a Cu interlayer.	28
1.6	Illustration of the ITER W monoblock design, including location in the divertor target. Reproduced from (Bonnin <i>et al.</i> 2017).	28
1.7	Upper: He-cooled modular divertor with jet cooling (HEMJ) concept (reproduced from (A. R. Raffray, R. Nygren, <i>et al.</i> 2010)). Lower: Mock-up of a helium-cooled divertor featuring a W foam insert manufactured using chemical vapour deposition (D. Youchison <i>et al.</i> 2007).	30
1.8	Different techniques for optimisation of a truss structure, where initial setups are shown on the left and optimised results on the right. a) Sizing (or geometric) optimisation where the size of individual features can be modified. b) Shape optimisation allows for the modification of already existing boundaries in the design. c) Topology optimisation allows for the creation of new boundaries and is therefore the most generic optimisation technique. Reproduced from (M. P. Bendsøe and O. Sigmund 2003).	33
1.9	Monoblock geometries for study using topology optimisation. Left: ITER-style monoblock. 1) W armour, 2) Sacrificial W armour layer to account for erosion during the component's lifetime. 3) Cu interlayer to relieve thermally induced stress. 4) CuCrZr coolant pipe. Right: novel monoblock design inspired by work presented in (Oh <i>et al.</i> 2021).	37
1.10	Simplified topology optimisation flow chart indicating some of the main steps in the topology optimisation process.	40

1.11	The variables utility can be used to define the material interpolation between specific parameters, and to parameterise material properties not easily available in the GUI.	41
1.12	COMSOL topology optimisation settings. This interface allows the specification of settings relating to filtering, projection and interpolation. Furthermore, it is where the design domain (where topology optimisation is to be performed) is defined.	42
1.13	Screenshot showing the specification of a point-wise inequality constraint. This type of constraint must be true at all elements in the specified region and is therefore useful for the specification of material operational temperature limits.	42
1.14	Topology optimisation algorithm settings, including the ability to specify the method and optimality tolerance (which controls the convergence criterion). Objective functions (defined using domain probes), the choice of minimisation or maximisation, the treatment of multiple objectives, and any additional constraints can also be defined here.	43
1.15	COMSOL GUI showing the application of a volume force to oppose flow and aid in the simulation of the transition from fluid to solid elements.	44
1.16	The parameters used by the physics interface are exposed in the GUI and are directly modifiable, allowing for the definition of additional topology optimisation parameters.	45
2.1	Illustration of the different plasma geometry in conventional versus spherical tokamaks. Reproduced from (Blagoev 2020)	53
2.2	Simplified depiction of modelling on different scales in fusion reactor research. In divertor design, a lot of decisions which have a very significant impact on design are made at a high level.	55
2.3	Speculative timeline for planned fusion development including a selection of national devices and programmes.	59
2.4	Cross-sections of internal tokamak geometry representative of a spherical tokamak showing the geometric differences in strike points: the regions where the magnetic field geometry (shown in blue) interacts with the PFCs. Reproduced from (I. Chapman <i>et al.</i> 2015).	66
2.5	Illustration of the He HEMJ divertor concept, assembly and location in the divertor. Reproduced from (Prachai Norajitra, Giniyatulin, <i>et al.</i> 2008).	79
2.6	Illustration of the ‘thermal break’ concept designed to minimise thermally induced stress around the upper face of the monoblock cooling pipe. Reproduced from (Domptail <i>et al.</i> 2020)	79
2.7	Representation of a castellated monoblock designed to minimise thermally induced stresses by allowing for thermal expansion. Reproduced from (Li Puma <i>et al.</i> 2002).	81

2.8	Photographs of monoblock sections with discoloured bands showing the result of surface melting in a high-field region (left) and cracking in a low field region (right). The damage is attributed primarily to localised intense heat fluxes resulting from small misalignments between tiles that expose leading edges. Adapted from (J. P. Gunn <i>et al.</i> 2021).	83
2.9	Schematic illustrating a swirl insert used to promote fluid mixing in the ITER monoblock concept, reproduced from (Wiggins, Cabral, and Carasik 2021) .	88
2.10	Shape optimised elliptical monoblock cooling pipe profiles designed to reduce heat flux concentration. Reproduced from (Lim <i>et al.</i> 2018).	91
2.11	Hypervapotron component schematic, reproduced from (Pascal-Ribot <i>et al.</i> 2007).	91
2.12	Liquid metal divertor module based on the capillary porous system concept. Arrows on the top surface indicate the direction of heat flux loading. Reproduced from (Rocella <i>et al.</i> 2020)	93
3.1	CuCrZr ternary phase diagram reproduced from (K. Zeng and Hämäläinen 1995) with the approximate regions relevant to the CuCrZr samples in this study highlighted.	99
3.2	CuCrZr phase diagrams for 0.5 at.% Cr (left) and 1.5 at.% Cr (right), with the relevant operating temperature and composition range highlighted. Reproduced from (K. Zeng and Hämäläinen 1995)	99
3.3	(1) Cylinders for LFA before machining to correct dimensions, showing discoloured surfaces due to heat treatment. (2) Larger diameter cylinders for LFA and smaller diameter cylinders for dilatometry after machining to correct diameter but before sectioning.	102
3.4	A selection of machined samples is displayed. The flatter samples on the left-hand side are for laser flash analysis and the small diameter cylinders on the right-hand side are for dilatometry. The image also includes the ends of the cylinders, which were not used for testing.	103
3.5	Push-rod dilatometer showing the sample placed in a heating element where it is raised to the required temperature and the push-rod through which its resulting expansion is measured.	104
3.6	Close-up view of push-rod dilatometer sample holder and inductive heating coil.	105
3.7	Schematic of a laser flash analyser showing the placement of the sample in the path of the laser power source and the detector on the opposing side. . .	106
3.8	Deviation of the measured platinum sample linear thermal expansion with respect to literature reference data from (Hahn <i>et al.</i> 1972), generated using Eq. 3.9. The negative values found here indicate that the measured sample expansion was greater than that found in the literature.	108
3.9	The calibration result when applied to the linear thermal expansion measurements obtained for the platinum reference sample is shown to be in good agreement with the literature values.	109

3.10	Calibrated linear thermal expansion plotted for samples heated between 30°C and 700°C. A linear function is fitted to the data and shows overall good agreement with the measured values apart from the highest temperature range for sample 1.3.	109
3.11	Mean coefficients of thermal expansion for the samples tested. The mean coefficients are calculated with respect to the temperature the sample is initially heated to (30°C). The first coefficient for sample 15.2 is significantly lower than the trends would suggest, which may have been caused by poor contact with the thermocouple or an off-centre placement of the sample in the dilatometer.	110
3.12	Raw voltage trace for sample 16.1 where the detected voltage corresponds to a temperature increase on the rear face of the sample. The thermal diffusivity is related to the gradient of the signal increase.	111
3.13	Thermal diffusivity results for samples machined from cylinder 1.	112
3.14	Thermal diffusivity results for samples machined from cylinder 5.	112
3.15	Thermal diffusivity results for samples machined from cylinder 11.	112
3.16	Thermal diffusivity results for sample 16.1, machined from cylinder 16. . .	113
3.17	Comparison of mean thermal diffusivity for all samples tested.	113
3.18	CuCrZr specific heat capacity data used in the estimation of thermal conductivities, reproduced from (Gonzalez <i>et al.</i> 2018)	114
3.19	Comparison of thermal conductivity estimates.	115
3.20	Initial testing was devised to test the thermal expansion up to 1000°C , however, the sample appeared to transition to a liquid phase at approximately 800°C (as measured by the dilatometer), significantly below the expected melting temperature of $\approx 1080^\circ\text{C}$	118
3.21	Photographs showing sample discolouration (left and centre) and location in the dilatometer before operation (right). A conservative test, considering the expansion up to 700°C was used to obtain finalised data, however, the samples still showed significant discolouration.	118
4.1	Illustration of checker-boarding in a topology optimisation problem, reproduced from (Diaz and Ole Sigmund 1995)	124
4.2	Left: Heat conduction topology optimisation domain and boundary conditions. Centre: topology optimised geometry with high conductivity material shown in black. Right: temperature distribution. Reproduced from (Ercan M Dede 2009).	124
4.3	Left: Fluid flow and heat transfer topology optimisation domain and boundary conditions. Centre: topology optimised geometry with fluid domain walls shown in black. Right: fluid velocity distribution. Reproduced from (Ercan M Dede 2009).	125
4.4	Influence of changing the conductivity ratio γ on optimised topologies. For full details of the displayed parameters, the reader is referred to the original publication (Dirker and J. P. Meyer 2013), from which this figure is reproduced.	127

4.5	Illustration of the differences between extrusion of a 2D topology optimised design (left) and a full 3D optimisation (right). Reproduced from (Pizzolato <i>et al.</i> 2017b)	128
4.6	Topology and streamlines for a density-based fluid channel topology-optimisation reversed flow example. Sub-figures a),b),c),d) show the impact of decreasing the Darcy number (Da) on the resulting topology. For more detailed analysis, the reader is referred to the initial figure, published in (Olesen, Okkels, and Bruus 2006).	131
4.7	Left: illustration of a standard reverse flow topology optimisation problem extended to 3D. Right: topology optimisation geometry showing the flow path for 1 inlet branching to two outlets. Reproduced from (Aage, Poulsen, <i>et al.</i> 2008) where a full discussion can be found.	132
4.8	Illustration of topology optimised bends with increasing Reynolds numbers (Re). Reproduced from (Deng <i>et al.</i> 2011).	133
4.9	Upper: design domain for topology optimisation of an air cooling system showing fluid and thermal boundary conditions. Topology optimised coolant channels are shown for $Re = 100$ (middle) and $Re = 1000$ (lower). Reproduced from (K. Lee 2012), where a full discussion can be found.	136
4.10	Optimised heat sink topology at iteration 200 (upper left), 400 (upper right), 600 (lower left) 1000 (lower right). Full details are available in the original publication (Alexandersen, Aage, <i>et al.</i> 2014)	138
4.11	Two views of the same optimised 3D flow manifold using the $k - \omega$ turbulence model. Streamlines are coloured based on the velocity magnitude. Reproduced from (S. B. Dilgen <i>et al.</i> 2018).	139
4.12	Left: CAD representation of topology optimised heat sink. Right: AM prototype. Reproduced from (Ercan M. Dede, Joshi, and F. Zhou 2015). . .	140
4.13	Topology optimised electric motor cover geometries. Left: high conductivity, low convection coefficient design. Right: low conductivity, high convection coefficient design. Reproduced from (Mingdong Zhou <i>et al.</i> 2016)	141
4.14	Left: parametric optimised design results (upper) and AM prototype (lower). Right: Topology optimisation result (upper left), AM prototype with manufacturing constraints (upper right) and without (lower half). Reproduced from (Lange <i>et al.</i> 2018).	142
4.15	Investment casting of a topology optimised heat sink. The images shown (from left to right) show: the topology-optimised design, the castable resin pattern, the plaster mold and finally the metal heat sink. Reproduced from (Lei <i>et al.</i> 2018).	142
4.16	99-Line MATLAB optimisation code. Left: optimised geometry for a static load on a 2D beam (with vertical symmetry condition). Right: thermal conduction geometry with voxels representing the placement of highly conductive material. The loads in each case are applied at the top of the domains, and the greyscale value is proportional to the material density. . .	146

4.17	PETSc topology optimisation minimum compliance default problem run on a desktop workstation and post-processed in Paraview. The colouration of the model represents the magnitude of the displacement field, in-keeping with the presentation of results in (Aage, Andreassen, and Boyan Stefanov Lazarov 2015).	148
4.18	Left: 2D projection of a low volume-fraction result colourised with material density. Right: a high volume-fraction result with colourisation representing displacement field. Both images were post-processed in Paraview.	149
5.1	Schematic of 2D geometries for thermal conduction topology optimisation studies, showing flat monoblocks with steady-state (A) and transient (B) heat loads and bevelled monoblocks with steady-state (C) and transient (D) heat loads. The schematic includes (1): The design domain (initially W), used for the topology optimisation. (2) W minimum armour thickness of 5mm. (3) Cu interlayer. (4) CuCrZr cooling pipe described by an internal forced convection heat flux boundary representing 423.15K water at 10m s ⁻¹	153
5.2	Optimised geometries for the flat (top row) and bevelled (lower row) monoblock objectives.	155
5.3	Temperature profiles during transient loading conditions along the upper boundary of the design domain for baseline and optimised geometries. Left: flat monoblocks. Right: bevelled monoblocks.	155
5.4	Contours showing the change in thermal gradient magnitude with respect to the conventional ITER baseline design, for temperature (left), thermal gradient (middle) and conductive heat flux (right) optimised flat monoblocks in 10MW m ⁻² steady state heat fluxes.	156
6.1	Sketch of 2D geometries for topology optimisation studies showing flat monoblock (left) and bevelled monoblock (right) with a 0.5mm bevel resulting in a higher heat flux over 92% of the top surface and a shadowed area on the left-most 8%. (1): The design domain (initially W), used for the topology optimisation. (2) W minimum armour thickness of 5mm. (3) Cu interlayer. (4) CuCrZr cooling pipe described by an internal forced convection heat flux boundary representing 120°C water at 10m s ⁻¹ and a 4MPa load on the internal boundary of the pipe representing water pressure.	160
6.2	Left: Variation in yield stress and conductivity with temperature for the monoblock constituent materials: tungsten (W (<i>Tungsten as a Structural Divertor Material</i> 2018)), pure copper (Cu (Karditsas and Baptiste 1995)) and copper-chrome-zirconium alloy (CuCrZr (Gonzalez <i>et al.</i> 2018)) Right: Conductivity variation with temperature for W, Cu (krishna <i>et al.</i> 2012), and CuCrZr (Gonzalez <i>et al.</i> 2018). Where material properties were not available in the built-in material library, representative properties were found in the literature and extrapolated linearly (in regions indicated with the ‘+’ symbol) when not available for the appropriate temperature range.	161

6.3	Results for the suspended flat monoblock reference design. a) Temperature distribution with contours highlighting Cu 500°C and W 1200°C temperature limits. b) Temperature relative to respective material limits. c) von Mises Stress. d) von Mises stress relative to yield stress. The maximum values of σ_{rel} are highlighted in each domain.	165
6.4	Results presented for suspended flat monoblock designs, identified by the objective function listed below the sub-plot. The difference plots are calculated by subtracting the data for the corresponding reference design.	166
6.5	Designs without a constrained sacrificial armour layer. (a) Cu fraction [%]. (b) Temperature difference with respect to the reference design, with contours highlighting -100°C . (c) Flux difference. (d) Difference in von Mises stress.	167
6.6	Results presented for fixed flat monoblock designs, identified by the objective function listed below the sub-plot. The difference plots are calculated by subtracting the data for the corresponding reference design.	168
6.7	Regions where the temperature falls outside the W operational range for flat (left), and bevelled (right) reference geometries.	169
6.8	Upper: Topologies for reduced surface area fraction designs for a range of average surface area fractions from 5-50%. Lower: Corresponding maximum stress and conductivity data. DD= design domain.	170
6.9	Temperature and stress results for the bevelled reference design.	171
6.10	Results presented for suspended bevelled monoblock designs, identified by the objective function listed below the sub-plot. The difference plots are calculated by subtracting the data for the corresponding reference design. . .	172
6.11	Design concepts for the four different monoblock scenarios, obtained with $\sigma_V + T$ optimisation and a surface area fraction constraint of 0.40.	173
7.1	Exploded view of the monoblock geometry inspired by a component developed in (Oh <i>et al.</i> 2021). The water coolant channel is used as the design domain for topology optimisation. A depth of 30mm, equivalent to 3 monoblocks, was chosen as a compromise between increasing the volume of the design domain, computational expense, and the need for any optimised geometry to be periodic.	180
7.2	Left: Interpolated thermal material properties using SIMP penalisation and inverse permeability α , which forms part of the Darcy interpolation scheme. Right: comparison between Darcy and SIMP material interpolation schemes for different values of penalisation parameters q and p	183
7.3	Optimised geometries thresholded at $\gamma \leq 0.3$ performed as initial tests of thermal compliance minimisation (7.3a), solid temperature minimisation (7.3b) and fluid temperature maximisation (7.3c) for laminar flow conditions and a coarse mesh which enabled faster evaluation.	187
7.4	Variation in the mean thermal compliance (ϕ): 7.4a, solid domain temperature T_S : 7.4b and fluid temperature T_F : 7.4c objectives objectives during the optimisation process.	188

7.5	The evolution of turbulent kinetic energy and turbulent dissipation rate for ϕ minimisation.	188
7.6	Optimised geometries thresholded at $\gamma \leq 0.1$ (upper row) and $\gamma \leq 0.3$ (lower row). The difference between the two rows is a thin layer of intermediate-density elements surrounding the optimised geometries. The decision was made to progress with the $\gamma \leq 0.3$ thresholded designs due to the potential for interpretation of the ϕ case as a continuous pipe insert.	188
7.7	Left: comparison of velocity contours at the outlets of the ϕ , T_S and T_F studies: 7.7a, 7.7b and 7.7c respectively. Right: comparison of Reynolds number contours at the outlets of the ϕ , T_S and T_F studies: 7.7d, 7.7e and 7.7f respectively, showing a maximum of above $> 10^6$, indicating the evolution of more turbulent flow downstream of the internal features.	190
7.8	Left: Temperature distribution at the outlet of the ϕ (7.8a), T_S (7.8b) and T_F (7.8c) designs. 7.8c includes an additional colour legend to display the extended temperature range in the upper right corner. Right: Outlet turbulent kinetic energy for the ϕ (7.8d), T_S (7.8e), and T_F (7.8f) results.	190
7.9	Regions of highest convective heat fluxes ($\geq 5\text{MW m}^{-2}$) in the ϕ , T_S and T_F geometries.	190
7.10	Post-processed and meshed inserts for the ϕ (7.10a), T_S (7.10b) and T_F (7.10c) results, which are then assembled for performance testing in elongated versions of the original geometries. Only the T_S and T_F designs make contact with the inside of the pipe, whereas 7.10b remains ‘suspended’ in the fluid.	191
7.11	Velocity streamlines around optimised geometries coloured by absolute temperature and velocity magnitude.	193

List of tables

2.1	PPCS reactor coolants. WCLL = water cooled Li-Pb, HCPB= He cooled pebble bed (Marbach, Cook, and Maisonnier 2002).	71
2.2	Parameters indicating the increases in technological capability between PPCS reactors A and D. Adapted from data in (D. Maisonnier <i>et al.</i> 2007).	72
2.3	Comparison of He cooled concept thermal hydraulic performance reproduced from (Hermsmeyer and Kleefeldt 2001)	89
3.1	CuCrZr chemical composition, (reproduced from a datasheet provided by 3T Additive Manufacturing).	99
3.2	CuCrZr chemical composition in at.% (primary constituents only).	99
3.3	Properties of the dilatometry test specimens chosen to provide an indication of the change in thermal properties for samples at the extremes of the laser power used.	107
3.4	Mean coefficients of thermal expansion.	110
3.5	Maximum and final length change.	111
3.6	Room temperature absolute densities and as a fraction of reference CuCrZr density (8.9g cm^{-3}) for samples used in laser flash analysis.	114
3.7	Sample build parameters when ranked by thermal expansion performance (where the lowest coefficient of thermal expansion is ranked 1 st) and diffusivity (where the highest diffusivity is ranked 1 st).	117
5.1	Design domain average values for temperature and thermal gradient for all geometries. The values are displayed as percentages of the baseline design steady-state performance.	156
6.1	Summary of material-based temperature limits. *These limits are ‘soft’ limits which are linearly interpolated in topology optimisation problems in order to account for the local mixing of materials.	162
6.2	Maximum relative stresses σ_{rel} for suspended flat monoblock sub-components	166
6.3	Fixed flat monoblock maximum relative stresses σ_{rel} for reference and optimised designs.	168
6.4	Relative stress with surface area fraction, presented to summarise the performance of reduced Cu content designs.	170
6.5	Maximum relative stresses σ_{rel} for suspended bevelled sub-components	173

6.6	Summary of results from the chosen four design concepts. The maximum value for the specified parameter is displayed in each case, as evaluated in the location given in the row below. Design domain is abbreviated to ‘DD’ and ‘Top’ and refers to the sacrificial armour layer.	174
7.1	Objectives used in the literature for topology optimisation of forced convection conjugate heat transfer systems. The first column divides studies with respect to whether the relevant property was minimised or maximised. . . .	185
7.2	Values of topology optimisation parameters	186
7.3	Completion times for turbulent flow topology optimisation simulations. . .	187
7.4	Average pressure drops for post-processed geometries. These results were obtained in 80mm long domains, however pressure drop per metre estimates are presented to facilitate comparison with other PFCs.	192
7.5	Average temperature differences between the outlet and inlet for the three geometries, evaluated over the 80mm design domain.	192

Abstract

Nuclear fusion has the potential to provide an energy-dense sustainable electricity supply, however, fusion power plants face a number of design challenges. In-vessel components designed for use inside fusion reactors must be capable of tolerating extreme heat and particle fluxes. This thesis investigates a methodology for re-introducing design freedom to the conceptualisation of in-vessel components for the divertor, a device responsible for handling the highest heat fluxes in the reactor. This is approached through the application of topology optimisation, a process which involves the distribution of material throughout a geometry in order to meet an objective, subject to constraints. The resulting geometries are often complex and may be dependent on progress in novel manufacturing methodologies. A review of divertor design finds that top-down requirements limit material selection, component geometry and coolant fluid choice. Furthermore, the need to tolerate a given heat load creates design challenges which often cannot be managed without driving device size, cost and complexity. Design requirements are also subject to significant uncertainty, caused by a lack of representative testing, the time associated with reactor construction and the large jumps in performance required of successive devices. An investigation into additive manufacturing (AM) of a divertor-relevant alloy (CuCrZr) was conducted as part of an industrial collaboration designed to assess contemporary AM material performance. The work finds the material to exhibit good thermal performance and establishes scope for process optimisation as a means of increasing build speed and reducing cost. Thermal topology optimisation of the divertor monoblock is performed using COMSOL Multiphysics and finds potential for optimised designs to reduce armour temperatures by over 200K during transient high heat flux events and to minimise thermal gradients. The incorporation of thermally induced stress minimisation leads to stress reductions of up to 65% and the potential for heat flux redistribution. The optimised geometries contain transitions between materials which could be interpreted for manufacture using a combination of functional grading and AM. The impact of asymmetric geometries designed to minimise leading edges and multiple attachment scenarios are also investigated, finding substantial differences in optimal design qualities. Finally, the methodology is extended to the treatment of conjugate heat transfer between armour plates and coolant fluid. The optimisation process employs $k-\epsilon$ turbulence and maximises heat transfer objectives whilst limiting pressure drop. The optimisation results in the development of internal features which promote convective and conductive heat transfer.

Declaration of originality

I hereby confirm that no portion of the work referred to in the thesis has been submitted in support of an application for another degree or qualification of this or any other university or other institute of learning.

Copyright statement

- i The author of this thesis (including any appendices and/or schedules to this thesis) owns certain copyright or related rights in it (the “Copyright”) and s/he has given The University of Manchester certain rights to use such Copyright, including for administrative purposes.
- ii Copies of this thesis, either in full or in extracts and whether in hard or electronic copy, may be made *only* in accordance with the Copyright, Designs and Patents Act 1988 (as amended) and regulations issued under it or, where appropriate, in accordance with licensing agreements which the University has from time to time. This page must form part of any such copies made.
- iii The ownership of certain Copyright, patents, designs, trademarks and other intellectual property (the “Intellectual Property”) and any reproductions of copyright works in the thesis, for example graphs and tables (“Reproductions”), which may be described in this thesis, may not be owned by the author and may be owned by third parties. Such Intellectual Property and Reproductions cannot and must not be made available for use without the prior written permission of the owner(s) of the relevant Intellectual Property and/or Reproductions.
- iv Further information on the conditions under which disclosure, publication and commercialisation of this thesis, the Copyright and any Intellectual Property and/or Reproductions described in it may take place is available in the University IP Policy (see <http://documents.manchester.ac.uk/DocuInfo.aspx?DocID=24420>), in any relevant Thesis restriction declarations deposited in the University Library, The University Library’s regulations (see <http://www.library.manchester.ac.uk/about/regulations/>) and in The University’s policy on Presentation of Theses.

Acknowledgements

I would like to thank Dr Lee Margetts, Dr Llion Evans and Dr Matthew Roy for their continued support throughout this project.

Chapter 1

Introduction

This thesis focuses on the design of a component known as the divertor, a crucial part of many fusion reactor concepts that performs a number of important functions which include maintenance of fuel purity, the safe handling of high heat fluxes and in some cases the supply of heated water for electricity generation. Before discussion of divertor design however, it is necessary to first cover some of the fundamentals of nuclear fusion, reactors, and some of the context surrounding their continued development.

1.1 Nuclear fusion

The project contained in this thesis relates to the study of nuclear fusion. Nuclear fusion is commonplace in nature, acting as the source of the energy radiated by stars, including our sun, and is therefore responsible for sustaining all life on earth. As implied in its name, nuclear fusion relates to the joining of light nuclei (those made up of comparatively few neutrons and protons) to form heavier elements. Fig. 1.1 shows the binding energy per nucleon for elements as the number of nucleons increases. It shows that the binding energy per nucleon, which can be thought of as a measure of how strongly bound the nucleons are, increases as the number of nucleons increases until the number associated with iron (Fe) is reached. For elements with fewer nucleons than Fe, the addition of more nucleons through nuclear fusion allows for stronger nuclear binding forces. For reactions with fusion products lighter than Fe, the addition of more nucleons through nuclear fusion typically allows for stronger nuclear binding forces. These reactions are exothermic and transfer kinetic energy to the reaction products.

Thermonuclear fusion implies the fuel has been heated to a temperature where the average kinetic energy of the particles is sufficient for fusion to occur. In order for this to happen, the matter must exist as a charged gas known as a plasma, where the electrons have been stripped from the nuclei. Stripped of their electrons, and with sufficient thermal energy, the nuclei can pass close enough such that they can overcome their natural repulsion (referred to as the Coulomb barrier) with the aid of quantum tunnelling effects, and fuse (Kikuchi 2010). Thermonuclear fusion is desirable in preference to other means of fusion (such as that which might occur in particle accelerators) as it is seen as a sustainable concept for an electricity-producing power plant. In a star, fusion occurs due to the pressure exerted

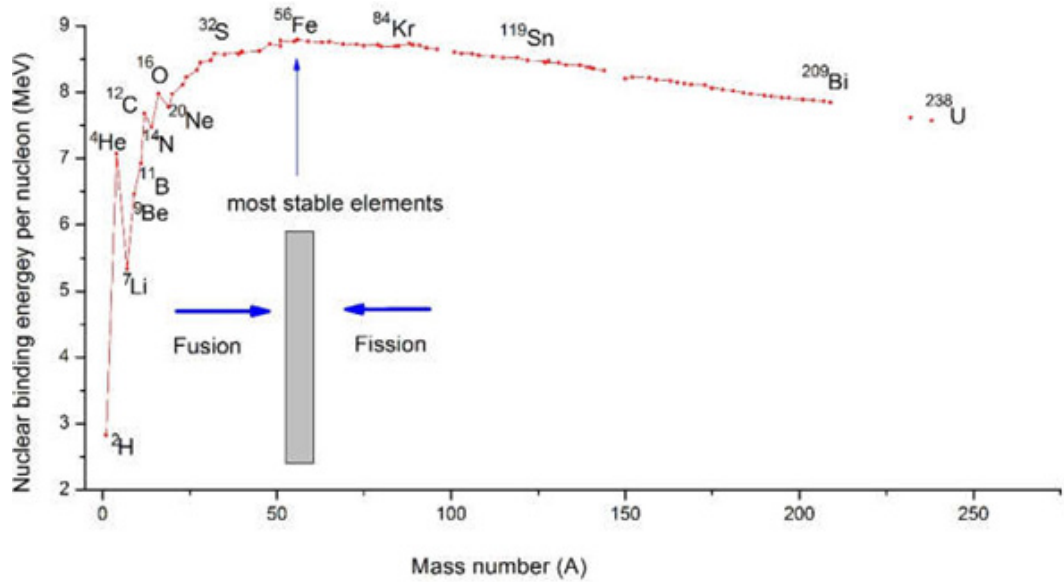
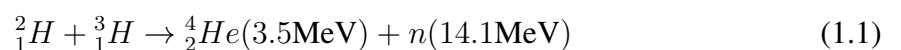


Figure 1.1. Binding energy per nucleon, showing the transition between the regimes where nuclear fusion and nuclear fission are energetically favourable, reproduced from (Girtan *et al.* 2021).

by gravitational forces due to its vast mass. This does not provide an achievable model for terrestrial fusion reactors, and suitable conditions for fusion must be reached by other means. This thesis discusses magnetic confinement fusion exclusively, where magnetic fields are used to contain a plasma in a ‘magnetic bottle’ in order to sustain the conditions required for thermonuclear fusion. The most widespread concept for a magnetic confinement reactor is known as a tokamak.

1.2 Tokamaks

This section is intended as a brief summary only and the reader is referred to the many books detailing tokamak operation such as Wesson’s ‘Tokamaks’ (Wesson 2011) for more information. Tokamaks are devices which use magnetic fields to confine ionised gases known as plasmas. The plasma is heated using a variety of techniques in order to produce suitable conditions for the constituent parts to undergo sustained nuclear fusion. The gases thought to present the best candidate fuels for the first generation of fusion power plants are two isotopes of hydrogen known as deuterium and tritium. These isotopes are chosen as their cross-section of interaction - a measure of the likelihood of interacting particles fusing - is greater at lower temperatures than it is for other reactions. As illustrated in Eq. 1.1, the reaction produces a neutron which carries the majority of the kinetic energy and an alpha-particle (a helium nucleus).



The goal is to heat the plasma such that a significant fraction of the ionised particles have enough kinetic energy to fuse, and that enough of the alpha particles produced go on to heat the plasma further, such that self-sustaining heating, known as ‘ignition’ is achieved. For

deuterium-tritium (D-T) plasmas, this is thought to be achievable if the ‘plasma temperature’ is in the range of 10 – 20keV. However, as keV is strictly measure of kinetic energy with a conversion factor of $1\text{keV} = 11,600\text{K}$, this can be thought of as a temperature range of 116 – 232 million K.

Whilst the alpha particles have a net electric charge and therefore interact with the magnetic fields, the neutrons can escape the plasma and collide with the inner walls of the reactor. The energy imparted to the reactor walls produces heat, which, if connected to a steam turbine system, could be used to generate useful electricity. This electricity generation system, whilst based on a centuries-old technology, has not yet been demonstrated in the context of a fusion reactor (Ciattaglia *et al.* 2020). Whilst deuterium is present in seawater, tritium is a short-lived isotope, with a half-life of approximately 12.3 years and is thus not present in significant quantities naturally. Tritium ‘breeding’ is thought to be necessary for commercially viable fusion reactor operation and is typically proposed through the decomposition of lithium implanted in the reactor walls, where it is hoped that enough tritium can be bred and extracted to provide a self-sustaining supply. Where the supply of tritium is limited, the use of deuterium-deuterium fusion reactions (which can produce a tritium product) has been proposed as a method of start-up (Zheng *et al.* 2016). Fig. 1.2 shows some of the major tokamak components as they are configured in the ITER tokamak. The poloidal and toroidal field coils generate magnetic fields which combine to produce a field with a toroidal geometry and helical field lines which cause the ionised plasma to circulate around the torus. The current passed through the central solenoid is increased rapidly, generating a changing magnetic field which induces a current in the plasma through Lenz’s law. The central solenoid is therefore important for plasma initiation and heating, but also contributes to plasma stability and shaping (Libeyre *et al.* 2009). The blanket protects other components such as the vacuum vessel and magnet systems and is responsible for tritium breeding. The divertor is engineered to handle the highest heat fluxes in the reactor and acts as an exhaust system for spent fuel. The divertor is the primary subject of this thesis and is introduced in more depth in Section 1.5.

1.3 ITER and future devices

The global fusion community is currently very focused on the development of the ITER tokamak. The device is part of the European Fusion Roadmap, a plan for fusion energy detailed in (Romanelli *et al.* 2012) and updated in (Nordlund 2018), which aims at proving the viability of fusion as a power source, with ITER’s successor, known as DEMO designed to demonstrate the feasibility to industry. ITER is funded by taxpayers in 35 countries, with its range of international collaborators including the USA, China, Japan, Russia, South Korea, India and the EU. Non-member participants include Canada, Thailand, Kazakhstan and Australia (ITER 2021). The ITER members contribute largely by providing services or components, enabling the local development of fusion-relevant manufacturing facilities. Those associated with ITER will share data produced from the device, which will inform the next generation of DEMO devices. This global collaboration is the main reason why there

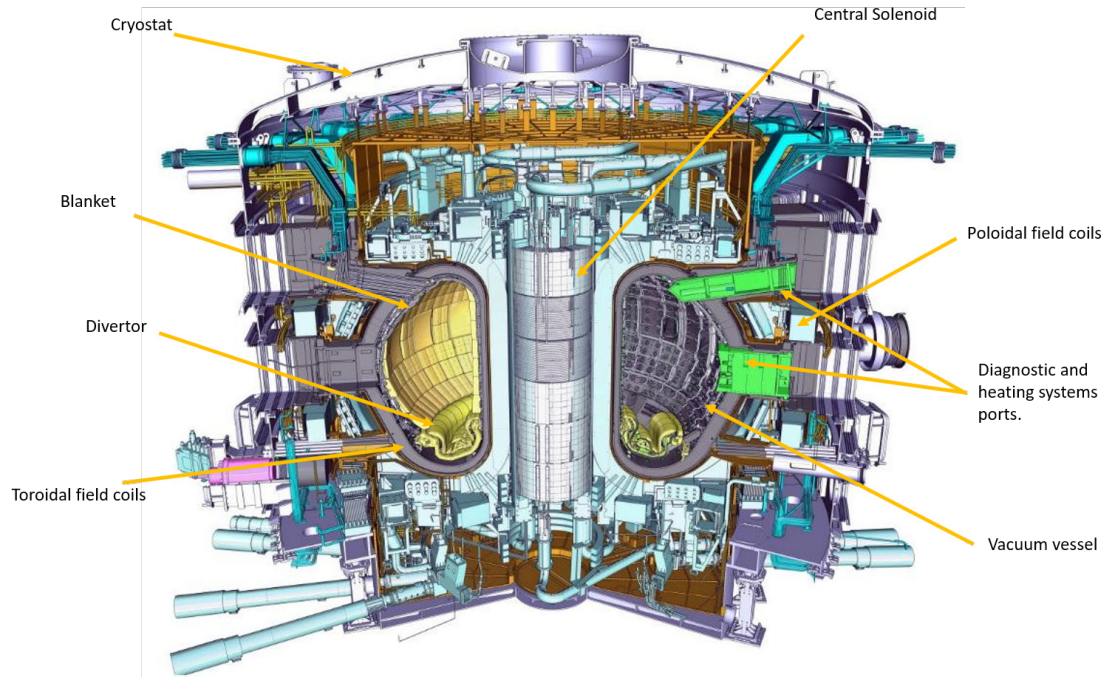


Figure 1.2. Schematic of ITER with some of the main components labelled. Reproduced from (Dubus 2014).

are not currently many ITER-scale devices being developed. Whilst ITER was never intended as an electricity-producing device, it is designed to be the highest-performing tokamak ever constructed. The following discussion regarding ITER is presented as context to the progress that still needs to be made before fusion reactors have a chance at commercial viability.

The ITER organisation claims the device will be the first in the world to produce a net surplus of fusion energy (Nordlund 2018). It is designed to operate in 400-600 second pulses and will be the largest tokamak to date when constructed. Despite this, there is a large gap between ITER-level performance and what is required from a commercially relevant reactor. This can be illustrated through the definition of a power amplification parameter, referred to as fusion gain ‘ Q ’. Q is the ratio of the power generated by fusion reactions P_{fus} to the heat successfully coupled into the plasma P_{heat} , with ITER aiming to produce 500MW fusion power for a heat input of 50MW, giving $Q = 10$. Fusion gain may be defined relative to any measure of power input, however, such as the power the reactor draws from the national electricity grid. The simplest interpretation for ITER (based on information available on the ITER website (*The Balance of Power* 2022)) gives 500MW fusion power produced for 300MW electrical input, resulting in $Q = 1.67$. This is intended for illustration only, because, as shown in Eq. 1.1, a fraction of the fusion power output is carried by alpha particles, some of which can contribute to plasma ‘self-heating’, which sustains the reaction. ITER’s successor DEMO aims to produce 500MW net electrical power for a fusion power of 2000MW, with a pulse length (burn time) of 2 hours (G. Federici, Bachmann, Barucca, Biel, *et al.* 2018), 4x the fusion power of ITER for 12-18 for times as long. A commercially relevant power plant would likely have a fusion gain which is higher still and require steady state operation in order to achieve a high enough availability (D. Maisonnier *et al.* 2007). The performance of tokamaks as electricity-producing devices remains a long way from economic attractiveness, even with dramatic performance increases envisaged between devices.

of reactors is likely to become more constrained and complex rather than less so.

1.5 The divertor

The divertor is a tokamak component which is the subject of significant active research and development and provides crucial functionality in mainstream tokamak designs. In work on fusion reactors in the 1950s, divertors were originally introduced to improve the plasma purity by removing plasma surface interactions from the region of confined plasma, altering particle flow to prevent dust and sputtered wall material from re-entering the plasma (Nuttall 2004).

The most widely implemented convention for divertor design relies on a single magnetic null point commonly referred to as a magnetic X-point due to the shape of the magnetic flux surface (illustrated in Fig. 1.4). The position of this magnetic null is dependent on the separatrix, which divides the toroidal plasma core from what is known as the scrape-off layer, (a plasma region which contains open flux surfaces) which is responsible for the majority of power transport to the divertor plates (Wesson 2011). The divertor receives the vast majority of the charged particle flux, as the motion of these ions is primarily along magnetic field lines. The particle flux, and therefore heat load, is particularly concentrated as it is limited by the scrape-off layer width (see Fig. 1.4), which can be on the order of several mm, leading to a target surface of only a few mm² that is perpendicular to the plasma. This area can be increased, however, by placing the targets at glancing angles, which stretch the contact surface vertically, or through having multiple magnetic null points (Wesson 2011).

The presence of impurities in the plasma often results in power loss, and maintaining high plasma temperatures is essential in order to maximise the probability of interaction between the deuterium and tritium fuels such that thermonuclear fusion can be sustained. Power loss can occur through Bremsstrahlung radiation, which has an emissivity that is proportional to atomic number Z^2 and is thus much more severe for the heavy materials such as W used in the reactor armour (Wesson 2011). As the destination for charged particles including spent fuel, the divertor is exposed to an intense heat flux which can be utilised for the generation of electricity through transfer to the fluid cooling system (Burchell *et al.* 1992). Further discussion on the additional challenges associated with using divertor heat for electricity generation is presented in Chapter 2. In many divertor designs, such as the ITER concept described subsequently, thousands of actively cooled armour tiles are attached to the divertor to help manage the incident heat flux. These are often made of materials like W, which has a melting point of approximately 3,400°C.

1.5.1 The ITER divertor design

The current ITER divertor target design includes a water-cooled CuCrZr pipe surrounded by a pure Cu interlayer (Hirai, Escourbiac, *et al.* 2014) designed to facilitate joining and act

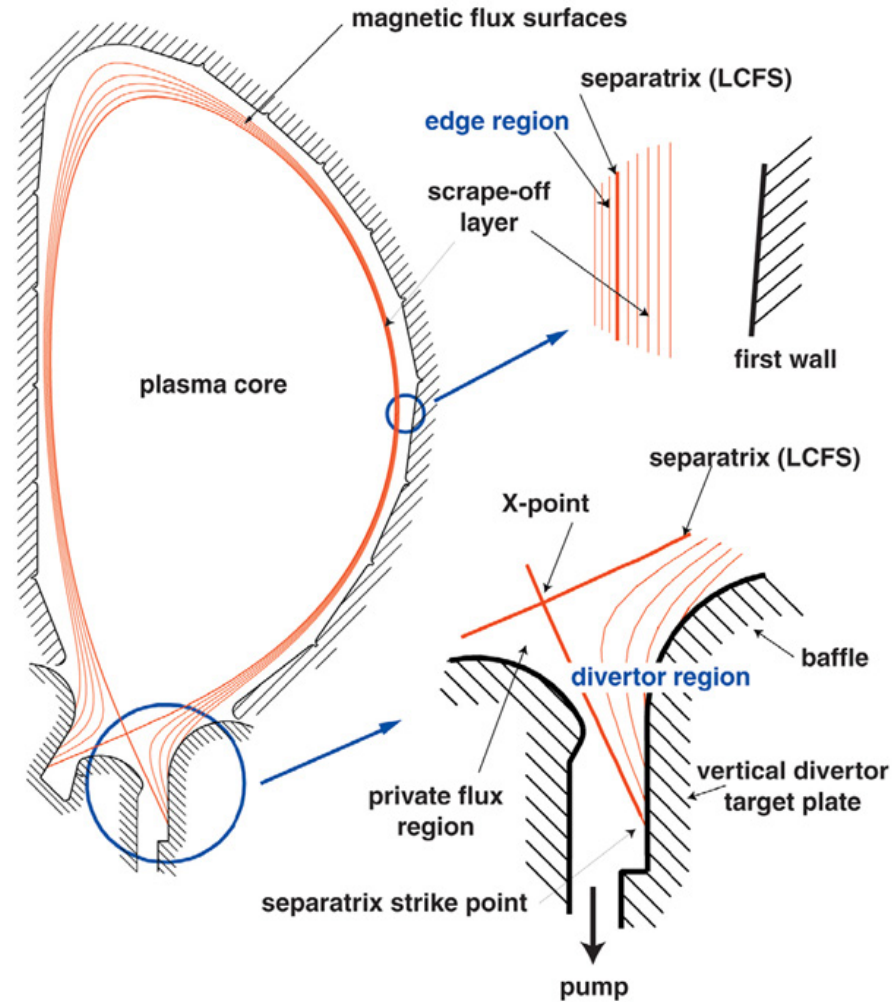


Figure 1.4. Cross section of a single magnetic null divertor configuration, with important features labelled. Reproduced from (G. Federici, Biel, *et al.* 2017)

as a compliant layer which relieves the thermal stress caused by the difference in thermal expansion coefficient α (T.R. Barrett *et al.* 2015). When the monoblock receives a heat flux, the CuCrZr parts (which have $\alpha \approx 17 \times 10^{-6}/\text{K}$) expand at faster rate than the W parts (with $\alpha \approx 4.4 \times 10^{-6}/\text{K}$). The interlayer accommodates this by undergoing plastic deformation (M. Fursdon, J. H. You, *et al.* 2018). The design is illustrated in Fig. 1.5. Rows of monoblocks are then assembled and fixed to structural cassette bodies as illustrated in Fig. 1.6 to form the divertor targets responsible for handling the highest heat fluxes in the reactor.

The ITER divertor is designed to operate with 54 divertor cassettes, resulting in many thousands of monoblocks (R. Pitts *et al.* 2013). W was chosen for its high melting point which allows for safe operation between 773 and 1723 K (Abernethy 2017), and relatively high thermal conductivity (174 W/(mK) at room temperature (D. S. Lee *et al.* 2019)) however there are associated compromises. W is considered low activation but does undergo significant transmutation, affecting its performance in ways which are difficult to predict (R. E. Nygren *et al.* 2016). It also poses significant safety issues. In the event of loss of coolant to the reactor and air ingress, W forms WO_3 which is volatile and creates a pathway for failure of the device through explosion (Denkevits 2010; Wegener *et al.* 2017). W was chosen over the previously considered carbon fibre divertor design due to its resistance to absorbing tritium (R. Pitts *et al.* 2013). The amount of tritium present in fusion reactors is likely to be strictly

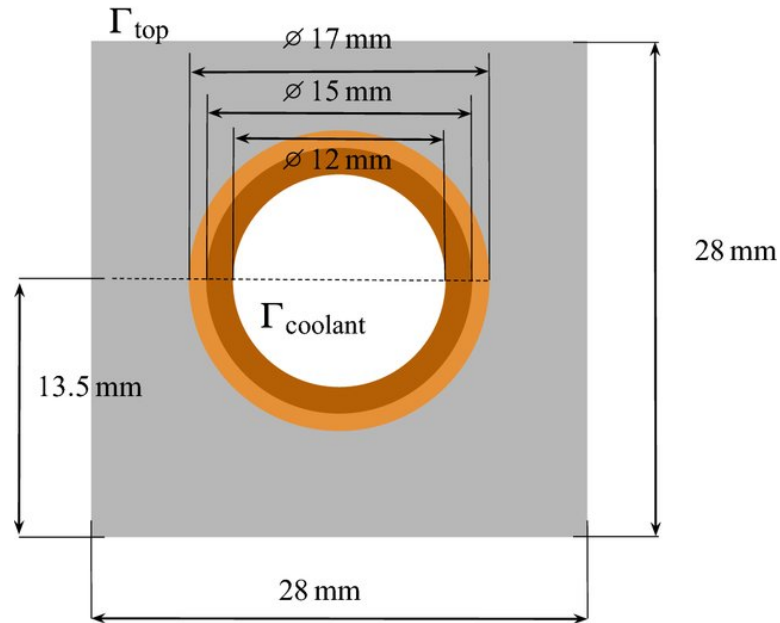


Figure 1.5. Sketch of ITER monoblock geometry reproduced from (Delaporte-Mathurin *et al.* 2020) which shows the inner CuCrZr cooling pipe set separated from the W monoblock by a Cu interlayer.

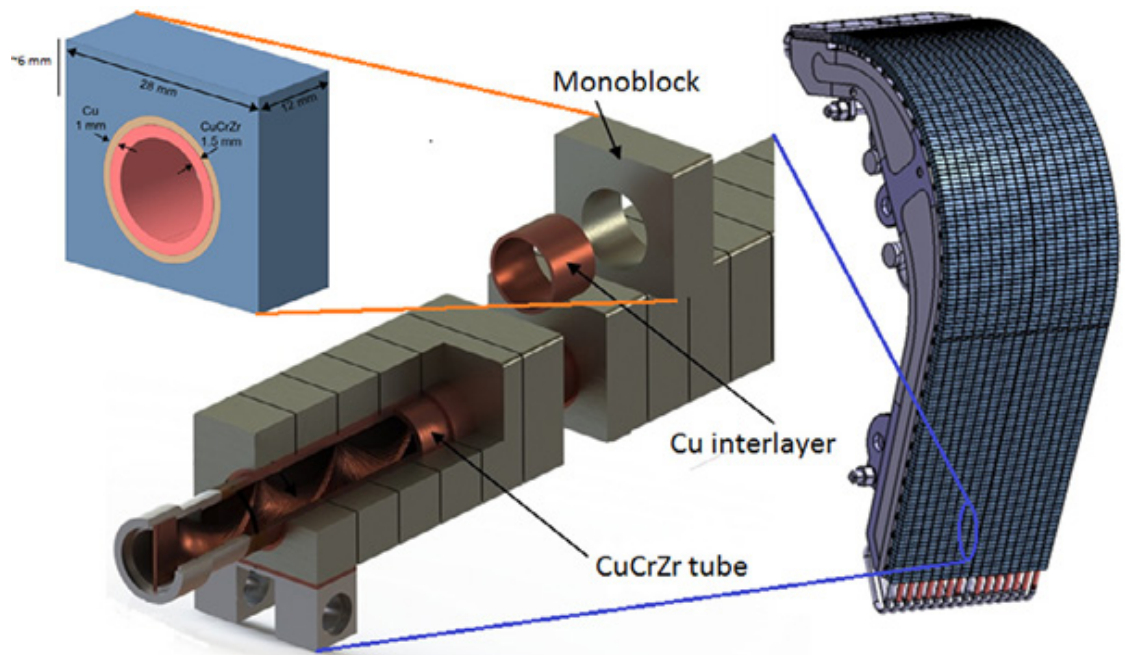


Figure 1.6. Illustration of the ITER W monoblock design, including location in the divertor target. Reproduced from (Bonnin *et al.* 2017).

controlled by nuclear regulators (Taylor, Ciattaglia, Boyer, *et al.* 2017). The CuCrZr pipe was chosen primarily for its thermal conductivity and strength and not its activation characteristics (Thomas R. Barrett *et al.* 2016). The rationale behind slotting many W monoblocks onto a single copper pipe has two parts. Firstly, there is a lower transference of stress between individual monoblocks as they are not bonded, thus it is more likely that a single monoblock fails than an entire row (T.R. Barrett *et al.* 2015). Despite this design, however, the current ITER protocol is to replace the entire divertor cassette (Thomas R. Barrett *et al.* 2016). The ITER divertor must be resistant to high heat flux fatigue such that it can withstand 10MW m^{-2} heat fluxes in normal fusion operation and slow transients of 20MW m^{-2} (M. Fursdon, J. H. You, *et al.* 2018). Similar criteria have been assumed when developing components for the Euro-

pean DEMO project (Muyuan Li and Jeong-Ha You 2017), which is intended ‘as a credible prototype for a power-producing fusion reactor, although in itself not fully technically or economically optimised’ (Romanelli *et al.* 2012, pp. 6). The requirements for ITER and DEMO divertor monoblocks are comparatively well documented and act as a guideline for the development of components using design optimisation in this thesis.

1.5.2 Alternative divertor concepts

There are many design constraints and requirements to consider when developing a divertor concept. The demanding performance requirements must be met whilst ensuring compatibility with other reactor systems such as the blanket, which is responsible for breeding tritium and extracting heat for power generation. The European Power Plant Conceptual Study (PPCS) project envisaged five different conceptual designs of fusion power plants reflecting a progressively more advanced technology and assessed them on the basis of systems integration over the course of a series of studies (D. Maisonnier *et al.* 2007). The PPCS assesses several different divertor concepts and includes discussion on non-traditional coolant fluids such as helium. A wide range of divertor concepts have been proposed, including those which rely on gas jet impingement (D. S. Lee *et al.* 2019), porous insets (Hermsmeyer and Kleefeldt 2001), liquid metal surfaces (Hirooka *et al.* 2015) and rotating targets (Mazul 2016), however these exist in different states of maturity and investigation. Fig. 1.7 illustrates two helium-cooled divertor concepts and indicates the diversity of concepts being proposed.

The paper presented in Chapter 2 discusses a range of these designs in the context of digital engineering and work modelling their performance, associated uncertainties and interaction with power plant design.

1.5.3 Design considerations for high heat flux components

High heat fluxes can lead to a range of different damage scenarios in plasma-facing components. Thermal stresses are induced in plasma-facing components due to thermal gradients and differing rates of thermal expansion in multi-material components due to steady state and cyclic heat loads (Linke *et al.* 2019). These loading conditions may be expected as part of standard reactor start-up and operation. Thermal shocks, however, associated with transient events (often resulting from plasma disruptions) represent a distinct loading condition that the components must tolerate (Hirai, Pintsuk, *et al.* 2009). Damage to components can be associated with both of these scenarios, in combination with the many additional interacting processes that occur in a fusion reactor including radiation and electromagnetic forces. In (Hirai, Pintsuk, *et al.* 2009) for example, which assesses the causes of damage in W armour tiles, plastic deformation at high temperature was found to result in micro-cracks, with major cracks associated with brittle behaviour in the W. W divertor monoblocks have also been shown to experience deep cracking due to thermal fatigue at heat loads approaching 20MW m^{-2} , (Muyuan Li and Jeong-Ha You 2015) and are at risk of bulk melting and lo-

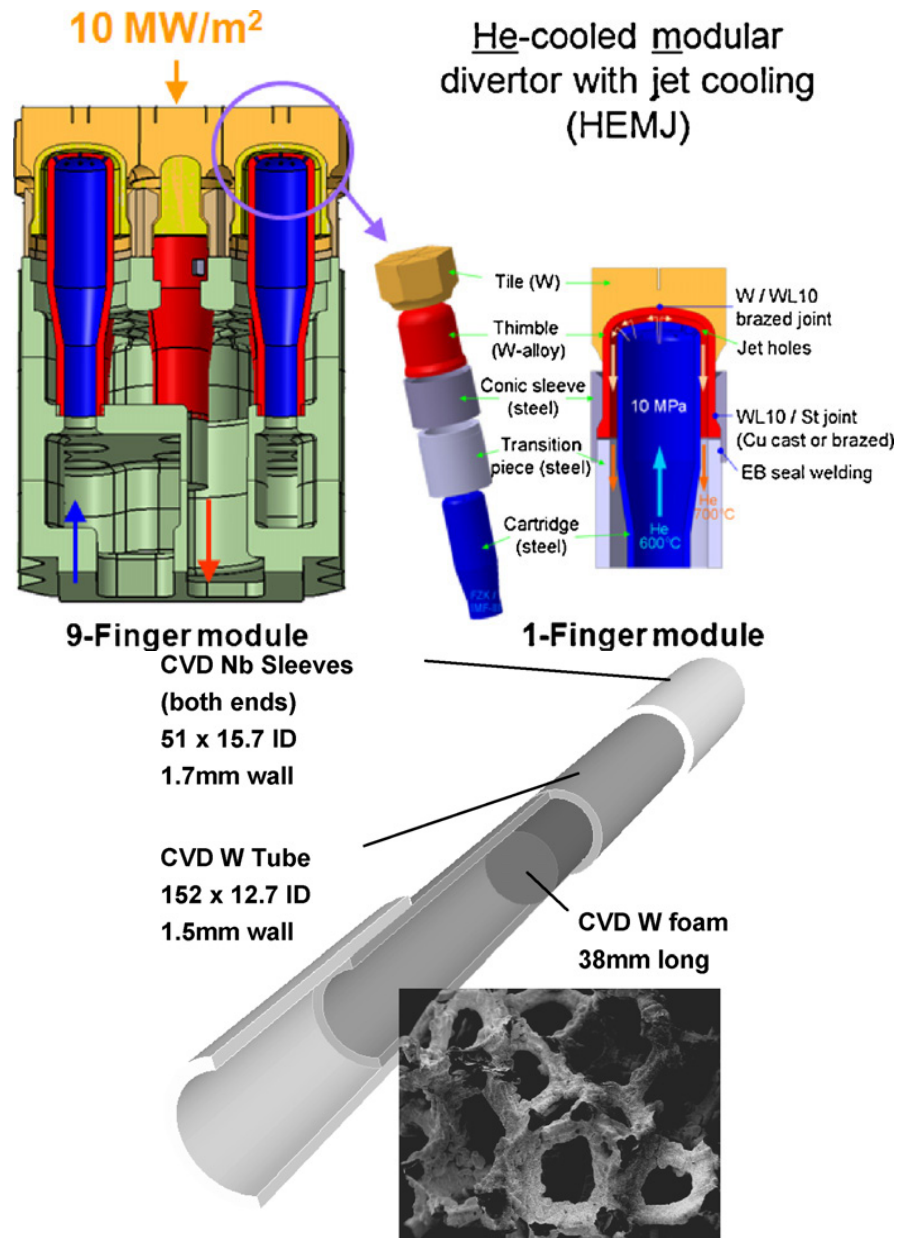


Figure 1.7. Upper: He-cooled modular divertor with jet cooling (HEMJ) concept (reproduced from (A. R. Raffray, R. Nygren, *et al.* 2010)). Lower: Mock-up of a helium-cooled divertor featuring a W foam insert manufactured using chemical vapour deposition (D. Youchison *et al.* 2007).

calised boiling on leading edges due to transient high heat flux events (J. Gunn, T. Hirai, *et al.* 2019).

In addition to tolerating high heat loads, plasma-facing components are subject to a number of other requirements. A series of functional requirements for High Heat Flux (HHF) materials, initially developed for ITER (Burchell *et al.* 1992) provide a perspective on some of the considerations associated with tokamak component design. The requirements are divided into functional and operational requirements. The operational requirements are:

1. to protect the (structural) components from plasma effects and
2. to protect the plasma from degradation by interactions with the plasma-facing materials.

Essentially, the HHF materials must form a barrier between the plasma and structure of the reactor without hindering the performance of either. The operational requirements are that:

1. HHF materials must not compromise the safety or environmental aspects of the plant (including fire, explosion, toxic and radioactive exposure);
2. shall not lead to unacceptable costs and operating schedules of the entire plant or
3. interfere with the operation of other requirements.

These requirements largely relate to integration challenges and focus development towards solutions that permit operation of a commercially viable reactor which does not require lengthy maintenance periods or expensive materials development programmes. Additional requirements state that HHF components must exhibit the following properties:

1. high thermal-shock resistance;
2. acceptable irradiation-induced property changes;
3. minimal tritium retention;
4. low erosion rates;
5. tailorable thermal conductivity;
6. low outgassing;
7. resistance to steam oxidation;
8. manufacturing compatibility and
9. maintainability.

These requirements were targeted specifically to the development of Carbon Fibre Composite (CFC) plasma-facing components and the reader is referred to (Burchell *et al.* 1992) for a full discussion. One point of note, however, is that in the development of a CFC divertor concept there was a desire for the (directional) tailoring of material properties. Whilst CFC plasma-facing components may have been deselected for ITER (due to cost and issues with tritium retention (Dolan 2014)), it is possible that similar tailoring of material properties may be possible with a combination of additive manufacturing and topology optimisation techniques (Alexandersen and Boyan Stefanov Lazarov 2015).

It is clear that these requirements place significant constraints on the design of plasma-facing components in addition to their primary function of handling heat loads. This contributes significantly to the challenge of designing plasma-facing components, as each additional requirement reduces the design space available. Another challenge for materials, set out by the European Fusion Development Agreement (EFDA) in (Romanelli *et al.* 2012) is that ‘at around 100 years after the reactor shutdown all the materials can be recycled in a new reactor’ (Romanelli *et al.* 2012, pp. 5). This and similar goals relating to minimising irradiated waste have contributed to the development of low activation materials as outlined in (Bloom *et al.* 1984) and influence the ITER divertor design. It could therefore be considered desirable to minimise the use of materials like Nb, Mo, Ni, and Cu which are likely to remain significantly activated for over 100 years (Okada, Noda, and Abe 1989).

1.6 Fusion technology readiness and development

A report on the idea of Technology Readiness Levels (TRLs), published in 1999 found that the maturity of a technology is one of the most important factors in its eventual success. The TRL classification system is based on 9 levels of readiness from basic scientific principles to a commercially fully functional product (*United States General Accounting Office* 1999). These principles have since been applied to many industries, and tokamak component development in (M. Tillack 2009), which provides several key results relevant to the development of the divertor. It is concluded that many ITER technologies are not reactor relevant and therefore do not advance the TRL. This includes heat and particle flux handling, which has a TRL of 3 (with no improvement expected due to ITER) and maintenance, which has the lowest TRL at 1. These technologies are crucial for the divertor as it is subject to the highest heat loads and therefore will likely require regular replacement in a reactor, particularly if it contains Cu alloys susceptible to radiation damage (Tobita, Ryoji Hiwatari, *et al.* 2019). In (Pearson *et al.* 2020), technology road-mapping for fusion startups is discussed. It is claimed that the linear development approach followed by publicly funded fusion research - inspired by 20th century success projects like fission power and the space race - has failed for fusion, in part due to the delays caused by strict adherence to the avoidance of risk of failure. Agile and lean development schemes, which originated in software and hardware development respectively, are proposed as the solution. These approaches emphasise rapid learning and adaptation to failure in order to iterate towards a minimum viable device which is scalable to commercial implementation. It is also argued that this approach prevents another risk - that of technologies becoming outdated over long development times.

1.7 Topology optimisation for design

Topology optimisation is a technique which involves the optimal distribution of material in a design domain in order to minimise (or maximise) an objective function, subject to a number of design constraints. Topology optimisation differs from other more traditional design optimisation techniques in that it allows for the creation of new boundaries in a design, rather than simply changing the size or shape of existing ones, as shown in Fig. 1.8.

Many different implementations of topology optimisation exist, including gradient-based methods and those based on genetic algorithms which take inspiration from biological processes. Topology optimisation can yield non-intuitive designs, established in a quantitative manner from a very generic initial problem statement. The implementation used in this project relies on gradient-based methods rather than heuristic techniques such as genetic (or evolutionary) algorithms. Gradient-based topology optimisation uses a single-valued objective function to characterise some aspects of system performance. Objective functions can be composed of multiple terms associated with different properties such as pressure drop or thermal gradient and given different weightings depending on the requirements of the optimisation problem. COMSOL Multiphysics 5.6[®] (COMSOL 2021), is used for the

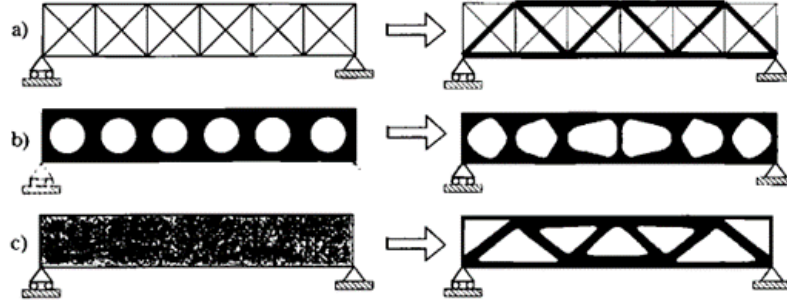


Figure 1.8. Different techniques for optimisation of a truss structure, where initial setups are shown on the left and optimised results on the right. a) Sizing (or geometric) optimisation where the size of individual features can be modified. b) Shape optimisation allows for the modification of already existing boundaries in the design. c) Topology optimisation allows for the creation of new boundaries and is therefore the most generic optimisation technique. Reproduced from (M. P. Bendsøe and O. Sigmund 2003).

topology optimisation performed in this thesis.

Whilst topology optimisation has traditionally been applied to compliance minimisation in structural problems, (M. P. Bendsøe and O. Sigmund 2003) the technique is gradually being applied to a wider range of systems. The publication of (Borrvall and Petersson 2003) has led to significant work applying topology optimisation techniques to fluid systems where the technique can be used to modify flow channels. Furthermore, as discussed in (T. Dbouk 2017), focus on thermal and in some cases thermal-fluid topology optimisation problems, has been increasing.

The topology optimisation problem can be formalised as shown in Eqs. 1.2 - 1.6, which are based on the formulation presented in (Jan H. K. Haertel, Engelbrecht, *et al.* 2018) as are Eqs. 1.7-1.10 apart from 1.7 which follows the COMSOL implementation (COMSOL 2021). Where $F = F(\gamma, s(\gamma))$ is the objective functional, subject to constraint functionals G_i (and M extra constraints). The local material density varies continuously throughout the design domain Ω and is given by γ which can have values between 0 and 1.

$$\underset{\gamma}{\text{minimise}} : F = F(\gamma, s(\gamma)) = \int_{\Omega} f(\gamma, s(\gamma)) dV \quad (1.2)$$

$$\text{subject to} : R(\gamma, s(\gamma)) = 0 \quad (1.3)$$

$$\text{and} : G_1(\gamma) = \int_{\Omega} \gamma dV - fV_{\Omega} \leq 0 \quad (1.4)$$

$$G_i(\gamma, s(\gamma)) \leq 0 \quad \text{with } i = 2, \dots, m + 1 \quad (1.5)$$

$$0 \leq \gamma(x) \leq 1 \quad \forall x \in \Omega \quad (1.6)$$

s is the state vector and R is the residual relating to the discretisation. G_1 is a volume constraint which controls the fraction f of the design domain volume V_{Ω} that the optimised geometry is permitted to occupy.

The choice of objective function and the associated constraints are crucial in the setup of

an optimisation problem. The objective function is a scalar quantity which is maximised or minimised according to a set of constraints and boundary conditions and may be composed of multiple individually weighted variables. Constraints on the problem can take a wide variety of forms. They can be geometrical such as a choice of design domain, based on maximum or minimum volume or surface-area fraction, or almost any physical property which has a well-defined derivative with respect to the design variables.

1.7.1 Interpolation and penalisation

The density-based method for topology optimisation implements changes to the objective function through modification of a continuously varying material density field γ . The material properties of an element at arbitrary density must therefore reflect any physical properties described in the objective function. This is performed by means of an interpolation function, which establishes values for intermediate material properties. This means that if the objective is to minimise compliance (maximising stiffness) for example, the material Young's modulus must be interpolated to provide values for intermediate-density elements.

One of the most commonly implemented interpolation techniques is the SIMP (Solid Isotropic Material with Penalisation) method (G. I. N. Rozvany 2009). The material properties of the extremes of the spectrum are usually well-defined, i.e. solid vs void or 'material 1' vs 'material 2'. However, the intermediate values of physical material properties are often hard to define in a physically meaningful way. This problem is tackled with the use of material penalisation. Penalisation reduces the number of elements with intermediate densities, justified on the basis that intermediate material densities would in most cases result in designs which are not suitable for manufacture by conventional techniques (M. Zhou and G. Rozvany 1991). In the SIMP method, the local value of material penalisation γ_p is calculated using a power law relation shown in Eq. 1.7. γ_{min} is the minimum penalised volume fraction, which is typically given a small positive value for numerical stability, p controls the level of penalisation.

$$\Gamma_p = \gamma_{min} + (1 - \gamma_{min})\gamma^p \quad (1.7)$$

The penalised volume factor Γ_p can be thought of as the local value of the design penalisation, or the degree to which different elements have their density pushed towards 0 or 1. Exponents of $p > 1$, therefore, reduce the values of γ where it is between 0 and 1. A continuation method whereby the value of p is slowly increased from 1 to 4 is often recommended to aid in avoiding convergence to local minima (Eschenauer and Olhoff 2001). Other common practices exist, including the recommendation of an exponent of $p \geq 3$ for materials with a Poisson's ratio on the order of $1/3$ (O. Sigmund 2001). Another penalisation scheme, sometimes referred to as 'Darcy' penalisation is associated with the topology optimisation of fluids, as shown in Eq. 1.8.

$$\Gamma_p = \frac{q[1 - \gamma]}{q + \gamma} \quad (1.8)$$

Here, the topology optimisation design domain is conceptualised as a porous medium, based on a methodology proposed in (Borrvall and Petersson 2003) where elements become part of the fluid or non-fluid domain when their properties tend towards full or zero permeability respectively. q is a constant which controls the strength of penalisation.

1.7.2 Techniques for design control

Projection and filtering are two commonly used techniques used to exert additional control on the optimisation problem. Filtering is used to enforce a minimum length scale and to reduce mesh dependency. The filter averages the density of similar nearby elements to produce a new value for local material density with a resolution corresponding to the specified filter radius, as shown in Eq. 1.9.

$$-r_{filter}^2 \nabla^2 \tilde{\gamma} + \tilde{\gamma} = \gamma \quad (1.9)$$

Where $\tilde{\gamma}$ is the filtered value of the continuous density field and r_{filter} is the filter radius. More detail on the use of this Helmholtz filtering technique can be found in (B. S. Lazarov and O. Sigmund 2011).

Projection is a technique which involves taking elements with intermediate material properties and amplifying their deviation from the projection threshold η to the closest extreme of density (either 0 or 1). COMSOL uses a form of Heaviside projection based on the implementation in (F. Wang, Boyan Stefanov Lazarov, and Ole Sigmund 2011), as shown in Eq. 1.10.

$$\tilde{\gamma} = \frac{\tanh(\beta\eta) + \tanh(\beta(\tilde{\gamma} - \eta))}{\tanh(\beta\eta) + \tanh(\beta(1 - \eta))} \quad (1.10)$$

Where β controls the gradient of the projection. Projection is used to combat the blurring of boundaries associated with filtering techniques. These techniques must be implemented with care, however, as they can move the problem away from a mathematically rigorous optimisation problem towards one where the subjective use of tuning parameters can make results difficult to replicate, as discussed in (G. I. N. Rozvany 2009).

1.7.3 The method of moving asymptotes

The Method of Moving Asymptotes (MMA) is an optimisation algorithm developed in 1987 in (Svanberg 1987) that is commonly employed for topology optimisation problems in the literature. These studies typically use the algorithm presented in (Svanberg 2002) which contains a MATLAB[®] script made available for academic usage. The MATLAB implementation is expanded upon and made globally convergent in (Svanberg 2007). The method is an iterative technique whereby the optimisation problem is split into a series of strictly convex approximate sub-problems. It is designed to handle a wide variety of element sizes, design variables and constraints, where the derivative of the constraint with respect to the design variables can be calculated numerically (Svanberg 1987).

1.7.4 Interaction with fusion research

Any results from plasma physics or material science research that can be translated into a material property or model input, such as a modified Ductile to Brittle Transition Temperature (DBTT) or a specifically tailored heat load, can be used to make the topology optimisation process more appropriate to the application area. As the techniques involved become more mature, it may also be possible to incorporate additional capabilities, such as, for example, optimisation for material properties that change in time over the course of component lifetimes.

1.8 Monoblock design exploration

The left side of Fig. 1.9 shows the ITER-style monoblock geometry considered for topology optimisation in Chapters 5, 6. The right side of Fig. 1.9 shows a geometry inspired by the monoblock variation presented in (Oh *et al.* 2021), which is discussed in Chapter 7. The concept combines the rectangular coolant channel of the hypervapotron with a monoblock armour concept. Apart from the coolant channel and explicit modelling of the sacrificial armour layer, the sub-components have similar material assignments to those in the ITER-style monoblock. It should be noted that whilst the sacrificial armour layer is shown as a separate part, this is to visually separate it from the topology optimisation domain, and it is part of a continuous armour plate.

The guiding methodology behind this project involved building up a topology optimisation workflow from the simplest possible case. Furthermore, the decision was made to constrain the work to existing geometries as much as possible, to facilitate comparison to published literature and constrain the otherwise broad and poorly defined design space. The sacrificial armour layer, coolant pipe and interlayer are left as unmodified in order to maximise compatibility with the baseline design, leaving the armour domain and the internal coolant pipe geometry available for topology optimisation.

For the case of the monoblock, the simplest relevant topology optimisation problem was identified as involving thermal conduction in the solid domain only. The results of this are presented in Chapter 5. The incorporation of thermally induced stress involved coupling the thermal simulation to a structural analysis, adding complexity to both the finite element modelling and the specification and weighting of multiple optimisation objectives. This methodology, implemented in Chapter 6 could be extended to include many more constraints and additional physics without significant additional effort as long as the software and computational resources allow for it. Recently, the top edge of the monoblock has been modified in some locations in the divertor to include a bevel which reduces the severity of heat flux concentration at leading edges (R. A. Pitts *et al.* 2017). Topology optimisation in Chapter 6 indicates the impact of this (seemingly minor) design change on optimum geometries and demonstrates the technique's ability to respond to asymmetric loading conditions. A discussion of published work regarding the design and enhancement of thermal-structural

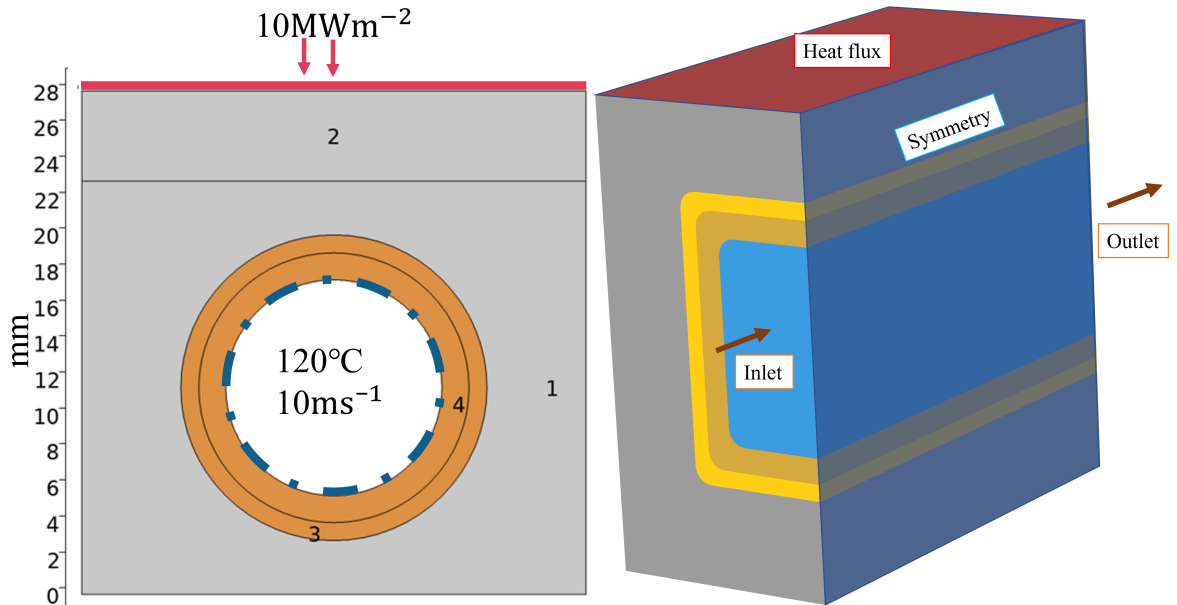


Figure 1.9. Monoblock geometries for study using topology optimisation. Left: ITER-style monoblock. 1) W armour, 2) Sacrificial W armour layer to account for erosion during the component’s lifetime. 3) Cu interlayer to relieve thermally induced stress. 4) CuCrZr coolant pipe. Right: novel monoblock design inspired by work presented in (Oh *et al.* 2021).

performance in plasma-facing component armour domains is presented in Section 2.4.3.

Finally, the problem is extended to the fluid domain. Compared to solid domain thermal-structural optimisation, topology optimisation of the fluid domain using Computational Fluid Dynamics (CFD) is more complex in its setup and computational requirements. In addition to the complexity which arises in the computational representation of fluid behaviour, the fluid domain optimisation geometry (shown on the right of Fig. 1.9) requires a 3D treatment, significantly increasing the computational resources required. The application of topology optimisation to the monoblock fluid domain was seen as the natural extension of the work performed in the solid domain as a means of testing the limits of the technique as implemented in commercially available finite element software. This approach was undertaken as opposed to, for example, a more detailed implementation of the currently accepted design-by-analysis rules presented in (M. Fursdon, J. H. You, *et al.* 2018) and discussed in Section 2.4.2. The justification for this decision is as follows: topology optimisation and the manufacturing techniques required to produce the resulting geometries are sufficiently immature that the design rules are likely to change before they can reliably be built, and consequently, the technique is currently best used for design space exploration. A discussion of the thermal-hydraulics of divertor plasma-facing components is presented in Section 2.4.8.

1.8.1 Previous studies on topology optimisation for fusion

To the best of the author’s knowledge, at the start of this project, there were no published applications of topology optimisation to fusion reactor plasma-facing components. As a result of this, the application of the technique to the divertor monoblock was pursued independently and cautiously, with the goal of building on an initial proof of concept application. The divertor monoblock was chosen as the target geometry for optimisation due to some

of the reasons outlined already, relating to the high-performance requirements and design challenges. It was thought that if techniques that result in a higher cost of manufacture were applied to fusion reactor component design, they are most applicable to the components currently facing the toughest design challenges. The divertor monoblock was also attractive, as some of the design challenges - particularly those of providing efficient heat transfer and acceptable pressure drop - can be characterised largely with physics commonly available in mainstream finite element software. This was necessary, as open-source topology optimisation codes were found to be used largely by their creators and respective research groups, with external users presented with long development times due to a lack of documentation or interest in collaboration.

Two significant studies have since published similar applications of topology optimisation to the divertor monoblock: (Curzadd *et al.* 2019), and (Kerkhof *et al.* 2021). Both of these implementations rely on in-house codes and focus on minimising von Mises stress and yield-criterion objectives in representations of the divertor monoblock, with emphasis on the stress-free temperature associated with residual stresses in AM components. (Kerkhof *et al.* 2021) uses finite volume techniques whereas (Curzadd *et al.* 2019) uses the finite element method. (Curzadd *et al.* 2019) tests the use of global volume fraction and cell-density constraints which limit the concentration of W or Cu in a particular element. The former is not found to be useful whereas it is claimed that the latter can be applied to act as a proxy for manufacturing constraints. (Kerkhof *et al.* 2021) implements temperature based constraints but does not investigate the use of temperature-based objective functions. Both studies result in designs that significantly outperform the baseline geometry. (Curzadd *et al.* 2019) suggests that more work needs to be completed investigating the influence of the stress-free temperature and the behaviour of W-Cu composite materials. (Kerkhof *et al.* 2021) indicates the need for optimised designs which perform well outside the conditions they have been optimised for, given the range of potential transient conditions plasma-facing components are exposed to and the need to account for lifetime effects such as cyclic loading in the formulation of objective functions. The unknowns associated with the stress-free reference temperature are also noted. Both papers ultimately attempt to formulate optimum geometries suitable for manufacture, with neither - by their own admission - succeeding. This shows a different approach to the perceived usefulness of topology optimisation in contemporary plasma-facing component design from the one followed in this thesis. In this project topology optimisation is used primarily as a design exploration tool, in the knowledge that as all the contributing technologies mature, design requirements will change and capabilities evolve. The power of topology optimisation is considered to be its flexibility to investigate multiple objectives, and its ability to start from a very generalised problem. Furthermore, the possibility to illustrate the impact of design changes such as the introduction of asymmetry in the monoblock through bevelling or different fixing mechanisms (explored in Chapters 5 and 6) or in concept development for novel plasma facing components (as explored in Chapter 7) became apparent.

Work presented in (Domptail *et al.* 2020) also performs optimisation of the divertor monoblock,

in the design of a thermal-break interlayer, however, the methodology used is that of traditional sizing optimisation (shown in Fig. 1.8), where the magnitude of different parameters is altered to find an optimum sizing, a technique which bears little similarity to topology optimisation as it requires a well-defined geometry and concept. The initial designs are combined with a design-search approach where a genetic algorithm is used to identify the optimum combination of parameters. Whilst this approach differs from the topology optimisation methodology, the detailed parameterisation of the design allows for the specification of more detailed constraints. It is therefore less useful as early-stage design exploration and more applicable to a concept that is intended for imminent manufacture and testing. The sub-components of the design are already well-defined and so the rules outlined in design codes and rules such as the Monoblock Elastic Analysis Procedure (detailed in (Thomas R. Barrett *et al.* 2016)) can be applied more easily. This paper does however provide a model for an optimisation procedure to be performed after initial topology optimisation concept development. Ideally, the techniques shown in Fig. 1.8 should be applied in reverse of the displayed order, with topology optimisation used to define the initial design concept, shape optimisation used to refine the boundaries and sizing optimisation used for localised control over the scale of features.

1.9 Overview of topology optimisation workflow

A simplified overview of the topology optimisation process is detailed in Fig. 1.10, which is broadly representative of the techniques used throughout the remainder of this thesis, however, projection and filtering techniques are not always used. As shown in Fig. 1.10, once the solution to this has been obtained, the geometry can be updated based on the local material densities, giving an intermediate result. Then, any filtering and projection is applied and the process is repeated until the convergence criteria are met.

The following series of figures illustrate some of the major workflow steps when performing topology optimisation in COMSOL Multiphysics. Some of the following steps can be carried out in scripting environments, however, they are shown here performed in the graphical user interface (GUI). This section is not a re-creation of the COMSOL Multiphysics user manual or online tutorials but is designed to illustrate some of the key elements of the process that differ from traditional finite element analysis. The point is not to show the finer points of the graphical user interface but to illustrate where the techniques outlined in the previous sections can be implemented. The standard process of setting up a standard simulation in the software is not detailed, as tutorials on this are readily available online and in COMSOL's user manual (COMSOL 2021).

The COMSOL project variables window - which facilitates easy parameterisation of the topology optimisation implementation - is shown in Fig. 1.11. These parameters can be set up to link material properties such as thermal conductivity (k), density (ρ) and heat capacity (C_p) between the relevant materials used in the optimisation to permit interpolation as shown in Eqs. 1.11, 1.12 and 1.13. Γ_p is the degree of penalisation defined in Eq. 1.7. The

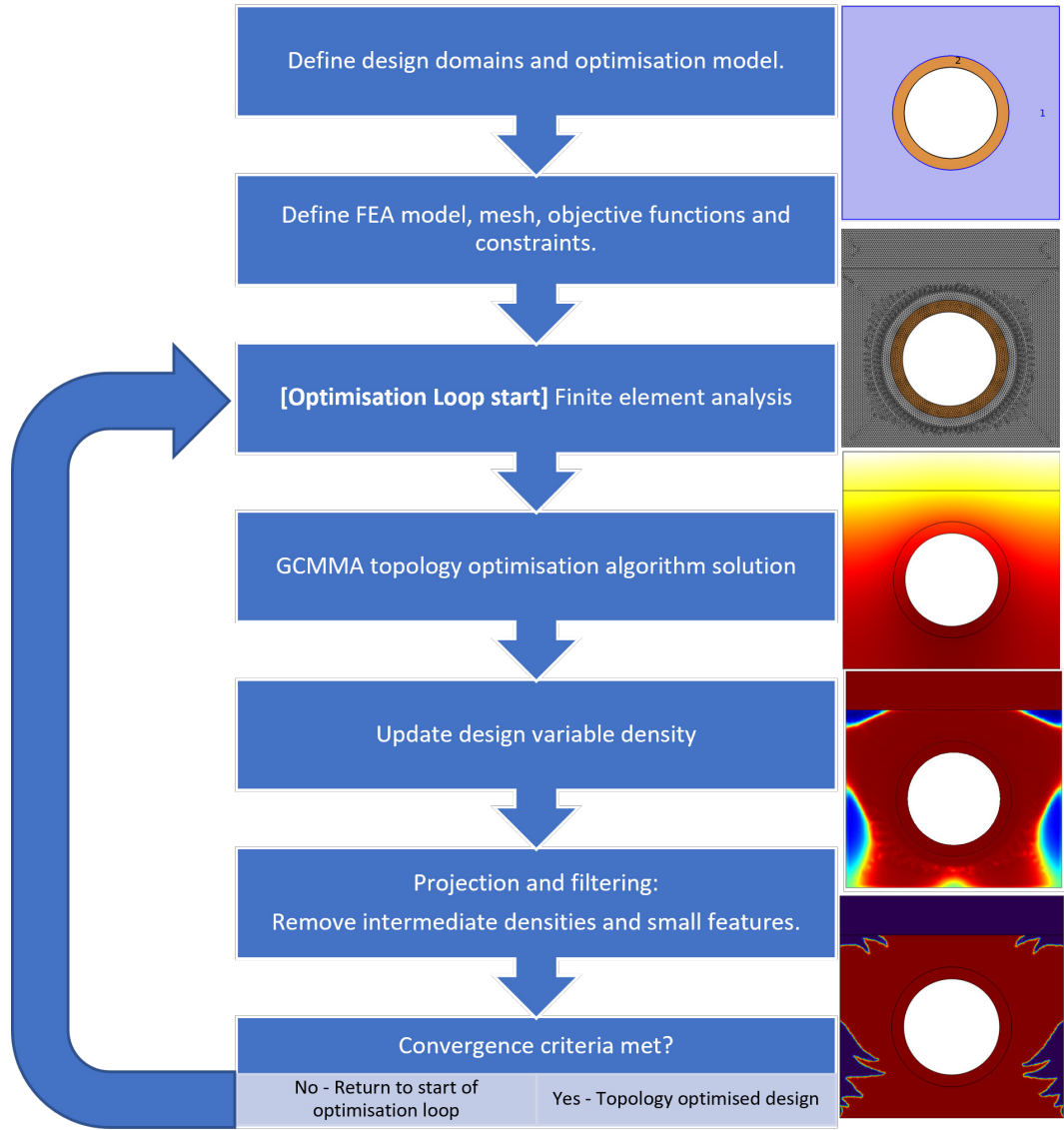


Figure 1.10. Simplified topology optimisation flow chart indicating some of the main steps in the topology optimisation process.

subscript ‘Cu’ refers to the variation of the property in copper and the subscript ‘W’ refers to its counterpart in W. More details regarding the implementation of suitable interpolation schemes, constraints and objectives are presented in Chapter 6.

$$k_p = (k_{Cu} - k_W)\Gamma_P + k_W \quad (1.11)$$

$$\rho_p = (\rho_{Cu} - \rho_W)\Gamma_P + \rho_W \quad (1.12)$$

$$C_p = (C_{p(Cu)} - C_{p(W)})\Gamma_P + C_{p(W)} \quad (1.13)$$

The use of Γ_p in Eqs. 1.11, 1.12 and 1.13 links the interpolation type (specified in the settings shown in Fig. 1.12) to these linked material properties. Once these parameters have been established, they must be specified in the relevant physics interface settings. For example, a variable containing the thermal conductivity interpolation must then be activated in the settings for the heat transfer interface. When performing multi-physics, multi-objective optimisation, as is required to capture thermally induced stress, it is important to ensure the

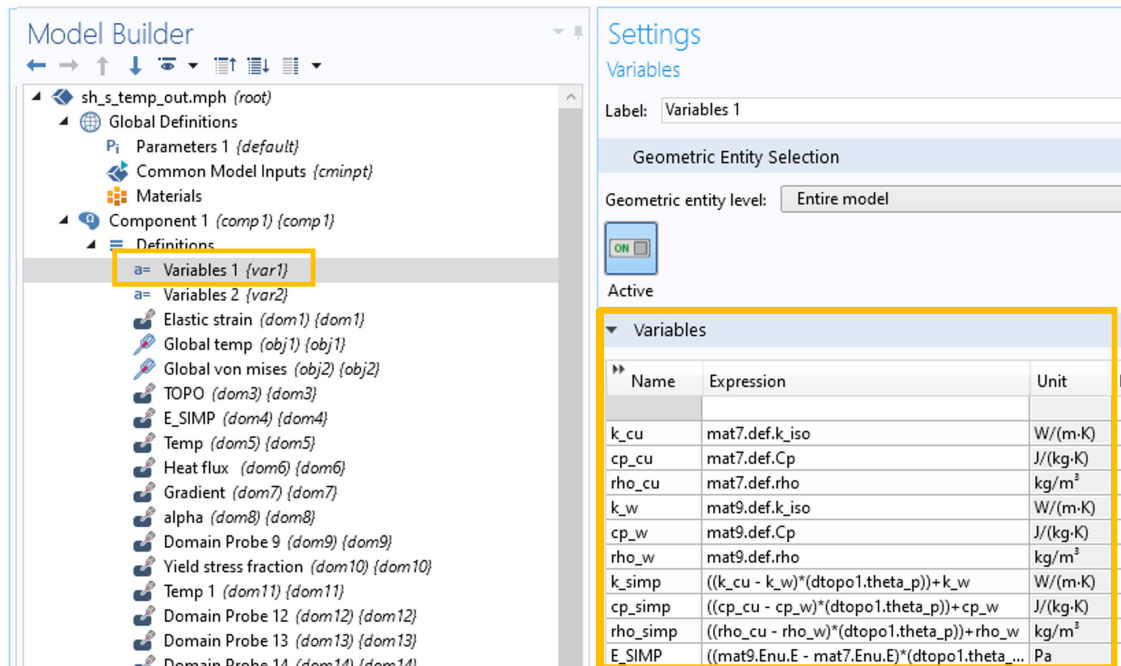


Figure 1.11. The variables utility can be used to define the material interpolation between specific parameters, and to parameterise material properties not easily available in the GUI.

relevant parameters are coupled and used consistently.

Fig. 1.12 shows the primary settings window for the specification of topology optimisation parameters. The decision regarding whether or not to use filtering and projection is problem-specific and dependent on the goal of the optimisation. Careful use of both can result in smoother, more manufacturable designs and can aid in the imposition of minimum feature size, however, they alter the optimisation problem and should therefore be approached with caution. The interpolation type can also be specified, with pre-defined options for SIMP, RAMP and Darcy interpolation available, as well as the possibility for user-defined interpolation. A discussion of the various merits of different interpolation schemes is presented in (Ramalingom, Cocquet, and Bastide 2018). The choice of design domain should also be approached with consideration of the tolerable level of design freedom and the design driving features. Constraints on the design can be applied such that they are satisfied by the average value across a domain, line or point, or such that they must be true for every element in a specific region, as is the case for the constraint shown in Fig. 1.13.

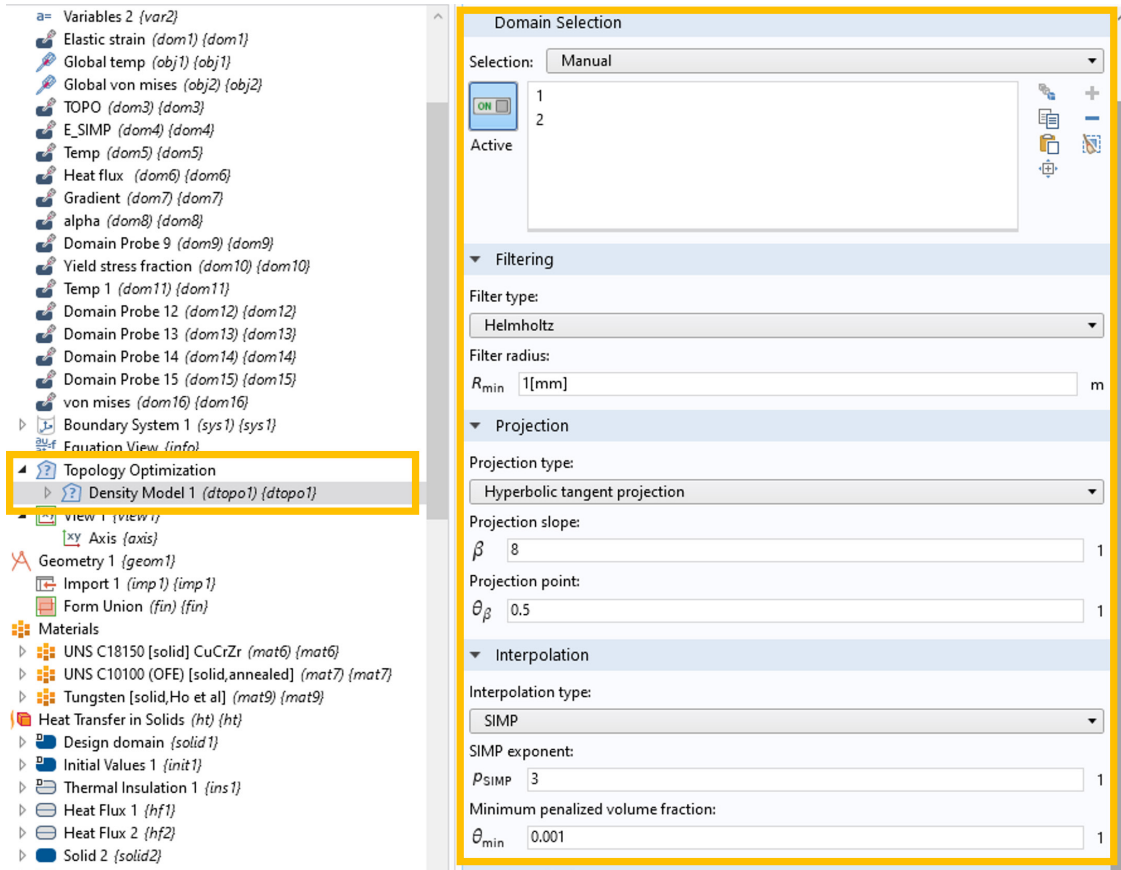


Figure 1.12. COMSOL topology optimisation settings. This interface allows the specification of settings relating to filtering, projection and interpolation. Furthermore, it is where the design domain (where topology optimisation is to be performed) is defined.

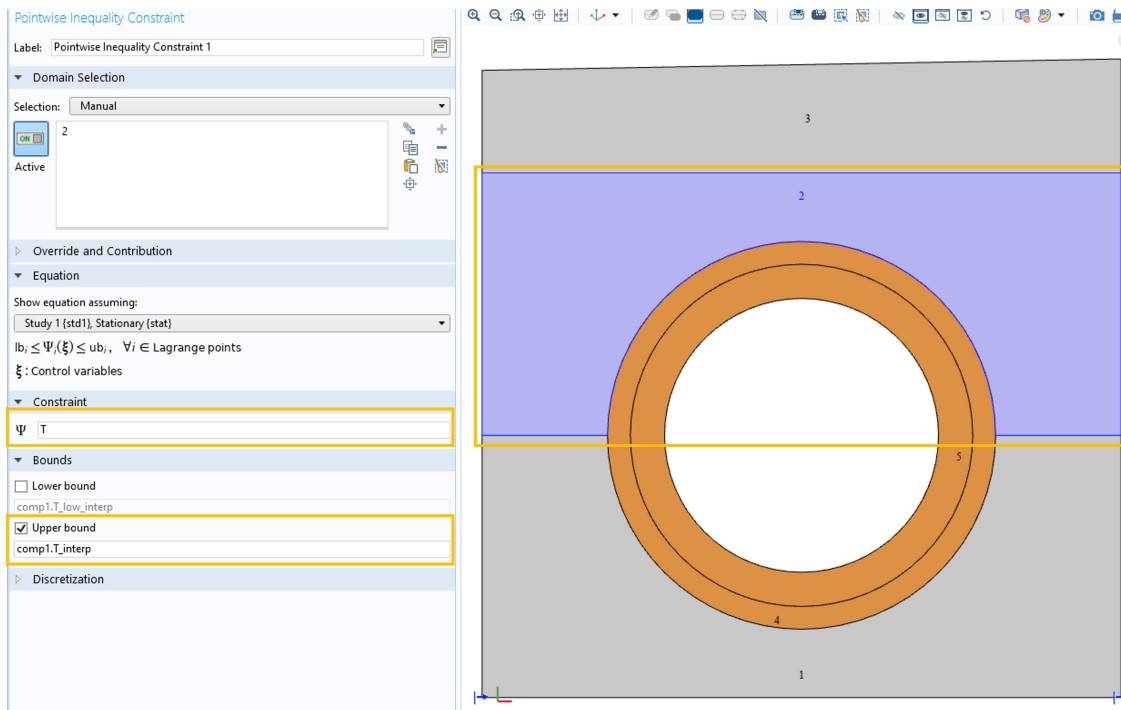


Figure 1.13. Screenshot showing the specification of a point-wise inequality constraint. This type of constraint must be true at all elements in the specified region and is therefore useful for the specification of material operational temperature limits.

Fig. 1.14 shows the settings pane for the topology optimisation algorithm, which can be used to define controls over convergence, objective functions and additional constraints. This is

typically where volume fraction constraints would be applied, however, constraints based on a domain probe can also be defined.

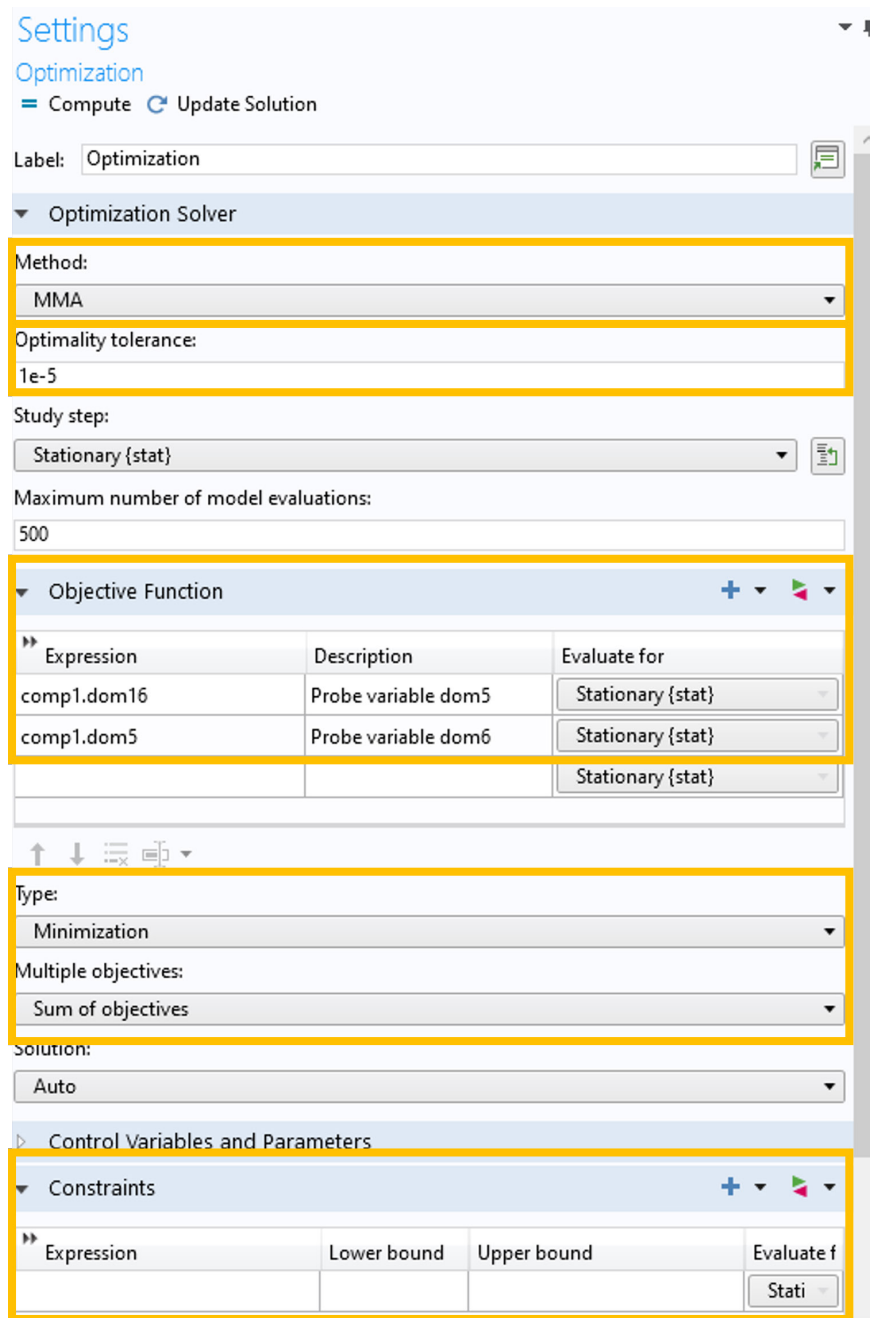


Figure 1.14. Topology optimisation algorithm settings, including the ability to specify the method and optimality tolerance (which controls the convergence criterion). Objective functions (defined using domain probes), the choice of minimisation or maximisation, the treatment of multiple objectives, and any additional constraints can also be defined here.

A key component of the fluid optimisation performed in Chapter 7 is the specification of a force which opposes flow, which can be implemented using a volume force in COMSOL as shown in Fig. 1.15. This is used to manage the transition between fluid and solid elements. In Chapter 7, this is described as a friction force \mathbf{f} , which is proportional to the fluid velocity (\mathbf{v}), and given by: $\mathbf{f} = -\alpha\mathbf{v}$, where $\alpha(\mathbf{r})$ is the inverse of the local permeability in the medium at position \mathbf{r} . As inverse permeability increases, the flow is restricted, with velocity tending to zero in ‘solid’ regions. The porous medium is described by the Darcy law $q = -\frac{k}{\mu}\Delta p$ where q is the instantaneous flow rate, k is the permeability, μ is the dynamic

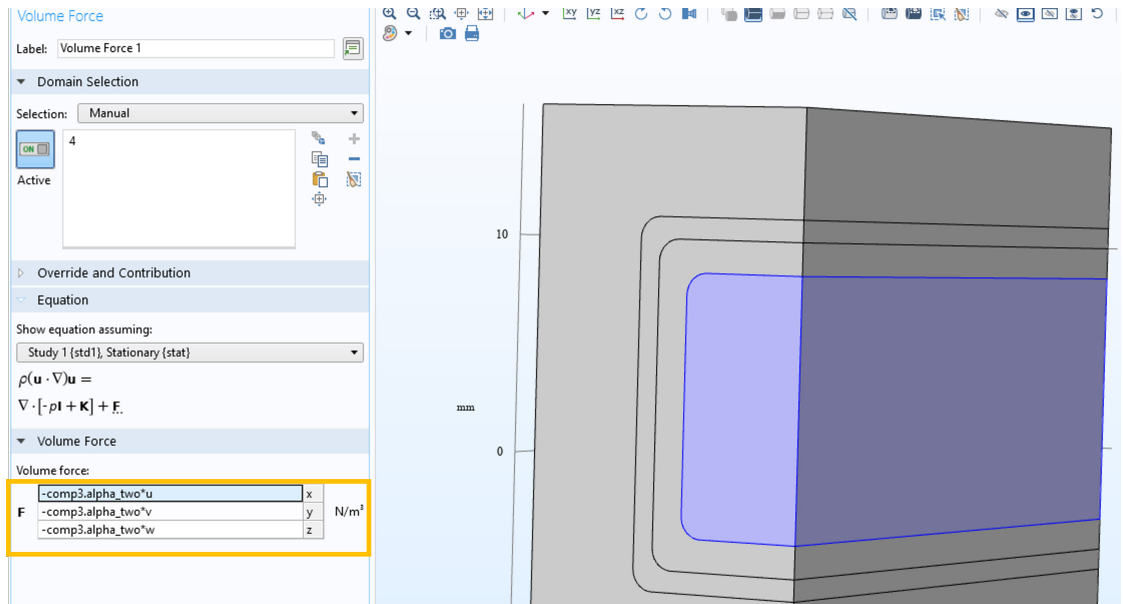


Figure 1.15. COMSOL GUI showing the application of a volume force to oppose flow and aid in the simulation of the transition from fluid to solid elements.

viscosity of the fluid and Δp is the pressure drop. The Darcy number (Da) represents the relative impact of the permeability of a medium over its cross-sectional area and is defined as $Da = \frac{k}{d^2}$ where d is the characteristic length.

If the topology optimisation GUI settings are insufficient for the physics required in the topology optimisation, the parameters used by the solver can be modified directly, as shown in Fig. 1.16. This can be used, for example, to modify the turbulence models in fluid topology optimisation problems, to ensure that turbulent parameters reduce to zero in solid domains and is implemented in Chapter 7.

Name	Expression	Unit	Description	Select
ht.cfluxMag	$\sqrt{ht.cfluxx^2 + ht.cfluxy^2 + ht.cfluxz^2}$	W/m ²	Convective heat flux...	Doma
ht.tfluxx	ht.dfluxx + ht.cfluxx	W/m ²	Total heat flux, x com...	Doma
ht.tfluxy	ht.dfluxy + ht.cfluxy	W/m ²	Total heat flux, y com...	Doma
ht.tfluxz	ht.dfluxz + ht.cfluxz	W/m ²	Total heat flux, z com...	Doma
ht.tfluxMag	$\sqrt{ht.tfluxx^2 + ht.tfluxy^2 + ht.tfluxz^2}$	W/m ²	Total heat flux magni...	Doma
ht.tefluxx	0	W/m ²	Total energy flux, x c...	Doma
ht.tefluxy	0	W/m ²	Total energy flux, y c...	Doma
ht.tefluxz	0	W/m ²	Total energy flux, z co...	Doma
ht.tefluxMag	$\sqrt{ht.tefluxx^2 + ht.tefluxy^2 + ht.tefluxz^2}$	W/m ²	Total energy flux mag...	Doma
ht.q0_u	0	W/m ²	Out-of-plane heat flu...	Doma
ht.q0_d	0	W/m ²	Out-of-plane heat flu...	Doma
ht.rflux_u	0	W/m ²	Radiative out-of-plan...	Doma
ht.rflux_d	0	W/m ²	Radiative out-of-plan...	Doma
ht.tflux_u	ht.q0_u + ht.rflux_u	W/m ²	Total out-of-plane he...	Doma
ht.tflux_d	ht.q0_d + ht.rflux_d	W/m ²	Total out-of-plane he...	Doma

Figure 1.16. The parameters used by the physics interface are exposed in the GUI and are directly modifiable, allowing for the definition of additional topology optimisation parameters.

1.10 Additive manufacturing and functional grading

Additive manufacturing (AM) takes the opposite approach to traditional subtractive manufacturing processes, which typically remove material to achieve the desired geometry. Instead, AM involves the use of a high-powered energy source to build components a single layer at a time from a base powder or wire. This technique allows for the creation of near-net designs directly from a virtual model and can increase design flexibility, allowing for the manufacture of complex geometries not previously possible. AM is an emerging industry, however, some application has already been made to tokamak high heat flux component design. In (Hancock, Tom Barrett, *et al.* 2015) and (Hancock, Homfray, *et al.* 2018), the application of AM to tile-based divertor designs incorporating tantalum as a structural material is explored. Functionally graded components are those with gradually varying spatial transitions between material properties which may be the result of structural differences (such as different levels of porosity) or differences in elemental composition. These components typically require advanced manufacturing techniques and functionally graded AM components have often been proposed (Loh *et al.* 2018). Functional grading of high heat flux components is also discussed in (R. E. Nygren *et al.* 2016), including the development of materials with layers of controlled porosity and features such as microfibrils or nanoparticles to capture transmutation products and limit tritium retention. Functionally graded components made possible by AM could allow smooth transitions between materials properties where needed, reducing some of the stress caused by differences in thermal expansion, as is common in divertor monoblocks between the W and the CuCrZr cooling pipe (Kato *et al.* 2018; Q. Li *et al.* 2019).

AM is not without challenges however, a recent assessment of AM (Tofail *et al.* 2018) identifies (among others) the following issues.

- AM fabrication machinery needs to be developed such that self-contained, robust, safe and user-friendly systems with appropriate build characteristics including power, scan motion, speed and energy are available.
- Parts often lack homogeneity in material properties and contain dimensional inaccuracies.
- AM components often need extensive surface treatment and finishing to resolve roughness and may still contain surface porosity.
- Several issues relating to metrology including providing adequate quality assurance, process optimisation, and diagnostic information that needs to be performed in real-time.
- Direct Metal Laser Sintering, an AM technique utilised to build the samples analysed in Chapter 3, is identified as relatively slow, with size limitations, a lack of structural integrity in the resulting parts, a high power requirement and a finish which is dependent on the precursor powder size.

Another review, (Loh *et al.* 2018), which focuses on functional graded AM (FGAM) components found the following challenges:

- AM parts frequently exhibit internal and external defects, including voids, areas of porosity, and unsintered material.
- Operational parameters are poorly understood and require manual fine-tuning for specific component builds.
- Most commercial AM focuses on single material builds, limiting the potential applications.
- Material characterisation is inadequate for FG-AM structures.
- There is a lack of predictability concerning the material phase and the transition in properties in built parts.

The resolution of these problems is not the focus of this thesis, however, they are mentioned here to illustrate the context around AM technology, which is undergoing significant growth in capability and commercial implementation (Tofail *et al.* 2018), with many seeing a potential for the development of high-performance metal parts (Herzog *et al.* 2016).

The functionally graded components proposed in (Curzadd *et al.* 2019), discussed in more detail in Section 1.8.1 rely on Cu infiltration of AM W components. This is one method for functional grading which doesn't fully rely on additive manufacturing. In the infiltration technique, Cu is drawn by capillary forces into the pores of a W skeleton structure, as described

in (J.-H. You *et al.* 2013). The development of stronger functionally graded interfaces which use Cu1CrZr instead of pure Cu as a monoblock interlayer to reduce thermally induced stress is explored in (J.-H. You *et al.* 2013). The study showed a linear dependence of coefficient of thermal expansion with CuCrZr content and a slightly better than linear relationship for yield stress with W content, attributed to the strength of the three-dimensionally networked W skeleton structure. Further characterisation of the material properties of functionally graded interfaces will enable better definition of interpolation schemes for topology-optimised components.

1.11 Summary of context and motivation

The goal of this thesis is to investigate the opportunity for applying a topology optimisation-focused design workflow to the fusion divertor, in the context of metal-based additive manufacturing techniques which permit the realisation of complex designs. It is envisaged that the ongoing development of these techniques may contribute to the development of fusion reactor components in one of two ways. Firstly, in line with the agile approach to fusion hardware development discussed in (Pearson *et al.* 2020), it could be used to rapidly generate prototypes with different performance characteristics for testing in a dedicated facility like IFMIF (a fusion test facility described in (Knaster *et al.* 2017)) or in a tokamak test facility that allows for easy exchange of components. Another approach involves application to the later stages of development in the linear approach to fusion commercialisation associated with the European fusion Roadmap described in (Romanelli *et al.* 2012). Development of a set of standardised concepts such as the monoblock could continue, in the knowledge that once the operating conditions and constraints present are known, techniques like topology optimisation could then be used to tailor the components to the needs of specific devices. This could be supported by advancements in techniques that target virtual qualification, such as Image Based Simulation (IBSIM) which uses techniques like X-ray tomography to scan real components for virtual analysis, as proposed in (Evans, Minniti, and Tom Barrett 2019). It should also be noted that additive manufacturing is not the primary focus of this thesis but an enabling technology. The focus is the potential of topology optimisation for application to component design and the identification of broader challenges and opportunities in fusion reactor design. This information is relevant to the consideration of material property interpolation for topology optimisation. Further research into the material properties of functionally graded materials will facilitate a more realistic generation of optimum geometries using topology optimisation.

1.12 Thesis structure

The thesis is presented in journal format as a series of papers. Papers 1 and 2 provide the fusion and manufacturing context for the topology optimisation presented in papers 3, 4 and 5. Paper 1 aims to demonstrate some of the design challenges associated with fusion reactors

and considers the impact of both reactor scale decisions and component-level performance results. It is postulated that because of the extreme challenge associated with designing components to survive fusion reactor conditions and the restrictions on design due to plant-level constraints and system integration issues, a design approach which is able to adapt to both upstream and downstream pressures is required. Paper 2 presents an investigation performed as part of a collaboration with an additive manufacturing company as part of a fusion CDT initiative to broaden the experience of PhD candidates and so the focus is somewhat different to the rest of the work. It is included as part of the thesis as it discusses optimisation of the build process for a fusion-relevant alloy - CuCrZr - which is present in the monoblocks which undergo topology optimisation in papers 3,4 and 5. Papers 1, 2 and 3, 4, 5 are separated by a chapter which includes a literature survey of topology optimisation focused on fluid and thermal problems and a software evaluation, performed in preparation for the topology optimisation work.

Paper 1 - A Review of Tokamak Divertor Design for Digital Engineering

This paper aims to illustrate the considerations required in the digital engineering design of plasma-facing components for the divertor. It details the constraints and design requirements, placed on the component, which occur on a range of different scales, from the device level to the component. The paper provides a high-level overview of the challenges in divertor design and is set in the context of motivation in the research community for integrated approaches to reactor modelling which combine simulation and experimental data. An example of this approach is the Integrated Nuclear Development Environment (INDE) presented in (E. A. Patterson *et al.* 2019) which aims to translate a hierarchical integration of experiment and simulation found to be successful in the aerospace industry to nuclear fusion. There is also a move towards greater design flexibility, as exemplified by the BLUEPRINT systems code presented in (Coleman and McIntosh 2019), which aims to facilitate evaluations of DEMO designs that differ more significantly from the baseline design by reducing development and testing time.

Paper 2 -Thermal Testing of Additively Manufactured CuCrZr Samples for Application to Nuclear Fusion

This section details a ‘Collaboratory Project’ undertaken as a required part of the Fusion CDT programme. Students were encouraged to seek collaborations outside of the normal scope of their project in order to develop research skills. Following approval of a proposal, a collaboration which included a placement with an additive manufacturing company - 3T AM - was undertaken. This consisted of working with engineers on process optimisation for CuCrZr material designed for high heat flux application. Subsequently, thermal testing of this material was performed at the University of Manchester. This testing consisted of Laser Flash Analysis (LFA) to establish the thermal diffusivity, which was calibrated using dilatometry in order to account for the effects of thermal expansion. LFA is based on the

measurement of the temperature rise on the rear face of a specimen in response to illumination of the opposing side by a laser pulse of known energy. Dilatometry measures the linear expansion of a sample of known length over a programmed temperature range. Thermal diffusivity (D) is then related to thermal conductivity (λ) through a known specific heat capacity (C_p), and mass density (ρ), as described in Eq. 1.14.

$$\lambda = DC_p\rho \quad (1.14)$$

The CuCrZr samples tested were part of ongoing work at 3T-AM to accelerate and optimise the build process. The change in the build parameters between samples produced measurable differences in the thermal properties, with the sample representing the fastest build process achieving the highest thermal diffusivity and the lowest coefficient of thermal expansion.

Topology optimisation literature survey and software evaluation

This chapter contains a review of the previous applications of topology optimisation to both thermal and fluid problems. Subsequently, a software evaluation process is presented which includes the evaluation of commercial and open-source software based on their availability, associated development time, and applicability to the modelling requirements. COMSOL Multiphysics is identified as the most promising candidate.

Paper 3 - Thermal Topology Optimisation of a Plasma Facing Component for use in Next-Generation Fusion Reactors

This paper is a proof of concept demonstration of thermal topology optimisation of the divertor monoblock. The paper was presented at the UKACM2021 virtual conference and is available online (see (O. H. R. Marshall *et al.* 2021)). Topology optimisation is applied to two different geometries, the first is based on a symmetric divertor monoblock design and the second introduces asymmetry through means of a bevel which is incorporated to reduce heat flux concentration caused by leading edges. A density-based topology optimisation method is implemented which uses the Solid Isotropic Material with Penalisation (SIMP) technique to ensure the formation of discrete material domains. The majority of the main armour block apart from the sacrificial armour layer is used as a design domain for topology optimisation. In the design domain, the thermal material properties are allowed to vary between those of W and Cu in order to meet an objective. Three objectives are investigated, with the first two based on the minimisation of thermal properties: temperature and thermal gradient, and the final one maximising conductive heat flux, for both flat and bevelled monoblocks. The resulting geometries are then subjected to transient heat fluxes representative of those expected in ITER.

Paper 4 - Multi-Objective Topology Optimisation of a Tungsten Divertor Monoblock,

with Consideration of Toroidal Beveling and Multiple Attachment Scenarios

This paper extends the established topology optimisation methodology to incorporate the simulation of thermally induced stress. Stress reduction is regarded as one of the most significant challenges to overcome with the divertor monoblock design. Thermally-induced stress is caused by the mismatch between the coefficients of thermal expansion (CTE) of W and CuCrZr, meaning that they expand at different rates in response to a temperature increase. This is compounded by the one-sided heat load and the concentration of heat flux around the circular cross-section coolant pipe. In addition to the flat and bevelled monoblocks already considered, the study is extended to investigate the consequences of modelling different attachment techniques present in the divertor monoblock design. Unlike in the previous paper, intermediate material properties are not penalised. This is done to allow the optimisation problem to create a smooth transition between material CTEs and permits physical interpretation through functional grading techniques. The impact of the differences in geometry and constraints is clearly evident in the optimised designs. Whilst the topology-optimised designs show significant reductions in von Mises stress and temperature, one of the main results of the paper is in demonstrating the sensitivity of optimal designs to loads and boundary conditions. This links to the findings of Chapter 2, where it is established that there is significant uncertainty remaining in divertor design requirements.

Paper 5 - Conjugate Topology Optimisation of Turbulent Flow for the Design of Novel Plasma Facing Component Geometries

This paper considers the extension of the topology optimisation technique to a monoblock coolant pipe. Material properties are allowed to vary between those representative of CuCrZr and H_2O in the fluid domain. The study uses a plasma-facing component geometry recently proposed in (Oh *et al.* 2021) as the basis for optimisation. This geometry is chosen for its high fluid volume and as the initial geometry likely requires additional manufacturing complexity. It is therefore identified as a good candidate for demonstrating the synergy between topology optimisation and AM, where the complexity of design is not always directly related to manufacturing costs. The topology optimisation investigates the influence of a number of thermal objectives on the design of internal features, performed with a maximum pressure drop constraint. The implementation of $k - \epsilon$ turbulence modelling in the computational fluid dynamics pushes the limits of the available computational resources but results in optimised geometries with internal features that promote convective heat transfer in the fluid.

Conclusions and further work

Chapter 8 summarises the work conducted, and details the potential for future work established by individual chapters.

Overall discussion

Chapter 9 presents an overall discussion of the project and a more general discussion of future work relating to the fields of plasma-facing component design and topology optimisation.

Appendix

This section includes a proposal selected as one of six finalists in the International Atomic Energy Association Net Zero Competition, which was held in preparation for the COP26 climate change conference (*IAEA Selects Winner of Net Zero Challenge on Policies for Clean Energy Transition 2021*). The competition called for policy proposals for the ‘clean energy transition’. The policy presented involved the establishment of a partnership between afforestation plans and the siting of Advanced Modular Reactors (AMRs) in order to improve public perception of nuclear power and accelerate the planting of trees in the UK. The submission progressed to the final round of judging, which occurred following a presentation on the margins of the 65th IAEA General Conference.

1.13 Statement of contributions

All work presented in the main body of the thesis was conducted by the author Oliver Marshall, apart from the Laser Flash Analysis (LFA) experimental work which was conducted by Andy Wallwork, Senior Experimental Officer in the Department of Materials at The University of Manchester. A subsequent analysis of LFA data was performed by Oliver Marshall. CuCrZr samples and initial build data were provided by 3T-AM. Appendix Section A.1 was prepared in collaboration with Angus Wylie, and Emre Yildirim, who at the time of writing were Fusion CDT PhD candidates at the University of Manchester.

Chapter 2

Paper 1 - A Review of Tokamak Divertor Design for Digital Engineering

A review of tokamak divertor design for digital engineering

Oliver H.R. Marshall^{1*}, Lee Margetts¹ and Mohammed Omer¹

¹ Department of Mechanical, Aerospace and Civil Engineering, George Begg Building, The University of Manchester, Manchester, United Kingdom

Abstract

A review of the digital engineering techniques employed when designing PFCs for the divertor, the region in the interior of a tokamak fusion reactor that receives the greatest heat flux. The goal of this review is to provide a high-level overview of divertor design including performance modelling and the associated interconnected series of requirements and constraints. Constraints on divertor design occur on many scales and include the impact of policies designed to limit environmental impact, the economics of fusion power, and performance constraints including the maximum allowable heat load. This is set in the context of the need to consider the long-term evolution of fusion reactor design towards a commercially viable power plant and the desire to incorporate emerging technologies. The first part considers a top-down approach, where decisions made on the reactor scale have knock-on impacts that manifest as requirements and constraints on divertor design. These power plant modelling studies also provide a perspective on the future of divertor design. The second part of the review describes a range of divertor component concepts, discusses performance modelling and mechanisms for failure.

2.1 Introduction

The design of a fusion reactor is a complex, interdependent problem, with a high degree of sensitivity to the project parameters and requirements. It is also a lengthy process, with design and construction often taking several decades to complete.

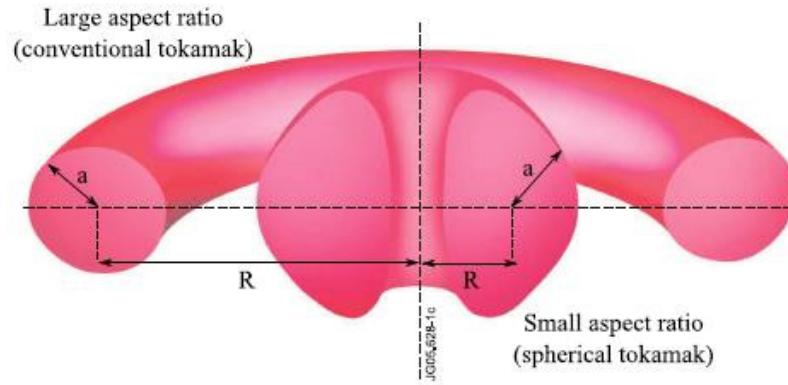


Figure 2.1. Illustration of the different plasma geometry in conventional versus spherical tokamaks. Reproduced from (Blagoev 2020)

2.1.1 Tokamaks

Tokamaks are the most widely studied type of fusion reactor and use magnetic confinement to sustain thermonuclear fusion in a plasma usually comprised of two hydrogen isotopes: deuterium and tritium. The machines confine the plasma in toroidal vacuum vessels and are categorised by the aspect ratio of the vessel: R/a where R is the major radius (measured from the central point of the torus to the centre of the toroidal vacuum vessel cylinder) and a the minor radius (the vacuum vessel radius). Fig. 2.1 illustrates the difference in plasma geometries. High aspect ratio devices, where the major radius is significantly greater than the minor radius are considered ‘conventional’ and are referred to simply as tokamaks. Low aspect ratio devices, however, are known as spherical tokamaks. To date, there are no commercially operating tokamak power plants and fusion power is currently limited to experimental devices, with operational parameters designed to investigate plasma physics, rather than all-out attempts at producing a power plant. This review focuses on the digital engineering techniques that contribute to the design of the divertor, which receives the highest heat flux of all the components, in the context of exploring the route between the current generation of devices and electricity-generating commercially relevant devices.

2.1.2 The divertor

The divertor is known as the tokamak ‘exhaust system’ but serves a number of purposes. Charged particles in the plasma are transported along magnetic field lines and eventually travel through the outer region known of the plasma known as the scrape-off layer. Whilst tokamaks use magnetic fields to confine the plasma, the confinement is not perfect, and charged particles migrate towards the walls of the device (Wesson 2011). The aim of the divertor is to move the point of contact for these charged particles outside of the last closed flux surface - outside the magnetically confined portion of the plasma - allowing for spent fuel and impurities to be removed. It also reduces the ease with which material generated from plasma-surface interactions (such as sputtering) is able to enter and pollute the plasma (Malizia *et al.* 2014). Maintaining the purity of the plasma is crucial for maintaining fusion conditions. For example, when the average atomic number Z of the plasma rises, Bremsstrahlung

radiation (which scales in power proportional to Z^2) will remove energy from the plasma, cooling it and making fusion harder to achieve. In the most widely used tokamak configuration, there is a single magnetic null and a divertor located on the bottom of the device, however designs with multiple divertors and advanced configurations do exist and are discussed later in this review.

2.1.3 Digital modelling techniques

Digital engineering design of the divertor interacts with development decisions made at multiple scales. The three levels targeted in this review are: stakeholder motivations (such as grid integration, environmental sustainability and regulation), conceptual reactor designs obtained using systems codes, and modelling of component performance.

2.1.4 A vision for comprehensive fusion reactor modelling

The ‘Integrated Nuclear Digital Environment’ (INDE) for fusion reactors proposed in (E. A. Patterson *et al.* 2019) is one vision for comprehensive fusion reactor modelling. This concept combines an array of digital and experimental data, inspired by the hierarchical structures used in the aviation industry in order to provide a framework for the design optimisation of fusion reactors prior to their construction. The goals of this framework are: to increase design freedom, decrease development time, exploit synergies with the fission industry and improve credibility, operability, reliability, and safety. The focus on credibility is somewhat unique to fusion reactor design, but is required due to unknowns in future device performance and requirements, the prevalence of one-of-a-kind devices and the large jumps in size and performance between devices. These factors all introduce uncertainty into modelling.

The lack of credibility in predictions has serious consequences for the design of components for future devices. The idea of credibility in engineering models is discussed in more detail in (E. Patterson 2015) where the lack of capability for comprehensive testing in fusion is emphasised. The recursive nature of design for fusion reactors, where for example changes to either the plasma or the divertor impacts the performance of the other, complicates the process further. The implication in (E. A. Patterson *et al.* 2019) is that the current state of fusion research leaves this component design over-constrained by regulation and design requirements, and under-defined due to uncertainties in the requirements of future devices. The INDE or any comprehensive equivalent is not yet a reality, however, and with current modelling technology and experimental data, it remains an ambitious goal. An illustration of the different scales at which divertor relevant decisions are made is presented in Fig. 2.2.

2.1.5 Structure

The review is split into two main parts. The first discusses the top-down approach to design, investigating the impact reactor-level design studies have on divertor design. The second

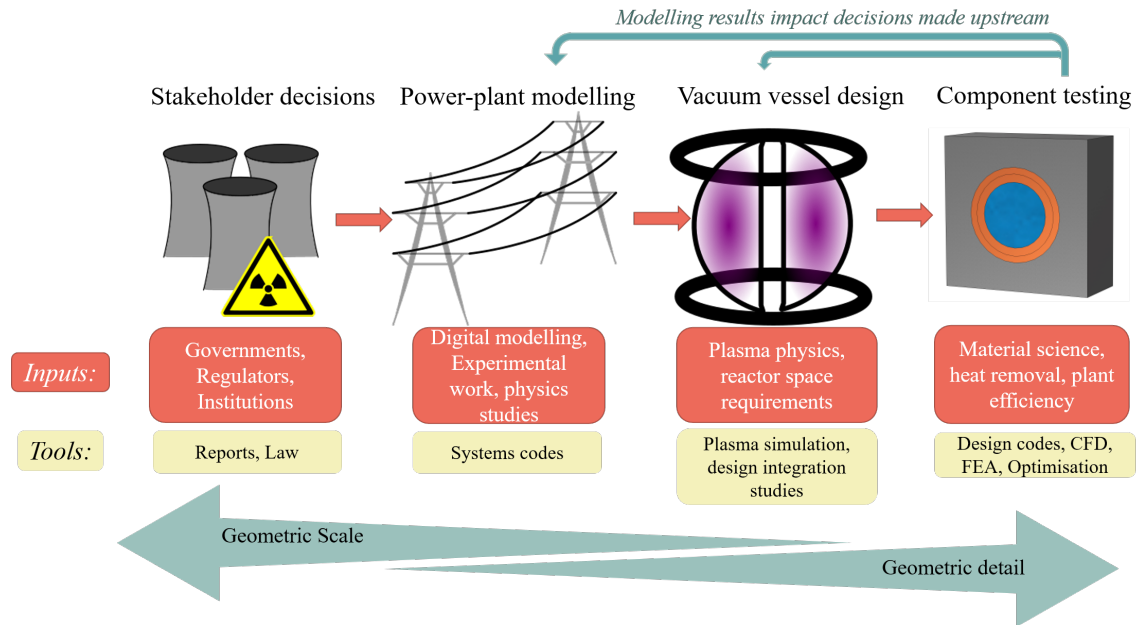


Figure 2.2. Simplified depiction of modelling on different scales in fusion reactor research. In divertor design, a lot of decisions which have a very significant impact on design are made at a high level.

part deals with component-focused modelling, and assesses how the characteristics of the Plasma Facing Components (PFCs) affect the design of the overall reactor. The scope does not include an in-depth discussion of the material science associated with PFCs, however, reference to the material science concepts and the impact of neutron damage is occasionally made. A brief outline of some of the external stakeholder decisions which impact divertor design is provided in Section 2.2. The top-down approach to modelling the divertor focuses specifically on reactor systems codes and is outlined in Section 2.3, with some commonly used codes outlined in Section 2.3.1. The impact of this approach on divertor geometry and specific devices is discussed in Sections 2.3.2 and 2.3.4 respectively. Design uncertainty is discussed in Section 2.3.5. Section 2.4 focuses on the design of the sub-components which make up the divertor. Section 2.4.2 describes divertor target design codes. Section 2.4.3 details the different armour concepts. Section 2.4.4 details the loading conditions which can lead to the damage described in Section 2.4.5. Section 2.4.6 introduces coolant fluid modelling. Section 2.4.9 describes the commonly employed coolant pipe geometries. Section 2.4.7 provides a brief overview of heat transfer modelling in divertor coolant fluids. Section 2.5 concludes the review.

2.1.6 The state of global fusion research

A significant proportion of the literature on digital modelling of the divertor is related to the development of ITER, which will be the world's largest tokamak when construction is finished. Fusion for Energy is the agency which organises the European Union's contribution to ITER and DEMO. F4E acts in accordance with the European Fusion Roadmap presented in (Romanelli *et al.* 2012). Whilst ITER is part of the European Fusion Roadmap, it is funded by a range of international collaborators including the USA, China, Japan, Russia, South Korea, India and the EU. Non-member participants include Canada, Thailand,

Kazakhstan and Australia (ITER 2021). A summary of some national and international fusion programmes including operational and proposed devices and an approximate timeline towards the realisation of commercial fusion energy is presented in Fig. 2.3. This figure is presented as a qualitative guide for the trajectory of fusion reactor development only. Due to the scale of international involvement, ITER is currently occupying a significant fraction of the world's fusion scientists. The plan is for ITER results to inform the next generation of DEMO devices. This global collaboration is the main reason why there are not currently many ITER-scale devices being developed. Whilst there is a European DEMO planned, the expectation is that many DEMO scale devices will be constructed using the shared knowledge acquired by the ITER members.

2.1.7 Previous reviews

As discussed in (E. A. Patterson *et al.* 2019), fusion research is device-led, with large gaps in between reactor size, capability and physics basis. This is reflected in the literature where substantial research effort is made tied to the development of a particular device. Where in other fields one might expect to find more general reviews, in fusion, reviews typically cover the progress made in the development of a particular device. The following papers were particularly useful in the preparation of this paper and related work and provide either overviews of large fusion projects or highly influential results with significant impact on fusion reactor design.

The European fusion programme

(Tomabechi 1991) provides an overview of ITER conceptual design activities. The estimates presented for the construction and cost of ITER here have proven to be too optimistic with a completion date of 2004 and a total cost of 4.9Bn US dollars. Furthermore, the remote maintenance of components, crucial to divertor operation in a tokamak operating DT plasma at high power, is assumed to have been resolved, however, this remains a challenge of considerable proportions (Damiani *et al.* 2018). An updated design review of ITER is provided in (Hawryluk *et al.* 2009), however, this still relies on the use of C divertor targets for initial operation, before installation of a full W divertor - a plan which was later rejected due to the associated cost, resulting in increased manufacturing requirements placed on the W divertor (Escourbiac *et al.* 2012). An overview of the Power Plant Conceptual Study (PPCS) - an attempt to conceptualise the pathway to a commercial tokamak power plant, with the aim of clarifying the goals for DEMO - is provided in (Marbach, Cook, and Maisonnier 2002) and updated in (D. Maisonnier *et al.* 2007). The PPCS study does however involve significant extrapolation of knowledge, particularly when considering longer-term solutions such as liquid-metal cooled components, which may prove infeasible.

A detailed overview of the DEMO design strategy and consequences for materials is discussed in (G. Federici, Biel, *et al.* 2017), of design progress in (G. Federici, Bachmann,

Barucca, Biel, *et al.* 2018), and the staged design approach in (G. Federici, Bachmann, Barucca, Baylard, *et al.* 2019). (G. Federici, Biel, *et al.* 2017) indicates that R&D of PFC heat sinks and structural materials that are resistant to radiation and the intense thermo-structural loading conditions are critical issues to the success of DEMO. It is stated that DEMO must learn from ITER's operation, however, it is also envisaged that construction of a near-term conservative DEMO reactor could begin in around 2036, which is approximately the same time ITER is due to start full-power DT operation (Windsor 2019). (G. Federici, Bachmann, Barucca, Biel, *et al.* 2018) acknowledges that the development of an electricity-producing DEMO by 2050 requires a change to EU fusion community culture including more modest extrapolations of physics and technology and targeted parallel R&D studies, in an admission of equivalent failures in the development of previous devices. The change in approach required is emphasised in (G. Federici, Bachmann, Barucca, Baylard, *et al.* 2019) where plans to evaluate high-risk solutions to the DEMO blanket are outlined, however, it remains to be seen whether this level of risk-tolerance is enacted in the programme.

(Bachmann *et al.* 2018) provides an overview of DEMO integration challenges with an emphasis placed on systems integration. Despite, this, it is acknowledged that whilst some of the materials used in divertor PFCs are prone to irradiation-induced swelling, it is also expected that individual divertor cassettes can be removed from ports using remote handling, with no discussion of possible ensuing difficulties. (Siccinio, Biel, *et al.* 2020) discusses DEMO physics challenges beyond ITER and indicates that the DEMO (and to an extent the ITER) plasma scenario is poorly understood, leading to difficulties in guaranteeing the safe termination of the plasma on PFCs after loss of control, within engineering limits. A long term European fusion 'roadmap' is discussed in (Romanelli *et al.* 2012), updated in (Nordlund 2018) and (Donné 2019). One of the increasingly well-documented flaws with the European fusion roadmap, is the idea that all reactor materials can be recycled into a new reactor 100 years after shutdown. (M. Gilbert *et al.* 2018) suggests that (depending on the choice of coolant), some components will need to be stored significantly longer before they can be recycled.

Other post-ITER devices

Progress on the design of a Japanese DEMO reactor is presented in (Tobita, Asakura, *et al.* 2017). The paper recognises the many challenges that remain in the design of a DEMO reactor. This includes plans to operate at a lower 1.5GW fusion power DEMO (reduced from 3.0GW in earlier designs) for which a feasible divertor power handling design exists, with plans to design a higher power reactor at a later date. An overview of activities relating to the Chinese CFETR reactor is provided in (Wan *et al.* 2017). CFETR plans also include a two-stage approach, with operational fusion power set to increase from 200MW to over 1GW. However, given the plan to begin operation in the 2030s, this may prove to be too ambitious given the plan to use ITER operational data.

Component development

(K J Dietz *et al.* 1995a) and (K. J. Dietz *et al.* 1995b), published halfway through the ITER engineering design process describe the physics and engineering basis for the ITER divertor before the concept was finalised. The analysis presented in (K. J. Dietz *et al.* 1995b) however uses lower divertor heat loads than have since been established. (Smid *et al.* 1997) presents a comparison between different hydraulic tube concepts, (C B Baxi and Wong 2000), reviews He cooling, as does (Hermesmeyer and Kleefeldt 2001). (Ferrari *et al.* 2001) provides a review of conceptual divertor designs for a fusion power plant and envisages designs tolerating maximum heat fluxes of only $5\text{-}7\text{MW m}^{-2}$. Divertor conceptual designs are reviewed in (Prachai Norajitra, Said I. Abdel-Khalik, *et al.* 2008). US work on He divertor concepts is presented in (M. S. Tillack *et al.* 2011), where the uncertainty in transient event severity is seen as a hindrance to design. The potential of water-cooled concepts as candidates for DEMO are discussed in (Li-Puma *et al.* 2013). (Jeong-Ha You 2015) compares two divertor concepts (one He-cooled and another water-cooled) and discusses the impact of the baseline materials choices on the mechanical performance of the concepts, including the evolution of this performance with radiation. The review concludes that the top-down structural design requirements are not compatible with the performance of the chosen baseline materials and a different design approach, open to the use of novel materials is required. This interaction between top-down constraints and performance-based modelling is discussed further in the proceeding sections.

(Mazul 2016) discusses the merits of alternatives to the ITER divertor design concept, however, finds critical issues with all the proposed designs. (Thomas R. Barrett *et al.* 2016) looks at the progress made in the engineering of the DEMO divertor and first wall PFCs, finding that full analysis of failure modes requires further development of elasto-plastic analysis codes and a more complete understanding of material behaviour under irradiation.

The engineering risks associated with the advanced divertor configurations are discussed in (Kembleton, G. Federici, *et al.* 2019), where it is acknowledged that the ITER divertor solution will likely not be appropriate for DEMO. It is also accepted that many of the proposed replacements are less well understood and may result in integration challenges that propagate through the design process resulting in significant delays.

Heat transfer and thermal-hydraulics

(Linke *et al.* 2019) presents an overview of the challenges presented to the development of PFCs. The review covers a wide range of stationary and transient loads including thermal transfer in solid armour tiles, ion and neutron bombardment. This review is of particular interest as it does not focus solely on W but discusses carbon fibre composite (CFC) tiles, noting their greater heat load tolerance 25MW m^{-2} (compared to "20MW m⁻²" for W) and drawbacks relating to tritium retention. Loading conditions which combine plasma neutron and thermal loads to study synergistic effects are seen as necessary to properly

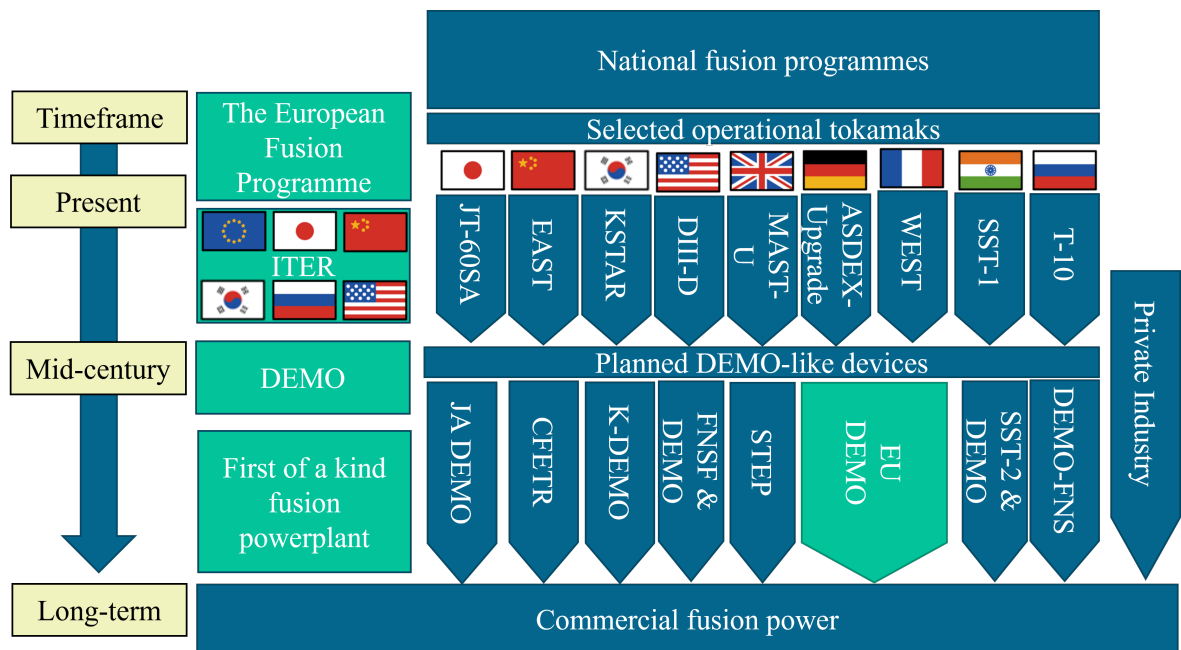


Figure 2.3. Speculative timeline for planned fusion development including a selection of national devices and programmes.

understand the behaviour of components in tokamaks. However, the current lack of fusion-relevant (14.1MeV) neutron sources for component testing is identified as a major challenge to performance validation.

(C. Baxi 2001) reviews the thermal hydraulics of water-cooled divertors, finding that well-optimised thermal-hydraulic systems not only require less pumping power but improve cooling performance and extend the life of components. This work presents the design basis used in the ITER divertor, including an assessment of Critical Heat Flux (CHF) correlations. (Yoda and S. I. Abdel-Khalik 2017) discusses the thermal hydraulics of He-cooled divertors. The experimental data used to assess one of He cooled designs reviewed in the paper was extrapolated to fusion-relevant conditions, and it is indicated that recent anomalous results may limit the validity of this data. This indicates the presence of a problem which is discussed further throughout this review. The use of one coolant over another often results in a choice between water, which is well-studied and has well-described behaviour and limitations and another ‘exotic’ choice. These coolants are typically He or liquid metal, about which there is promising initial data but for which there are unknown challenges. This is particularly problematic in fusion as the long time frame for device construction and operation makes it difficult to integrate higher-risk technologies without potentially compromising reactor operation for several decades.

2.2 Stakeholder decisions

Many of the decisions which have a significant impact on the design of the divertor are made by politicians, regulators and those not directly involved in the construction of the devices. The low activation criterion associated with the EU fusion programme, for example, requires that fusion reactor components must be disposable in landfill sites not specifically designed

for active waste 100 years after use in a reactor (El-Guebaly 2007). Whilst this might seem like a simple condition, it has far-reaching consequences, affecting the material choices for both structural and PFCs, including the divertor. As discussed in (Nicholas *et al.* 2021), recent modelling suggests that fusion reactors will produce more intermediate-level waste - which requires geological disposal under current UK law - than fission for equivalent power production. If similar activation criteria are enforced, components like the divertor may require significant re-design, causing delays to fusion commercial viability and harm to its eventual competitiveness. A full analysis of the impact of this criterion on materials is outside the scope of this review, however, a critical assessment of the impact on the development of suitable steels can be found in (M. J. Gorley 2015). The preparation of the safety case for DEMO, designed to satisfy a nuclear regulator is investigated in (Taylor, Ciattaglia, Boyer, *et al.* 2017) and (Taylor, Ciattaglia, Coombs, *et al.* 2019) where it is hoped the tritium retained by the divertor can be kept at ITER levels due primarily to higher operating temperatures which allow for tritium removal.

2.2.1 Tokamak accident scenarios involving the divertor

Fusion reactors are widely considered to be safer to operate than fission reactors in concept, with most off-normal plasma events resulting in plasma shut-down rather than a runaway nuclear reaction. An in-depth look at the safety case for fusion reactors can be found in (J. Raeder 1995), and the more recent (Gulden, Raeder, and Cook 2000) and (Flanagan *et al.* 2010), which focus on potential for radiation leaks if the ITER tokamak cooling water system fails. (Malizia *et al.* 2014) finds that in the case of vacuum vessel failure, the divertor must be designed in a way that mitigates the impact of unexpected plasma behaviour but also such that the risks associated with its own failure are minimised. (Rivas *et al.* 2016) finds that transient heat fluxes associated with a loss of plasma control risk causing severe melting in the divertor. It is suggested that the recovery time for the plasma control system must be an order of magnitude lower than the confinement time to protect the divertor.

In a Loss of Coolant Accident (LOCA) in a water-cooled device, the interaction between steam and W dust in the divertor has been identified as a risk for hydrogen production and subsequent explosion (D'Onorio *et al.* 2020). It is argued that in a He-cooled device, a much larger coolant storage option is required in the case of a LOCA as the gas cannot readily be condensed. This is likely to increase the cost of the device, changing the economic prospects as well as the safety case. The release of tritium dust in accident scenarios is discussed in (Mazzini, Kaliatka, and Porfiri 2019), which also considers the divertor as a potential source of a LOCA in the case of a large rupture.

The formation of a fusion-specific Generic Site Safety Report (GSSR) study is detailed in (Porfiri *et al.* 2020), where reliability and the need to minimise reactor complexity are highlighted as integral to the safety case. This represents one of the criteria against which the performance improvements associated with advanced divertor geometries will likely have to be measured. The safety case for a reactor goes beyond the operational phase and includes

safe decommissioning and disposal of waste. (Porfiri *et al.* 2020) finds that activation of waste is particularly dependent on the presence of materials like Cu in the divertor, which are strongly activated by neutron radiation and influenced by the coolant used for the first wall. Here the influence on divertor design is indirect, as often the use of a single coolant fluid is preferred for both the divertor and first wall. In (M. Gilbert *et al.* 2018) it is found that a water-cooled DEMO design becomes predominantly low-level waste after 100-300 years whereas He cooling resulted in intermediate-level waste beyond 1000 years. A recent UK government publication as part of a consultation (see (Secretary of State for Business 2021)) on the regulation of fusion reactors, confirms that the main divertor-relevant focus of regulators is likely to be on the handling of tritium, activated in-vessel components that are replaced during operation and in decommissioning the plant after closure. However, due to the immaturity of the field, the true impact of the requirements imposed by national regulators on fusion reactors, and more specifically divertor design, remains to be determined.

2.3 The top-down approach to modelling the divertor

The next section discusses a top-down approach to divertor design, based largely on the results from reactor systems codes. Systems codes typically take design requirements and (experimental) performance data as inputs and form a self-consistent reactor design. Due to their broad scope, these codes are typically based on simplified models for individual systems and aim to produce a self-consistent result which encompasses all of the reactor requirements, often including high-level economic constraints and environmental policies. System codes typically use optimisation algorithms to balance high and low-level constraints, (Hartmann 2013) however, some of this balance is subjective and subject to variation based on the wider context of the study. Decisions regarding the planning of future power plants, the direction of experimental programs and the outlook of the fusion community are made using these codes and as such they can have significant influence over divertor design. The results can also provide insight into the pressures placed on the divertor in current devices.

2.3.1 Commonly used systems codes

The following systems codes were found to be used frequently in the literature. They feature different levels of detail regarding modelling of the divertor. The divertor is commonly viewed as a design driving component, as discussed in (G. Federici, Giruzzi, *et al.* 2013), where uncertainty in divertor heat load modelling leads to conservative employment of protection techniques that increase the size and cost of the device. The treatment of the divertor in different systems codes will therefore influence their prediction of device operation and the specification of optimal designs.

PROCESS

PROCESS is a reactor systems code used widely in fusion reactor design. Descriptions of the physics and engineering implementation can be found in (Kovari, R. Kemp, *et al.* 2014) and (Kovari, Fox, *et al.* 2016) respectively. It optimises fusion reactor parameters based on a figure of merit chosen by the user and includes reactor physics, electricity production, buildings, cost and limited plasma physics simulation capabilities. Regarding the divertor, it is possible to specify whether or not the divertor coolant is used as a primary heat source for the production of electricity. This is important to the overall efficiency of the plant. Power deposition on the divertor surface is calculated using neutron and secondary particle transport calculations. The deposition of pumping power in the (water or He) coolant, is based on preliminary values derived from calculations for a European DEMO reactor. The first wall however is modelled as a series of parallel pipes, and functionality for different divertor geometries is therefore limited. In (Wenninger, Kembleton, *et al.* 2017), the continuous improvement of generalised systems codes such as PROCESS through comparison with more specialised modelling techniques is highlighted. The parameters used in the code include design requirements, geometric constraints, operating conditions and physics parameters, many of which can have a direct impact on divertor design.

SYCOMORE

SYCOMORE is a modular systems code developed by CEA in France in order to meet the requirements of DEMO (Reux, Di Gallo, *et al.* 2015). The divertor and edge modules do not account for divertor erosion or multiple-null configurations but use a two-point divertor transport model to obtain parameters including target temperature and maximum heat flux on the inner/outer targets. The divertor module can be configured with either He or water cooling (Reux, Kahn, *et al.* 2018).

BLUEPRINT

BLUEPRINT, a systems code described in (Coleman and McIntosh 2019) aims to provide an alternative methodology to that used in PROCESS, reducing the time it takes to create 3D representations of optimised reactors with the goal of increasing the diversity of reactor types studied. This is done by decreasing the development time associated with designs that deviate from a baseline configuration. It is argued that traditional systems codes like PROCESS limit the exploration of EU-DEMO design space and that only 5-10% of studies are being conducted into designs which differ significantly from the EU-DEMO baseline due to the time cost involved. (Coleman and McIntosh 2019) claims a four order of magnitude speed increase for DEMO design activities.

HELIOS

HELIOS, developed by CEA in France and described in (Jean 2011) has been used to study ITER, DEMO, the PPCS, and in relation to other devices including the JT60-SA tokamak. Whilst HELIOS is fundamentally a 0-D code (like PROCESS), it places increased emphasis on plasma shape precision, numerical efficiency, precision in plasma density and temperature profiles. An ITER design review, described in (Hawryluk *et al.* 2009) presents the usage of HELIOS to investigate ITER sensitivity to changes in machine parameters.

ARIES Systems Code

The ARIES Systems Code (ASC) (Dragojlovic, Kessel, *et al.* 2009), is developed as part of the Advanced Reactor Innovation and Evaluation Study (AIRES) in the United States. It has a modular structure consisting of physics, engineering and costing and also aims to explore a broad design space instead of variations on a baseline design. The code is designed to model a ‘tenth of a kind’ commercial fusion power plant with a high aspect ratio (above 3) (Dragojlovic, A Rene Raffray, *et al.* 2010). In one example of the impact on the divertor, designs which do not meet the required heat flux constraint are filtered out in ASC, from over 2 million plasma scenarios, 6811 were found to be compatible with a divertor heat flux limit of 12MW m^{-2} and 2337 with a limit of 5MW m^{-2} , indicating a strong design-driving relationship (Carlson *et al.* 2011). (Carlson *et al.* 2011) also recommends a divertor heat flux limit of $5 - 8\text{MW m}^{-2}$, based on material considerations.

TREND

TREND (Tokamak Reactor Code for the Evaluation of Next-step Devices) is developed by IPP in Germany and is based on physics design guidelines for DEMO including a 5MW m^{-2} heat flux limit (Hartmann 2013). It uses a simple divertor model based on the one implemented in ASC, chosen due to results suggesting that the predictive capabilities for divertor modelling in HELIAS and PROCESS are limited with little chance of improvement in the near term.

TPC

Developed in Japan, the TPC systems code is detailed in (Fujieda, Murakami, and Masayoshi 1992) (in Japanese). A study benchmarking TPC and PROCESS (Kemp, Nakamura, *et al.* 2012), indicates that the divertor heat flux limit has a significant impact on the resulting device optimisation. Compared to PROCESS, which takes a flexible set of inputs and constraints and will only converge to a solution if reasonable initial values are chosen, TPC requires a fixed set of inputs and outputs and will produce a solution which may or may not satisfy technology limits. (Kemp, Nakamura, *et al.* 2012) details disagreement between PROCESS and TPC regarding impurity radiation, which is particularly relevant to the calculation

of DEMO divertor heat loads. One contributing factor to the disagreement is the lack of experimental data with which to calibrate the models.

FUSAC

FUSAC, also developed in Japan, is a systems code aimed at modelling tokamaks capable of generating net electric power (Hiwatari *et al.* 2004). It is formed of three parts: a plasma physics module (based on ITER physics design guidelines), an engineering design program and an economic analysis model. More details on the development of an integrated modelling system which links FUSAC to engineering analysis codes can be found in (NAKAMURA *et al.* 2009).

Systems codes typically rely on dimensionally reduced models for parameters such as divertor heat load. It is therefore important that in the design process, these codes are used responsibly and iteratively in order to best capture realistic divertor conditions. There are several techniques used in reactor design, however, that can reduce the loads the divertor is required to tolerate, as discussed in the following section.

2.3.2 Divertor geometry and protection

This section focuses on a number of approaches to divertor protection and modifications to divertor position and geometry which bridge the gap between plasma physics considerations and divertor target engineering. These techniques typically involve protecting the divertor through a combination of modifying its overall geometry and position, or through creating a buffer layer of gas to disperse the incoming heat load. Both techniques have trade-offs and may lead to additional expense, more difficult maintenance, poorer plasma performance, among a number of other factors. A review of the impact of different 2D divertor geometries on the plasma can be found in (Alberto Loarte 2001). Divertor geometry was found to interact with a number of parameters including local energy diffusion, whether detached operation (a form of gas shielding) can be maintained efficiently, the recycling of impurities, plasma flows and plasma pressure. These upstream considerations must be balanced against the operational performance limits discussed later in this review.

Divertor protection techniques

One technique for divertor protection is known as flux expansion, where the divertor target is placed at a glancing angle to the incident plasma exhaust in order to maximise the surface area over which the heat load is deposited. This technique is due to be used in ITER (Campbell *et al.* 2019). Another technique employed for divertor protection is the use of gas pumping in the vicinity of the divertor to encourage the absorption and uniform re-radiation of the energy contained within the plasma before it reaches the target plates. This process allows the divertor to operate in a ‘detached’ configuration and reduced the incident heat flux

to the PFCs. (Siccinio, G. Federici, *et al.* 2019) presents a simplified model for assessing the maximum DEMO radius and magnetic field above which sufficient divertor protection cannot be guaranteed. (I. T. Chapman and A. W. Morris 2019) states that the current understanding of divertor detachment, including the movement of the detached plasma is inadequate, however, the upgraded spherical tokamak MAST-U aims to improve understanding. (Siccinio, Biel, *et al.* 2020) finds that ITER techniques for managing instabilities are not fully applicable to DEMO, and that because of the potential for damage to PFCs, and a lack of characterisation, a certain frequency of disruption events must be expected and tolerated by the divertor. Typically, plasma disruptions result in damage to the PFC surface through melting and cracking (Jeong-Ha You 2015). Sweeping the power load over the divertor targets to reduce the steady-state heat load is also considered necessary and is discussed in relation to EU DEMO in a number of publications, including (Bachmann *et al.* 2018; G. Federici, Bachmann, Barucca, Baylard, *et al.* 2019; Maviglia *et al.* 2016; Siccinio, Biel, *et al.* 2020; Siccinio, G. Federici, *et al.* 2019).

Divertor protection in systems codes

Systems codes treat divertor protection in a number of different ways. TREND specifies increasing machine size and power radiation from the plasma as the two main methods for facilitating divertor protection (Hartmann 2013). (Wenninger, Kembleton, *et al.* 2017) discusses PROCESS results which suggest that a significant fraction of power must be re-radiated by seeded impurities before reaching the DEMO divertor to stay within the material heat load limit of 10MW m^{-2} . However, it is argued that these impurities pollute the plasma and may reduce fusion power, possibly driving an increased device size. The creators of BLUEPRINT argue that the development of models which rely on advanced divertor configurations are more achievable in their code compared to PROCESS due to the lower time cost associated with exploring off-baseline designs (Coleman and McIntosh 2019). Challenges for the EU-DEMO divertor are discussed in (Siccinio, Biel, *et al.* 2020), which includes results from a PROCESS simulation and highlights the need to protect the PFCs in the case of loss of plasma control.

Influence on divertor design

Advances to the physics basis for European DEMO design discussed in (Wenninger, Arbeiter, *et al.* 2015) suggest that because of the perceived need to radiate a significant fraction of power before incidence on the divertor, the total divertor power must be limited to 30MW. It is also suggested that a good compromise between divertor protection and loss of fusion power is currently difficult to achieve, with the development of an economically optimal solution identified as a key issue to the DEMO conceptual design. The DEMO first wall armour thickness in (Siccinio, G. Federici, *et al.* 2019) is limited to approximately 3mm in order to accommodate tritium breeding. This makes it less robust than the ITER wall, and therefore novel strategies are required for the protection of PFCs and divertor power

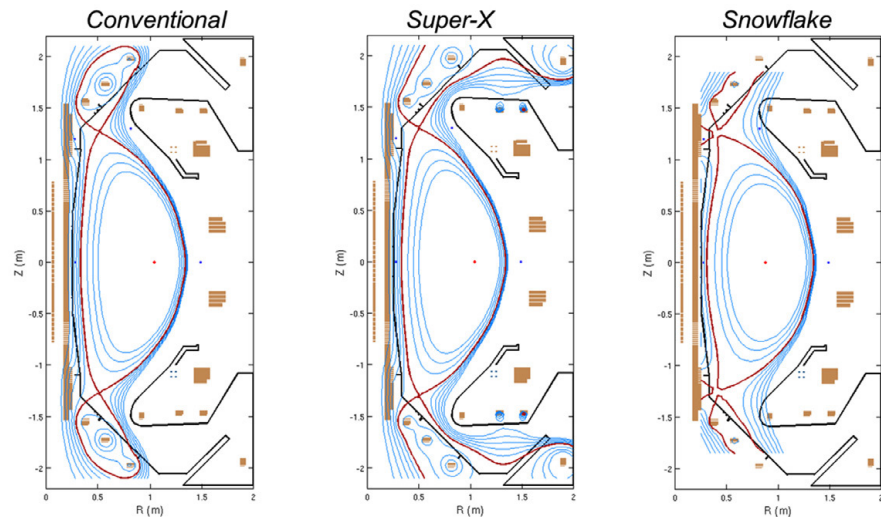


Figure 2.4. Cross-sections of internal tokamak geometry representative of a spherical tokamak showing the geometric differences in strike points: the regions where the magnetic field geometry (shown in blue) interacts with the PFCs. Reproduced from (I. Chapman *et al.* 2015).

management. It is indicated that in the case of an emergency shut-down, plasma reattachment would cause the coolant to exceed the CHF after only 3 seconds, and could only be delayed by tens of seconds with common techniques such as divertor sweeping.

PROCESS and SYCOMORE results in (G. Federici, Bachmann, Barucca, Biel, *et al.* 2018) lead to the assessment of adequate divertor protection as one of the ‘three overarching criteria’ used in the early design phase used to set the minimum reactor size. A number of alternate divertor configurations for EU DEMO including the snowflake and double null are discussed, however, only modest extrapolations are currently being made from ITER technology to minimise integration risks. A related paper (G. Federici, Bachmann, Barucca, Baylard, *et al.* 2019) investigates minimum EU-DEMO size and establishes that divertor protection is key to further size reduction, where a single ELM event can be sufficient to melt the divertor target W surface. It is argued that the divertor must be able to withstand accidental re-attachment, likely contributing to the size and cost of the component. (Maviglia *et al.* 2016) investigates divertor sweeping for DEMO and finds a $4\times$ reduction of heat transfer to the coolant is possible for heat loads of $15 - 30\text{MW m}^{-2}$. Additionally, divertor armour thicknesses of up to 10mm are found to extend the time before coolant CHF is reached, which is considered more severe than the possibility of armour surface melting. The uncertainty surrounding divertor heat loads and other factors such as the difficulty of inspection means that components in EU-DEMO are currently not expected to fulfil a safety function as their integrity cannot be guaranteed (Bachmann *et al.* 2018).

2.3.3 Advanced divertor configurations

Advanced configurations change the geometry of the divertor and either move the strike point away from the main plasma to maximise the wetted area (and reduce heat flux concentration) or add magnetic null points, which allow the heat load to be spread across additional targets and facilitate additional control over factors such as radiative power management. Fig. 2.4

illustrates the geometric differences between a conventional (spherical tokamak) divertor geometry and the proposed super-X and snowflake concepts. Advanced divertor geometries such as the snowflake have been tested in the TCV tokamak (Donné 2019), DIII-D and NSTX (Buttery *et al.* 2019), where they have been found to be effective at distributing heat flux over a larger surface area. The super-X design is discussed in (Muldrew *et al.* 2020) in relation to PROCESS studies of spherical tokamaks, where modelling is seen as unreliable until the geometry can be verified experimentally.

In DEMO reactors

An investigation of double null configurations for DEMO in (Pearce *et al.* 2019) using PROCESS finds attractive performance benefits to divertor protection and electrical power generation, which come at the cost of higher plasma control requirements. Advanced divertor configurations are modelled and discussed in (Tobita, Gianfranco Federici, and Okano 2014) where it is argued that at the time of publication, divertor simulation codes have not been adequately verified by experiment and that this is not likely to change until a DEMO scale reactor is built. The choice of divertor target plate for DEMO is questioned as it is suggested that whilst water-cooled W/Cu is preferred by the EU as a conservative approach, this setup is not resistant to the higher radiation damage expected in DEMO, and a Reduced Activation Ferritic Martensitic (RAFMs) pipe alternative can only remove 5MW m^{-2} heat flux. It is further cautioned that for any advanced divertor configuration proposed to overcome these obstacles, the choice of remote maintenance scheme must be carefully evaluated as a larger volume of components will need to be replaced more often in DEMO than ITER.

The DEMO ‘broader approach’ is a name given to the collaboration between the EU and Japan aimed at making progress towards resolving key DEMO design issues. In addition to the benchmarking of PROCESS against TPC (Kemp, Nakamura, *et al.* 2012), the collaboration included a study investigating the application of advanced divertor configurations. (G. Federici, Giruzzi, *et al.* 2013) finds that the lack of confidence in DEMO-relevant divertor heat loads has a significant impact on the direction taken in systems code modelling. As a result, high radiation models are preferred, which drive up machine and divertor volume as well as plasma current. The implication of this is that influential design decisions are being made on the basis of a lack of reliability in the systems codes. Despite the potential advantages in power handling, the snowflake divertor was found to be subject to additional forces and result in a decreased plasma volume for the device size. In (Okano, Gianfranco Federici, and Tobita 2014) the results of the joint EU-Japan studies into advanced divertor designs show that for the snowflake divertor the wide divertor opening causes issues for the control of impurities and neutral particles, for the super-X it is anticipated that severe engineering difficulties will emerge from the need to place the divertor inside the toroidal field coils. (Buttery *et al.* 2019) emphasises the need for any radiative divertor geometry and protection scheme to be compatible with the upstream plasma operation if high-performance steady-state fusion conditions are to be maintained.

In spherical tokamaks

(Sykes *et al.* 2018) discusses double null configuration modelling using PROCESS in the context of spherical tokamaks manufactured by Tokamak Energy Ltd, and finds the configuration attractive for high plasma power operation, however, it is acknowledged that there are uncertainties in divertor heat load. (Muldrew *et al.* 2020) also applies PROCESS to spherical tokamaks but urges caution due to significant remaining uncertainties associated with the design and limited modelling capability. (A. E. Costley 2019) stresses that divertor power loads in a compact spherical tokamak pilot plant will likely mean operating on the edge of material limits, however, it is hoped that R&D associated with DEMO reactors will be transferable. Similarly, it is hoped that the flexible divertor system recently installed in MAST-U will be able to improve the theoretical models for the divertor exhaust system that EU DEMO will be heavily reliant on given the large jump in size and power (I. T. Chapman and A. W. Morris 2019).

2.3.4 Power plant modelling

Modelling of prospective fusion power plants can provide insight into the constraints placed on divertor design, the direction of divertor development and the progress required to accommodate the demands of a (commercially viable) reactor. Proposed operating conditions and economic assessments for fusion power plants vary dramatically, reflecting not only the different visions of scientists and institutions, but also the uncertainty in design requirements and operating conditions. As before, much of the information discussed results from a combination of experimental and theoretical knowledge that is combined with systems code results to provide conceptualisations of reactors based on a range of different influences and constraints.

The ITER power plant

ITER will be the world's largest, most powerful fusion reactor when it is operational, however, is not designed to be a power plant. In (Janeschitz 2019), the author's vision of an economically viable tokamak based on ITER experience is presented, using modest extrapolations from current technology and including results from systems codes. The paper postulates that an ITER-style power plant would need to generate 2.5GWe, at an overall efficiency of 30% implying thermal power generation of greater than 6GW, 12 times the expected (500MW) thermal power output of ITER. The cost of operating devices with large toroidal magnetic field volumes drives an attempt to minimise divertor volume, however, this is in competition with the durability of the divertor. Plasma disruptions including Edge Localised Modes (ELMS) are identified as dangers to the divertor which would lead to rapid erosion of the targets, shortening their lifespan and causing operating problems for the device. Another study, using the HELIOS (Jean 2011) found that for a 1GWe ITER-like reactor, constraints including a 10MW m^{-2} divertor load limit result in a large machine with a major

radius of $R=10\text{m}$, almost double the figure for ITER. These two studies demonstrate the disparity between current technology, and what may be required in terms of future divertor performance.

Intermediary reactors

(Wan *et al.* 2017) details the China Fusion Test Reactor (CFETR) designed to help bridge the technological gaps between ITER and a demonstrator reactor. Results from a systems code developed by General Atomics were used to determine the initial parameters for CFETR. A conservative 200MW fusion power design (referred to as Phase I) and a high fusion power 1GW design (phase II) are established. Phase II, however, involves a divertor heat load of 20MW m^{-2} (double the proposed EU-DEMO heat load) and it is noted that despite the employment of additional heat removal and flux expansion techniques, this heat load could prevent long pulse or steady-state operation. This makes the phase II design of questionable use as a prototype power plant, where availability would seemingly be crucial to demonstrating economic viability. Both water and He cooled divertor systems are considered for phase II.

Water, He and carbon dioxide coolants for Generation IV fission reactors and fusion power plants are compared in (Garrett and Watson 2019). Water was determined to be the best coolant overall due to its ability to minimise armour temperature. The use of beryllium armour, however, limits the maximum operating temperature, making the efficiency gains from operating with He less substantial. The study uses TRACE/Relap, a combination of 4 systems codes and envisages significant technological crossover with generation IV fission reactors, which could be beneficial to the development of future tokamaks.

The European DEMO reactor

Based on an extrapolation of ITER physics and technology basis, the European DEMO reactor aims to bridge the gap between ITER and a first-of-a-kind fusion power plant. Recent design activity updates (G. Federici, Bachmann, Barucca, Baylard, *et al.* 2019; G. Federici, Bachmann, Barucca, Biel, *et al.* 2018) suggest a change in European fusion community culture towards an emphasis on systems integration, using only modest extrapolations from the ITER design and focused R&D studies into high-risk technologies. The conceptual design for EU DEMO is not yet finalised, however, and a lack of reliability in systems codes regarding divertor heat loads and impurity radiation impacts the predicted performance of conceptual designs.

The formulation of a self-consistent design point for DEMO is discussed in (Kemp, Ward, *et al.* 2014), where characterising the key features of the plant is seen as important in order to better understand technological, physics and engineering limitations. Variations on EU-DEMO are discussed, with a more conservative DEMO1 pulsed design based largely on ITER technology and a more optimistic steady-state device termed DEMO2. DEMO2 devel-

opment, described in (Giruzzi *et al.* 2015) requires significantly more recirculating power to support the current drive, potentially increasing the heat load to the divertor. It is noted, however, that a steady-state machine would however reduce fatigue due to thermal cycling. In (Reux, Di Gallo, *et al.* 2015) it is found using SYCOMORE that for a DEMO1 design, He and hot water divertor coolants provide similar net electric power efficiencies. The increase in pumping power associated with He was offset by the increase in thermodynamic cycle efficiency permitted. Further work optimising DEMO designs using SYCOMORE is presented in (Reux, Kahn, *et al.* 2018), which focuses on the influence of technological constraints. It is found that He and Pressurised Water Reactor (PWR) temperature (325°C) water permit equivalent reactor sizes. The cold water case allows for an increase in maximum tolerable heat flux from 5MW m⁻² to 10MW m⁻² for the same reactor size as in the hot water case.

The expected operational performance of a CuCrZr water-cooled heat sink proposed for DEMO is described in (Bachmann *et al.* 2018), where it is found that the high conductivity of the CuCrZr enables a relatively low thermal gradient through 1.5mm armour, at heat loads up to 20MW m⁻². By contrast, an equivalent Eurofer component limits power load to 1-1.5MW m⁻². Sub-cooled flow boiling in water is used to achieve a high convection coefficient, thought to be a factor of 5 better than what is achievable with gas coolants. However, the irradiation lifetime of Cu alloys means that the components would have to be replaced after a DEMO full power year. This contrasts with guidelines proposed in (Zohm *et al.* 2013) where there is a 5MW m⁻² projected divertor heat flux limit for DEMO, due to the requirement to use different, more neutron-tolerant materials.

A comparison between PROCESS, which uses a 1-D divertor model, and results from the more detailed SONIC 2-D divertor simulation code is made in (J. Morris *et al.* 2020). It is highlighted that systems codes are used to enforce engineering limits and calculate the heat load and therefore the impact of any simplifications in systems codes may result in the inaccurate application of constraints which may be carried through the design process. Despite this, PROCESS was generally found to agree well with the results from SONIC, but requires further testing to determine whether the prediction of attachment is reliable, as this is influential to divertor design.

Other DEMO reactors

In (Tobita, Asakura, *et al.* 2017) the status of the Japanese DEMO project is discussed. It is suggested that a fusion power of 1.5GW may be achieved using a water-cooled W armoured CuCrZr pipe divertor with a peak heat load of 5-10MW m⁻². Despite the comparatively low heat load, very high rates of divertor armour erosion are predicted, ranging from 0.03 – 0.3m per full power year. This results in the assessment that partial divertor attachment is not tolerable for a W divertor and fully detached operation is required. With significantly higher divertor heat fluxes proposed in other studies, it is clear that claims about prospective divertor performance should be approached with caution. (Batet *et al.* 2014) models the power cycle for a Spanish proposal for DEMO using the RELAP5-3D cooling systems code developed

Table 2.1. PPCS reactor coolants. WCLL = water cooled Li-Pb, HCPB= He cooled pebble bed (Marbach, Cook, and Maisonnier 2002).

Reactor	Coolant	
	Divertor	Blanket
A	H ₂ O	WCLL
B	He	HCPB
C	He	Self,He
D	Li-Pb	Self

for nuclear fission plants. A super-critical CO_2 power conversion cycle is recommended to maximise thermal efficiency where coolants of different temperatures (from the blanket and divertor) are used for the generation of electricity.

The Power Plant Conceptual Study (PPCS)

The power plant conceptual study, detailed in (Marbach, Cook, and Maisonnier 2002) was launched in 1999 in an effort to develop a viable power plant concept that upholds the claims made for the environmental sustainability and safety of fusion power. The PPCS was designed to provide direction for research to be conducted in parallel to ITER construction and operation, in preparation for DEMO. The technological parameters of the reactors described range from those based on ITER to those which assume significant technological development. The PPCS reactors have the following operational goals: steady-state electricity at a power of 1GWe; a lifetime of 40-60 years, and maintenance procedures that should be compatible with 75-80% availability.

The choice of coolant has a significant impact on divertor design. The choices made in the PPCS are detailed in Table 2.1. PPCS C and D both use ‘self-cooled’ blanket concepts which would require significant R&D. The Pressurised Water Reactor (PWR) conditions implemented in (Marbach, Cook, and Maisonnier 2002) for PPCS reactor A limit the maximum allowable heat flux to $7MW\ m^{-2}$, and $12MW\ m^{-2}$ with compromises to efficiency (by reducing water temperature). A power plant using ITER-like technology would face fluxes of $15MW\ m^{-2}$ or above. It is further suggested that ITER-based water-cooled technology with a CuCrZr cooling pipe is the only solution compatible with these loading conditions. This limits the coolant temperature, and therefore plant efficiency whilst simultaneously requiring an increased major radius. Divertor heat load was however found to be a limiting factor to the economic benefit of increasing the blanket wall load (which allows for an increased rate of water heating for electricity production).

Progress in optimising the water-cooled divertor for the PPCS reactor A detailed in (Li Puma *et al.* 2002), finds that for a $15MW\ m^{-2}$ heat load, the CuCrZr cooling pipe remains within the acceptable temperature range. It is suggested that as the divertor receives on the order of 18% of thermal power, an acceptable CoE is likely only obtainable if this power is used to drive electricity production. The proposed approach involves using the divertor output water to preheat the turbine feed water, increasing plant efficiency to 33%, in line with PWR reactors. Whilst He is typically preferred from a thermodynamic efficiency standpoint, it

Table 2.2. Parameters indicating the increases in technological capability between PPCS reactors A and D. Adapted from data in (D. Maisonnier *et al.* 2007).

	Reactor		
	A	D	
Fusion power	5	2.53	GW
Major radius	9.55	6.1	m
Divertor peak load	15	5	MW m ⁻²
Fusion gain (Q)	20	35	
Electrical power	1.5	1.5	GW

showed little efficiency improvement due to the high pumping power required. The WCLL divertor concept is discussed in (Sardain *et al.* 2003), where it is argued that quantification of uncertainties combined with advanced modelling techniques such as image-based modelling (as proposed in (Evans, Minniti, and Tom Barrett 2019)) will be necessary for the qualification of divertor components for a fusion power plant. The 0-D HELIOS code used in (Jean 2011) finds that for a PPCS C reactor, the combination of the low heat removal capability of the He coolant and the divertor heat load limit mean that a very high level of argon seeding is required for divertor protection. In addition, the high level of pumping power required is found to result in poor plant electrical efficiency. An update to PPCS progress presented in (D. Maisonnier *et al.* 2007) includes a summary of the operational criteria, again derived from PROCESS simulations where the cost of electricity is minimised. The increases in efficiency and reduction in current drive envisioned in progressively more advanced reactors result in the change in parameters shown in Table 2.2. Not indicated in the PPCS, is a framework for the practicalities of transitioning to untested divertor technology in only a few devices. A study on post-ITER design (Prachai Norajitra, Said I. Abdel-Khalik, *et al.* 2008) describes the divertor conceptual designs that form part of the PPCS. One advantage of the water-cooled design is that experimental data from PWR fission reactors can be extrapolated to inform modelling. To avoid excessive design complexity, reactors with the same coolant for the divertor and blanket systems are preferred, tying divertor design to blanket design, and further constraining the system. The He cooled designs considered have a peak heat load limit of 13MW m⁻² whereas the water-cooled divertor is able to operate at a heat flux of up to 20MW m⁻² but is considered unsuitable for application to power plant scenarios due to its use of CuCrZr which is vulnerable to embrittlement. The study seems however to compare the (experimentally derived) material problems of the water-cooled design to the theoretical advantages of the He cooled design, where the associated uncertainties might make it seem unduly attractive.

Accelerating development of a commercially viable tokamak

A series of papers published introduced in (Windsor 2019) on the topic of accelerating the development of tokamak-based fusion energy include some discussion of power plant modelling. The impact of plasma physics on power plant timescale is investigated in (Wilson 2019), where it is argued that divertor detachment and advanced designs including the super-X and snowflake divertors may be required for successful fusion power plasma operation.

(I. T. Chapman and A. W. Morris 2019) discusses UKAEA capabilities to address challenges to delivering fusion power, and includes a discussion of rapid prototyping and virtual engineering twins to accelerate the design and testing workflow. (Kembleton, A. W. Morris, *et al.* 2020) covers design issues standing in the way of fusion commercialisation, many of which stem from system integration and the low technology readiness level of tokamaks, which provides significant uncertainty when modelling power plant designs. The divertor is singled out as a significant source of complexity in the design of the fusion reactor and efforts to construct it from standardised parts like the monoblock allow for the efficiencies of scale in manufacturing. The author also suggests that component design must be driven by commercial concerns such as reliability, ease of manufacture and assembly. It is estimated that only 3-4 disruptions per full plasma year are acceptable to minimise unplanned downtime for divertor maintenance. This implies that tolerance of disruptions may be an important parameter when considering divertor design and ultimate cost.

Commercialisation and the cost of electricity

As discussed throughout this review, tokamaks are far from ready to enter the commercial electricity market, however, if this goal is to be achieved, it is important to consider how their operation will impact the cost of electricity (CoE). An approximation of the economy of fusion energy in (Entler *et al.* 2018) finds a high degree of uncertainty in modelling fusion CoE but identifies a strong dependence on fusion industrial technologies. Steady-state operation of power plants is investigated in (Buttery *et al.* 2019) where work on the DIII-D tokamak has improved compatibility between plasma physics and divertor requirements in order to reduce disruption frequency, thereby decreasing erosion of the divertor. In (Takeda, Sakurai, and Konishi 2020), a fusion power plant compatible with a deregulated electricity market is modelled, where it is established that the economic performance of fusion power plants is particularly sensitive to unplanned outages. This is of particular importance to consider in conjunction with divertor protection and may influence choices regarding divertor durability versus cost. A study looking at the minimisation of the cost of electricity (CoE) in fusion reactors (Tokimatsu *et al.* 1998) finds that a water-cooled design is compatible with a minimised CoE and that He or Li cooling are not required.

Spherical tokamak power plants

Spherical tokamaks present a different optimisation problem to that of the conventional high aspect ratio tokamak. (Voss *et al.* 2000) uses PROCESS to model thermodynamic, neutronic and mechanical design parameters for a spherical tokamak power plant with a 1GWe electrical output. The resulting reactor design involves water-cooled divertor coils with a highly elongated plasma designed to protect the components through the more uniform distribution of the neutron load. The divertor configuration uses a double null system with an upper and a lower divertor effectively halving the load per target. There is however very limited space for the construction of the inboard targets due to the compact low aspect ratio design. The small

central column however means that it may be easier to remove for maintenance, including the replacement of the divertor. In (A. Costley, Hugill, and Buxton 2015) the author presents a vision of future spherical tokamaks based on the observed scaling of the fusion energy gain (Q) which scales with absolute fusion power and energy confinement, and only weakly on major radius. This inevitably leads to a concept of small reactors, which will need robust methods for dealing with even higher heat and neutron loads to components like the divertor. The route for compact spherical tokamaks is perhaps therefore even more reliant on novel divertor geometries and protection techniques. An argument for the vision of a spherical tokamak power plant is developed in (A. E. Costley 2019), which suggests that careful design could result in a power load that is compatible with material limits. A 5-10MW m^{-2} divertor heat load is suggested in a double null configuration where divertor engineering is a key aspect of spherical tokamak power plant viability.

2.3.5 Uncertainty in divertor design

The unverified nature of many fusion power plant concepts means there is a high degree of uncertainty in the values of many parameters which may need to be used as inputs in a systems code. The risks associated with undefined components and system integration in DEMO is discussed in (Gliss *et al.* 2018), where it is noted that cost saving and design simplification needs to be performed once design uncertainties are reduced in order to allow for effective design integration. In (Lux *et al.* 2017) a Monte Carlo sampling technique is used in conjunction with PROCESS. Significant uncertainty in power flow to the divertor is noted, as PROCESS lacks a robust model and instead uses a proxy value based on current data. The reliability of systems code modelling becomes harder to prove for reactors the further they progress from the current experimental capability. For this reason, (Marbach, Cook, and Maisonnier 2002) benchmarks PROCESS against existing ITER calculations and finds good agreement with ITER geometry and cost, however, uncertainties in ITER operation still exist. As stated in (Zohm *et al.* 2013), the assumptions made in systems code modelling of DEMO are largely dependent on the optimism of the author, where it is suggested that out of all the areas requiring improvement in technology and understanding, the power exhaust system (including the divertor) is where the most progress is needed.

(Bachmann *et al.* 2018) discusses the design integration challenges envisaged for the construction of a European DEMO reactor. It is stressed that divertor performance is an outstanding issue which creates a challenge for design integration. Furthermore, it is suggested that the DEMO divertor may have to rely on the sub-cooled boiling regime associated with liquid coolants (water) rather than gas coolants in order to deal with heat loads. This again leads to the contradiction that a water-CuCrZr coolant-pipe combination is required in order to manage heat loads in DEMO but is also considered unsuitable due to its poor radiation resistance. The power density from which divertor operation can be recovered without significant damage if detachment is lost is assessed as affecting the net electrical power by $\pm 3\%$ when it is modified by $\pm 10\%$ (Kembleton, G. Federici, *et al.* 2019). In a review of design integration issues regarding power exhaust in the transition from ITER to DEMO, (A. Loarte

and Neu 2017) finds that contamination of the core plasma is a central issue with W divertor PFCs. Liquid metal is presented as a solution, however, it is subject to potentially hazardous interactions with the magnetic fields.

2.4 Divertor target modelling

This section focuses on the modelling of plasma-facing divertor targets, which are typically composed of rows of actively cooled armour plates. The discussion is divided into two sections, one which focuses on the modelling of armour processes and another which describes issues relating to the coolant fluid.

2.4.1 Divertor armour modelling

The armour provides a number of different functions in the divertor: it is the first point of contact for the most intense tokamak heat load, it provides neutron shielding and heat transport. It must be able to perform these functions without melting or unacceptable activation, undergoing fracture, retaining excess tritium, resulting in unacceptable arcing from the plasma, or allowing He ingress (Malizia *et al.* 2014). It is unlikely that any armour component will perfectly satisfy all of these constraints and so compromises are made with different devices emphasising some functionalities over others. For example, experimental reactors may be able to use parts designed to be replaced more regularly than would be possible in a commercial reactor with high availability.

2.4.2 Design codes

Design codes can include rules for manufacture, failure testing methodology, performance requirements and other processes related to component design. In the case of one concept known as the monoblock, for example, only the pipe is considered a structural component and the armour is subject to different design standards (Muyuan Li, Werner, and Jeong-Ha You 2015). This section does not constitute an exhaustive list of codes but highlights the existence of some of the major ones used in the design of the divertor.

SDC-IC and RCC-MR

Full details on the development of an ITER-relevant design code - the ITER Structural Design Criteria for In-Vessel Components (SDC-IC) - and recent developments can be found in (Sannazzaro *et al.* 2013). The SDC-ICC is based on the earlier RCC-MR, as stated in (Martinez *et al.* 2011), which also discusses the challenges in developing structural design criteria for fusion in-vessel components. (Kalsey and Porton 2014) notes that current nuclear power plant codes are all designed for fission and are of limited relevance to fusion applications. It is argued that they do not adequately account for effects like cyclic softening

(including ratcheting and creep-fatigue) and non-ductile material behaviours. RCC-MRx is a French design code resulting from the merger of two other design codes. It is developed in the context of a materials test reactor and aims to be applicable to ITER-relevant components (De Meis 2015).

The MEAP

The Monoblock Elastic Analysis Procedure (MEAP) was developed as part of the ITER Work Package Divertor (WPDIV) as a method for the simple but accurate assessment of monoblocks under steady-state operating conditions (M. Fursdon, J. H. You, *et al.* 2018). Monoblock sub-components are made of materials which have different yield strengths and coefficients of thermal expansion. This leads to the proposal of a hybrid elasto-plastic analysis technique for proper characterisation of the stress state. It is established that even when plastic analysis is included, the results only provide an estimate of the cyclic stress range, rather than the absolute stress state. (M. Fursdon, J. H. You, *et al.* 2018) also notes that a new code based on elasto-plastic methods, known as the DEMO Design Criterion (DDC), is being developed. The MEAP includes selected structural rules from the ITER SDC-IC and three thermal rules (Crescenzi *et al.* 2017). Firstly, the cooling tube bulk temperature must be within the prescribed temperature range limited by irradiation embrittlement, irradiation creep and or thermal softening. Secondly, the tube wall heat flux must be lower than the CHF. Finally, the W surface temperature should be less than 1800°C to prevent bulk re-crystallisation. There are also additional rules relating to failure through processes including ratcheting that consider distinct load cases. It is stressed in (Thomas R. Barrett *et al.* 2016) that the MEAP is intended primarily for comparative purposes, and to inform design by analysis.

Design by analysis

The concept of design by analysis for PFCs is discussed further in (M. Fursdon, J.-H. You, and M. Li 2019), where a number of specific design rules for an Inelastic Analysis Procedure (IAP) are proposed. ITER is described as a design-by-experiment device due to historical difficulty in predicting cracking, which was identified as a dominant failure mechanism. As the monoblock cooling pipe is the only sub-component designated as structural, the standard elastic design rules do not apply to the other sub-components. A number of key points are highlighted, some of which are summarised as follows:

- I W is brittle and no formally validated design assessment rules exist.
- II The dissimilar metals and joining methods in monoblocks can lead to singularities for stress and strain in finite element analysis.
- III Material property modification by radiation is poorly characterised.

2.4.3 Armour geometries and concepts

The following section describes common divertor armour geometries and their performance where sufficient data is available.

The 'ITER' style monoblock

The monoblock design features a continuous armour block with an integrated cooling pipe. The concept has been selected for a number of reactors including ITER (Hirai, Escourbiac, *et al.* 2014) and CFETR (Wan *et al.* 2017). Early designs used CFC armour. (Cardella *et al.* 1993), models the CFC armour concept in a 3D thermo-mechanical analysis in support of experimental results and finds no degradation after 1700 cycles at a heat flux of 13MW m^{-2} and over 1000 cycles at 15MW m^{-2} . Whilst CFC was evaluated as a divertor plasma facing material (K J Dietz *et al.* 1995a), it was rejected for ITER due to reasons of cost and tritium retention (Dolan 2014). The replacement design includes a CuCrZr cooling pipe separated from W armour by a stress relieving Cu interlayer (Hirai, Panayotis, *et al.* 2016). Two design issues identified are the stress induced due to differing material coefficients of thermal expansion (Schlosser, F. Escourbiac, *et al.* 2005) and the use of a circular cross-section pipe, which leads to uneven heating (Araki, Ogawa, *et al.* 1996). The influence of the ITER divertor on future DEMO reactors is likely to be widespread due to the number of national members of the ITER organisation.

Other monoblock concepts

(Hermsmeyer and Kleefeldt 2001) highlights a number of different He-cooled concepts, all of which are designed to be compatible with a monoblock armour geometry, and discusses the use of a porous wick to enhance thermal contact. In the concept proposed in (J.H. Rosenfeld *et al.* 1997), the porous medium is placed at the outer region of the coolant channel with the flow in the porous region directed such that the heated coolant fluid flows away from the top region which receives the peak heat flux. The multi-channel concept presented in (D. L. Youchison *et al.* 2000) also features circumferential flow in an outer porous region, however, two channels are present in a single armour block. A coolant tube concept proposed in (C B Baxi and Wong 2000) consists of an annular vanadium tube with ridges cut into the internal surface in order to break the laminar boundary layer which is found near the solid-fluid interface. The ridges are more pronounced in the top portion of the tube, where the highest heat fluxes are experienced. Other concepts presented in (Hermsmeyer and Kleefeldt 2001) including the 'eccentric swirl promoter' and a slot concept, do not seem to have been investigated further.

Flat tile

The flat tile concept typically involves an armour plate bonded to a higher thermal conductivity heat sink with an internal cooling pipe (Araki, Akiba, *et al.* 1992). The dangers associated with an early ITER flat tile concept involving a CFC or beryllium armour layer bonded to a Cu pipe with an external rectangular cross-section Cu (alloy) heat sink are described in (Merola and Vieider 1998). The consequences of tile detachment are modelled in ANSYS (and EUPITER for heat transfer coefficients), and result in a heat flux of 120MW m^{-2} on a 1mm area of the adjacent tile causing rapid temperature rise and melting (of Be armour) in 17ms. The von Mises stress was found to increase rapidly in the adjacent tile and was thought to lead to further detachment. It is concluded that a monoblock solution is significantly more robust in this application. The microchannel designs investigated in (D. Y. Lee and Vafai 1999) rely on plasma-facing armour plates where the opposing side is actively cooled with coolant forced between finely spaced high aspect ratio fins. This allows for a large contact surface area and a high temperature gradient within the water coolant.

Tile-finger geometries

The jet impingement concept presented in (Ihli *et al.* 2005), discussed in the context of DEMO in (Prachai Norajitra, Said I. Abdel-Khalik, *et al.* 2008), and optimised in (Widak and P. Norajitra 2009), uses hexagonal armour tiles which are not cooled directly but are brazed onto caps to minimise cracking. Jets of high velocity He travel along He tubes or ‘fingers’ perpendicular to the armour tiles and impinge on the underside of these caps. The He cooled modular divertor with jet cooling (HEMJ) design, based on the tile-thimble concept is illustrated in Fig. 2.5. An integrated finger and plate concept presented by (A. R. Raffray, Malang, and X. Wang 2009), has a unit size tailored to the heat flux profile and uses small components which are better at heat removal in areas of high flux and more reliable, larger plate components elsewhere.

Interlayer engineering

Interlayers are typically added to divertor monoblock designs in order to relieve stress. The ITER monoblock interlayer is designed to yield plastically, minimising excessive thermal stresses (Q. Li *et al.* 2019). Interlayers have been the subject of a number of recent design studies aimed at improving monoblock performance, and the emergence of novel manufacturing techniques capable of producing designs with more complex internal geometries may provide further opportunities for development.

A thermal barrier concept which aims to improve heat flux repartition and reduce thermal gradients with the addition of a graphite layer to the top surface of the interlayer is introduced in (Giancarli *et al.* 2005). The design is based on the monoblock concept and uses a Eurofer cooling pipe and W armour, chosen over a flat tile concept to limit the consequences of failure (due to tile detachment). A 2D thermal analysis was performed and found that the design

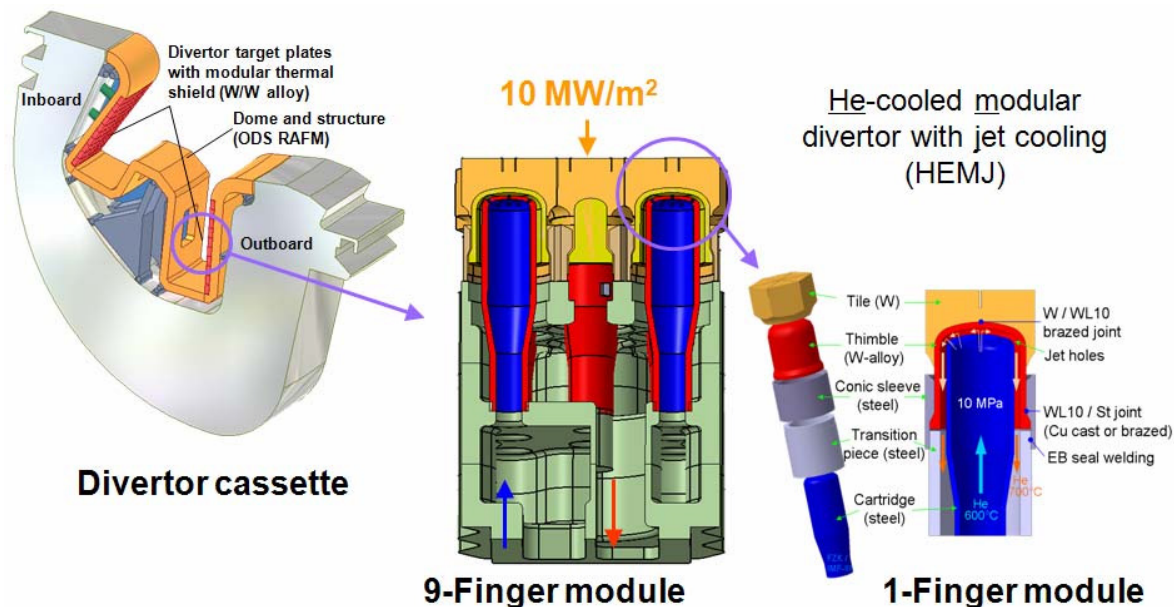


Figure 2.5. Illustration of the He HEMJ divertor concept, assembly and location in the divertor. Reproduced from (Prachai Norajitra, Giniyatulin, *et al.* 2008).

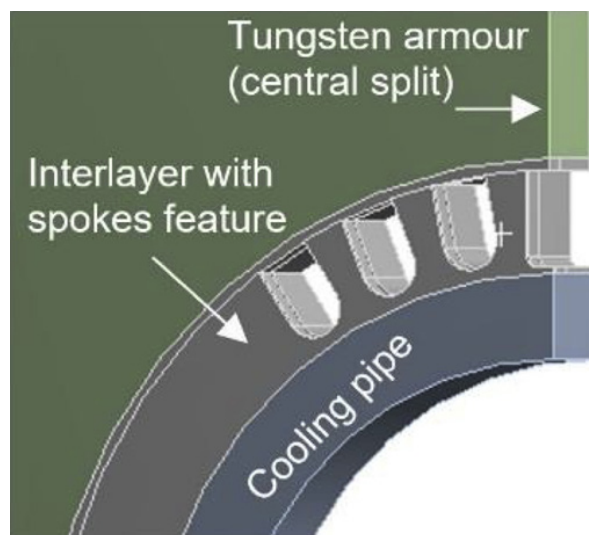


Figure 2.6. Illustration of the ‘thermal break’ concept designed to minimise thermally induced stress around the upper face of the monoblock cooling pipe. Reproduced from (Domptail *et al.* 2020)

was able to withstand an incident surface heat flux of 15MW m^{-2} . The thermal barrier is applied to the top half of the pipe and is 0.075mm at its thickest point. The repartition effect of the thermal barrier reduces this heat flux to 13MW m^{-2} at the pipe interface, giving a safety factor of 1.28 between this and the CHF (16.7MW m^{-2}).

A design search performed in (T.R. Barrett *et al.* 2015) with the goal of exploring interlayer engineering, produced a concept known as the ‘thermal break’. The thermal break is designed to reduce the stress induced by the CTE mismatch between the CuCrZr and the W in an ITER-style monoblock. Fig.2.6 illustrates a design developed based on the thermal break low conductivity interlayer concept and presented in (Domptail *et al.* 2020). The interlayer ‘spokes’ increase thermal resistance, resulting in greater W thermal expansion and therefore less induced stress due to the more rapid CuCrZr cooling pipe expansion.

The counter-intuitive concept of deciding to reduce overall conductance is justified by refer-

ence to its proposal in (Li-Puma *et al.* 2013). The optimisation in (T.R. Barrett *et al.* 2015) uses response surface methodology to minimise a stress-based objective function, combined with a genetic algorithm to identify optimal designs. The optimisation resulted in a thick compliant interlayer with a low Cu fraction, which was found to re-distribute stress around the pipe, reducing the peak value. Whilst the optimised design met the ITER SDC-IC rules, the W maximum temperature was near the imposed limit, described as potentially design driving. This somewhat calls into question the chosen reduction in conductance. The authors also note the potential for the development of ultra-compliant interlayers which structurally decouple the pipe and armour. The thermal break concept is further developed in (Fursdon 2017) where the design features machined spokes in the upper portion of the interlayer, chosen as a compromise between strain in the interlayer and stress in the pipe. The SDC-IC rule used describes a limit on progressive deformation which the thermal break design satisfies, exceeding the performance of the ITER design. (Galatanu *et al.* 2019) investigates the manufacture of functionally graded thermal barrier interfaces for DEMO in an attempt to combat the different operating temperature ranges of the W armour and CuCrZr pipe. Results from a finite element simulation suggest that it is possible to maintain W in its operational temperature window (given as 300 – 1200°C) with the chosen design concept. In (Q. Li *et al.* 2019) the number and thickness of Functionally Graded (FG) interlayers are optimised with the goal of reducing the impact of thermal stress and irradiation-induced degradation in the Cu. The FG interlayer was particularly effective at reducing the stress in the CuCrZr heatsink (by more than half), however, the modelling of functionally graded layer behaviour was somewhat limited. The maximum temperatures in the W and CuCrZr were found to exceed the W re-crystallisation limit (given as 1300°C) and the CuCrZr limit for stable operation (400°C which moves to 300°C under irradiation). The author proposes the development of new alloys as the solution, however, it is clear that there is significant variation in the operational limits of these materials in the literature. The SAT (Swept Armour Target) introduced in (Mazul 2016) involves a water-cooled W armour block with a Eurofer pipe and a LiPb liquid metal interlayer which minimises the thermally induced stresses due to differences in material CTEs. A Korean ‘K-DEMO’ monoblock based on a modified ITER design is presented in (Im, Kwon, and J. S. Park 2016), where a vanadium interlayer and RAFM steel cooling tube is used. The RAFM steel is used instead of CuCrZr despite its lower thermal conductivity to minimise activation (Kwon, Im, and J. S. Park 2017), however, to combat this, the pipes must be very thin and managing stress becomes more difficult.

Advanced armour design

(Li Puma *et al.* 2002) performs a thermal-hydraulic analysis on a castellated divertor monoblock component concept optimised for a water-cooled Li-Pb (WCLL) blanket (and divertor) concept associated with the PPCS (Power plant Conceptual Study). The component was found to tolerate the heat flux without failing, with minimum temperatures in the CuCrZr and W falling 27°C and 300°C below the respective lower limits for a steady state heat flux of 15MW m⁻². It is suggested that the castellated W design (illustrated in Fig. 2.7) needs to be

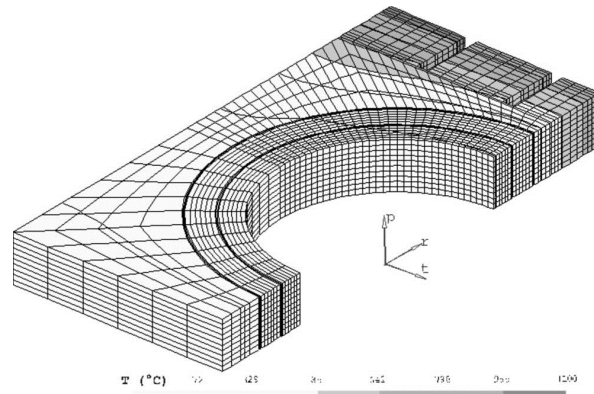


Figure 2.7. Representation of a castellated monoblock designed to minimise thermally induced stresses by allowing for thermal expansion. Reproduced from (Li Puma *et al.* 2002).

further investigated to ensure it does not increase the likelihood of the cracking it is designed to alleviate. An ITER-like divertor concept for DEMO is evaluated in (Crescenzi *et al.* 2017) as part of a design study which uses the MEAP (Monoblock Elastic Analysis Procedure). A sizing optimisation problem is performed with the objectives of minimising the maximum temperature and the maximum von Mises stress in the cooling pipe. The interlayer is assumed to be elasto-plastic and the pipe and armour are treated elastically in the finite element analysis. The optimisation leads to a modified geometry with reduced dimensions that had sufficient safety margin for the three loading cases studied.

A novel vision for plasma-facing component design and manufacture is established in (R. E. Nygren *et al.* 2016), where it is proposed that PFCs made from homogeneous armour materials would have insufficient lifetimes for operation in reactors like DEMO. It is suggested that future PFCs will require features like functional grading, nano-structures, and controlled porosity, enabled by advanced manufacturing techniques.

In (Curzadd *et al.* 2019), topology optimisation is used to address the problem of stress in the divertor monoblock system. The localised material composition of part of a generalised topology optimised monoblock is allowed to vary between the properties of W and Cu in accordance with a gradient-based optimisation algorithm with the objective of minimising (peak von Mises) stress. The result is a continuous mixture of Cu and W intended for manufacture using FG technology, with a minimum upper W armour thickness of 5mm. The lack of proper characterisation of FG materials and the importance of the residual stress state on the results are noted. (Kerkhof *et al.* 2021) also implements topology optimisation for stress minimisation but uses a full 3D model and investigates the influence of temperature limits on optimisation alongside residual stress and modifications to the objective function to include the influence of a yield criterion. The resulting designs are found to exhibit improved performance for the loading conditions used in the optimisation but were outperformed by reference designs in other loading scenarios.

2.4.4 Divertor target loading conditions

This section discusses the performance of the various divertor solid domain designs when subjected to fusion-relevant loading conditions. PFCs must be able to tolerate a wide range of loading conditions through fusion initiation, steady state operation and shutdown, not including the additional demands placed on components by transient power surges resulting from a variety of plasma events. Most fusion devices proposed for commercial application rely on steady-state operation to maximise availability for electricity production (Kembleton, A. W. Morris, *et al.* 2020). Most current tokamak designs, however, which rely on ramping a current through a central solenoid to induce a toroidal plasma current, are inherently cyclic. Start-up and shut-down cycles can be particularly damaging to PFCs, both as they introduce mechanisms for cyclic damage, but also because they can result in higher thermal loads to the divertor (A.R Raffray *et al.* 1998). Furthermore, it is currently unclear to what extent future PFCs will be subject to damaging transient events including plasma disruptions known as Edge Localised Modes (ELMs). Whilst ELM-free operation is being investigated, it is currently poorly understood (Siccinio, Biel, *et al.* 2020) and it is thought that future devices must be able to tolerate several ELMs without failure (Sizyuk and Hassanein 2018).

Heat flux concentration

One design challenge present even in steady-state operation is caused by small misalignments that arise between monoblocks in assembly, exposing a leading edge to an increased heat flux. In (J. Gunn, Carpentier-Chouchana, *et al.* 2017) it is shown that a 0.5mm bevel in the toroidal direction can protect the monoblock from bulk melting under steady-state heat loads. The introduction of this bevel, however, changes the exposure of the monoblock to the magnetic fields, increasing the overall heat flux, and leading to a greater danger of surface melting and if detached operation is lost (R. A. Pitts *et al.* 2017). Uncontrolled ELMs also become a more severe threat to the divertor. This analysis is extended in (J. Gunn, T. Hirai, *et al.* 2019) where a poloidal-toroidal bevel is considered (but not recommended for ITER) and it is highlighted that ELMS on bevelled components may be intense enough to trigger boiling of the W armour. (J. P. Gunn *et al.* 2021) includes experimental verification of the impact of heat loads on leading edges between monoblocks and predicts that ITER monoblocks may undergo cracking in the first stages of operation which could act as nuclei for further cracking under steady-state operation. Fig. 2.8, reproduced from (J. P. Gunn *et al.* 2021) illustrates the potential for damage due to exposed leading edges.

Transient events

Slow transients of 20MW m^{-2} over 10 seconds are the most demanding heat load requirements PFCs in ITER are designed to handle (A.R. Raffray *et al.* 1999). However, (Mazul 2016) envisages the worst-case scenarios for divertor loading, with loss of detachment in ITER resulting in transient heat loads of 40MW m^{-2} . A range of engineering solutions are

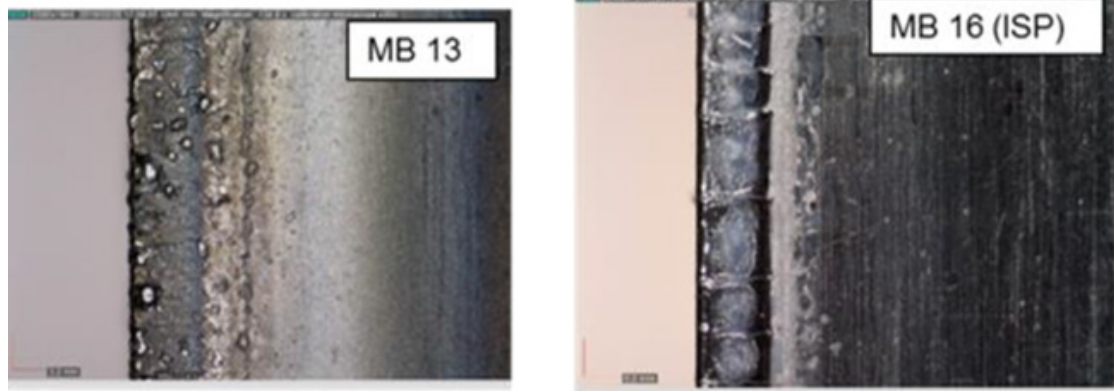


Figure 2.8. Photographs of monoblock sections with discoloured bands showing the result of surface melting in a high-field region (left) and cracking in a low field region (right). The damage is attributed primarily to localised intense heat fluxes resulting from small misalignments between tiles that expose leading edges. Adapted from (J. P. Gunn *et al.* 2021).

proposed including the use of functionally graded materials, however, it is argued that the potential thermo-mechanical improvement would be insufficient for loads above $15\text{-}20\text{MW m}^{-2}$. The authors present the idea that it may be difficult to integrate an adequately performant divertor into an already optimised DEMO design. A number of solutions are proposed which rely on the movement of either the plasma or the target including liquid metal or a system involving continually refreshed metal spheres. A rotating target is proposed as an alternative to sweeping the plasma across a stationary target in order to reduce electromagnetic loading. (Maviglia *et al.* 2016) discusses DEMO relevant ITER-style monoblocks designed to handle slow 10-second transients. A thermal-hydraulic analysis involving a sudden ramping of power from a steady state load to a value above the CHF found that when the coolant temperature was above 160°C , the design driving constraint is the CHF and pipe burnout, whereas for coolant temperatures below 160°C , melting of the armour surface was the primary source of failure during high transient heat loads. It is found that thicker W armour would allow for a longer period of time in an extreme heat load scenario (up to 30MW m^{-2}) before pipe burnout occurs, at the expense of higher surface temperature. An in-depth simulation of transient events resulting from ELMS in ITER is presented in (Sizyuk and Hassanein 2018). It is found that the ITER design has the potential for localised heating of PFCs a distance away from the divertor targets, leading to damage and vaporisation of both surface and hidden components. It is suggested that a single transient could leave ITER inoperable and that damage to hidden components could involve a lengthy maintenance time. (Hassanein and Sizyuk 2021) goes further and suggests that the ITER divertor design will not work properly during transient events without significant redesign. A snowflake divertor configuration is suggested as a potential solution to this problem.

Transient stresses in a He cooled W divertor target during startup and shutdown considered in (X. R. Wang, A. R. Raffray, and Malang 2009) show that a jet impingement design operated within the stress and temperature limits, but risked W re-crystallisation in the thimble. It is suggested however that transients on the scale of 10 seconds, perhaps associated with emergency shutdowns, may exceed these limits. The 3D thermo-mechanical and thermo-fluid analyses were performed for a reactor startup scenario involving ramping power to

10MW m⁻² over 400 seconds.

2.4.5 Deformation, damage and failure

Modelling of the mechanisms of deformation, damage and failure in PFCs in conjunction with experimental work, is crucial to improving the ability of digital modelling techniques to continuously evaluate a broad range of design concepts, including those not currently in use in experimental devices. Some of the main mechanisms for deformation and damage in PFCs (detailed in (M. Fursdon, J.-H. You, and M. Li 2019)) are:

- i Residual stresses (stresses which remain present in materials after the external forces which initially caused the stress have been removed).
- ii Thermal fatigue (induced by repeated cyclic expansion and contraction of materials), which is especially problematic in multi-material divertor components due to differences in CTEs.
- iii Plastic deformation (permanent distortion of a material which occurs when it is subjected to stresses beyond its yield stress).
- iv Ratcheting. Also referred to as cyclic creep, ratcheting involves the accumulation of plastic deformation due to thermo-mechanical cyclic stresses.

Modelling damage in monoblock concepts

Cracking has been found to occur in the upper portion of the W armour of monoblock concepts. In (T.R. Barrett *et al.* 2015) the three sources of stress in the monoblock pipe are listed as the internal coolant pressure; the temperature gradient due to the plasma heat flux and the differences in thermal expansion. Cracking in W armour is modelled in (Muyuan Li and Jeong-Ha You 2015), where cracks were initiated with heat loads of 15MW m⁻² and 20MW m⁻², with the most probable causes of cracking detailed as low cycle fatigue. Surface cracks initiated during operation were found to grow during cooling, reaching 5mm into the armour. Furthermore, crack growth was found to continue during subsequent high heat flux heating, extending to the region directly above the interlayer in some cases. An elasto-plastic thermo-mechanical analysis of the ITER monoblock cooling tube and interlayer in (Muyuan Li, Werner, and Jeong-Ha You 2015) for DEMO operating conditions, establishes that the cooling tube is unlikely to fail under an 18MW m⁻² heat flux. It is noted however that un-irradiated material property data was used. The Cu interlayer however was shown to experience significant plastic deformation at the upper boundary with the cooling tube and loads greater than 15MW m⁻² were found to reduce the low cycle fatigue lifetime. Consequently, the component was seen as unlikely to meet the design requirements for DEMO operating conditions.

The heat flux limit in a W/RAFM (Reduced Activation Ferritic-Martensitic) divertor design for CFETR is investigated in (Mao *et al.* 2018). The design uses a RAFM steel pipe with

a Cu interlayer. The ITER in-vessel design code SDC-IC is used to analyse structural integrity under with ITER-like conditions due to uncertainty in the expected CFETR operating conditions. The temperature limit for the Cu interlayer was found to limit maximum allowable surface heat flux to below 10MW m^{-2} with a maximum coolant flow rate of 20m s^{-1} . This was caused by the low thermal conductivity of the RAFM steel pipe. The included geometric optimisation, therefore, generated designs with thin pipes, which showed increased performance but a potential vulnerability to failure through accelerated corrosion. Somewhat surprisingly, reducing the heat load from 10MW m^{-2} to 9.19MW m^{-2} was found to extend the lifetime from 0.55 years to 2 years. A thermo-mechanical analysis of the same monoblock with a China Low Activation Martensitic (CLAM) steel pipe is presented in (Peng Liu *et al.* 2018) using the EU DEMO MEAP and the hybrid model detailed in (M. Fursdon, J. H. You, *et al.* 2018). Whilst the CLAM steel tube was predicted to satisfy the requirement for cyclic fatigue, creep is predicted to be an issue for operating times exceeding 1460 hours.

2.4.6 Coolant fluid modelling

Cooling the divertor armour involves removing an intense one-sided heat flux, which creates challenges for both concept design and the modelling of fluid processes in the coolant. Digital design typically relies on Computational Fluid Dynamics (CFD) to model coolant flow as part of a conjugate heat transfer problem coupled to a thermo-mechanical analysis of the solid parts. A significant source of complexity arises from the multiple engineering objectives associated with the system. The cooling pipe must be capable of adequate heat conduction to the coolant, where mixing and convective transfer occurs, in order to carry away heat without involving a pumping power that is unacceptable from the perspective of maintaining reactor efficiency. Equally, a balance must be maintained between removing enough heat from the armour to prevent melting and maintaining operation below the fluid CHF.

The choice of coolant has a large impact on the design of PFCs. It is both influenced by ‘upstream’ decisions regarding power plant regulations and goals for safety, efficiency, cost of electricity and maintenance and ‘downstream’ constraints such as the maximum tolerable heat flux and the need to operate within the operating temperature ranges of PFC materials. Water is the best-characterised coolant, and the most common choice for past and present experimental tokamaks. The phase change as water undergoes boiling, however, can add complexity to modelling, engineering and operating safety. Water has a high heat capacity, which in turn leads to high heat flux handling capability. It is traditionally associated with Cu alloy coolant pipes which do not permit operation beyond approximately 350°C under irradiated conditions (Li-Puma *et al.* 2013). Helical swirl tapes are typically used as turbulence promoters (Schlosser, F. Escourbiac, *et al.* 2005) and increase the heat transfer coefficient by increasing effective flow velocity and mixing (C B Baxi and Wong 2000).

He has some theoretical advantages over water including its compatibility with the plasma in

case of a leak and its chemical and neutronic inertness, allowing for corrosion-free operation in metal cooling pipes (C B Baxi and Wong 2000). Furthermore, it is used as a single-phase coolant and as such does not involve the modelling and engineering challenges associated with fluid CHF. He has a low heat capacity, which may be compensated for with high fluid velocity, however, this can also mean that a high pumping power is required. Furthermore, in areas receiving greater heat load, the He gas can expand significantly, reducing density and increasing pressure drop (D. L. Youchison *et al.* 2000).

Exotic coolants including liquid metal are another option proposed for next-generation reactors (C B Baxi and Wong 2000). They typically feature high boiling points and heat transfer coefficients but are highly chemically active (Ferrari *et al.* 2001). Furthermore, as liquid metals are conductive, internal currents and Lorentz forces can be induced in the presence of magnetic fields, as is the case in a tokamak. Their use in divertors (and breeder blankets) often results in additional drag forces and therefore increased pressure drops (Abdou *et al.* 2015). The behaviour of electrically conductive fluids in magnetic fields can be described using magnetohydrodynamics (MHD).

A liquid metal plasma-facing surface concept designed to remove heat fluxes in excess of 20MW m^{-2} is proposed in (Kurihara 2002). The liquids suggested for use are Li, Ga and a molten salt (LiF-BeF₂) known as FLiBe. The concept aims to reduce the need for maintenance and eliminate the problems of thermally induced stress and crack growth. FLiBe has a high electrical resistance and so MHD-related pressure loss is predicted to be less significant. A liquid metal armour concept discussed in (Roccella *et al.* 2020) aims to increase the PFC lifetime with a self-healing divertor that is also less susceptible to neutron damage, with concepts proposed using either Li or Sn-based coolants. (Segantin *et al.* 2020) details FLiBe molten salt coolant and dynamic flow adaptation to permit an efficient load following design where the inlet and outlet temperatures can be modified to protect against stress peaks and cyclic fatigue. Whilst liquid metals and molten salts are arguably the least mature of the three coolants discussed, they are the subject of active research and could drastically change the design of future divertors if successful.

2.4.7 Fluid heat transfer modelling

The fusion environment provides a unique conjugate heat transfer environment, even for a coolant as well-studied as water. An extreme heat flux is transferred through a (multi-material) solid domain to highly pressurised hot fluid through one side of the cooling pipe. Literature describing similar heat transfer scenarios was not widespread before works including (Schlosser, Chappuis, and Deschamps 1993) were performed in preparation for ITER. It was established in (Araki, Ogawa, *et al.* 1996) that previously-established heat transfer coefficient correlations for non-boiling to sub-cooled partial nucleate boiling conditions were unsuitable for ITER purposes. FILM-30 (successor to FILM) is a code developed to calculate heat transfer properties for the inside of an OFHC (oxygen free high thermal conductivity) PFC coolant channel that is non-uniformly heated (T. D. Marshall 2001). The code is writ-

ten in FORTRAN and when combined with FEA, was found to be in good agreement with experimental data for OFHC-Cu mock-ups.

2.4.8 Thermal-hydraulics

As the coolant fluids used in the divertor are circulated using forced convection, the nature of their mechanical behaviour, and the interaction of this with their thermal performance is of significant interest. Whilst the thermal-hydraulic behaviour of water-cooled components is dominated by investigation of the CHF and phase change behaviour, He-cooled components operate entirely in the gas phase.

In water-cooled components

The CHF of a fluid describes the upper limit of efficient heat transfer to a fluid, beyond which heat transfer dramatically deteriorates. In a fluid undergoing nucleate boiling (where bubbles of gas break away from the heated surface). The process is typically characterised by the formation of an insulating vapour film between the cooling pipe wall and the main body of the coolant fluid (Donnelly 1985). The CHF ratio is the ratio of the CHF to the incident heat flux at the boundary of the coolant channel. Analysis of the ability of the ITER divertor to handle 20MW m^{-2} transients over 10s and the impact of the CHF on the design is presented in (A.R. Raffray *et al.* 1999). It is found that a suitable CHF safety margin (with 2.0 stated as desirable) is possibly achievable with the since deprecated ITER-style CFC monoblock for heat loads up to 25MW m^{-2} . A detailed analysis of film boiling in water-cooled divertor systems with a swirl tape is presented in (Yagov and Dedov 2009) and finds good agreement between turbulence modelling and experimental data at moderate pressures. The relationship between CHF and flow rate, including a calculation method, is discussed in (Dedov 2010). Divertor components often rely on sub-cooled boiling flow, where the bulk average temperature is less than the saturation temperature. This is favoured for many high heat flux situations due to the increased efficiency associated with the latent heat of vaporisation which increases cooling performance over single-phase flow (Alatrash *et al.* 2022). An analysis of correlations for the description of sub-cooled boiling flow is presented in (Ping Liu *et al.* 2021), which finds average errors in literature correlations of between 18.18-78.69%. A new correlation is developed which reduces this error to around 10%.

(Domalapally and Entler 2015) notes that the thermo-mechanical advantages of the swirl tube could be combined with the thermal-hydraulic advantages possessed by the hypervapotron in the form of a screw-tube: a pipe with helical grooves also referred to as rifling. This is not the first time this solution has been suggested, however, with (C. B. Baxi 1995) recommending a similar approach (discussed further in Section 2.4.9).

The thermal-hydraulic performance of the water-cooled twist tape for use in ITER-style monoblock divertors is discussed at length in (Clark 2017). Twisted tapes (also known as swirl tapes) were found to improve thermal performance but result in greater pressure losses.

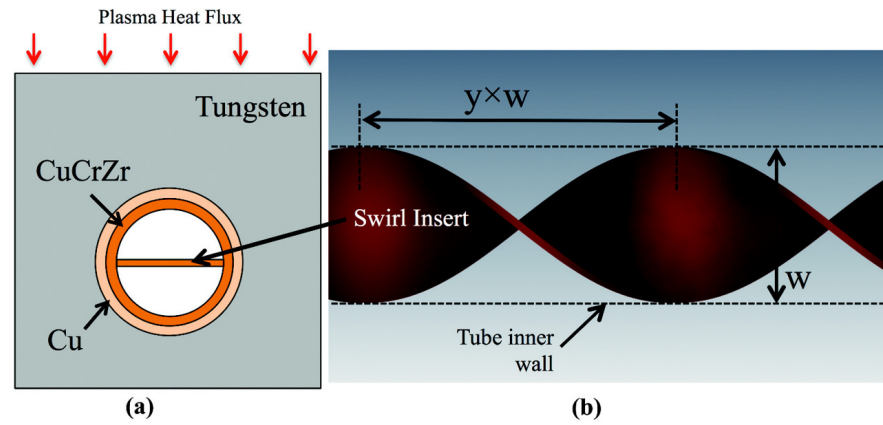


Figure 2.9. Schematic illustrating a swirl insert used to promote fluid mixing in the ITER monoblock concept, reproduced from (Wiggins, Cabral, and Carasik 2021)

Twisted tape simulations at conditions representative of the W7-X stellarator resulted in boiling in several regions, limiting the applicability of results from studies relying on single-phase heat transfer correlations. Furthermore, despite attempts to experimentally verify flow conditions, it was not clear which turbulence model most accurately represented the flow. (El-Morshedy 2021) finds that an ITER monoblock under a heat load of 15MW m^{-2} without a swirl tape has a minimum CHF margin of under 1.4, which is the minimum allowable value for ITER. The addition of a swirl tape increases the ratio to 2.38 at 20MW m^{-2} . Melting of the upper W surface was found to occur, however, the Cu temperatures were found to remain below the melting point. This indicates that, for the swirl tape design, more heat could be extracted to reduce the likelihood of melting without exceeding a safe CHF ratio. (Wiggins, Cabral, and Carasik 2021) finds that surface roughness caused by thermal fatigue from the cyclic loading of a twist tape geometry (illustrated in Fig. 2.9 leads to increased heat transfer and pressure drop. The design reduces in efficiency over time, however, which may lead to the materials exceeding operational temperature limits. The study is limited to the investigation of a uniform heat flux but it is proposed that the scenario would likely be worse in a more realistic one-sided loading configuration.

The impact of using Eurofer as a structural material for an ITER-like DEMO monoblock design is investigated in (Richou, Li-Puma, and Visca 2014), where water velocity is maximised to enhance heat transfer. In the most favourable thermal-hydraulic case analysed, the design was found to be limited by the CHF and rules against progressive deformation and ratcheting. Modelling of transient loads on an ITER-like monoblock concept for DEMO in (Maviglia *et al.* 2016) shows that if the water temperature is above 160°C , the limiting factor is the CHF (causing vapour film build-up and loss of cooling) but below this temperature, the limiting factor is the melting of the W armour surface. The THAMES code, discussed in (Thomas R. Barrett *et al.* 2016) has been developed to enable rapid design exploration for thermal-hydraulic concepts.

Table 2.3. Comparison of He cooled concept thermal hydraulic performance reproduced from (Hermsmeyer and Kleefeldt 2001)

Divertor concept	Max fluid/structure interface [°C]	Ratio of pumping power to thermal power [%]
Porous medium	880	1
Multi-channel	1240	2.3
Swirl rod	1170	2.5
Eccentric swirl promoter	1080	2.3
Slot	1090	0.7

In He-cooled components

Typical parameters for evaluating thermal-hydraulic performance of divertor components are pressure drop and a temperature metric (either surface or wall temperature). Numerical thermal-hydraulic benchmarking for porous He-cooled concepts was performed in (Hermsmeyer and Kleefeldt 2001) based largely on heat transfer correlations derived in (J. Rosenfeld and Lindemuth 1993) and is shown in Table 2.3.

Table 2.3 shows significant variation in the ratio of pumping power to thermal power, where lower values represent more efficient cooling. The slot and porous medium concepts perform best on this measure, however, the study represents an early stage of development. It is noted that further research is needed to assess the impact of surface roughness on heat transfer and to better understand heat transfer coefficients in porous material. More details on the geometry of these designs can be found in Section 2.4.9. Furthermore, it is noted that the porous medium concept has the highest level of uncertainty. This is a recurring problem in fusion research where a lack of consistent knowledge about component performance tends to favour poorly characterised designs. (Prachai Norajitra, Giniyatulin, *et al.* 2008) evaluates the performance of the EU He-cooled divertor for DEMO at 600°C and 10MPa. Mock-ups of the component were found to handle heat fluxes of up to 11MW m⁻² for 100 cycles without observable deterioration.

Thermal-hydraulic optimisation

The thermal hydraulics of water cooled divertors is discussed in (C. Baxi 2001) where it is found that pumping in a poloidal direction requires an order of magnitude less power than in the toroidal direction due to the highly peaked heat flux in the poloidal direction. If the flow is directed in the poloidal direction, the cooling geometry can accommodate the localised peak in heat flux without needing to support it over its entire length. Heat transfer enhancement techniques (of which the swirl tape is the most mature) are found to reduce the required pumping power, flow rate and pressure drop. The paper also includes recommendations such as the best practice of maintaining a CHF ratio factor of at least 1.5, and a recommended method of analysis for fusion thermal hydraulic studies. A recent modification to the monoblock concept in (Kwon, Im, and J. S. Park 2017) investigates reversing the convention established in (C. Baxi 2001) for poloidally directed cooling channels, arguing that toroidal channels enable local modifications to material properties. This concept employs CuCrZr heat sinks in the high heat flux regions and RAFM heat sinks, which permit higher

coolant temperatures, suitable for power generation, in lower heat-flux regions. This was found to be effective, however, the use of two separate coolant scenarios adds complexity to the system. Further optimisation of the design using statistical tools and CFD in (Kwon, Im, and J. S. Park 2018) results in a thinner tube and smaller monoblock for the RAFM design. The use of thermal-hydraulics to lead design optimisation results in a distinct concept for the divertor not seen in other approaches. An investigation into the optimisation of cooling circuit manifolding for the DEMO divertor cassette in (Di Maio *et al.* 2018) finds that a more gradual expansion of flow in the supply of coolant to the monoblocks results in a lower pressure drop with less turbulent re-circulation.

2.4.9 Cooling pipe geometries and design concepts

The next section describes the range of techniques that are commonly used to improve heat transfer in PFCs.

Internal heat transfer enhancement

(C B Baxi and Wong 2000) includes a general discussion on PFC heat transfer enhancement techniques, and it is speculated that heat transfer enhancement techniques which rely on increasing the thermal conductivity of the system through the addition of micro-fins or porous media will be unsuitable for future devices that rely on low activation, low thermal conductivity materials. Jet impingement cooling is also criticised for its reliance on high fluid velocity (and therefore high pressure drop) and manifolding difficulty. The addition of particulates to coolant gases is identified as a method to improve heat transfer, but it is thought to lead to complex filtering systems and erosion/blockage of the coolant channels. The preferred solution is a variation on the swirl tape known as the swirl rod insert, which has fins instead of a twist.

(Lim *et al.* 2018) uses CFD and shape optimisation to compute the optimal cross-section for a monoblock concept. The ratio of incident heat flux at the monoblock surface to the peak heat flux at the top of the cooling pipe is usually 1.4 – 1.5 for circular cross-section pipes, concentrating an already difficult to tolerate heat flux. A 3D CFD verification study using $\kappa - \epsilon$ turbulence and a two-phase flow model finds a 78% reduction in heat flux concentration for the elliptical cross-sections illustrated in Fig. 2.10.

Hypervapotrons

The ‘hypervapotron’ technique (illustrated in Fig. 2.11) involves placing fins in the cooling pipe, transverse to flow direction and allows the base of the fin to operate above the CHF while the rest of the fin operates near the condition for stable nucleate boiling, allowing for very efficient heat transfer (Cattadori *et al.* 1993).

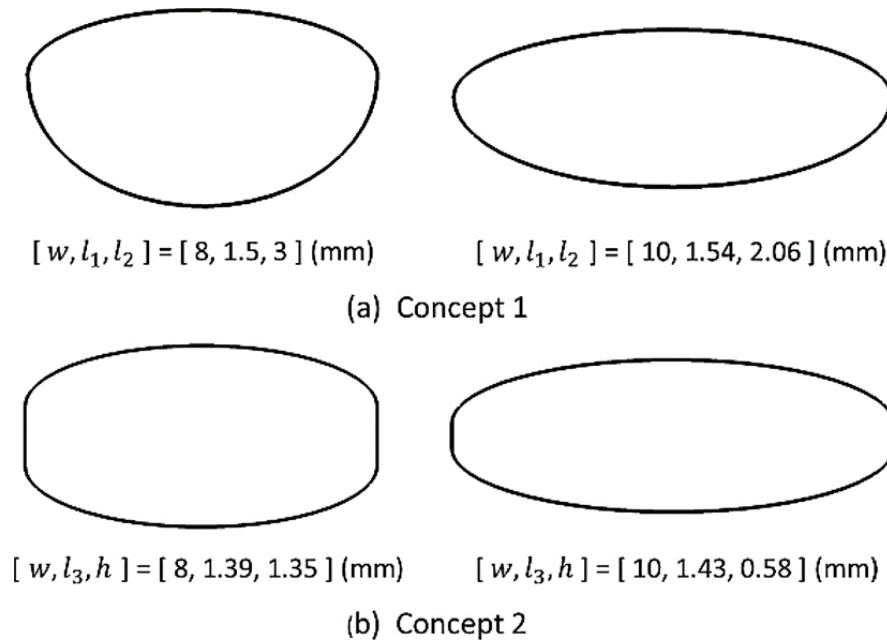


Figure 2.10. Shape optimised elliptical monoblock cooling pipe profiles designed to reduce heat flux concentration. Reproduced from (Lim *et al.* 2018).

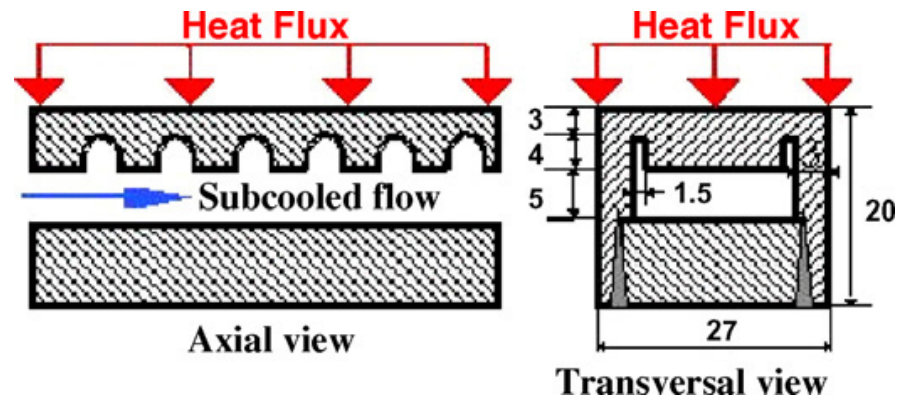


Figure 2.11. Hypervapotron component schematic, reproduced from (Pascal-Ribot *et al.* 2007).

(C. B. Baxi 1995) compares hypervapotrons and swirl tape concepts for application to the ITER divertor, finding that the hypervapotron requires approximately 10% higher pumping power and has a CHF of approximately 8% lower than the swirl tube for similar flow conditions. The swirl tube is recommended for ITER vertical targets, however, the comparative ease of manifolding with the hypervapotron is suggested as a reason for application to the central divertor dome area. A comparison is made between four monoblock variations including dual pipe designs, annular flow tubes and hypervapotron tubes. Thermal-hydraulic analysis indicated that one of the hypervapotron models showed a 30% higher incident CHF than the dual tube swirl tape configuration. Operation above 20MW m^{-2} was found to be limited by temperature and stresses in the associated Cu alloy heat sinks. A combination design containing a circular channel monoblock design with helical fins is suggested as the best compromise between durability and high heat flux performance.

(Milnes, Burns, and Drikakis 2012) demonstrates a new boiling model, developed and implemented using modified commercial CFD software to describe heat transfer of sustained fluxes of $20\text{-}30\text{MW m}^{-2}$ in hypervapotrons. The new model is described as an effective tool to be used for design optimisation and virtual prototyping of hypervapotrons for future fu-

sion reactors. (Oh *et al.* 2021) combines the hypervapotron concept with a monoblock-style armour plate. The hypervapotron includes rounded corners to the rectangular cross-section pipe designed to minimise stress concentration in the monoblock armour and assesses a number of different fin configurations in accordance with the MEAP. One of the concepts satisfies all of the MEAP rules and is proposed as a novel design for divertor vertical targets.

Jet impingement cooling

Jet impingement cooling is commonly associated with He cooling and enables a high heat removal capability using jets of coolant incident perpendicular to the plasma-facing surface. (Ihli *et al.* 2005) details a high-velocity jet design where He is filtered out of a thimble-like tube and impinges on the underside of the hot armour surface. The highly turbulent flow of the jet impinging on the wall increases coolant mixing and therefore heat transfer performance. The design involves a W armour tile that is castellated to reduce thermal stress and brazed to a W alloy cap also known as a thimble. The performance was assessed with a CFD analysis at fluxes of $8\text{-}15\text{MW m}^{-2}$ and with sufficient mass flow, the design was able to maintain a maximum thimble temperature below the stated 1300°C W recrystallisation limit.

A micro-channel geometry is compared to an early investigation of a jet-impingement design in (D. Y. Lee and Vafai 1999). The comparison is made difficult due to the fundamental differences in the designs, however, at their respective optimal operational conditions, it is found that the jet impingement design requires a high coolant flow rate but has a comparatively low pressure drop. The micro-channel exhibits a large pressure drop but has lower coolant flow requirements. (Yoda and S. I. Abdel-Khalik 2017) discusses the thermal hydraulics of several impinging-jet concepts due to recent anomalous experimental results and finds potential for optimisation of the He-cooled modular divertor with multiple jets (HEMJ) design. (D. S. Lee *et al.* 2019) investigates these anomalies experimentally and finds manufacturing discrepancies as a potential explanation.

Porous cooling media

A dual channel porous metal He cooled divertor module is discussed in (D. L. Youchison *et al.* 2000) where finite element software was used to model the effective heat transfer coefficient inside the divertor module. One drawback with multichannel designs is a flow instability known as ‘dynamic plugging’ where a decrease in pressure due to localised heating of one channel leads to a density decrease and associated pressure drop. The colder channel then experiences an increased mass flow which equalises the pressure drop, however, this results in increasingly uneven cooling performance, possibly leading to failure. In addition to their use in gas-cooled components, porous geometries have also been proposed for liquid-metal-cooled systems. (J. Rosenfeld and Lindemuth 1993) discusses a He/Cu porous heat exchanger tested for fusion, which demonstrated tolerance of 15 MW m^{-2} heat fluxes without failure.

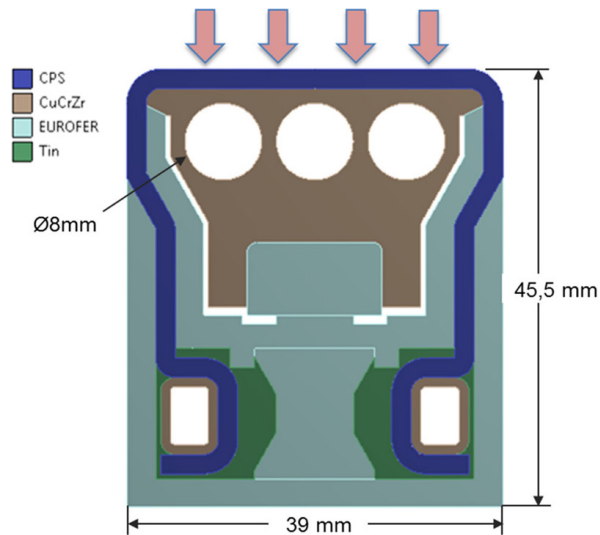


Figure 2.12. Liquid metal divertor module based on the capillary porous system concept. Arrows on the top surface indicate the direction of heat flux loading. Reproduced from (Roccella *et al.* 2020)

Liquid metal geometries

Liquid Metal PFC concepts have been proposed for use in tokamaks as early as 1974 (Wisconsin Univ 1974), as discussed in (Muraviev 1995) which considers Ga as a PFC material. Liquid metal plasma-facing surfaces have been tested in operational tokamaks, including NSTX (Ono *et al.* 2013), where they were found to reduce peak flux by more than 50% due to radiative heat transfer by vaporised Li. The application of liquid Li to W PFC surfaces such as those found in ITER is also proposed, if a way to maintain purity and re-supply is found. Liquid Li-Pb components were also considered as part of the PPCS (A. Li Puma *et al.* 2003).

Liquid metal PFCs are reviewed in (R.E. Nygren and Tabarés 2016), which focuses on Capillary Pore Systems (CPS) that use a pore structure to supply a plasma-facing surface with liquid metal using capillary action. CPS are considered the most mature technology and are engineered to enhance liquid surface stability. Liquid Li PFCs were found to suffer from low maximum temperatures, however, vapour shielding, whereby a dense cloud of evaporated neutrals protects the surface from further evaporation, could allow for higher operating temperatures. Liquid Li PFCs were also found to contribute to plasma disruption suppression and confinement time increases. A forced convection liquid metal divertor concept discussed in (Ferrari *et al.* 2001), uses both Pb¹⁷Li and SnLi, with SiC insulation to reduce MHD-induced pressure drops. The concept was found to be capable of tolerating a maximum heat flux of 5MW m^{-2} . Two evaporation-based liquid metal concepts are discussed in (Reimann *et al.* 2001), where it is recommended that the concepts be combined with liquid metal or gas-cooled blankets to take advantage of the efficiency gained by operating at higher temperatures. The concepts proposed in (Kurihara 2002) include one which utilises liquid-solid multi-phase flow to exploit the latent heat of fusion associated with melting suspended particles to increase the heat capacity. In (Roccella *et al.* 2020), a liquid metal CPS concept (illustrated in Fig.2.12) is presented that demonstrates the use of liquid Sn as both the armour and coolant. The armour surface is made up of a porous mesh infiltrated with liquid Sn to

prevent excessive MHD interaction. This is refilled by capillary action from three coolant channels. Whilst initial results place the concept in-line with required DEMO performance characteristics, further development of 3D FEA and CFD models is required.

2.5 Summary of findings

This review has discussed divertor design at a number of different levels, from the performance of individual components to the impact divertor choice has on the operation of a power plant and potential influences on the safety case of a reactor. It was found that much of the world's fusion research capability is tied to the development of ITER, delaying progress and increasing the risk for the development of alternate technological pathways. Top-down constraints such as the low activation criterion were found to create additional challenges for material selection, with several recent studies suggesting that operating within the required activation limits may be unfeasible, hindering the development of commercially viable fusion reactors.

The discussion of reactor systems codes established that some codes, including PROCESS, are seen as not conducive to significant design deviations, due to the long associated implementation time. It is also clear that the heat flux handling requirements for future divertor targets have significant levels of uncertainty which challenge efficient design and make progress difficult to assess. Furthermore, as the design of fusion reactor components is device-led, with large periods of time between devices, research progress tends to be non-linear. Concepts are pursued up to the engineering design of a device and then abandoned for many years. Consequently, there are surprising similarities in the content and results of some papers published 20 years apart. Significant progress has been made in the development of advanced divertor configurations with extended legs or additional strike points. These may lower the heat flux handling requirements of the target plates, however, their operation is not fully understood and therefore they cannot be fully relied upon. Divertor design is further constrained due to systems integration issues, including the desire in some cases to use a single coolant for the divertor and first wall. Where divertor heat is used for electricity generation, this must be incorporated into the power plant thermodynamic cycle, possibly resulting in compromises to its primary functionality. It is also clear that divertor heat flux handling capability strongly drives design complexity, size and cost. Additionally, the transition to more advanced divertor technologies including liquid metal, is challenged by the difficulty of implementing novel technologies in a multi-decade reactor project and by the lack of representative test facilities to develop operational confidence. This also presents a challenge to effective decision-making. Water cooling, for example, is well-characterised, reliable, and thought to be unsuitable for commercial devices. Other coolants are less well understood and therefore their drawbacks are less well characterised, which appears to provide them with false attractiveness. Conductive liquid metals, for example, can be subject to enhanced pressure drops as a result of induced Lorentz forces from the magnetic fields in the tokamak. This may pose unquantified challenges to coolant circulation.

Design codes such as the MEAP are starting to accelerate progress towards design by analysis for divertor components, and many advanced monoblock concepts have been proposed. Despite this, some reactor design codes are still based on fission pressure-vessel codes that are of limited applicability. Finally, significant risks to future divertor operation include poorly characterised transient events which may result in heat loads several times the engineering limit, cyclic loading, and heat concentration on leading edges.

2.6 Additional commentary on Chapter 2

The uncertainties in divertor target operational requirements and in the viability of different armour-coolant combinations undoubtedly slow fusion development. Due to the interplay between extreme heat loads, neutron radiation damage, safety, environmental concerns and cost, engineering design for nuclear fusion requires inherent compromise. To make these compromises effectively, without subjective tweaking of designs and disputes between stakeholders who envisage vastly different operating conditions, engineers need to be able to fully understand the environment in which the components will be used. It is suggested that, as a significant level of design uncertainty still exists, more attention is devoted to design methodology, including novel techniques for optimising designs and areas of rapid development such as machine learning, emerging manufacturing techniques such as additive manufacturing and functional grading. These techniques may be able to exploit the growing trend towards design by analysis, supported by advances in computational power, and new modelling techniques. It is also clear that more work needs to be done to develop an understanding of complex components such as the hypervapotron which until recently have defied attempts at computational description.

Progress in digital modelling techniques may eventually enable engineering development to be decoupled from the timescales involved in building fusion reactors. This may be important in order to design components which capitalise on developments made in emerging fields relating to computing and manufacturing, which evolve on much shorter timescales than fusion. It is also not clear that the large jumps in technological maturity expected between ITER and DEMO are optimal for the time-efficient development of a fusion power plant. This is compounded by the ongoing lack of facilities for testing components in fusion-relevant conditions outside of experimental reactors, which are designed primarily to investigate plasma physics scenarios. Whilst devices such as the Divertor Test Tokamak (DTT) (Crisanti *et al.* 2017) and the IFMIF-EVEDA project (Knaster *et al.* 2017), aim to close this gap, they have not yet been realised.

At any point in the development and construction of a fusion reactor, the emergence of novel technologies, data or modelling techniques may render any part of the device obsolete. If this happens mid reactor-cycle, it is important that the implications are taken seriously for the development of future designs. Whilst some fusion programmes run parallel research and development studies looking at the viability of alternate component designs, it is put forward that a set of reactor ‘digital cousins’ could be maintained, consisting of reactor ‘digital twins’

with different choices made for the design of critical components such as the divertor. These could then be updated to include contemporary results relating to reactor operation and emerging manufacturing technologies. Whilst there would be an inherent error and some subjectivity in ‘translating’ operational results into a different design, these models could be used to inform long-term design decisions, somewhat similar to the use of systems codes to optimise designs before construction. Fusion reactor design has a history of returning to previously abandoned ideas when it is time to build a new device. Work on a more flexible system which permits some level of mid-cycle redesign could perhaps help fusion reach commercial competitiveness on a shorter timescale than might otherwise be possible.

Chapter 3

Paper 2 - Thermal Testing of Additively Manufactured CuCrZr Samples for Application to Nuclear Fusion

Thermal testing of additively manufactured CuCrZr samples for application to nuclear fusion

Oliver H.R. Marshall^{1*}, Lee Margetts¹, Llion M. Evans^{2,3} and Matthew J. Roy^{1,4}

¹ Department of Mechanical, Aerospace and Civil Engineering, George Begg Building, The University of Manchester, Manchester, United Kingdom, oliver.marshall@manchester.ac.uk, lee.margetts@manchester.ac.uk, matthew.roy@manchester.ac.uk

² College of Engineering, Swansea University, Swansea, United Kingdom, llion.evans@swansea.ac.uk

³ United Kingdom Atomic Energy Authority, Culham, United Kingdom

⁴ Henry Royce Institute, University of Manchester, United Kingdom

Abstract

Additively manufactured CuCrZr has been considered for application to heat exchange components exposed to high heat fluxes. Additive Manufacturing (AM) permits the creation of parts with complex geometries, such as those with high surface areas, designed to maximise heat transfer. One potential application area is nuclear fusion, where components designed using topology optimisation and enabled by AM could help meet the high barrier to entry associated with cooling the inside of fusion reactors. Whilst AM may permit complex geometries, the components will only be suitable for high heat flux applications if they demonstrate desirable thermal properties. This study measures the thermal expansion and diffusivity of AM CuCrZr samples using push-rod dilatometry and Laser Flash Analysis (LFA) for a temperature range of 30°C to 700°C. The samples tested were manufactured by 3T-AM as part of efforts to accelerate the build process by using high laser powers (370W to 900W). The samples built using the highest laser power (900W) and greatest layer thickness (60µm)

were found to have the highest thermal diffusivities and the lowest coefficients of thermal expansion, indicating a potential for a reduction of the associated build time.

Confidentiality

This report details the outcomes of a collaboration between the author and 3T AM, an additive manufacturing company based in Newbury, Berkshire, UK. Some details relating to the materials provided are not specified here for reasons of confidentiality, however, the testing methodology is based on standard methods.

3.1 Introduction

Additive Manufacturing (AM) enables rapid prototyping, low lead times for unique components, and the manufacture of complex geometries which would either require specialised tooling or would be unobtainable with conventional manufacturing methods. The testing performed in the present study is designed to inform the modelling of optimised heat exchange components for use in fusion reactors. Components designed for use in this context have challenging design requirements and may require both good thermal properties and a manufacturing technique that permits the creation of complex internal geometries for use in future devices (R. E. Nygren *et al.* 2016).

This study uses push-rod dilatometry to obtain material coefficients of thermal expansion. This data is then used in the correction of thermal diffusivity data, obtained using Laser Flash Analysis (LFA).

3.1.1 CuCrZr properties

CuCrZr is a precipitation-hardened alloy, in which Cr and Zr particles improve the strength and thermal conductivity of the material, but exhibit low solubility, which limits their addition (Brotzu *et al.* 2019). Furthermore, the resulting mechanical properties are highly dependent on heat treatments (Barabash *et al.* 2011). Unlike other Cu alloys which have low absorption coefficients for infra-red light, CuCrZr allows for dense part fabrication using laser sintering AM techniques due to its higher absorption coefficient (Wallis and Buchmayr 2019). CuCrZr has found application in integrated circuits, network cables, high-speed railways and heat sinks for aerospace and nuclear fusion, however, it has been associated with manufacturing difficulty, such that that AM has been proposed as a solution (F. Sun *et al.* 2020).

The CuCrZr samples used in this study were manufactured by 3T Additive Manufacturing as part of ongoing research to optimise the build process. The material composition for the CuCrZr in wt. % is presented in Table 3.1 with the corresponding at. % of the main constituents shown in Table 3.2. A ternary phase diagram (showing possible phases of

constituent elements at constant pressure and temperature) for CuCrZr at 940°C is presented in Fig. 3.1. Vertical cross sections (showing variation with temperature) at relevant at.% of Cr are presented in Fig. 3.2. In both cases, the operational space relevant to this study, given the uncertainty in chemical composition shown in Tables 3.1 and 3.2, is highlighted. It is evident that whilst two different phases may exist in the material, at the maximum operating temperature of 800°C (1073.15K) the material should remain in the solid regime, with no liquid phases expected. The presence of (Cu)+(Cr)+5 and 5+51+(Cr) particles in the material in unknown quantities may however be the cause of some variation in the thermal performance. The operational temperature limit for CuCrZr in the divertor is thought to be around 350°C due to the effects of radiation damage and thermal creep (Galatanu *et al.* 2019), however, for purposes of characterisation, a wider temperature range is investigated in this study. The goal of this study is to establish the thermal characteristics of the CuCrZr samples both for application to fusion reactor components and as part of ongoing process optimisation at 3T AM.

3.1.2 The importance of process optimisation

It is sometimes said about AM that, ‘complexity is free’. This statement may be considered correct to the extent that the process does not require the development of new tooling for novel designs and thus additional complexity can be added to existing geometries without requiring extensive development of new machinery. Conversely, it is not the case that the addition of geometrically complex features does not incur costs associated with an extended build time and the potential for lower material quality. More complex parts may take significantly longer to build and can consume more material (Pradel *et al.* 2017). The acceleration of build speed is considered crucial to making AM components commercially competitive (Thomas and S. W. Gilbert 2014), and the possibilities for bespoke components with optimised geometries may only be considered if the price is not prohibitive.

3.2 Methodology

Coefficients of thermal expansion are obtained using push-rod dilatometry. Thermal diffusivity is measured using a laser flash analyser. The methodology reported here is designed to comply as much as possible with the ASTM standards established in (ASTM-E1461-13 2013) and (ASTM-E228–17 2017), for obtaining thermal diffusivity by the laser flash method and linear thermal expansion of solid materials with a push-rod dilatometer respectively.

3.2.1 Material and preparation

The Direct Metal Laser Sintering (DMLS) process used for manufacture uses a laser to sinter the CuCrZr powder, creating a part which is manufactured one layer at a time with

a layer thickness on the order of tens of μm (Yadroitsev and Smurov 2010). Increasing the laser power from the standard level of approximately 300W (Buchmayr *et al.* 2017) to 900W allows for these layers to be sintered more quickly as it takes less time for the powder to reach the required temperature. The decrease in build time results in a cost reduction as machine time is a key limiting factor in the speed of manufacture (Thomas and S. W. Gilbert 2014). Any increase in power must be balanced with a number of other parameters including hatch distance (the separation between consecutive laser paths) and layer thickness to maintain a reasonable energy density.

3.2.2 Process optimisation

The optimisation of build parameters and any post-build heat treatments are key influences on the final performance characteristics of metal AM parts. In (Wallis and Buchmayr 2019), untreated as-built CuCrZr had a thermal conductivity of $100 \pm 2\text{W}/(\text{m K})$, approximately a third of the thermal conductivity expected for conventionally manufactured parts. The highest recorded thermal conductivity after solution annealing and age hardening was $297 \pm 6\text{W}/(\text{m K})$, still significantly less than the expected $320\text{W}/(\text{m K})$.

The CuCrZr samples used in this study for experimental testing were built using a modified EOS 290 metal sintering machine with a 1kW Yb-fibre laser, capable of a build speed of $2 - 8\text{mm}^3 \text{s}^{-1}$ (dependent on material) and a layer thickness of 20-100 μm . The Archimedes method was used to measure the as-manufactured density by engineers at 3T AM, finding an average relative density of 98.54%, where the standard deviation across these results was 0.23%. The build parameters for each laser power were chosen to ensure material sintered correctly without burning, taking into account factors such as material reflectivity, conductivity and powder size. After building, the components were subjected to a proprietary heat treatment process. More information on standard heat treatments for AM CuCrZr alloys can be found in (Ivanov *et al.* 2002). The energy density used in the build process can be described as a function of laser power (P), scan speed (ν), hatch distance (d_H) and layer thickness (t) as shown in Eq. 3.1.

$$E = \frac{P}{\nu \times d_H \times t} \quad (3.1)$$

The exact values of some process parameters including scan speed, scanning pattern, atmosphere, powder bed temperature and hatch distance - which may all influence part quality (Yadroitsev and Smurov 2010) - are kept confidential by 3T Additive Manufacturing due to the associated business opportunity related to build speed optimisation.

Layer thickness influences the stability of the material sintered by the progress of the laser across the build plate and needs to be balanced carefully to avoid “balling” of the material and instability (Yadroitsev and Smurov 2010). In this study, the samples were built for two separate layer thicknesses, 30 μm and 60 μm . The thinner the layer thickness, the longer a component takes to build as more layers are required for a given volume, and therefore the



Figure 3.3. (1) Cylinders for LFA before machining to correct dimensions, showing discoloured surfaces due to heat treatment. (2) Larger diameter cylinders for LFA and smaller diameter cylinders for dilatometry after machining to correct diameter but before sectioning.

higher the associated cost. An optimum layer thickness provides the detail and material properties required in the part, allowing for sufficient penetration of the laser without unnecessarily increasing build time (Yadroitsev and Smurov 2010). The balance between build parameters for all different laser powers was chosen by engineers at 3T Additive Manufacturing in an attempt to maximise part density, as this is a good predictor of suitable material properties (Wallis and Buchmayr 2019).

3.2.3 Build parameters

The laser power is increased from the standard 370W CuCrZr process to 900W with samples built at 370W, 540W, 710W and 900W. In this study, samples from the extremes of laser power are tested to assess the difference between the standard process and the highest laser power, representing the fastest build time.

3.2.4 Machining

Fig. 3.3 shows the samples before any machining was performed (labelled as (1)), and after the discoloured surface layer was removed by engineers at 3T-AM (labelled as (2)). Electrical Discharge Machining (EDM) was the chosen technique for sectioning the sample cylinders into discs suitable for LFA and dilatometry. For LFA, discs with a 12.5mm diameter, and a 4mm depth were required. A thicker than average 4mm sample depth was chosen due to the high thermal conductivity of copper alloys. The dilatometry setup required cylinders with a 6mm diameter and a 10mm depth. EDM was chosen as it modifies a smaller region of material than other cutting techniques, however, it does have an associated recast layer caused by local heating of the material, and beyond that, a Heat Affected Zone (HAZ) (Newton *et al.* 2009). Residual stresses caused by EDM of mild steel were found to affect a layer



Figure 3.4. A selection of machined samples is displayed. The flatter samples on the left-hand side are for laser flash analysis and the small diameter cylinders on the right-hand side are for dilatometry. The image also includes the ends of the cylinders, which were not used for testing.

approximately 10 times the Centre Line Average (CLA) - a measure for surface roughness. This residual stress arises due to the thermal dilation of the heated material. The heated material exceeds the maximum elastic strain limit and deforms plastically. Plastic deformation during material cooling leads to layers of deformed material that are now shorter than the unaffected material and thus residual stress arises between the two layers (Barash 1962). The impact of this is not included in the results, however, due to a lack of data for CuCrZr in the literature and the lack of processes available to reliably remove this layer without causing further damage. It is however thought that any impact is likely to be negligible compared to other sources of uncertainty in the methodology. After machining, samples are referred to with two-digit names ($X.Y$) where the first digit of the sample name refers to the cylinder it was built in, and the second digit refers to the location in that cylinder. Samples with the same first digit have therefore been manufactured using the same parameters. A selection of machined samples can be seen in Fig. 3.4.

3.2.5 Method for obtaining coefficients of thermal expansion

Material expansion with temperature is required for the calibration of the laser flash experiments, and as most of the samples have been made with different build parameters, it was reasonable to expect that the coefficient of thermal expansion would vary for each sample. Due to the constraints imposed on the time frame for experimental work, this study focuses on the extremes of the sample laser power build parameters: 370W and 900W for the 30 μ m and 60 μ m layer thicknesses. The linear thermal expansion is representative of the change in length ΔL with respect to the initial specimen length L_0 and is calculated as shown in Eq. 3.2 between temperatures T_0 and T_1 . This ratio is typically displayed in units of $\mu\text{m m}^{-1}$.

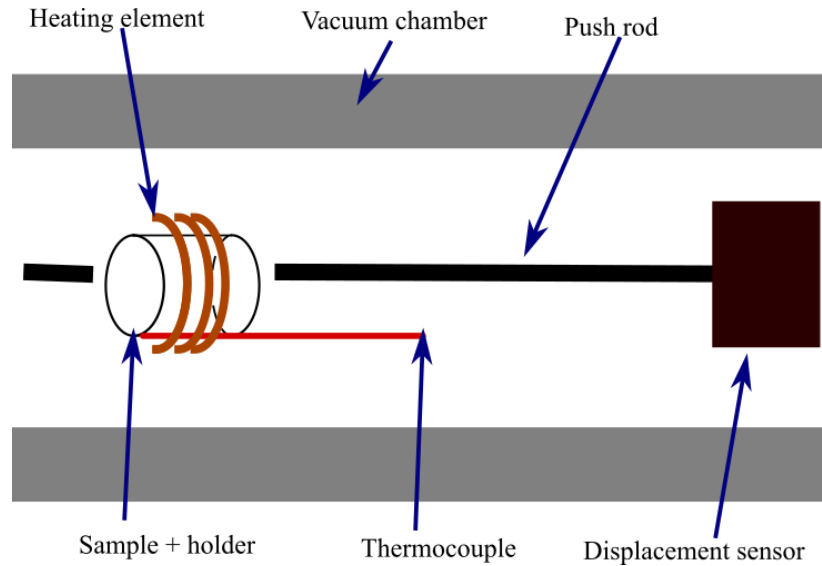


Figure 3.5. Push-rod dilatometer showing the sample placed in a heating element where it is raised to the required temperature and the push-rod through which its resulting expansion is measured.

$$\frac{\Delta L}{L_0} = \frac{L_1 - L_0}{L_0} \quad (3.2)$$

The mean thermal expansion coefficient is defined as the ratio between the material expansion and the temperature difference it is caused by, as shown in Eq. 3.3. In Ref. (ASTM-E228–17 2017), this coefficient is always determined from the initial temperature and so when the mean thermal expansion coefficient is determined for a series of increasing temperatures, each subsequent coefficient is a progressive estimate of an overall mean coefficient of thermal expansion.

$$\alpha_m = \frac{1}{L_0} \frac{\Delta L}{\Delta T} \quad (3.3)$$

The coefficient of thermal expansion was measured for the CuCrZr samples using push-rod dilatometry. The dilatometer used was the TA Instruments DIL805 A/D/T and the work was performed at the University of Manchester, in the School of Materials. A diagram of a push-rod dilatometer is shown in Fig. 3.5.

The goal of push-rod dilatometry is to measure the thermal expansion of a sample. This is obtained simply by measuring the change in length of a sample whilst it is subjected to a thermal cycle. The method requires careful calibration, however, in order to provide accurate results, as material thermal expansion at standard temperature ranges is typically a small fraction of the overall sample length. The machine also relies on many moving parts and care must be taken during operation not to damage any components. The sample holders, for example, are typically made from quartz or glass, as can be seen in Fig. 3.6.

In push-rod dilatometry, a sample is placed in a sample holder and in contact with a push-rod. The push-rod can move in response to thermal expansion, enabling registration of change in length data. The sample then slides horizontally such that it is placed inside an inductive heating coil. The machine is then sealed so that the air can be evacuated and the test chamber can be backfilled with inert gas. The machine then needs to be zeroed to establish an initial

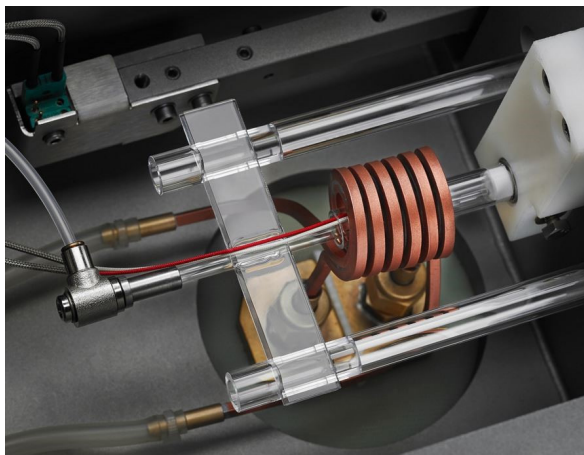


Figure 3.6. Close-up view of push-rod dilatometer sample holder and inductive heating coil.

starting point for obtaining change in length data. The sample can then be subjected to a thermal test cycle.

Sample preparation is important. The opposing faces need to be perpendicular and evenly machined and the dimensions need to be suitable for the target machine. Furthermore, a thermocouple needs to be attached directly to the sample to ensure accurate readings during the heating cycle. Thermocouples are typically attached to the samples under test by spot welding, however, due to the high conductivity material used in this study, the thermocouple wires were wrapped around the sample, as discussed in Section 3.4.5. The sample holder and push-rod must be made of the same material to ensure a consistent rate of thermal expansion. Despite this, the machine must be calibrated before use, as detailed in Section 3.3.1. The specific details of the testing parameters used are presented in Section 3.3.1 and an in-depth description of the test method can be found in (ASTM-E228–17 2017).

3.2.6 Method for obtaining thermal diffusivity

The thermal diffusivity (D) of the CuCrZr was measured using the technique of Laser Flash Analysis (LFA), performed at the University of Manchester, using the Netzsch 427 machine in the School of Materials. A diagram of a typical laser flash analyser is shown in Fig. 3.7.

The technique involves a high-intensity energy pulse directed at the front face of a thin cylindrical specimen heated to the temperature for which the thermal diffusivity data is required. The laser pulse is absorbed, transferred through the material, and the temperature rise on the rear face is measured. The technique therefore measures the transient thermal response of the material. As the laser pulse is directed perpendicularly to the material, the thermal diffusivity is only measured in one direction and any material anisotropy is not accounted for. In LFA, the thermal diffusivity is calculated using the half-rise time $t_{1/2}$, (the time taken for the sample to reach half of the maximum recorded temperature) and the specimen thickness L through the relation shown in Eq. 3.4.

$$D = 0.13879L^2/t_{1/2} \quad (3.4)$$

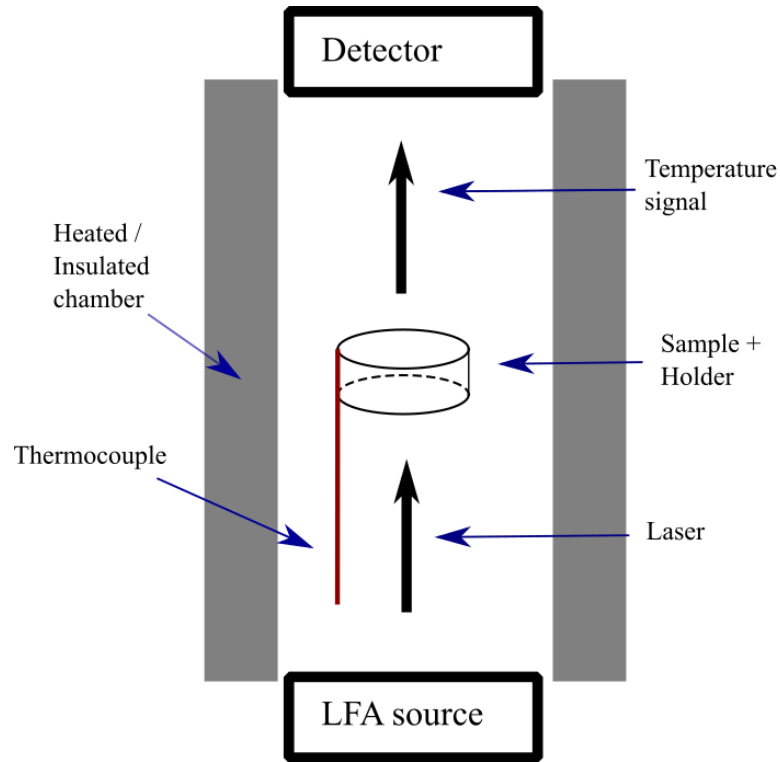


Figure 3.7. Schematic of a laser flash analyser showing the placement of the sample in the path of the laser power source and the detector on the opposing side.

Thermal diffusivity (D) can be related to thermal conductivity (λ) if the specific heat capacity (C_p) at constant pressure, and the mass density (ρ) are known, as described in Eq. 3.5. Note that all of these quantities are functions of temperature.

$$\lambda = DC_p\rho \quad (3.5)$$

As the time taken for the heat imparted by the laser pulse to be conducted through the sample is typically on the order of milliseconds, several successive measurements can be made quickly. In this study, the average of five shots is taken. This also ensures that any poorly performing shots do not require full repeats of the experiment. The sample is then heated to the next test temperature before the laser pulses are repeated. Full discussion of the test method is provided in (ASTM-E1461-13 2013).

Correction for thermal expansion

Thermal diffusivity is dependent on sample length (cylinder height) as seen in Eq. 3.4, and therefore on density, as shown in Eq. 3.5. This dependence is corrected for by incorporating the thermal expansion measurements obtained through dilatometry. Rearranging Eq. 3.3 results in an expression for ΔL which can be added as a length correction to Eq. 3.4 and evaluated as shown in Eqs. 3.6, 3.7 and 3.8.

$$\Delta L = \alpha_m \Delta T L_0 \quad (3.6)$$

$$D = 0.13879(L + \Delta L)^2/t_{1/2} \quad (3.7)$$

Table 3.3. Properties of the dilatometry test specimens chosen to provide an indication of the change in thermal properties for samples at the extremes of the laser power used.

Sample name	Laser power [W]	Layer thickness [μm]
1.3	900	60
5.2	370	60
11.3	370	30
15.2	900	30

$$D = 0.13879(L + \alpha_m \Delta T L_0)^2 / t_{1/2} \quad (3.8)$$

Correction for pulse width

The laser pulse has a non-zero width and the energy is not all deposited into the sample instantaneously, which means that an additional correction must be made to the thermal diffusivity. This correction is performed by the LFA software used to interpret the recorded data and is combined with the correction for thermal expansion obtained through dilatometry to form a final corrected result.

3.3 Results

3.3.1 Dilatometry

The samples names and process parameters for the samples tested are detailed in Table 3.3.

The push-rod dilatometer used was the DIL 805A/D/T model manufactured by TA instruments, operated in α -mode. The temperature was measured with an S-type thermocouple made of 90%Pt, 10%Rh-Pt by weight. After pumping down the system to a vacuum it was then filled with a N_2 gas, to prevent reaction with the sample at elevated temperatures. In accordance with (ASTM-E228–17 2017), a testing program was devised where the sample is heated at a constant rate of 5°C min^{-1} throughout testing. The sample is heated between $20 - 30^\circ\text{C}$ to ensure a consistent start temperature for expansion calculations despite possible variations in initial ambient temperature. It is then heated from $30 - 700^\circ\text{C}$, held at 700°C for 30 minutes and then cooled at 5°C min^{-1} . Calibration is performed through comparison to results obtained for a platinum reference material and literature data for a specified temperature range. Eq. 3.9, published in (Hahn *et al.* 1972) shows the empirical relationship between temperature and the linear expansion of platinum between 293K and 1900K used to produce the ‘Empirical equation’ data plotted in Fig. 3.8.

$$\begin{aligned} \frac{L_T - L_{293}}{L_{293}} \times 10^6 = & -2279 + 6.117T + 8.251 \times 10^{-3}T^2 - 1.1187 \times 10^{-5}T^3 \\ & + 9.1523 \times 10^{-9}T^4 - 3.6754 \times 10^{-12}T^5 + 5.893T^6 \end{aligned} \quad (3.9)$$

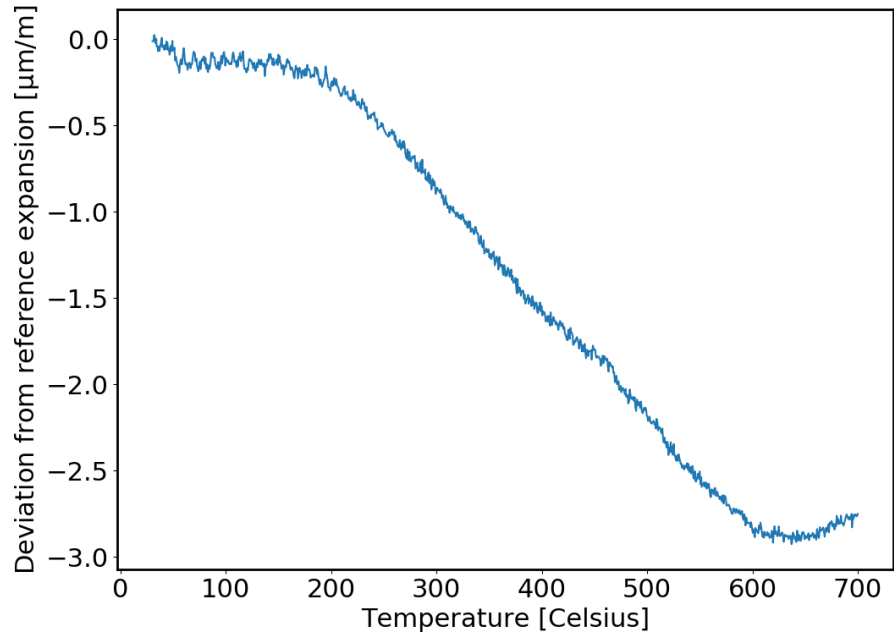


Figure 3.8. Deviation of the measured platinum sample linear thermal expansion with respect to literature reference data from (Hahn *et al.* 1972), generated using Eq. 3.9. The negative values found here indicate that the measured sample expansion was greater than that found in the literature.

A platinum sample with an initial length of $10.05 \times 10^3 \mu\text{m}$, was tested under the previously discussed test program and the difference between the measured value of $\frac{L_T - L_{293}}{L_{293}} \times 10^6$ (where L_T is the length recorded at a specific temperature T , and L_{293} , is the length recorded at 293K) is compared to that obtained from Eq. 3.9. The difference between the recorded platinum reference material and the literature expansion rate is plotted in Fig. 3.8. The experimental results are calibrated using: $A_{T_i} = [(\frac{\Delta L}{L_0})_t - (\frac{\Delta L}{L_0})_m]_{T_i}$ where the subscripts m , t and T_i refer to measured, true, and the value at temperature ‘i’, respectively. This constant is then used in the final calculation of linear expansion. Once the calibration was performed it was compared to the values for the linear thermal expansion of platinum found in (ASTM-E228–17 2017) and the values obtained from Eq. 3.9 and found to be in good agreement, as shown in Fig. 3.9.

The deviations shown in Fig. 3.9 could be influenced by impurities in the platinum sample, however, platinum is chosen as a thermal expansion reference material due to the ease of obtaining pure samples and its lack of phase changes between absolute zero and its melting point (Kirby 1991). Therefore it is likely that the deviations result primarily from the many potential mechanical, thermal and environmental factors that could cause inconsistencies in the push-rod dilatometer.

Linear thermal expansion

The linear thermal expansion of the samples tested is presented graphically in Fig. 3.10, which shows good agreement with a linear fit in all cases apart from a deviation which appears in the upper range of sample 1.3. The mean thermal expansion coefficients for the samples at intervals of 100°C are presented in Fig. 3.11. The overall coefficients of thermal

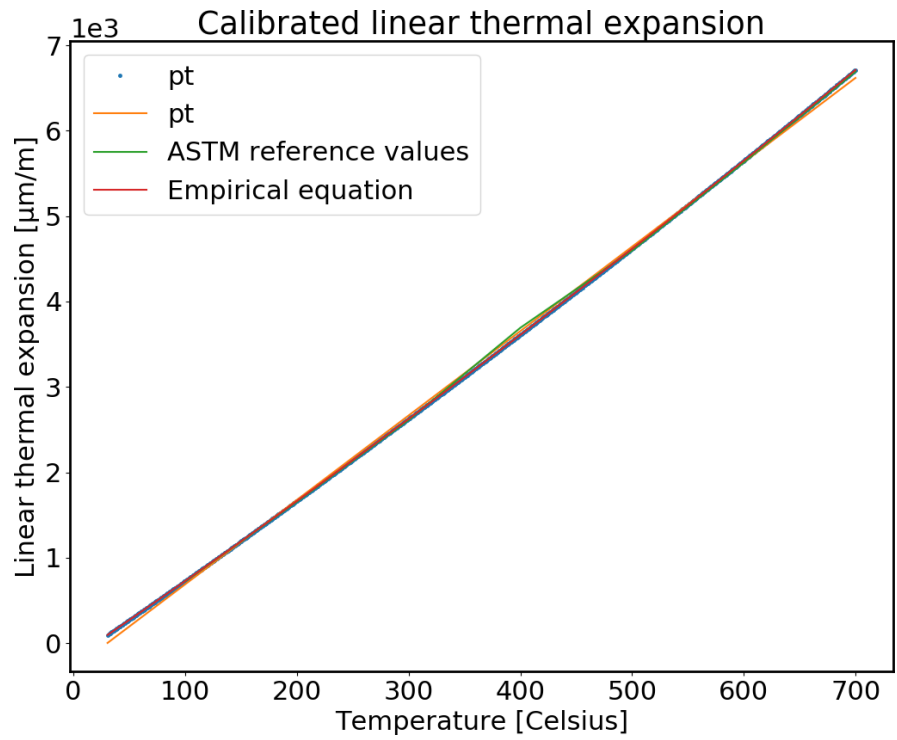


Figure 3.9. The calibration result when applied to the linear thermal expansion measurements obtained for the platinum reference sample is shown to be in good agreement with the literature values.

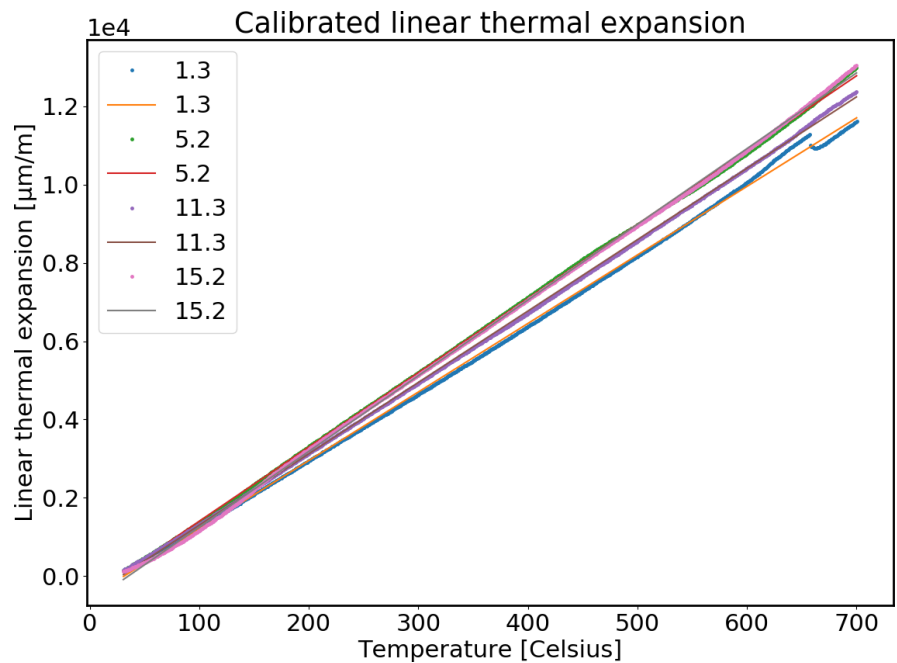


Figure 3.10. Calibrated linear thermal expansion plotted for samples heated between 30°C and 700°C. A linear function is fitted to the data and shows overall good agreement with the measured values apart from the highest temperature range for sample 1.3.

expansion, averaged over the temperature range, are detailed in Table 3.4. These are used in the calibration of the density values.

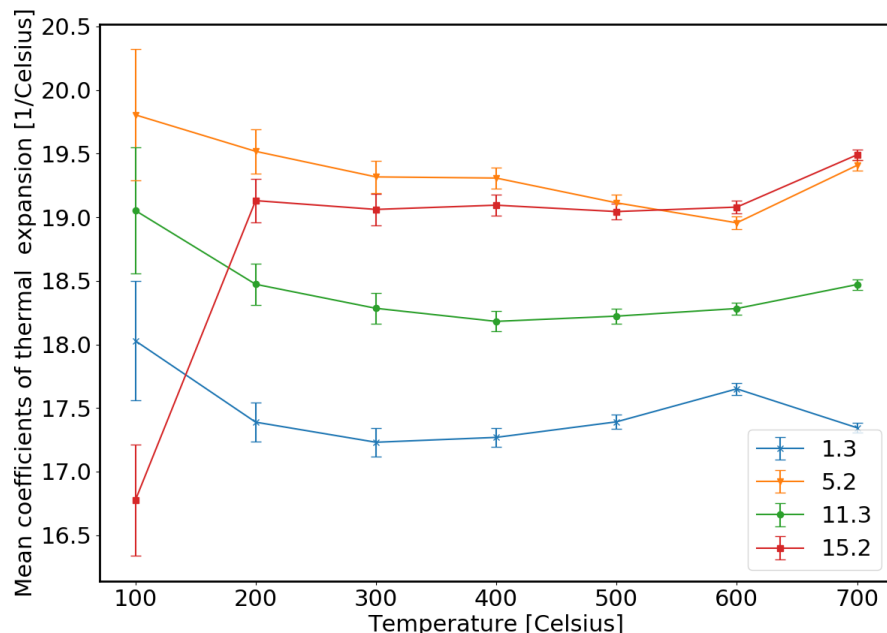


Figure 3.11. Mean coefficients of thermal expansion for the samples tested. The mean coefficients are calculated with respect to the temperature the sample is initially heated to (30°C). The first coefficient for sample 15.2 is significantly lower than the trends would suggest, which may have been caused by poor contact with the thermocouple or an off-centre placement of the sample in the dilatometer.

Table 3.4. Mean coefficients of thermal expansion.

Sample name	Laser power [W]	Mean coefficient of thermal expansion [$\mu\text{m}/\text{m}^\circ\text{C}$]
pt	n/a	9.97
1.3	900	17.3
5.2	370	19.39
11.3	370	18.45
15.2	900	19.47

Change in length data

The initial and final lengths of individual samples are measured using digital callipers. The values for the maximum and final length change for the samples tested are presented in Table 3.5. (ASTM-E228–17 2017) requires that any permanent deformations of above $20\mu\text{m m}^{-1}$ are reported. This is equivalent to $0.2\mu\text{m}$ for a 10mm sample. The same document however requires that the measuring tool must have a precision of $\pm 25\mu\text{m}$, which is much greater than the allowable deformation for a sample length on the order of tens of mm. The permanent deformation (the last recorded length change data point) for all the samples can be seen in Table 3.5. All samples, including the reference samples, exceeded the stated limit as measured by the dilatometer and so are reported.

3.3.2 Laser flash analysis

The laser flash analysis is carried out in accordance with the guidelines established in (ASTM-E1461-13 2013) where possible and it is stated where deviations are made. An example of the raw voltage signal obtained during the LFA pulse can be seen in Fig. 3.12

Table 3.5. Maximum and final length change.

Sample name	Maximum ΔL [μm]	Final ΔL [μm]	Final ΔL [$\mu\text{m m}^{-1}$]
pt	69.89	-4.66	-466
1.3	118.92	1.93	193
5.2	149.19	-0.69	-69
11.3	130.45	6.34	634
15.2	133.2	-0.28	-28

which shows a clean signal with little noise, indicating a good shot.

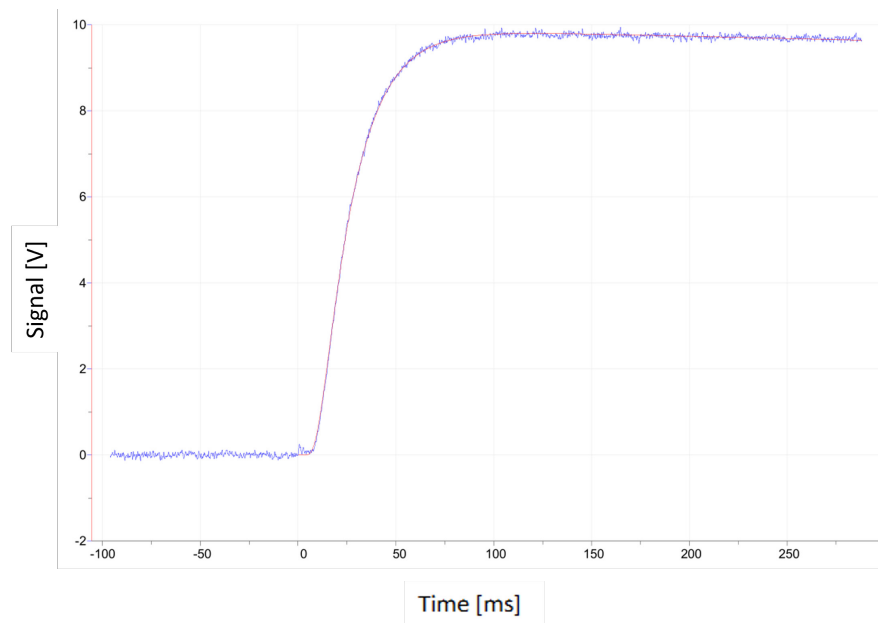


Figure 3.12. Raw voltage trace for sample 16.1 where the detected voltage corresponds to a temperature increase on the rear face of the sample. The thermal diffusivity is related to the gradient of the signal increase.

Thermal diffusivity

Thermal diffusivity for the laser flash specimens was calculated using the length corrections obtained from dilatometry. The results for thermal diffusivity, in $\text{mm}^2 \text{s}^{-1}$ are presented in Figs. 3.13, 3.14, 3.15, and 3.16. Fig. 3.16 depicts one graph only, as only one sample from cylinder 16 was tested via the laser flash method (which was built using the same parameters as sample 15 used for dilatometry). A comparison of the differences in thermal diffusivity between samples where the 5-shot mean is taken at each temperature increment for all the samples tested is presented in Fig. 3.17. It was expected that samples taken from the same cylinders (indicated by a shared first digit in the sample name) would exhibit similar thermal diffusivities. This holds true for all sample pairs shown in Fig. 3.17 apart from 1.1 and 1.8 where a significant difference is observed. Interestingly, sample 1.8 behaves more like samples 11.1 and 11.8. In addition to this, the similarity in naming means that it is strongly believed that a sample from cylinder 11 was mistakenly tested and recorded as sample 1.8. In addition to the uncertainty which arises due to assumptions of sample homogeneity and instantaneous heat deposition associated with the laser flash technique, it is found in (Vozár and Hohenauer 2005) that uncertainty reduces with temperature. This is

because the sensitivity of infrared temperature sensors increases with temperature, meaning that thermal diffusivity measurements at higher temperatures may be more reliable. This is supported by the results presented in Figs. 3.13, 3.14, 3.15, and 3.16, where the values are grouped much more closely at higher temperatures.

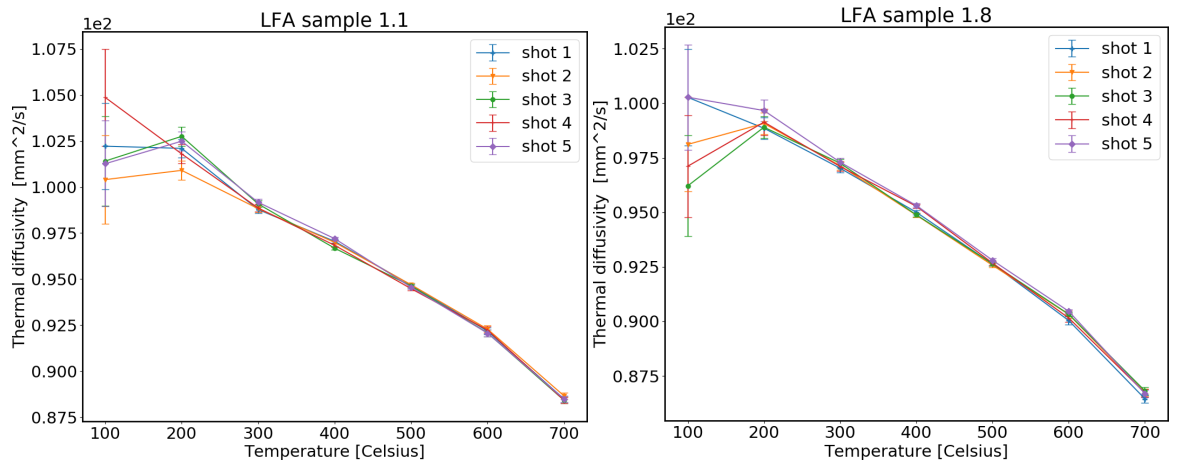


Figure 3.13. Thermal diffusivity results for samples machined from cylinder 1.

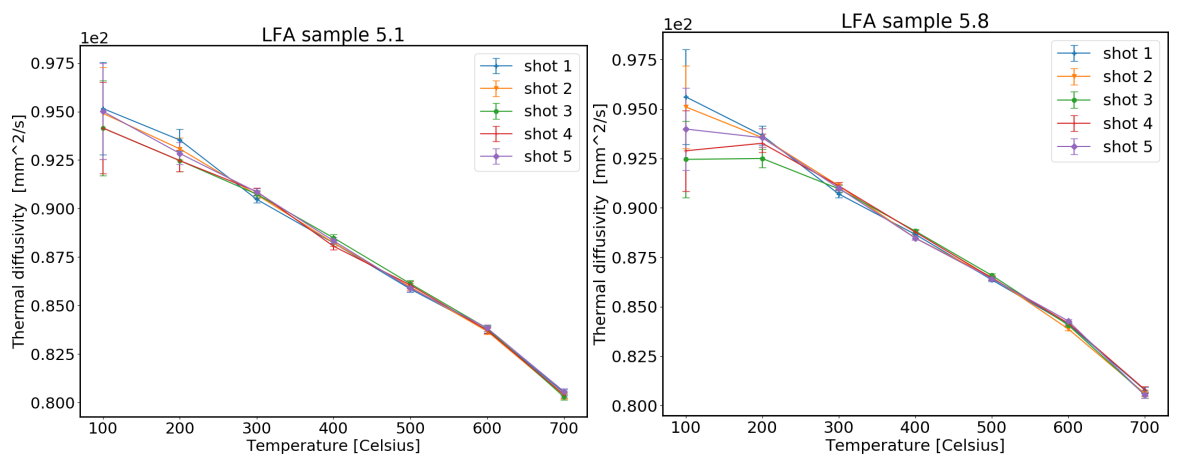


Figure 3.14. Thermal diffusivity results for samples machined from cylinder 5.

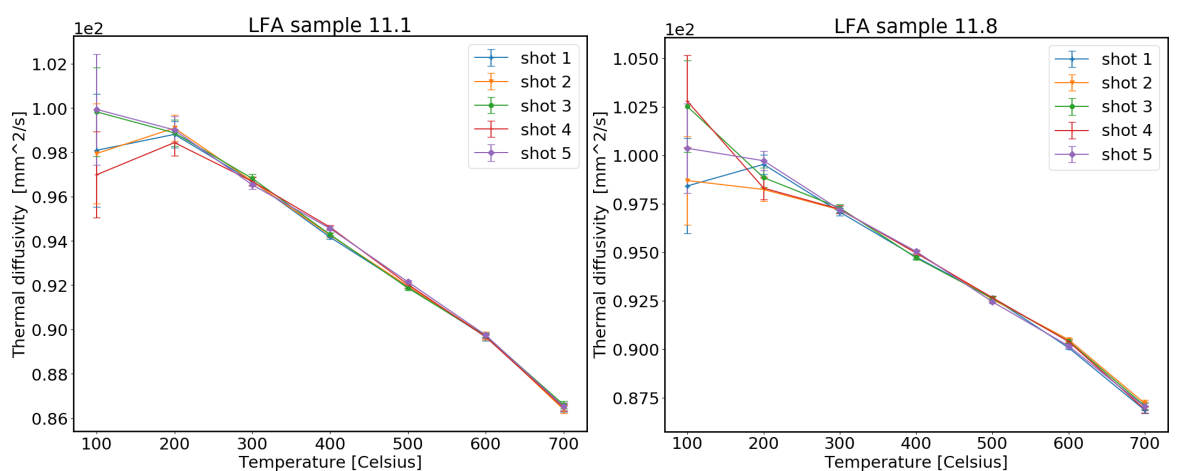


Figure 3.15. Thermal diffusivity results for samples machined from cylinder 11.

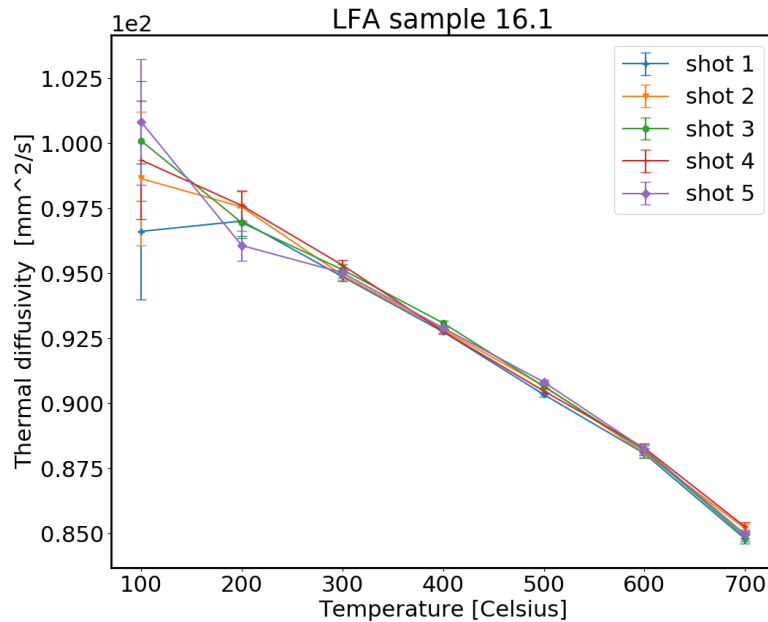


Figure 3.16. Thermal diffusivity results for sample 16.1, machined from cylinder 16.

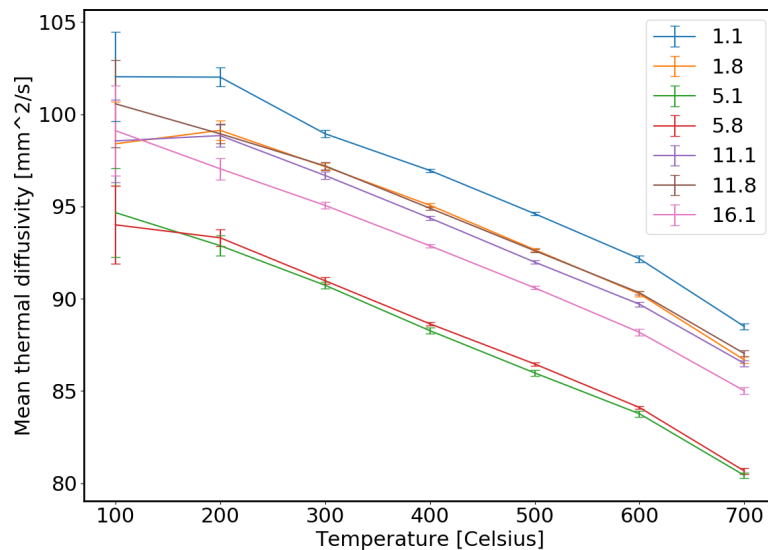


Figure 3.17. Comparison of mean thermal diffusivity for all samples tested.

3.3.3 Thermal conductivity

An estimate for the thermal conductivity can be made using Eq. 3.5, however, due to difficulties in obtaining access to a Differential Scanning Calorimeter (DSC) and Archimedes density testing equipment, the results presented in Fig. 3.19 are presented as estimates. They rely on (fusion relevant) literature values for specific heat capacity presented in (Gonzalez *et al.* 2018) and shown in Fig.3.18. Specific heat capacity refers to the quantity of heat required to raise a unit mass of material by a unit in temperature. Whilst it is widely accepted that factors such as the process parameters and build direction can influence the microstructure and final material properties of AM materials (Leonard *et al.* 2012), this is likely not a major issue regarding the use of this data. Unlike thermal diffusivity which describes thermal transport, heat capacity does not depend on the microstructure but is influenced solely by material composition (Arrizubieta *et al.* 2020). The CuCrZr material used in (Gonzalez *et al.*

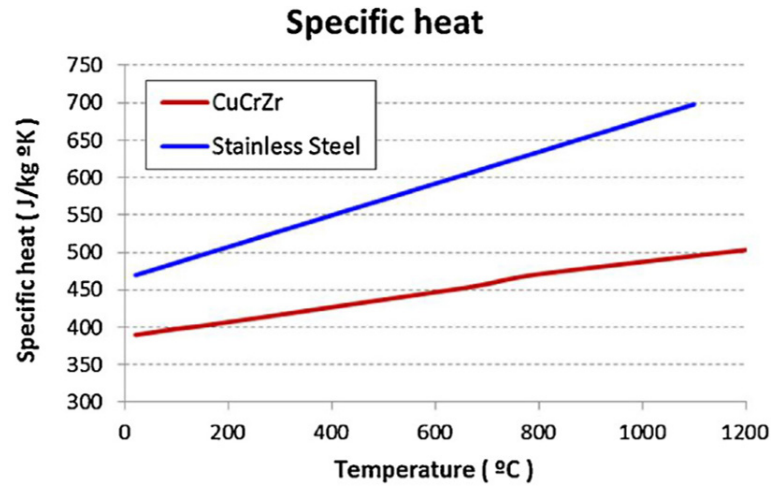


Figure 3.18. CuCrZr specific heat capacity data used in the estimation of thermal conductivities, reproduced from (Gonzalez *et al.* 2018)

Table 3.6. Room temperature absolute densities and as a fraction of reference CuCrZr density (8.9 g cm^{-3}) for samples used in laser flash analysis.

Sample name	d_{layer} [μm]	P_{Laser} [W]	Mass [g ± 0.0005]	Vol. [$\text{mm}^3 \pm 0.1$]	ρ [$\text{g cm}^{-3} \pm 0.03$]	Fractional ρ [% ± 0.4]
1.1	60	900	4.3118	495.6	8.70	97.8
1.8	60	900	4.3371	492.6	8.81	98.9
5.1	60	370	4.1632	494.8	8.41	94.5
5.8	60	370	4.1820	490.6	8.52	95.8
16.1	30	900	4.3121	492.6	8.75	98.4
11.1	30	370	4.3191	495.6	8.72	97.9
11.8	30	370	4.2677	490.8	8.70	97.7

2018) is ITER grade CuCrZr which has a composition in wt.% of Cu (balance), Cr (0.6-0.90) and Zr (0.07-0.15), detailed in (*CuCrZr Tube Procurement Specification for Divertor* 2014). As this composition overlaps with the composition data presented in Table 3.1, the specific heat capacity is treated as applicable to the estimation of thermal conductivity data.

Measurement of density was made using digital callipers and a mass balance with associated estimated uncertainties of $\pm 0.0005\text{g}$ and $\pm 0.001\text{mm}$ respectively. These uncertainties are propagated through subsequent calculations of volume and density in combination with errors in diffusivity and the previously obtained corrections to thermal expansion. The resulting data is shown in Table 3.6. Fig. 3.19 shows that samples 5.1 and 5.8 display significantly poorer thermal conductivity than the others, with sample 1.1 exhibiting the highest values. This is consistent with previous results presented.

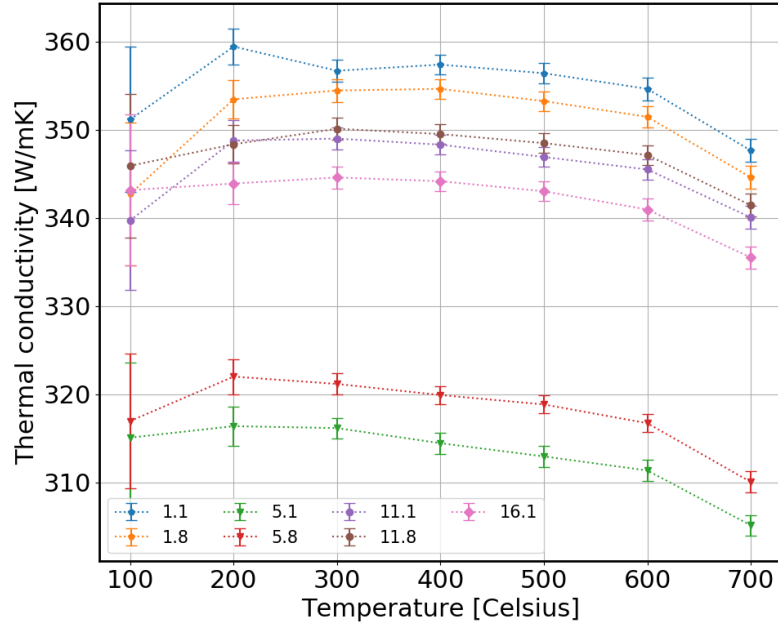


Figure 3.19. Comparison of thermal conductivity estimates.

3.4 Discussion

3.4.1 Uncertainty estimation

Dilatometry

The ASTM standard detailed in (ASTM-E228–17 2017) details the limit of precision for a vitreous silica dilatometer as 4% when carefully calibrated. Random error is introduced into the measurement through calibration issues and fluctuation in the measured values of length, temperature, and any associated voltages. The error in $\Delta L/L_0$ is estimated as:

$$\delta\left(\frac{\Delta L}{L_0}\right) = \pm[(\delta E)^2 + (\alpha_T L_0 \delta T)^2]^{1/2} \quad (3.10)$$

where the initial length $L_0 = 10^{-2}\text{m}$, the precision in length measurement $\delta E = \pm 5\mu\text{m}$, $\alpha_T = 18.65\mu\text{m m}^{-1}\text{ }^\circ\text{C}$ (which is an averaged coefficient for all samples used) and $\delta T = 0.5^\circ\text{C}$. The error is calculated as $\pm 25.01 \approx \pm 25\mu\text{m m}^{-1}$. In order to estimate the error in the mean thermal expansion coefficient α , the error in $\Delta L/L_0$ is combined in quadrature with that associated with the temperature measurement ($\delta T = 0.5^\circ\text{C}$) where average values of $\Delta L/L_0$ are used for each temperature interval, giving the fractional errors seen in Fig. 3.11.

Laser flash analysis

The estimation for the thermal diffusivity calculation is more involved than that for the coefficient of thermal expansion and is detailed in depth in (Migliorini 2009). Some of the

sources of uncertainty in the laser flash procedure are related to deviations in the sample properties from the assumptions made of isotropy, homogeneity, parallelism, and uniform heat pulse distribution (which allow for the treatment of one-dimensional heat flow) (Vozár and Hohenauer 2005). Errors are introduced through temperature measurement, detector performance, data acquisition board performance and data analysis. Additional sources include the finite pulse time effect and heat losses. As some of these sources of error relate to the internal performance of the laser flash equipment, and the correction to thermal diffusivity due to length change is very small, the percentage error calculated by the laser flash software is used in Fig. 3.17.

3.4.2 Comparison to conventional CuCrZr alloy

Data for a traditionally manufactured CuCrZr alloy with a similar composition to the one studied here is available online (Copper Institute 2021). The stated mean thermal expansion coefficient for a temperature range of 20 – 300°C is 17°C⁻¹. This is of similar magnitude to the values presented in Table 3.4. Sample 1.3 had the closest thermal expansion to this value at 17.3°C⁻¹, with the other samples exhibiting higher thermal expansions. As shown in Fig. 3.17, the thermal diffusivity of the best performing samples reduces linearly from around 100 mm² s⁻¹ at room temperature to around 95mm² s⁻¹ at 500°C, which is comparable to the 100-90mm² s⁻¹ decrease for CuCrZr published in (Rohde *et al.* 2014) where the mean was calculated based on testing using the laser flash method in 9 different laboratories. Laser flash samples 1.1 and 1.8, made with the same build parameters as the best-performing dilatometry sample (1.3), also exhibited the highest thermal diffusivity.

3.4.3 Thermal expansion

The mean coefficients of thermal expansion displayed in Fig. 3.11 show a variation between samples of 2 – 3°C⁻¹ with the maximum coefficients of thermal expansion found in samples 5.2 and 15.2. The lowest and second-lowest overall coefficients of thermal expansion were found in samples 1.3 and 11.3 respectively. When considered for use as part of a cooling pipe in a tungsten (W) component (W has a thermal expansion coefficient of $\approx 4^\circ\text{C}^{-1}$), a lower CuCrZr coefficient of thermal expansion reduces the thermally induced stress at the material interface. When a component featuring interfaces between different materials is heated, the expansion of one material at a faster rate than the other leads to the application of stresses where they meet, which can lead to cracking and component failure. A summary of results is presented in Table 3.7 where thermal expansion and diffusivity are used to rank sample performance, based on the premises that a high diffusivity is beneficial for heat transfer and a lower coefficient of thermal expansion would likely result in lower stresses at the material interface.

Table 3.7. Sample build parameters when ranked by thermal expansion performance (where the lowest coefficient of thermal expansion is ranked 1st) and diffusivity (where the highest diffusivity is ranked 1st).

Dilatometry sample	LFA sample	Laser power	Layer thickness	Thermal expansion rank	Diffusivity rank
1.3	1.1,1.8	900	60	1	1,n/a
11.3	11.1,11.8	370	30	2	3,2
15.2	16.1	900	30	3	4
5.2	5.1,5.8	370	60	4	7,6

3.4.4 Relationship to laser build power

Sample 1.3 displayed the lowest coefficient of thermal expansion. As mentioned previously, the corresponding LFA sample (1.1) had the highest thermal diffusivity. These samples were made with a laser power of 900W and a layer thickness of 60µm. The other samples manufactured with the highest - 900W - laser power, 15.2 (dilatometry) and 16.1 (LFA) had a layer thickness of 30µm and displayed high thermal expansion coefficients and moderate thermal diffusivities. The rankings of the sample thermal expansion coefficients and diffusivities, presented in Table 3.7 are consistent with each other, meaning that if a sample has a lower thermal expansion coefficient it has a higher diffusivity and vice versa. It is interesting that the best overall performing sample set was [1.3, 1.1] as this suggests that increasing the laser power combined with a greater layer thickness not only decreases build time but may increase material quality over those manufactured at 370W. Sample 1.8 was not included as it is suspected to have been sample 11.8 tested in error.

3.4.5 Experimental difficulties

The thermal expansion experimental work was complicated by dealing with a high electrical conductivity material, which also appeared to melt at a lower temperature than expected. The initial dilatometry heating program was designed to operate up to 1000°C, however, it became clear, that a phase change was occurring at approximately 800°C, as measured by the thermocouple. The resulting sample can be seen in Fig. 3.20. Even with a reduced temperature range with a maximum of 700°C the dilatometry samples were significantly discoloured and an outer layer of material flaked from the main bulk as shown in Fig. 3.21, indicating potential phase change.

3.4.6 Possible causes for sample phase change

The high electrical conductivity of the CuCrZr material made the standard process of spot welding the thermocouple to the dilatometry sample infeasible. After several attempts working with different welding techniques, it was necessary to wrap the thermocouple wires around the sample following a method recommended for a Gleeble thermodynamic testing system. The attachment of the thermocouple can be seen in Fig. 3.21. As the thermocouples are not directly bonded to the sample, this technique may have introduced error into the

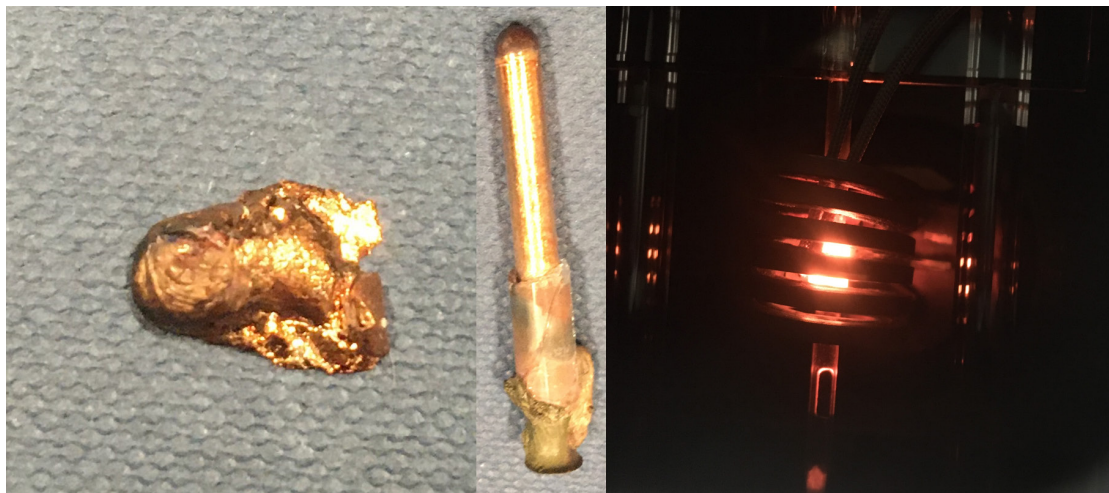


Figure 3.20. Initial testing was devised to test the thermal expansion up to 1000°C , however, the sample appeared to transition to a liquid phase at approximately 800°C (as measured by the dilatometer), significantly below the expected melting temperature of $\approx 1080^{\circ}\text{C}$.

dilatometer temperature reading, however, it seems unlikely that it could contribute fully to the observed discrepancy in behaviour.

It is speculated that the unexpected phase change observed in the CuCrZr is a result of the heating method used in the dilatometer. The machine employs the principle of inductive heating, which involves circulating an alternating electrical current in the coil visible in Fig. 3.21, which acts as a solenoid. This generates a transient magnetic field inside the coil, causing eddy currents in the sample that result in heating due to electrical resistance. The presence of intermetallic phases or pockets of unsintered material in the sample may exhibit higher electrical resistivities than the bulk material, causing hot spots and regions of excessive heating not measured by the thermocouple. It is proposed that the phase change observed may have been initiated by regions of excessive localised heating in this manner. Further work including accurate characterisation of the material melting point (using a Differential Scanning Calorimeter) in combination with visualisation of internal defects, would likely be required to better understand this behaviour.

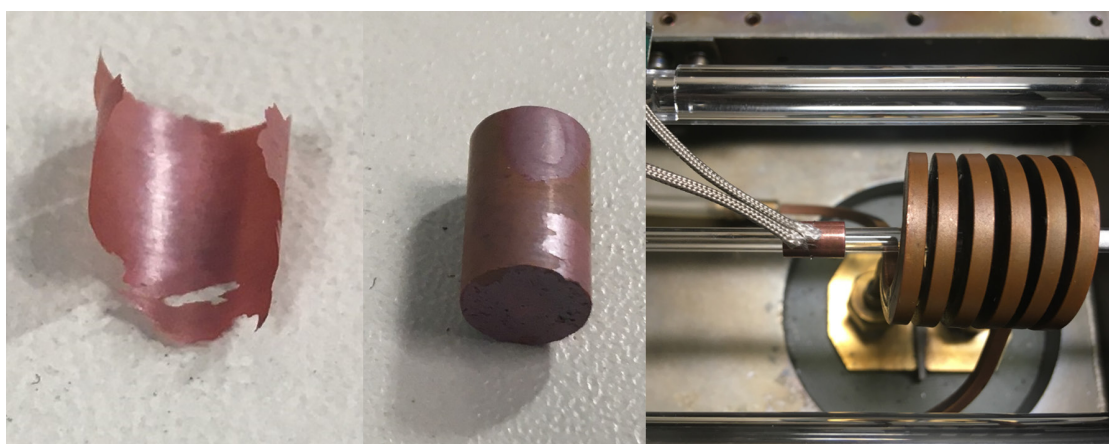


Figure 3.21. Photographs showing sample discolouration (left and centre) and location in the dilatometer before operation (right). A conservative test, considering the expansion up to 700°C was used to obtain finalised data, however, the samples still showed significant discolouration.

3.5 Conclusions

A set of additively manufactured CuCrZr samples were produced by 3T Additive Manufacturing based on a range of laser powers (370-900W) and layer thicknesses (30 μ m and 60 μ m) as part of ongoing work to optimise the build process. A subset of these samples, representing the extremes of the laser powers, were analysed using push-rod dilatometry and the laser flash method to ascertain the coefficients of thermal expansion and thermal diffusivities. Despite experimental difficulties relating to spot welding thermocouples to highly conductive material and unanticipated phase changes, data was obtained for a temperature range of 30 – 700°C. The samples manufactured with the highest laser power (900W) and greatest layer thickness (60 μ m) were found to have the most desirable thermal properties for application to a fusion reactor cooling component: high thermal diffusivity and low coefficient of thermal expansion. This indicates that a reduction of the associated build time by increasing laser power is possible without compromising thermal performance. Additionally, samples manufactured using the lowest laser power (370W) and the smallest layer thickness (30 μ m), representing the most conservative build process, performed the worst. Further testing would be required to fully optimise the process parameters, however, the results in this study indicate that changes to the build parameters produce observable differences in the thermal properties which could impact the performance and lifetime of manufactured parts. This is of particular importance when considering the application of the material to high-temperature environments such as a fusion reactor cooling system. Further investigation is however required in order to establish the cause of the observed sample phase change.

Acknowledgements

This work was performed in collaboration with 3T Additive Manufacturing, Laser Flash Analysis was carried out by Andy Wallwork of the University of Manchester, School of Materials. This study was supported by the Engineering and Physical Sciences Research Council [EP/L01663X/1].

3.6 Additional commentary on Chapter 3

The preceding chapter discussed the details of a collaboration with an additive manufacturing company with the capability to produce and sell CuCrZr. This in itself demonstrates that there is a viable market for additively manufactured metal products at the present level of technological capability. 3T AM's motivation for the investigation was related to the optimisation of the build process and cost reduction. The CuCrZr samples tested in the preceding chapter approached full density, with as-built relative densities of 98.54%. There are many factors to consider in the assessment of applicability for fusion. As discussed in Chapter 2, CuCrZr is currently proposed primarily for use in water-cooled divertor systems in conjunction with a W (alloy) armour plate. The operational temperature limit of CuCrZr is thought

to be around 350°C (Galatanu *et al.* 2019), so any AM part should feature comparable material properties up to this temperature. The coefficients of thermal expansion and thermal diffusivities were tested up to 700°C and were found to be approx. 17-19°C⁻¹ and 100-90mm² s⁻¹ respectively, values which are comparable to those obtained in literature for conventionally manufactured CuCrZr alloys. Design codes and criteria such as the Monoblock Elastic Analysis Procedure (MEAP) go further and specify a limit of $T_{max} < 300^\circ\text{C}$ to avoid creep and softening after irradiation (Oh *et al.* 2021). There is some evidence that radiation damage may affect additively manufactured materials differently, in part due to the anisotropy of the mechanical properties which arise from the printing process (Song *et al.* 2019) which will likely be a significant focus for future research. Regions of porosity associated with AM may also result in different behaviour under irradiation.

The MEAP also contains mechanical rules which relate to ratcheting and fatigue that any AM CuCrZr component would have to meet. There are many additional factors which go into the consideration of whether a manufacturing process is suitable for use in a tokamak, including cost, ease of mass production, systems integration and availability of materials. Assessment of all these criteria is beyond the scope of this thesis, for which AM is primarily of interest as an enabling technology for topology optimisation.

AM components have already been installed in operational nuclear fission power plants (Hui Li *et al.* 2022), and so, from a technological maturity perspective, AM could be considered more mature than nuclear fusion. Chapter 3 indicates that adequate thermal properties may not be a limiting factor for the application of AM techniques to fusion components, and so there are no explicit penalties applied in the topology optimisation discussed in Chapters 5, 6 and 7. The proposed application area for topology optimisation is to high-value components where suitable performance cannot be obtained by other means and so any additional costs associated with AM may be seen as acceptable. On the other hand, the practicality of producing complex components and the issues associated with the functional grading of material properties described in Chapter 6 are likely to require significant further development. Chapters 5, 6 and 7, follow an approach where the material properties used are treated as targets, where the exact details of the material and manufacturing approach remain unknown. If it had emerged that the presently obtainable thermal properties of AM Cu alloys were significantly worse, another approach could have been considered.

Chapter 4

Topology optimisation literature survey

This chapter presents a review of topology optimisation literature, required to establish an understanding of the methodologies employed in topology optimisation studies and a plan for numerical implementation. The focus of this chapter is on thermal and fluid optimisation and the application of topology optimisation to 3D engineering-relevant problems using standard workstation computing resources.

4.1 Introduction

Topology optimisation is a term which encompasses a broad range of mathematical techniques for the distribution of material in a design domain in order to comply with objectives and constraints specified by the user. There are a number of ways of performing this operation, and mathematical approaches vary from rigorous gradient-based methods to heuristic methods inspired by biological reproduction in cells. The technique has its roots in structural mechanics, where the optimisation objectives have typically been focused on weight reduction. There is a significant quantity of literature on this topic, and reducing weight or maximising stiffness remain the most mainstream industrial applications of the technique, as reviewed in (Eschenauer and Olhoff 2001) and (G. I. N. Rozvany 2009).

Design for products and components in all industries is a process of balancing costs, constraints and performance requirements. Topology optimisation can be used to explore non-traditional design concepts as, unless specifically implemented, it makes no account for preconceptions or intuitions (whether well-justified or not) on the part of the engineer or designer. There are many ways such a technique may be integrated into a design workflow. One approach might be to establish an optimisation implementation based on a simple model that includes what are thought to be the key physical processes, in order to explore design concepts and sensitivity. Another method might be to try and encapsulate the constraints and requirements as realistically as possible in order to generate a topology which can be exported directly for manufacture. The former approach informs designers as part of a more conventional design process, whereas the latter essentially automates design with the goal of removing subjective input. Both of these processes hold value, however, it seems that as the field matures, there is likely to be a push towards topology optimisation as a way of automating the design process, perhaps supported by other emerging techniques applicable to design, such as machine learning.

4.2 Additional background and context

Whilst some topology optimisation background was introduced in Section 1.7, additional theory and context are required in order to discuss the literature.

4.2.1 Optimisation algorithms

A crucial component of topology optimisation software is the algorithm used to solve the optimisation problem. In addition to the gradient-based MMA introduced in Section 1.7.3 (repeated below for convenience), there are a number of possible ways of solving any generic problem. Common alternative formulations in the literature include the level-set method (LSM), Evolutionary Structural Optimisation (ESO) and the use of Genetic Algorithms (GA).

The method of moving asymptotes (MMA)

The MMA has already been introduced in Section 1.7.3, however, due to its use in the remainder of the work, that introduction is repeated here for convenience. The MMA is an optimisation algorithm developed in 1987 in (Svanberg 1987) that is commonly employed for topology optimisation problems in the literature. These studies typically use the algorithm presented in Ref. (Svanberg 2002) which contains a MATLAB[®] script made available for academic usage. The MATLAB implementation is expanded upon and made globally convergent in (Svanberg 2007). The method is an iterative technique whereby the optimisation problem is split into a series of strictly convex approximate sub-problems. It is designed to handle a wide variety of element sizes, design variables and constraints, where the derivative of the constraint with respect to the design variables can be calculated numerically (Svanberg 1987).

Level set methods

Initially developed in (Osher and Sethian 1988), the level set method (LSM) is based around the level-set function, which is a real-valued function of a number of variables that is equal to a constant value or ‘level’. The zero level represents material domain boundaries. Due to its formulation, the level-set method explicitly tracks material boundaries. Due to this capability, it is used commonly in fluid problems, where it is important to know the exact location of the edge of the fluid domain. Additional formulation is required in order to include the creation of holes in the method, however, and different configurations of holes in the initiation can significantly affect the end result (Chungang Zhuang, Zhenhua Xiong, and Ding 2013).

An overview of the LSM for topology optimisation is presented in (van Dijk *et al.* 2013), where geometry is parameterised based on an implicit description of material boundaries rather than the density. One of the features and common reasons for using an LSM is the

generation of crisp designs without the ‘grey areas associated with the density-based methods. Density-based level-set methods are also discussed, which combine the LSM with a more traditional topology optimisation approach. In particular, the author notes that the differences between level-set and density-based approaches have narrowed and the need to consider topology optimisation as a single field of research within which ideas are shared is emphasised. It is recommended that future research look at the contributions of individual components of LSMs in order to identify the causes of difficulties associated with convergence and computational cost. Techniques used to extend LSMs such as the addition of hole nucleation schemes to extend the topological changes possible are discussed. Challenges to the method are detailed, including the dangers of LSMs converging to local minima, a feature inherent in their use formulation. Seeding of the initial domain with a large number of holes has been used to combat this. However, this approach could in itself lead to numerical problems and does not remove the dependency on the initial design.

4.2.2 Evolutionary Structural Optimisation

The Evolutionary Structural Optimisation (ESO) approach is a heuristic method based on the progressive removal of elements. ESO is a discrete approach to topology optimisation and is described in (Ole Sigmund and Kurt Maute 2013) as a modified density approach. The approach was developed from methods which involve removing elements with the lowest strain energy known as hard-kill techniques. Bidirectional variations of the techniques have been developed, which allow for the re-introduction of elements previously removed.

4.2.3 Genetic algorithms

Genetic algorithms are inspired by the biological processes of reproduction, including mutation and crossover (exchange of genetic material between chromosomes during reproduction). The basic approach to genetic optimisation is as follows. Firstly, a random population of initial design solutions is generated. The optimality (or ‘fitness’) of each of those solutions is then evaluated individually. Having found the fittest solutions, information is allowed to be transferred between these designs, producing hybrids of the initial solutions. Then a new generation of solutions is generated containing the features selected for by the proceeding generation. This process is repeated many times in the hope it converges towards an optimal solution (G. Rozvany 2001; Zargham *et al.* 2016).

4.2.4 Numerical instabilities

Topology optimisation - like many other numerical techniques - is subject to numerical instabilities, including what is known as the checker-boarding problem. Checker-boarding is where regions of the design domain exhibit an alternating pattern of elements of zero and full density (as shown in Fig. 4.1) that do not represent an optimal material distribution (Diaz

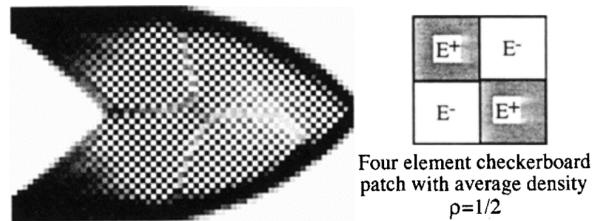


Figure 4.1. Illustration of checker-boarding in a topology optimisation problem, reproduced from (Diaz and Ole Sigmund 1995)



Figure 4.2. Left: Heat conduction topology optimisation domain and boundary conditions. Centre: topology optimised geometry with high conductivity material shown in black. Right: temperature distribution. Reproduced from (Ercan M Dede 2009).

and Ole Sigmund 1995). This was found to arise from an incorrect finite element formulation and mesh dependence. Checker-boarding is resolved by using higher order finite elements or prevented through the proper implementation of restriction methods (such as filtering and projection) that ensure mesh independence (Ole Sigmund and Kurt Maute 2013).

Another issue is the convergence of optimisation problems to local minima, a problem which is approached differently by individual topology optimisation implementations. In density-based methods this problem is often approached with the use of continuation techniques, whereby the strength of the penalisation of intermediate density elements is gradually increased as the optimisation progresses, reducing the likelihood of quickly converging to local minima (M. P. Bendsøe and O. Sigmund 2003).

4.3 Thermal optimisation studies

The number of topology optimisation studies concerned with thermal studies has been slowly increasing, ranging from simple case studies to new methodologies that push the field towards greater complexity and computational efficiency. The most basic studies are 2D heat conduction problems, which are sometimes extended by incorporating heat transfer to a fluid requiring a formulation that includes convection. Fig. 4.2 and Fig. 4.3, reproduced from (Ercan M Dede 2009), show examples of a typical 2D thermal conduction and convective heat transfer topology optimisation setups respectively.

Thermal optimisation problems often take the form of systems designed to transfer heat from a solid to a coolant fluid or between two fluids. For this reason, the development of thermal

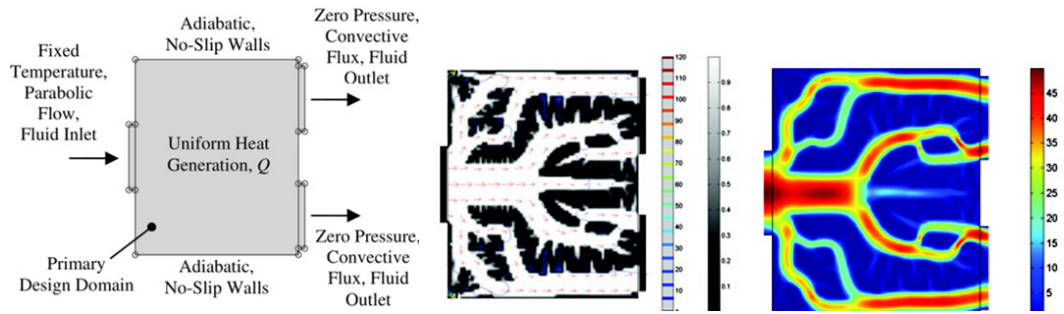


Figure 4.3. Left: Fluid flow and heat transfer topology optimisation domain and boundary conditions. Centre: topology optimised geometry with fluid domain walls shown in black. Right: fluid velocity distribution. Reproduced from (Ercan M Dede 2009).

topology optimisation is tied to the development of fluid optimisation, which is often the source of technical developments, incorporating more complex forms of flow and developing methodologies that track the effect of the changing geometry of solid-fluid interfaces during optimisation.

4.3.1 Previous reviews

The work presented in (T. Dbouk 2017) represents the first major review of the application of topology optimisation to thermal transfer problems. The lack of comparison between numerical methods for topology optimisation was observed to have a negative impact on the field's reputation for finding optimal designs. It was noted that the majority of thermal conduction problems in the literature are performed in 2D, with only a few extending the problem to 3D. Furthermore, it was suggested that in most thermal topology optimisation studies, sufficient detail regarding the performance of the most commonly used MMA optimisation algorithm is not presented. Developments made in computing power were found to have permitted the study of more complex fluid flow systems. This has resulted in the increase in popularity of topology optimisation over shape optimisation for fluid systems, with the important distinction that topology optimisation allows for the creation of new boundaries. Despite this progress, the author did not consider topology optimisation to be a mature technique for the development of optimal systems for thermal transfer at the time of publication. Problems are identified in numerous areas including computational time, meshing techniques, optimisation algorithms, transient state modelling, parallelisation, filtering techniques and experimental validation.

4.3.2 Conduction focused optimisation

Heat sinks are a common focus for topology optimisation studies. In (Srinivas 2006), the authors optimise a passive electronic cooling device that uses a phase-change material such as paraffin wax along with aluminium. Transient heat conduction analysis and topology optimisation were performed with COMSOL Multiphysics, which was chosen as it permits users to modify the governing partial differential equations. This allowed for the description of phase change in the wax. The topology optimisation was performed using a density-based

method with SIMP interpolation. The optimal design was considered 35% better than an “intuitive” design. In 2007, multiple load cases for heat conduction topology optimisation are considered in (ChunGang Zhuang, ZhenHua Xiong, and Ding 2007). The approach uses the level-set method to implicitly represent the geometric boundaries of the structure, avoiding the need for user-specified design thresholding. The topological derivative (a technique which involves the introduction of infinitesimal changes to topology) is used to generate new holes in the design. It is claimed that the combination of topological derivative and shape optimisation used, reduces the influence of the initialisation on the final design. (T. Gao *et al.* 2008) presents an implementation of a bidirectional ESO method for steady-state heat conduction problems, including design-dependent heat loads. The bidirectional ESO method involves analysing the sensitivity to the objective of elements in an initially fully-solid structure. Elements are then removed or added depending on their sensitivity. The work deals with the problem of applying boundary conditions to a changing topology, which is important in solid-void optimisation, where boundary conditions are applied directly to the design domain. A related approach is used in (Anflor and Marczak 2009), where a hard kill material removal algorithm is used for the optimisation of non-isotropic heat transfer problems. The technique uses the Boundary Element Method (BEM) which does not have the same meshing requirements of finite element techniques and allows for the creation of designs with no intermediate density elements, however, the formulation of constraints is found to be more challenging than in density-based techniques.

(Deaton 2009) performs thermoelastic topology optimisation based on the typical approach for structural optimisation. The work represents the first published application of topology optimisation to thermally induced stress, combining two common application areas for the technique. A custom formulation of the problem was developed in MATLAB. Thermal loads are implemented in as boundary conditions in a compliance minimisation problem. The topology optimisation was shown to break down when thermal loads (and resulting restrained thermal expansion) were significant compared to mechanical loads. An alternate formulation appeared to result in improved stress-related performance however in this formulation, stress was not explicitly considered. Stress-based design criteria were introduced, allowing for the direct targeting of thermal stress as an optimisation objective.

(Dirker and J. P. Meyer 2013) presents an implementation of heat transfer topology optimisation for electronic cooling systems. The results were found to resemble tree structures with branching regions of high-conductivity material. It was found that for a 2D heat conduction domain, these structures were consistent regardless of the domain dimensions but were dependent on the formulation of the cost function and the ratio of conductivity between the two materials used. The influence of changing the conductivity ratio γ on the shape of high conductivity tree structures is illustrated in Fig. 4.4, however, for a full discussion of the figure, the reader is referred to the original publication (Dirker and J. P. Meyer 2013).

The transient heat conduction topology optimisation problem presented in (Chungang Zhuang, Zhenhua Xiong, and Ding 2013) and extended in (Chungang Zhuang and Zhenhua Xiong 2014) uses a density-based implementation and the MMA optimisation algorithm. The






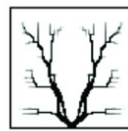



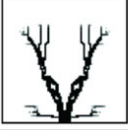

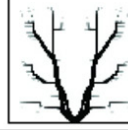
$p = 3$	Scheme 2A			Scheme 2B		
	$\gamma = 100$	$\gamma = 200$	$\gamma = 500$	$\gamma = 100$	$\gamma = 200$	$\gamma = 500$
τ_{\max}	0.1858	0.1315	0.0723	0.0900	0.0554	0.0247
$\varepsilon_{\text{final}}$	0.9732	0.9750	0.9561	0.9444	0.9364	0.8826
$\mathbf{x}_{\text{final}}$						
$p = 3$	Scheme 4A			Scheme 4B		
	$\gamma = 100$	$\gamma = 200$	$\gamma = 500$	$\gamma = 100$	$\gamma = 200$	$\gamma = 500$
τ_{\max}	0.1860	0.1319	0.0742	0.0903	0.0567	0.0302
$\varepsilon_{\text{final}}$	0.8874	0.9452	0.9332	0.9550	0.9408	0.9001
$\mathbf{x}_{\text{final}}$						

Figure 4.4. Influence of changing the conductivity ratio γ on optimised topologies. For full details of the displayed parameters, the reader is referred to the original publication (Dirker and J. P. Meyer 2013), from which this figure is reproduced.

main contribution of the work is the automation of peak heat flux identification in a transient problem, leading to an optimisation result that is more effective at tolerating maximum loads than if an average value had been used. The main difficulties encountered were numerical instabilities in the density-based formulation, including problems of mesh dependence and intermediate densities.

In (Pizzolato *et al.* 2017b), the optimisation of energy storage systems is approached through the distribution of highly conductive and poorly conductive material. The study represents a deviation from the literature surrounding fin design which is described as having high physics complexity and low design freedom. The topology optimisation problem is posed such that the maximum amount of energy is extracted from the low-conductivity material in a given period of time. The optimised 3D design includes aspects of alternative designs tried by researchers such as the addition of radial and pin fins but in a non-intuitive configuration. The 3D design shows an improvement of approx. 30% due to the added design freedom. Fig. 4.5 illustrates the differences between the extruded 2D design and the full 3D optimisation result produced in this study, which display significantly different topologies.

In an application of topology optimisation related to the development of hypersonic vehicles, (Yang *et al.* 2019) finds the topology-optimised design of an integrated thermal protection system based on minimising net heat transfer rate and net strain energy. The optimised designs exhibit lower temperature, deformation and component stress. In (Kang and James 2019), a novel multi-material topology optimisation methodology is presented and follows a parametric representation in which finite-element style shape functions are used to determine the local material properties in each element. The technique relies on adjoint sensitivity analysis and optimises for structural stiffness and thermal insulation. The technique permits

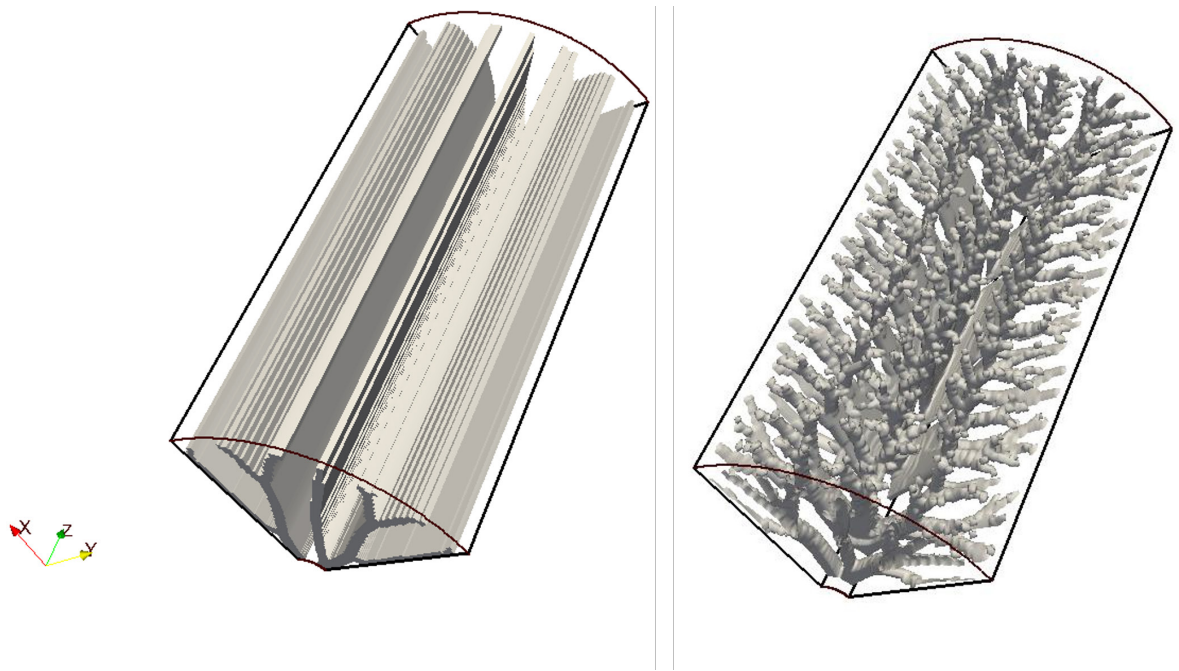


Figure 4.5. Illustration of the differences between extrusion of a 2D topology optimised design (left) and a full 3D optimisation (right). Reproduced from (Pizzolato *et al.* 2017b)

the application of individual temperature constraints to the different materials. Topology optimisation inspired by nature is implemented in (Lin, J. Wang, *et al.* 2019). A method for conduction optimisation based on leaf venation is presented. The process was found to visually resemble leaf growth, and the performance in solving a volume-to-point heat conduction problem was superior to the density-based approach. This technique is inspired by the constructal approach developed in (Bejan 2003).

Improvements to computational techniques

In (Lin, Hong, *et al.* 2018), a deep learning approach combined with the density-based method is presented to accelerate topology optimisation of conductive heat transfer. The deep learning implementation is based on a fully convolutional neural network. The deep learning is applied to the later stages of the density-based process which typically involves only small-scale changes to material distribution. The deep learning approach was able to reduce the convergence time by 71.65% compared to the standard topology optimisation approach. The inputs to the deep learning system are based on topology optimisation iterations and the final results of pseudo-random problems, resulting in a training data set of 10,000 problems. The accuracy of the deep learning approach was validated successfully using volume-point problems. Computational techniques for exploring the performance of evolutionary algorithms are explored in (Ikonen *et al.* 2018). Parametric L-systems (described as developmental recipes) are applied to evolutionary topology optimisation for heat conduction. The implementation, which involves the finite volume method, requires 2 orders of magnitude fewer iterations and results in better designs most of the time than a reference method and lower average temperatures than a density-based implementation. It is based on a model for interpreting the development of trees (the L-systems method).

A novel technique for the design of transient heat conduction systems is presented in (Wu, Y. Zhang, and Shutian Liu 2019) where a new performance index is introduced, known as the Regional Temperature Control Function (RTCF). This is used as an objective function which represents the maximum temperature of specific areas during the full transient analysis. This is proposed in response to findings showing that the results for transient topology optimisation studies on different time scales result in different geometries. The study uses the MMA in conjunction with density-based methods and is demonstrated as effective at minimising temperature in specific areas in transient systems.

Experimental verification

(Jensen 2018) describes a new application of a code which implements fast anisotropic mesh adaptation for the topology optimisation of 2D/3D heat conduction problems. (Q. Xia, Shi, and L. Xia 2018), presents an efficient method for solving heat conduction topology optimisation problems that combines ESO and LSM methods in order to overcome the inability of the LSM to nucleate new holes in the domain. This reduces design sensitivity to initial conditions. In (Vignaesh Subramaniam, Talib Dbouk, and J.-L. Harion 2018) topology optimised designs are tested experimentally using infrared thermography, representing one of only a few cases where topology-optimised designs are experimentally verified. The topology optimisation implementation uses the MMA, SIMP interpolation and a finite volume method. The optimised results were found to reduce the overall temperature and agreed with the simulation and another similarly manufactured component.

Topology optimisation is applied to a refrigerator cooling system in (Lu *et al.* 2019). The topology optimisation was performed in MATLAB using an optimality criteria based optimiser and uses an objective function based on heat dissipation. The topology-optimised parts were manufactured in copper, with the component displaying a 32% higher specific cooling power than a conventional design.

4.3.3 Incorporating convection

Numerical modelling of convection does not necessarily require explicit fluid modelling, with the use of convective boundary conditions allowing for direct application of the techniques used in conduction-based topology optimisation without modification to include computational fluid dynamics (CFD).

(T. E. Bruns 2007) presents a framework for topology optimisation of non-linear steady-state heat transfer with conduction convection and radiation, without explicitly accounting for fluid motion. The study focuses on the numerical instabilities arising from convection-dominated problems, which are known to significantly affect the optimisation results. This paper employs a variation on SIMP interpolation based on the hyperbolic sine function and known as the SINH method (described in (T. Bruns 2005)). The SINH method enables element penalisation such that intermediate-density material is made less volumetrically effective

than either solids or voids. A new topology optimisation implementation is proposed in (Yamada, Izui, Nishiwaki, and Takezawa 2010) based on the ability to adjust geometrical complexity using the level-set method. The approach is developed further in (Yamada, Izui, and Nishiwaki 2011), where a concept based on maximising thermal diffusivity is presented. This methodology is then applied to numerical examples of conduction and convection. The 3D convection problem presented shows the emergence of fins to aid convection, however, it is acknowledged that the design is strongly influenced by the design-dependent convection coefficient, where lower convection coefficients were found to increase the length of the heat convection boundary.

In (Cheng *et al.* 2018), a novel technique for managing the limitations of density-based methods is explored with lattice structures. Instead of designs with intermediate material densities, the technique produces regions of fully dense material and lattice structures where less material is required. It is argued that this technique allows for more reliable manufacturing. The projection of grey areas generated by density-based methods is criticised as it constitutes a deviation from the optimal design. An asymptotic homogenisation technique is used to interpolate the thermal conductivity of the lattice structure. The proposed methodology is applied to the optimisation of cooling channels, resulting in significant reductions in maximum temperature. The topology-optimised lattice-based design is also built using AM.

4.4 Topology optimisation for fluids

The development of topology optimisation techniques for fluid systems began later than structural optimisation, spurred primarily by the publication of (Borrvall and Petersson 2003), which presents a methodology for the topology optimisation of fluids in Stokes flow (viscous or creeping fluid). A generalised Stokes flow problem is derived from a plane flow assumption (Couette flow). The optimisation problem is formulated to minimise the dissipated power in the fluid. The methodology conceptualises the fluid domain as a porous media, where a penalty to flow is applied to reduce fluid velocity in non-fluid regions. Here, a density of 0 corresponds to a high flow rate representing an open element and a density of 1 represents a low flow rate indicative of a closed (low permeability) element. The problem was found to be well posed, with no regularisation techniques required. Subsequent studies have largely focused on extending optimisation techniques to more complex forms of flow, the addition of turbulence and multi-objective optimisation. There is a divide between studies that use a porous media formulation often associated with density-based implementations and those that criticise that approach, often implementing LSM formulations.

4.4.1 The development of fluid topology optimisation methodology

(Allan Gersborg-Hansen 2003) extends the methodology in (Borrvall and Petersson 2003) to treat incompressible Newtonian flow at moderate Reynolds numbers. The Reynolds number represents the ratio of inertial to viscous forces in a fluid and is used to characterise the onset

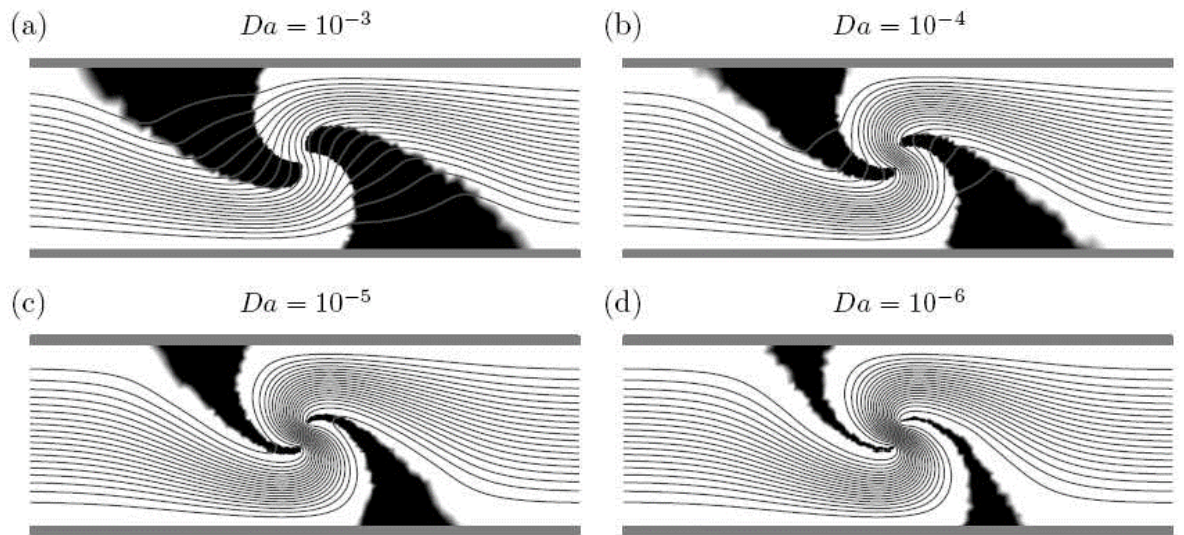


Figure 4.6. Topology and streamlines for a density-based fluid channel topology-optimisation reversed flow example. Sub-figures a),b),c),d) show the impact of decreasing the Darcy number (Da) on the resulting topology. For more detailed analysis, the reader is referred to the initial figure, published in (Olesen, Okkels, and Bruus 2006).

of turbulent flow. In (Guillaume and Idris 2004), topological sensitivity analysis is incorporated into the shape optimisation of Stokes flow in an attempt to avoid the numerical issues associated with the topology optimisation. (A. Gersborg-Hansen, O. Sigmund, and Haber 2005) focuses on the development of an optimisation methodology for steady incompressible laminar viscous flows at low to moderate Reynolds numbers and the inclusion of inertial effects, to find the optimal layout for channels in fluid network systems. Inertial effects are found to be significant even for moderate Reynolds numbers. The need to extend modelling to three dimensions to properly capture more complex, design-altering effects is stressed.

The minimisation of Stokes flow power for given velocities at the fluid boundary of the domain using the Darcy-Stokes or Brinkman equations is considered in (Evgrafov 2005). It is shown that the introduction of a requirement specifying zero power dissipation due to flow through the material makes the system a well-posed mathematical problem. It is argued that in (Borrvall and Petersson 2003), the generation of fully dense internal walls in the domain is not possible, preventing changes to the connectivity of the domain, and therefore that it cannot strictly be considered topology optimisation. In (Evgrafov 2005) however, pure flow and fully solid regions are possible, and the method is shown to provide optimal solutions. In (Guest and Prévost 2006), topology optimisation is performed using a novel method for conceptualising the flow as a porous medium that allows for efficient simulation of the no-slip condition at solid-fluid boundaries. (Olesen, Okkels, and Bruus 2006) describes an implementation of non-linear topology optimisation exemplified with Navier-Stokes flow using commercial FEMLAB software (an early name for the software which became COMSOL Multiphysics), extending work in (Borrvall and Petersson 2003). A numerical example, treating the standard reversed flow case, is reproduced in Fig. 4.6. The Darcy number (Da) represents the permeability of the medium, with lower values corresponding to thinner, less permeable topologies. The study focuses on reducing the computational difficulty in the formulation and is designed to be broadly applicable to a range of applications. A nu-

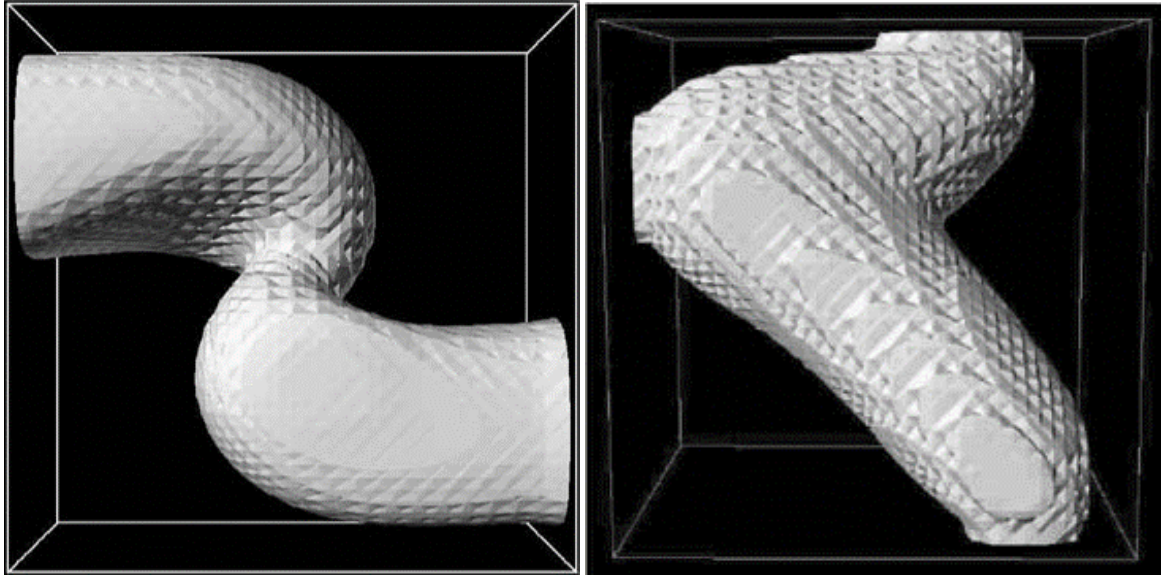


Figure 4.7. Left: illustration of a standard reverse flow topology optimisation problem extended to 3D. Right: topology optimisation geometry showing the flow path for 1 inlet branching to two outlets. Reproduced from (Aage, Poulsen, *et al.* 2008) where a full discussion can be found.

merical example looking at a four-terminal device indicates that, for problems associated with the optimisation of systems with multiple competing local minima, the solution can be strongly dependent on the initial conditions. (Georg Pingen, Evgrafov, and Kurt Maute 2007) presents 2D and 3D optimisation performed using the Lattice Boltzmann Method (LBM) to approximate Navier-Stokes flow. The use of the LBM allows for a representation of the flow which does not rely on varying permeability. The method is the first of its kind but is found to require improvements to the convergence behaviour before application to engineering problems.

(Wiker, Klarbring, and Borrvall 2007) involves the topology optimisation of Darcy-Stokes flow, as another extension of the work in (Borrvall and Petersson 2003). The implementation is tested on area-to-point flow systems similar to those considered in (Bejan 2000, 2003). This study however sets up the problem as two domains: free flow using Stokes' equations and porous flow using Darcy's equations. The objective is the minimisation of the total potential power of the system. Furthermore, the authors do not agree with the conclusion of Guest 2006 (Guest and Prévost 2006) who claims regularisation is not required to prevent an ill-posed problem. 'Large-scale' Stokes flow optimisation is considered in (Aage, Poulsen, *et al.* 2008). The problem is posed in 2D and 3D with approx. 125,000 elements. The formulation uses slightly compressible flow to ensure the problem was well-posed. COMSOL Multiphysics was used to verify the constraints and to ensure the no-slip boundary along the solid-fluid interface is maintained. An illustration of the extension of the reverse flow problem to 3D is presented in Fig. 4.7.

(Carsten Othmer, de Villiers, and Weller 2007) implements 3D topology optimisation of flow splitting in OpenFOAM. (C. Othmer 2008) develops a method for sensitivity calculation for the finite volume method including the implementation of a continuous adjoint into OpenFOAM to produce sensitivity maps, indicating where changes to the topology should be

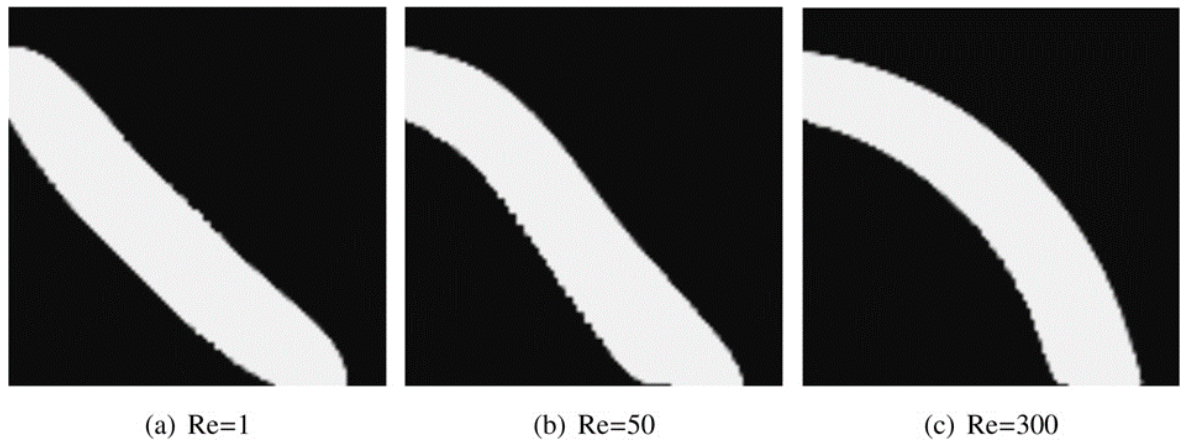


Figure 4.8. Illustration of topology optimised bends with increasing Reynolds numbers (Re). Reproduced from (Deng *et al.* 2011).

made. The system considered involved steady-state incompressible Navier-Stokes flow with Darcy porosity and frozen turbulence. The proposed workflow uses topology optimisation for an initial design draft followed by fine-tuning with shape sensitivities. (Georg Pingen, Evgrafov, and Kurt Maute 2009) performs porous fluid topology optimisation using the LBM. The technique was shown to enable accurate implementation of no-slip boundary conditions and it was found that a shaping factor in the porosity condition produced optimal designs consisting of “0-1” solutions (with low levels of intermediate values). A novel approach to two and three dimensional Stokes flow optimisation problems is presented in (M. Abdelwahed, M. Hassine, and Masmoudi 2009). The approach relies on the insertion of perturbations (small obstacles) in the fluid domain and is presented as accurate and fast for Stokes flow, with only a few iterations required to construct a final domain. It is acknowledged however that the technique may lead to local minima and that further development is required.

4.4.2 Consideration of additional fluid flow scenarios

A computational method for the optimisation of unsteady flows is developed in (Deng *et al.* 2011), using Brinkman penalisation to ensure flow in the porous material is zero. The Brinkman method is similar to the technique introduced in (Borrvall and Petersson 2003) but originates from an earlier work (Arquis and Caltagirone 1984) which penalises the fluid momentum equations, conceptualising obstacles to flow as porous media. The study focuses on the development of a material interpolation approach and the mitigation of numerical instabilities in the porous material. The inability of the Brinkman approach to prevent pressure diffusion through solid areas, is noted, with geometric boundary representation proposed as a solution. Fig. 4.8, reproduced from (Deng *et al.* 2011), shows the influence of increasing Reynolds numbers on optimal topologies.

(Kreissl, G. Pingen, and K. Maute 2011) details a methodology for unsteady flow problems at low Reynolds numbers. Brinkman penalisation is used to enforce zero flow velocities in the solid material, and examples show that designs based on unsteady flow differ from their steady counterparts. Topology optimisation for incompressible, laminar and turbulent

ducted flows is presented in (Papoutsis-Kiachagias *et al.* 2011), which implements the one-equation Spalart-Allmaras turbulence model. The method does not use frozen-in turbulence but includes the changes to turbulent flow which result from changes in the topology that are typically ignored.

(Mohamed Abdelwahed and Maatoug Hassine 2014) considers the optimisation of a non-stationary Navier-Stokes system including the minimisation of dissipated energy. An algorithm for topology optimisation of Stokes flows based on Chebyshev's iteration is presented in (Evgrafov 2015) which saves computation time. The reduction in computational time is the focus of significant effort in the field of fluid-based topology optimisation, often with the goal of permitting the study of more complex geometries and flow regimes. In (Jenkins and Kurt Maute 2015), the LSM is combined with the extended finite element method (XFEM) for the design of fluid-structure interaction problems. The fluid model includes Navier-Stokes flow and uses a fluid mesh which deforms with the structure. The method is compared with density-based topology optimisation, and it is indicated that the LSM-XFEM approach converges well, requiring fewer elements and resulting in better-defined geometries than is possible with the density-based approach. The LSM-XFEM approach does exhibit some problems with discontinuous design evolution, however, including the disconnection of thin members. Topology optimisation of unsteady incompressible fluid flows using the LBM is demonstrated in (Nørgaard, Ole Sigmund, and B. Lazarov 2016). A partial bounce-back model is implemented, which models fluid flow at the fluid-solid boundary during optimisation. It is found that the topology optimisation can account for more complex fluid effects such as vortex shedding and time-varying boundary conditions at moderate Reynolds numbers. Extension of the problem to 3D is, however, thought likely to cause computational difficulties.

The computational performance of fluid-based optimisation is explored in (Chen *et al.* 2018) where a threshold dynamics method is presented for topology optimisation of fluids. The implementation relies on minimising an energy function, which contains a measure of dissipation power in the fluid. The algorithm is shown to converge in significantly fewer iterations than other methods (including the MMA used in (Borrvall and Petersson 2003)). It is also shown that the algorithm is insensitive to the initial guess. Porosity is considered explicitly in the optimisation process presented in (Bastide, Cocquet, and Ramalingom 2018) where a methodology for including material porosity in the optimisation procedure through a perturbation to the Navier-Stokes equations is developed. A method for combining shape and topology optimisation is presented in (Feppon *et al.* 2019). The technique is applied to a fluid-structure interaction problem using the level-set mesh evolution framework. The simulation is only weakly coupled, however, as the equations for fluid and solid regions are solved consecutively.

4.5 Thermo-fluid problems

The following discussion focuses on topology optimisation studies which include explicit fluid flow and heat transfer modelling. Much of the theoretical complexity arises from the implementation of the fluid-based topology model, however, (turbulent) convective heat transfer processes create additional challenges to implementation. These problems are multi-physics by definition, and additional complexity is introduced into the topology optimisation process by the need to consider how to compose objectives made up of multiple terms and the impact that individual weightings can have on the results.

(Ercan M Dede 2009) couples COMSOL Multiphysics with an MMA technique in a custom COMSOL/MATLAB script. The study includes conduction, convection, diffusion and Navier Stokes flow and results in the optimisation of heat exchanger geometries. The weighting of multiple objectives was found to have a significant impact on optimal geometries and it is suggested that further work should focus on automating this process. (Yoon 2010) demonstrates the creation of a design for dissipating heat that relies on convective heat transfer, where the MMA was used in conjunction with SIMP interpolation for coupled Navier-Stokes and heat transfer equations. Thermal compliance – the product of temperature and the conductive heat flux vector – was used as an objective function. It was found that the balance between the conduction and convection of fluid is of central importance to the design of heat-dissipating structures.

(K. Lee 2012) investigates the topology optimisation of 2D and 3D convective cooling systems using Brinkman penalisation for Stokes flow. The stabilised finite element method and adjoint sensitivity formulation were found to be cost-effective, accurate methods for weakly coupled multi-physics optimisation. Numerical instabilities such as element-scale voids and boundary oscillations were found to cause convergence problems that became more apparent at higher Reynolds numbers. The element-scale instabilities were found to be distinct from traditional checker-boarding and were not easily suppressed with a filtering technique. Further numerical instabilities were found at the fluid-solid boundary due to the rapid change in velocity. Convective cooling systems were also investigated, with the goal of maximising cooling efficiency in cooling channels as shown in Fig. 4.9. Physically impossible cooling systems, in which no coolant could flow, were produced initially. This was resolved by fixing the flow path or by adding pressure drop minimisation as an additional objective.

In (Marck, Nemer, and J.-L. Harion 2013), the finite volume method is used in combination with the discrete adjoint method in order to conduct topology optimisation to minimise pressure drop and maximise recoverable thermal power. The methodology is applied to several numerical examples concerning heat and mass transfer, however, the study only considers laminar flow. Further work is suggested based on the investigation of heat exchanger design through maximisation of internal heat generation rate. (Matsumori *et al.* 2013) demonstrates a density-based topology optimisation implementation for coupled thermal-fluid interactions using Navier Stokes flow. The focus is on the design of heat exchangers which are

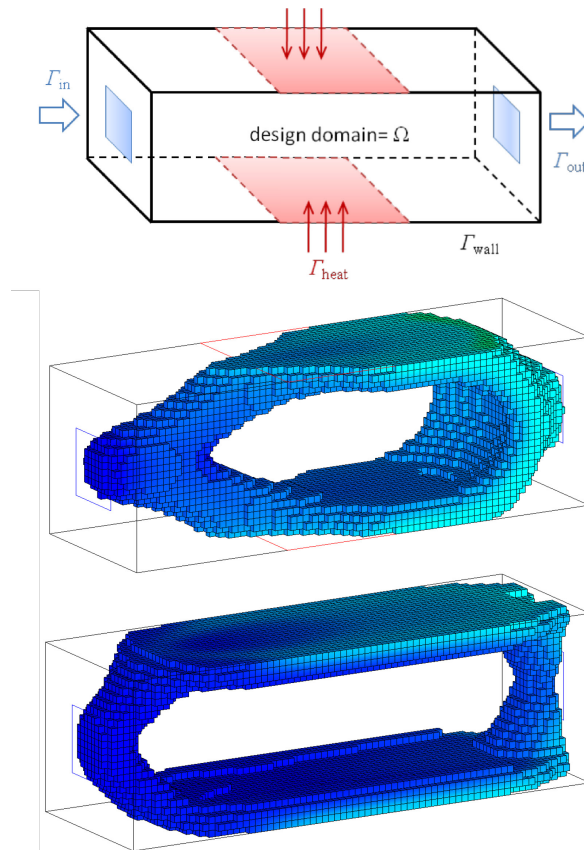


Figure 4.9. Upper: design domain for topology optimisation of an air cooling system showing fluid and thermal boundary conditions. Topology optimised coolant channels are shown for $Re = 100$ (middle) and $Re = 1000$ (lower). Reproduced from (K. Lee 2012), where a full discussion can be found.

optimised under constant input power. The porous media approach is used, and it was found that optimised geometries were Reynolds number and mesh dependent.

(Alexandersen, Aage, *et al.* 2014) investigates the application of density-based topology optimisation to the design of heat sinks and micro-pumps based on natural convection effects. Steady-state laminar flow is modelled using Navier-Stokes equations coupled to the convection-diffusion equation with the Boussinesq approximation (ignoring density differences except where they are associated with gravity). The Brinkman approach is used to penalise velocities inside the solid domain. The importance of design-dependent values for the convection coefficient is emphasised. The optimisation of natural convection systems is found to be challenging as a result of the strong coupling between the fluid and solid regions and the underlying non-linearity in the system. The extension of the methodology to three-dimensional problems is considered trivial, apart from a dramatic increase in computational cost.

Topology optimisation for a coupled thermal fluid problem based on two and three dimensional Navier-Stokes flow is presented in (Yaji, Yamada, Kubo, *et al.* 2015). The problem is posed as a heat transfer maximisation problem, with heat exchange governed by the interaction between structure and fluid. It is argued that many topology optimisation implementations produce overly complex geometries, which are unsuitable for engineering applications. The level-set method is seen as a viable way of generating more easily manufacturable, yet still ‘optimal’ geometries. A regularisation method is also introduced which allows for con-

trol of design complexity. In (Coffin and Kurt Maute 2016) the development of an LSM topology optimisation methodology targeting convective heat transfer in two and three dimensions is presented. The model is however thought to over-predict convective heat flux and result in overly thin fluid channels. (Xu *et al.* 2017) uses COMSOL Multiphysics to perform topology optimisation of a micro-channel heat sink in 2D with a high 3MW m^{-2} heat flux. The study minimises pressure drop and maximises heat dissipation, however, the weighting factor between these objectives was found to significantly affect the results. A new technique which interpolates material properties using sigmoid functions is applied to multi-objective optimisation of a convection problem in (Ramalingom, Cocquet, Maleck, *et al.* 2018). The study focuses on natural convection in an asymmetrically heated channel, considering objectives relating to fluid power dissipation minimisation and the maximisation of thermal recoverable power. Steady-state laminar flow and natural convection are assumed and it is found that the new formulation avoids the use of filtering techniques.

(Jan H. K. Haertel, Engelbrecht, *et al.* 2018) presents pseudo-3D topology optimisation of a heat sink, assuming steady-state laminar flow. The design is not fully optimised in 3D, but instead involves a 2D heat sink base plate and thermo-fluid design layer, which are thermally coupled. Symmetry conditions were used to minimise the computational load. The optimisation objective was the minimisation of heat transfer resistance for pressure drop and heat load constraints. It is acknowledged, however, that the pseudo-3D model only serves as a first estimation for the optimisation of flows in three dimensions, as the model does not account for heat exchange in the extruded perpendicular to the 2D models. Thermal topology optimisation problems conducted in full 3D are rare, with many studies simply extruding the 2D results. Extrusion provides a different result to 3D optimisation as the optimiser has more freedom when implemented in 3D. Studies that perform fully 3D optimisation are becoming more common as the field matures and computing power is better utilised by scalable codes. Topology optimisation of a volume-to-surface thermal conduction problem is presented in (Burger, Dirker, and J. P. Meyer 2013). The average temperature in cubic domains was minimised with an implementation which makes use of the MMA.

The development of high-performance topology optimisation software

In order to fulfil the desire to incorporate more physics, including turbulence and convective heat transfer in topology optimisation problems, there has been a focus in recent years on the development of high-performance topology optimisation codes. Currently, however, this appears to be limited primarily to the development of academic software and the simulation of standard topology optimisation geometries in higher resolution.

(Alexandersen, Ole Sigmund, and Aage 2016) details density-based topology optimisation for the design of three-dimensional heat sinks cooled by natural convection using cluster computing facilities. The study represents a significant step towards the implementation of topology optimisation codes which are able to make use of large-scale computational facilities. Fig. 4.10 illustrates the evolution of one of these heat sinks at increasing topology optimisation

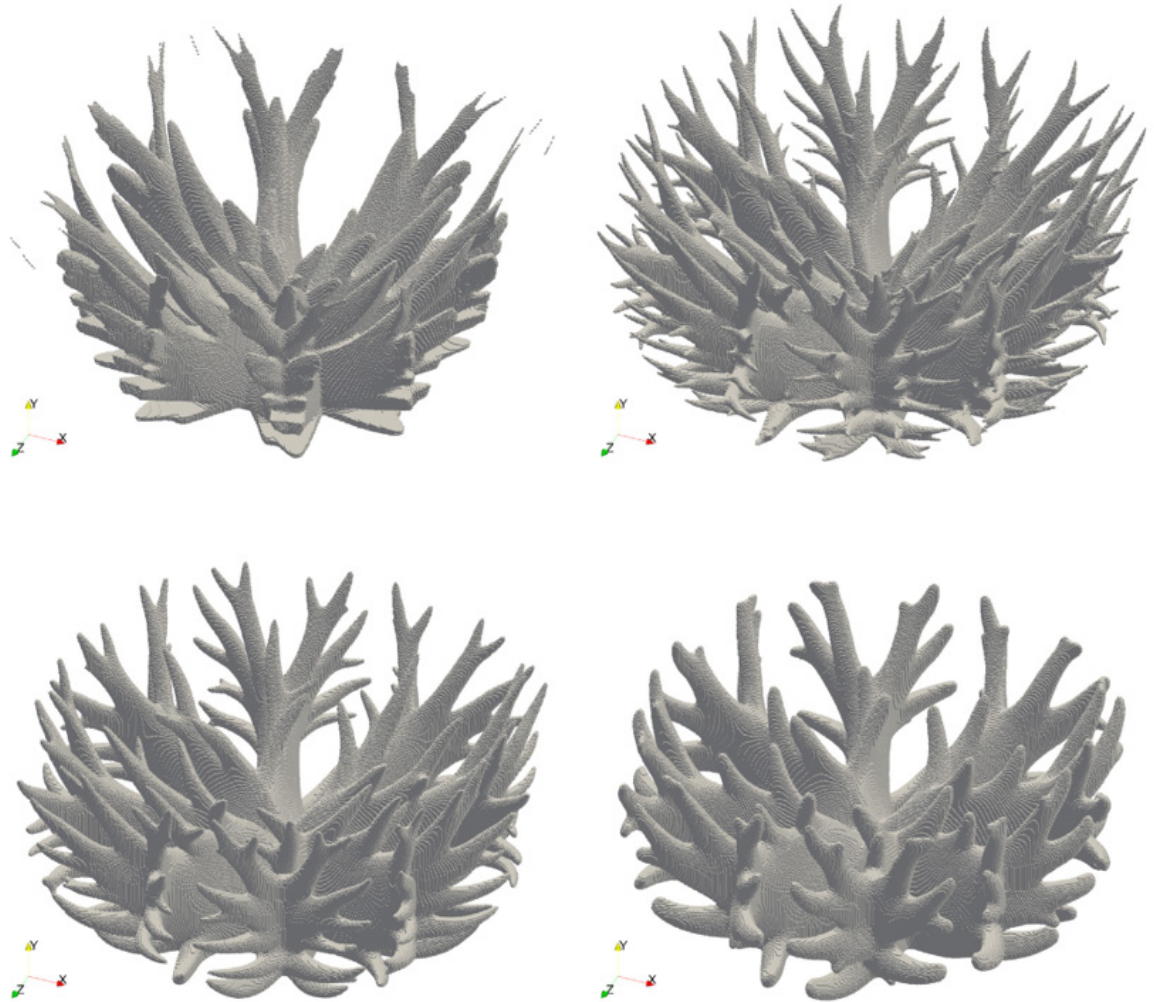


Figure 4.10. Optimised heat sink topology at iteration 200 (upper left), 400 (upper right), 600 (lower left) 1000 (lower right). Full details are available in the original publication (Alexandersen, Aage, *et al.* 2014)

iterations. As the optimisation progresses, a continuation approach progressively penalises intermediate density values and results in the removal of smaller features at later iterations. The study treats the optimisation of a typical heat sink problem, however, it is important that high-performance codes are sufficiently accessible such that they permit the study of the complex systems that are most likely to benefit from increases in computing power.

A methodology for the topological optimisation of heat sinks with turbulent forced convection is presented in (S. B. Dilgen *et al.* 2018) to demonstrate the scalability of a previously developed solver to coupled multi-physics and large 3D problems. The study represents progress in the topology optimisation of coupled thermal-fluid problems with turbulent flows. Comparison between the 2D and 3D designs showed that the performance is particularly dependent on the fluid-solid contact interface. A 3D design was shown to provide a more even temperature distribution than an extruded 2D result. The resulting 3D flow manifolds are shown in Fig. 4.11.

A multi-resolution 3D topology optimisation is used to design a multi-material structure for efficient heat dissipation in (J. Park *et al.* 2019). The problem is decomposed into a number of binary distribution problems for each material. The optimality criteria method is used with a multi-resolution scheme that allows for better material boundary representation than the

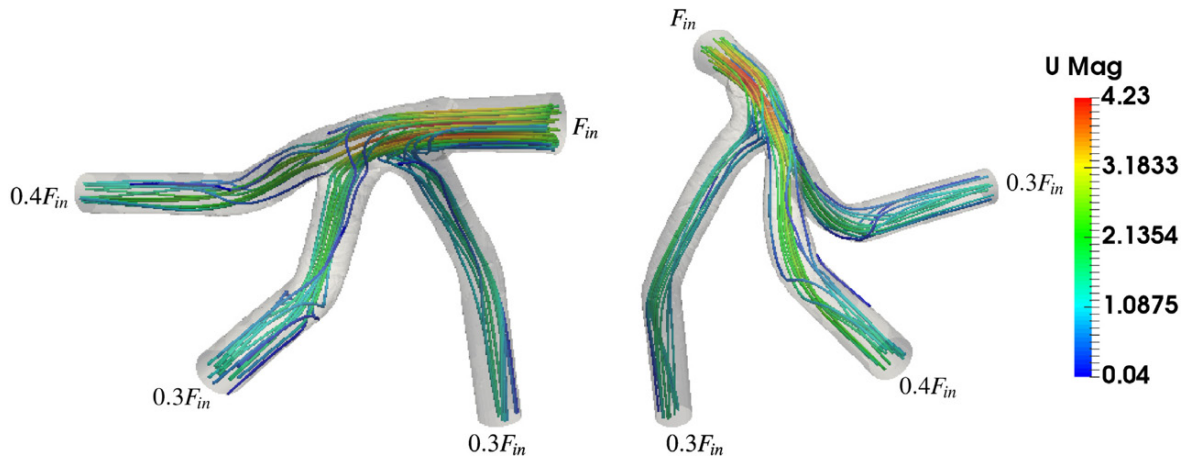


Figure 4.11. Two views of the same optimised 3D flow manifold using the $k - \omega$ turbulence model. Streamlines are coloured based on the velocity magnitude. Reproduced from (S. B. Dilgen *et al.* 2018).

conventional SIMP approach without needing massively parallel codes. It is noted that the technique is currently limited to application to small conduction-dominant systems.

4.6 Engineering applications

Much of the literature discussed so far has involved the application of topology optimisation techniques to ‘numerical examples’. These are typically simple heat conduction or flow systems that can be set up easily and enable a superficial level of comparison (limited by differences in boundary conditions) between studies. Whilst this is to be expected of a developing technology, there is a growing focus on the application of topology optimisation to experimental and industrial scenarios, targeting more complex systems and considering ease of manufacture.

A multi-physics optimisation method for the design of a multi-pass branching micro-channel heat sink for electronics cooling is presented in (Ercan M. Dede 2012). The topology optimisation was performed with two objectives, minimising fluid power dissipation and domain average temperature. The design was found to lower the thermal resistance with nearly negligible pressure drop. The work is extended in (Ercan M. Dede and Y. Liu 2013), which focuses on the manufacture of the resulting multi-pass branching micro-channel heat sink for high heat flux applications. The performance of the system is evaluated for a range of different flow conditions however the study lacks a baseline device to compare with. A full development cycle for the optimisation of small-scale heat sinks is demonstrated in (Koga *et al.* 2013), which focuses on minimising pressure drop (considering Stokes flow) and maximising heat dissipation. Small auxiliary channels were observed in the optimised design which did not contain flowing fluid but improved heat distribution (at the expense of additional pressure drop). Numerical simulation and experimental testing were carried out on the manufactured design, and showed good agreement with the optimisation study.

The thermo-hydraulic design of micro heat sinks is presented in (Van Oevelen and Baelmans 2014) with the goal of taking advantage of the design freedom associated with topology opti-

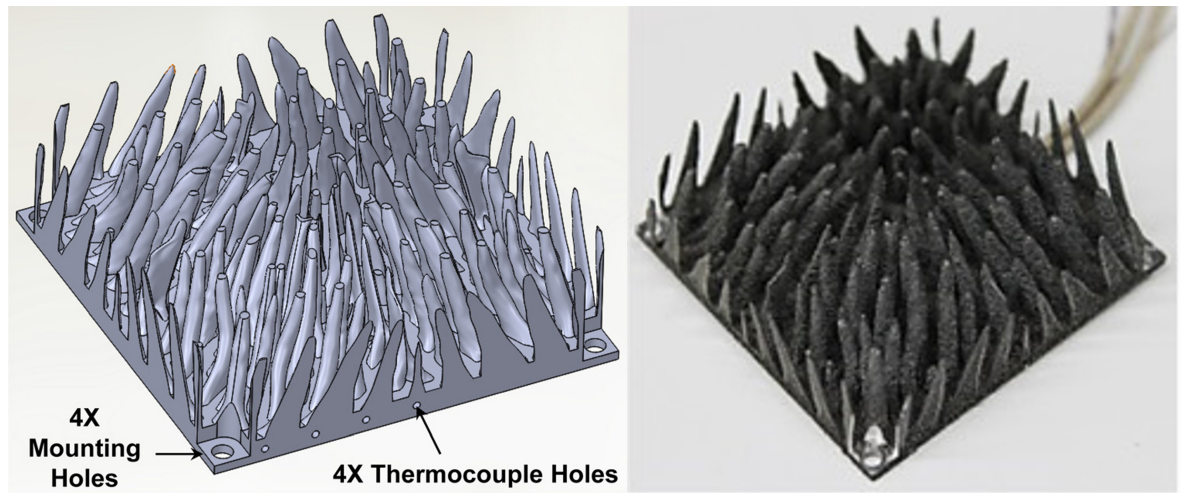


Figure 4.12. Left: CAD representation of topology optimised heat sink. Right: AM prototype. Reproduced from (Ercan M. Dede, Joshi, and F. Zhou 2015).

misation. The performance improvement associated with the resulting geometry is attributed to increases in surface area and the corresponding increase in heat transfer coefficients. In (J H K Haertel *et al.* 2015) topology optimisation is applied to the performance of an air-cooled copper heat sink based on a coupled 2D thermo-fluid model with forced convection. The study uses density-based optimisation implemented in COMSOL Multiphysics to minimise the heat sink temperature and pressure drop for two-dimensional incompressible laminar flow. Brinkman penalisation, in conjunction with a Rational Approximation of Material Properties (RAMP) interpolation function, is used to modify thermal material properties. Another topology optimisation implementation for an air-cooled heat sink, this time with side-surface convection, is presented in (Ercan M. Dede, Joshi, and F. Zhou 2015). The topology optimisation was conducted using COMSOL Multiphysics in conjunction with an MMA implementation. The AM prototype design made from AlSi12 material is visualised in Fig. 4.12.

The performance is experimentally validated and found to be superior to that of conventional designs machined out of aluminium and copper in two separate cases despite high levels of porosity leading to a reduction in thermal conductivity of almost 50%. The authors recommend further work on the numerical modelling of as-built material composition and final finish complexity including porosity and surface roughness. (Soprani *et al.* 2015) presents work to improve active cooling for down-hole tools used by the oil and gas industries. The thermal design was optimised using SIMP interpolation in COMSOL Multiphysics software. The density-based topology optimisation distributes highly thermally conductive materials to minimise the temperature of sensitive electronics. Density filtering and projection were used for design regularisation. Topology and shape optimisation for the design of the air-side of a heat exchanger is presented in (Bacellar *et al.* 2016). The optimisation was performed using a multi-objective genetic algorithm based using in-house code. The optimisation reduced approach temperature by 10%, pumping power by >20% and size by >20%. The authors note that this technique did not require secondary heat transfer surfaces such as fins, potentially resulting in lower manufacturing costs.

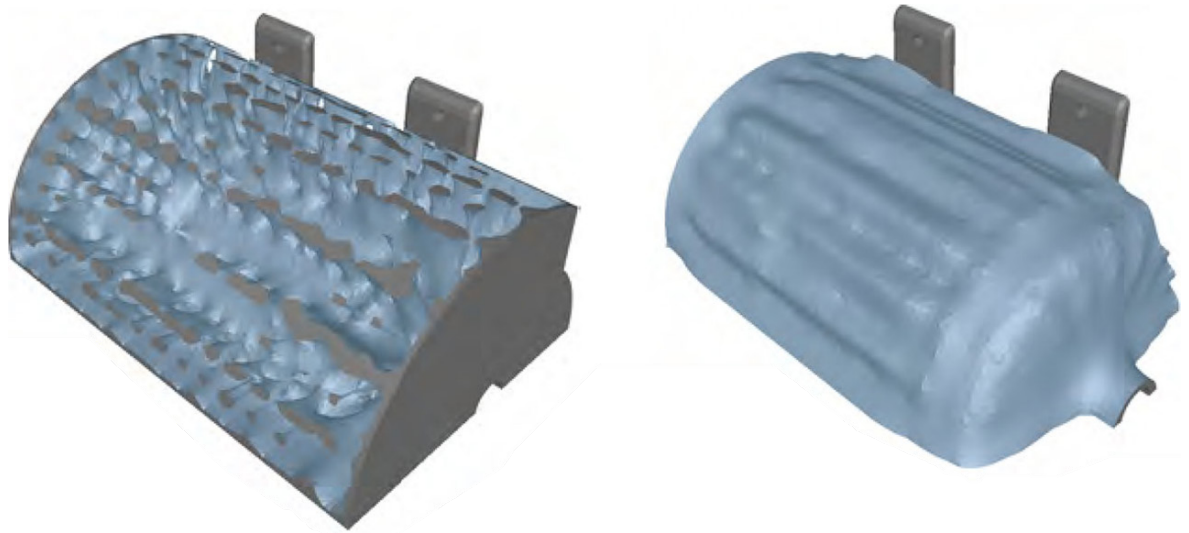


Figure 4.13. Topology optimised electric motor cover geometries. Left: high conductivity, low convection coefficient design. Right: low conductivity, high convection coefficient design. Reproduced from (Mingdong Zhou *et al.* 2016)

An approach for performing conjugate heat transfer topology optimisation in SIMULIA software is presented in (Mingdong Zhou *et al.* 2016). A minimum member size is introduced to control the finest structures and a symmetry constraint is introduced partly for aesthetic reasons and partly to compensate for numerical inaccuracies. The thermal compliance is minimised with a 20% volume fraction constraint. Fig. 4.13 illustrates the differences in the resulting topology optimised geometries for an electric motor cover as a result of changing the ratios of convection coefficient and thermal conductivity between air and the design domain material. This serves as an effective demonstration of the importance of well-defined material properties in topology optimisation studies.

(Jan H. K. Haertel and Nellis 2017) presents a density-based topological optimisation of the air-facing side of a dry-cooled power plant condenser. This is performed to improve the efficiency to achieve commercial competitiveness with traditional, environmentally demanding water-cooled solutions. The computational cost associated with the system is reduced by using geometric periodicity and symmetry to reduce the model to a 2D section of the unit cell. Fluid flow through the solid area is penalised with a Brinkman friction term. COMSOL Multiphysics was used to implement the topology optimisation module using the globally convergent GC-MMA with filtering and projection. The topology-optimised designs outperformed the reference geometry by up to 71% when the minimum fin width of the slot geometry is set to 0.3 mm and by up to 36% when an unconstrained slot geometry is considered. It is noted however that the study only involves a one-way coupling of the thermal problem to the convection model.

In (Lange *et al.* 2018), topology optimisation is performed for a heat sink in COMSOL Multiphysics and compared with a parametric optimisation in terms of performance and computational effort. A comparison between the parametric and topology-optimised geometries is shown in Fig. 4.14. Experiments were performed on AM prototypes and both the parametric and the topology-optimised designs improved performance over the conventional

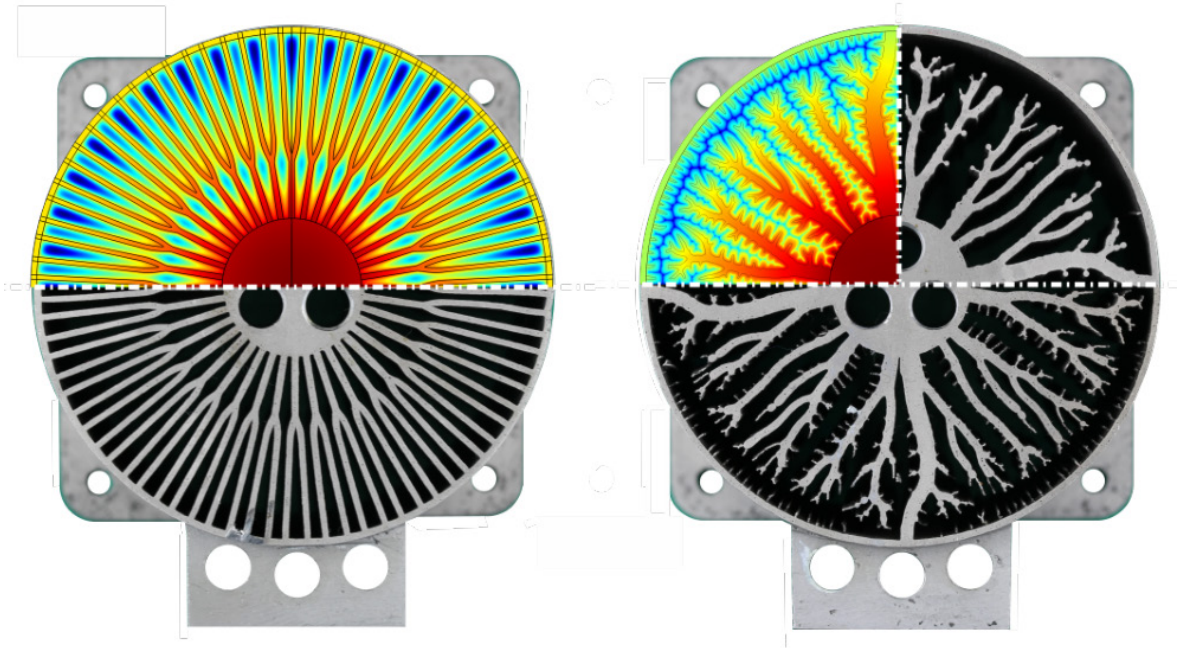


Figure 4.14. Left: parametric optimised design results (upper) and AM prototype (lower). Right: Topology optimisation result (upper left), AM prototype with manufacturing constraints (upper right) and without (lower half). Reproduced from (Lange *et al.* 2018).



Figure 4.15. Investment casting of a topology optimised heat sink. The images shown (from left to right) show: the topology-optimised design, the castable resin pattern, the plaster mold and finally the metal heat sink. Reproduced from (Lei *et al.* 2018).

design. The parametric approach had a less costly computational implementation but the topology optimisation approach provided a more universal solution.

A conjugate heat transfer optimisation problem is presented in (Lei *et al.* 2018). The paper considers Investment Casting (IC) and stereolithography as methods for manufacturing topology-optimised designs for 3D heat transfer devices. There is significant discussion of the issues with additive manufacturing as a method for producing topology-optimised designs. Porosity is common in AM components and it is argued that low levels of porosity have a significant impact on thermal conductivity and that not enough data is available on the performance of AM parts. The results presented were obtained with computation times of approximately 1 day using 2000-4000 CPUs, demonstrating industrially-relevant application of the technique to large computational facilities. An illustration of the steps required between obtaining a topology-optimised design and a heat sink produced using investment casting can be seen in Fig. 4.15. The topology-optimised designs were found to display superior results for the situations they were optimised for but under-performed outside of these scenarios.

Topology optimisation is used to design a wick for use inside a heat pipe in (Lurie, Rabinskiy, and Solyaev 2019). The problem involves distributing the wick material to minimise power dissipation and minimum total pressure drop over the heat pipe. This involves producing optimal pathways for liquid and vapour flow which are directed in opposing directions and are subject to many forms of interaction. This treatment of multiple-phase flow in a highly non-linear system indicates that topology optimisation is being applied to increasingly complex systems. COMSOL Multiphysics is used for the FEA and topology optimisation. The heat transfer capability was increased in the range of 25-100% without exceeding the maximum allowable temperature.

4.6.1 Optimisation for manufacturing

Whilst a full discussion of the incorporation of manufacturing simulation is outside the scope of this review, work has been done to incorporate geometric uncertainties and processes specific to additive manufacturing in topology optimisation software. AM-specific constraints could include more traditional minimum feature size constraints, overhang placement rules, and those relating to residual stress.

This is becoming increasingly important to the field with the move towards engineering-relevant applications. A 2016 review (K *et al.* 2016) notes that AM has been associated with a recent resurgence of interest in topology optimisation prompted by the possibility of efficiently producing geometrically complex designs in small batches. The review covers 20 different software packages with topology optimisation capabilities, including commercial and educational offerings and finds that the commercial software was not capable of implementing sufficient manufacturing constraints to enable the direct manufacture of topology-optimised designs. Non-commercial tools were, however, found to be unsuitable for use in industrial settings due to limitations on design export functionality and workflow integration. It is noted that the prevalence of density-based methods in commercial software that rely on thresholding techniques to export the final design result in the re-introduction of design subjectivity that topology optimisation aims to avoid. The author also notes the lack of AM-specific manufacturing constraints regarding build direction, overhangs, supports and thermal gradients in metal-based AM.

4.7 State of the field

It is clear that there has been significant development in the field of thermal and fluid topology optimisation over the last two decades. The literature shows a progression from 2D proof of concept studies (such as the widely used fluid methodology presented in (Borrvall and Petersson 2003)) and attempts to increase computational efficiency, to more advanced descriptions of physical phenomena such as turbulence ((Deng *et al.* 2011)) and convective heat transfer ((Yoon 2010)). Furthermore, high-resolution 3D problems are beginning to take advantage of large computational facilities ((Pizzolato *et al.* 2017a)). It is also clear that

as the field matures, it is finding greater application to engineering problems, where manufacturing constraints are being considered ((Lei *et al.* 2018)). (T. Dbouk 2017) concludes that topology optimisation is not a robust approach to finding the optimal designs of thermal systems. However, it is clear that in the years since that review, advances continue to be made and the technique is reaching the point of maturity where it is of interest to a broad range of industrial applications. There does seem to be a lack, however, in the exploration of some issues faced by many studies, including the impact of material properties and the exploration of different design objectives and weightings for multi-objective optimisation. These issues have the potential to impact topology-optimised designs in ways not currently accounted for, and greater agreement on best practices within the field needs to be established. The following section discusses the availability and practicality of using some of the software packages used by the literature surveyed here for the optimisation performed in the remainder of this work.

4.8 Software evaluation

This section contains a brief breakdown of the process of identifying the suitability of various topology optimisation codes available at the time of writing, for application to the fusion divertor. The option to define thermal and fluid parameters as objective functions was one of the most important factors when deciding on the software to use. In many commercial software packages, which often do not permit the modification or extension of the underlying code, the applicability is limited by the built-in functionality. In contrast, many open-source implementations of topology optimisation make the modification of functionality possible, at the expense of significant development time. The goal here was to find a solution which was sufficiently modifiable in order to facilitate novel research but sufficiently mature not to require several years of development time before moving beyond the demonstration of a trivial example.

4.8.1 Commercial software

Dassault Systèmes software

There is some optimisation functionality, including topology optimisation, built into Abaqus CAE. As detailed in the Abaqus User's guide (*SIMULIA™ Support Documentation - Dassault Systèmes®* 2019), it is possible to set strain energy; eigenfrequencies; internal and reaction forces; weight and volume; centre of gravity and moment of inertia as objective functions.

Topology optimisation using TOSCA is detailed in (Larsson 2016) and is implemented in two ways, the first of which is a modified optimality criteria (OC) method that is applicable only to stiffness problems with a volume constraint. The second method is a sensitivity-based algorithm that uses the MMA. This approach allows for the specification of manufacturing

constraints, including adaptation to specific manufacturing techniques and the ability to specify member-size constraints. A detailed study implementing conductive and convective topology optimisation using TOSCA was performed by Zhou et al in 2016 (Mingdong Zhou *et al.* 2016). The workflow established allows for the possibility of using the TOSCA optimiser with an alternate finite element package. This study allows for the treatment of the thermal problem through an optimisation objective based on reaction forces. However, it was later established that the code used in (Mingdong Zhou *et al.* 2016) was unreleased and not available to the public, and as such, this software was found to be unsuitable.

4.8.2 COMSOL Multiphysics

COMSOL Multiphysics a popular software package for implementing topology optimisation of thermal problems, with the following studies (among others) using COMSOL Multiphysics for thermal topology optimisation in some manner: (Ercan M Dede 2009; J H K Haertel *et al.* 2015; Jan H. K. Haertel, Engelbrecht, *et al.* 2018; Lange *et al.* 2018; Soprani *et al.* 2015; Srinivas 2006; Xu *et al.* 2017) and fluid optimisation: (A. Gersborg-Hansen, O. Sigmund, and Haber 2005; Allan Gersborg-Hansen 2003). It is unusual among commercial topology optimisation software packages in that it does not place many constraints on the formulation of objective functions, allowing for the explicit specification of thermal and fluid objectives. It is often used in conjunction with an MATLAB optimisation script, as demonstrated in (Ercan M Dede 2009).

4.8.3 Educational tools

The 99-line MATLAB script

A 99 line topology optimisation code for MATLAB is presented in (O. Sigmund 2001). It includes an optimiser and a finite element routine and can handle multiple load cases, although it is designed primarily for education. The topology optimisation scheme is based on the SIMP method, which uses a power law to interpolate between material properties at solid and intermediate densities. The code is easy to understand and modify and was tested in its default configuration, which aims to maximise stiffness for a given volume fraction for a static load (2D). The code can also be extended to treat other problems (such as 2D heat conduction) with a few modifications. The script includes support for passive elements such as a hole in a pipe which must exist in the final design. The results from modifying and running this code are visualised in Fig. 4.16. The code is run using the following command:

```
top3d(nelx,nely,nelz,volfrac,penal,rmin)
```

Top3d is the name of the function, 'nelx', 'nely' and 'nelz' are the number of elements in the three coordinates (x,y,z) which make up the domain. 'volfrac' is a constraint on the fraction of the design domain that the result is allowed to occupy, 'penal' is the level of penalisation

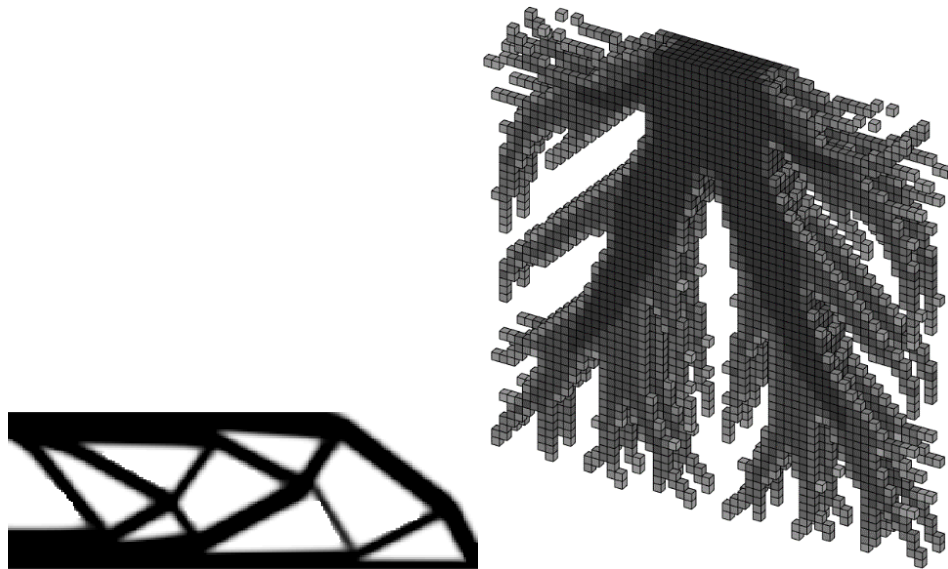


Figure 4.16. 99-Line MATLAB optimisation code. Left: optimised geometry for a static load on a 2D beam (with vertical symmetry condition). Right: thermal conduction geometry with voxels representing the placement of highly conductive material. The loads in each case are applied at the top of the domains, and the greyscale value is proportional to the material density.

given to intermediate density elements and ‘rmin’ is the filter size. More details are available in (O. Sigmund 2001).

An updated, more computationally efficient 88-line implementation is presented in (Andreassen *et al.* 2011). The code lacks any sort of import/export workflow or the ability to handle complex geometries. This, in addition to the need to develop many additional features, made the code unsuitable for application to the present work.

Level-set MATLAB code

A MATLAB implementation of the level-set method is presented in (Challis 2010), and is designed for topology optimisation of statically loaded structures. The code is inspired by the 99-line MATLAB code and is also compact, at 129 lines long. The code can be used as an educational tool and as a comparison to the SIMP method. Another MATLAB level-set implementation inspired by (Challis 2010) is presented in (Otomori *et al.* 2015). The code presented uses a reaction-diffusion equation to update the level set function and claims to be computationally efficient, implementing loop vectorisation and memory preallocation techniques described in (Andreassen *et al.* 2011).

Other MATLAB codes

A number of other codes inspired in part by (O. Sigmund 2001) have been implemented in MATLAB, including (Suresh 2010) which uses a sequential element rejection method, (Talischi *et al.* 2012) which uses unstructured polygonal finite element meshes, (Tavakoli and Mohseni 2014) which focuses on reducing multi-phase optimisation problems to a series of binary optimisation problems, and (Q. Xia, Shi, and L. Xia 2018) which focuses on materials

with extreme properties. The 99-line MATLAB code has been very influential and forms the basis for a lot of open-source topology optimisation codes, including those designed for application to high-performance computing systems. These codes were rejected for similar reasons to those associated with the 99-line MATLAB code.

4.8.4 Large scale optimisation

Codes designed for use on large computing facilities are commonly open source, and in general, have a higher barrier to entry regarding their usage and more limited documentation than commercially available packages. A number of topology optimisation codes have been designed to use on supercomputing facilities, including a parallel framework for topology optimisation using the MMA (Aage and Boyan S. Lazarov 2013) published in 2013, and an approach which uses the multiscale finite element method (H. Liu *et al.* 2018). Other approaches aim to make high resolution problems tractable on desktop systems including (Amir, Aage, and Boyan S. Lazarov 2014) and others implement topology optimisation techniques on GPUs (Martínez-Frutos and Herrero-Pérez 2016; Schmidt and Schulz 2011; Wadbro and Berggren 2009) and (Herrero, Martinez, and Marti 2013).

PETSc topology optimisation

A code based on the Portable and Extendable Toolkit for Scientific computing (PETSc) is presented in (Aage, Andreassen, and Boyan Stefanov Lazarov 2015), and made freely available. The authors claim it has led to the discovery of new effects in comparatively well-studied design problems. PETSc contains most of the elements required for large-scale topology optimisation including sparse matrices, vectors, iterative linear solvers, non-linear solvers and a time-stepping scheme. PETSc libraries have been tested extensively and are actively maintained. The application is scalable to thousands of cores. The code is written in object-oriented C. (Aage, Andreassen, and Boyan Stefanov Lazarov 2015) presents visualisations of topology optimisation results performed with 111.8 million design elements, run on 1800 cores with a completion time of 4h32m. The code is organised into modules where the most likely to need modification are the simplest to use and the least likely to need modification are the most complex. The code is divided into 5 C++ classes and a core program. There is a default problem included with the code which consists of a minimum compliance problem using a sensitivity filter with a radius of 0.08 and a volume fraction of 0.12. The flexibility of the system allows for extension to a number of problems, with the main barrier to entry being development time and effort. After a discussion with one of the developers, this effort was deemed such that it is likely not appropriate for this project. Fig. 4.17 shows the optimised structure from the example minimum compliance problem after being post-processed in Paraview (Ahrens, James, Geveci, Berk, Law, Charles n.d.). The case was run on a desktop workstation with 16Gb RAM and a quad-core processor. After installing and compiling the required packages, the code was run using the command:

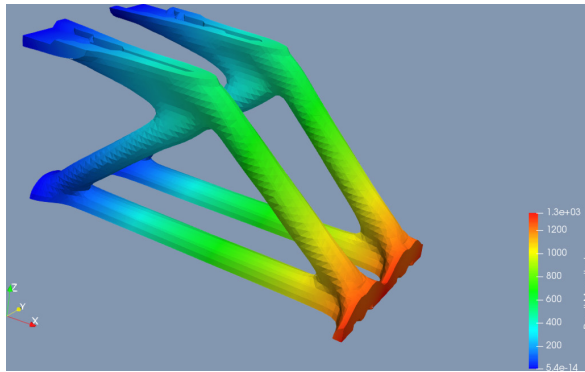


Figure 4.17. PETSc topology optimisation minimum compliance default problem run on a desktop workstation and post-processed in Paraview. The colouration of the model represents the magnitude of the displacement field, in-keeping with the presentation of results in (Aage, Andreassen, and Boyan Stefanov Lazarov 2015).

```
mpiexec -np 4 ./topopt -filter 2 -rmin 0.2 -volfrac 0.3 -maxIter 200
```

These options are similar to those specified for the 99-line MATLAB code, but also include more options for the filtering method and a maximum iteration constraint. The post-processing in Paraview requires user input with regard to a density threshold, above which the domain is considered to be part of the final design.

GPU based optimisation

A study looking at topology optimisation of heat conduction problems using a GPU is presented in (Wadbro and Berggren 2009). Here, the material domain is represented as a large array of voxels. A standard SIMP approach, using gradient-based methods for optimisation is implemented. In (Schmidt and Schulz 2011), a GPU-based open-source topology optimisation code is presented which makes use of the SIMP method, and the Compute Unified Device Architecture (CUDA), a programming language designed for parallel computation using graphics cards made by Nvidia.

It is argued that graphics cards can now be used as powerful tools for scientific computing. CUDA was chosen due to its popularity and the availability of commodity graphics hardware. Different operations are performed by the CPU and GPU according to the potential for their parallelisation. The GPU used by the authors was found to perform better than a 48-core shared memory system. Due to the differences in the architectures, the GPU and CPU implementations have different bottlenecks and take more time in different subroutines.

The study considers a 3D body deformed under forces which are modelled using linear elasticity with respect to displacement. Similarly to the previously discussed codes, the default problem is a minimum compliance problem, however the pathway for modification is less clear than that of the PETSc code, and issues with the installation of the correct drivers on Linux operating systems for stable CUDA operation were encountered. The code is run from an executable and design variables including the size of the domain, the number of iterations and the convergence condition can be specified interactively. The results, as visualised in Paraview, are displayed in Fig. 4.18.

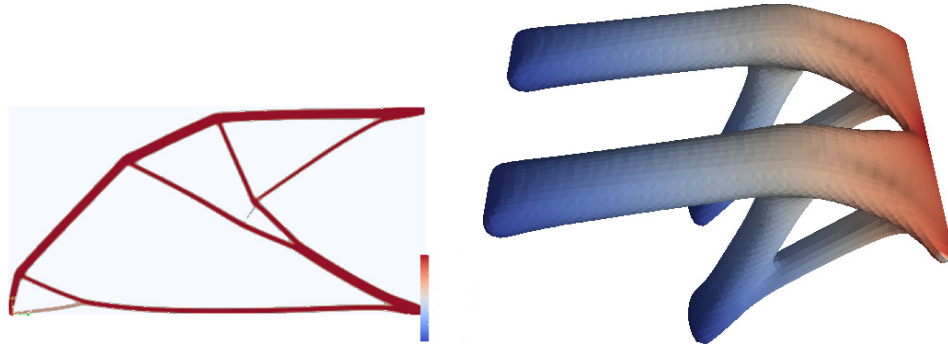


Figure 4.18. Left: 2D projection of a low volume-fraction result coloured with material density. Right: a high volume-fraction result with colourisation representing displacement field. Both images were post-processed in Paraview.

4.8.5 Other codes

Software designed for CFD has been used for topology optimisation focusing on fluid flows, including OpenFOAM, with methods implemented in (Pietropaoli *et al.* 2017) and others. A number of other codes, including ToOptix (Martin 2019) a code integrated with the open-source 3D creation suite Blender (*The Blender Foundation* 2019) were tested but could not be made to function correctly and several other codes including a Dofin-adjoint optimisation framework (Funke and Farrell 2013) and others ((M2DOLab 2019) and openMDAO (Chung *et al.* 2019)) were either found to require too much development time or were otherwise unsuitable for the application area.

4.9 Conclusions and strategy for computational work

It is clear that there is a large variety of topology optimisation codes being developed in the research community, based on a range of different algorithms. However, some of these are developed exclusively for the use of individual research groups and are either not made available to external researchers or are provided in a rudimentary form with varying levels of documentation. The prevalence of lots of codes with small user bases can make it difficult for newcomers to the field and those interested in using topology optimisation in an engineering context. This is likely due to the relative immaturity of the field, however, and it is likely that better-supported open-source codes and more functional commercial packages will emerge in the near future. The use of GPU-based codes for the computation of high-resolution problems using easily obtainable consumer-grade hardware is a promising development in the field, and will likely gain popularity as the implementation becomes more mature.

After consideration of the available literature on topology optimisation for thermal and fluid problems, the decision was made to proceed with COMSOL Multiphysics for the remainder of the project. This software is used in a number of thermal topology optimisation studies and demonstrates flexibility regarding the specification of objectives and the modular treatment of multi-physics modelling. It is also well documented and made available to the general public, unlike some research codes. When this decision was made, the optimisation

methodology was untested, and an approach was pursued based on the development of increasing complexity through the treatment of different elements of the fusion divertor monoblock system through papers which treat problems of increasing complexity. Thermal optimisation objectives in the monoblock armour domain are investigated in Chapter 5. Next, the problem is extended to incorporate thermally induced stress, temperature-dependent material properties and investigation of different attachment scenarios in Chapter 6. Finally, the methodology is applied to the conjugate heat transfer system associated with the cooling channel in Chapter 7.

Chapter 5

Paper 3 - Thermal Topology Optimisation of a Plasma Facing Component for use in Next-Generation Fusion Reactors

This paper was submitted to UKACM2021 and is published online (O. H. R. Marshall *et al.* 2021))

Thermal Topology Optimisation of a Plasma-Facing Component for use in Next-Generation Fusion Reactors

Oliver H.R. Marshall^{1*}, Lee Margetts¹, Llion M. Evans^{2,3} and Matthew J. Roy^{1,4}

¹ Department of Mechanical, Aerospace and Civil Engineering, George Begg Building, The University of Manchester, Manchester, United Kingdom, oliver.marshall@manchester.ac.uk, lee.margetts@manchester.ac.uk, matthew.roy@manchester.ac.uk

² College of Engineering, Swansea University, Swansea, United Kingdom, llion.evans@swansea.ac.uk

³ United Kingdom Atomic Energy Authority, Culham, United Kingdom

⁴ Henry Royce Institute, University of Manchester, United Kingdom

Abstract

The ITER tokamak, the experimental fusion reactor designed to be the first to produce net energy, has had a monoblock concept selected for use as a plasma-facing component in the divertor region. This design currently consists of a CuCrZr cooling pipe surrounded by a Cu interlayer and embedded in a W armour plate. Additive manufacturing may facilitate a geometry capable of greater efficiency through the introduction of greater design freedom whilst maintaining compatibility with the monoblock concept. This is achieved through the addition of high-conductivity material to the armour domain surrounding the coolant pipe. Finite element simulation of the heat transfer system combined with a topology optimisation methodology has been used to find the optimal distribution of high thermal conductivity

material (such as Cu) for three thermal objectives: minimising temperature and thermal gradient, and maximising conductive heat flux. The topology optimisation relies on a density-based approach which makes use of the globally convergent method of moving asymptotes technique (Svanberg 2002). The optimised geometries have been tested for both steady-state operation and transient heat flux events for both a symmetric, flat monoblock design and an asymmetric component designed to minimise leading edges. In high heat flux transient events, the optimisation resulted in temperature reductions of over 200K and reduced thermal gradients. These techniques may be used to help protect divertor components from damage in future devices.

Key words: *heat transfer; topology optimisation; nuclear fusion; additive manufacturing;*

5.1 Introduction

The planning, design and construction of new fusion reactors (tokamaks) is a long process. ITER will be the world's largest tokamak when it is completed, however, in the 47 years between the beginning of Conceptual Design Activities (1988) (Tomabechi 1991) and planned full power operation (2035) (Bigot 2019), the power of design tools and the capabilities of novel manufacturing techniques available to engineers and designers will surely continue to advance. The plasma-facing components which protect the inside of the fusion reactor face unique operational conditions including high steady-state heat loads, damaging transient events, neutron and gamma radiation, sputtering, arcing and a number of other damage mechanisms which challenge engineering design. It is important that emerging design tools and techniques are considered even before they are fully mature, to assess their potential to influence future fusion reactor design. The divertor, which is responsible for handling the most intense heat loads in ITER consists of 54 cassettes containing thousands of monoblocks: W armour blocks with a CuCrZr water-cooled heat pipe in the centre. Divertor components may receive heat fluxes of $\geq 20\text{MW m}^{-2}$ either in steady state or in the form of transient events occurring over tens of seconds, leading to extremes of temperature and a thermal gradient with the potential to cause melting, cracking and ultimately component failure (R. A. Pitts *et al.* 2017). This paper incorporates thermal topology optimisation to re-introduce design freedom in order to solve a set of temperature-based objectives whilst maintaining compatibility with the monoblock concept. The technique is subsequently applied to asymmetric, bevelled monoblocks, designed to limit heat flux concentration by reducing the prominence of monoblock leading edges exposed to the plasma. The design concepts are enabled by the prospect of emerging manufacturing technologies, including functional grading achieved with additive manufacturing.

5.2 Problem description

The divertor monoblock design used in this study (Fig. 5.1) has a 5mm minimum pure W armour thickness (sometimes referred to as a sacrificial armour layer) at the top of the design to ensure integrity after erosion of material by plasma processes. This sacrificial armour layer is continuous with the rest of the armour plate and is only shown as separated in Fig. 5.1 in order to distinguish the design domain for topology optimisation. The geometry of the CuCrZr pipe and surrounding interlayer are maintained in order to maximise compatibility with the baseline ITER monoblock design. This leaves the remaining W to use as the design domain for thermal topology optimisation. Cu is used as the high-conductivity material for topology optimisation. These materials choices are made as they are already present in the conventional ITER monoblock design, however, it is envisaged that any eventual finalised design using similar heat transfer enhancement techniques would use materials more suitable to the requirements of future devices. Interlayer engineering approaches have been used in the past to develop thermal barriers (T. R. Barrett *et al.* 2019) which reduce overall conductance (Li-Puma *et al.* 2013) of the monoblock but relieve thermally induced stress due to the mismatch in coefficients of expansion between the Cu alloy and W. This work considers designs with increased conductance, on the basis that this may be a desirable way of handling high heat flux events.

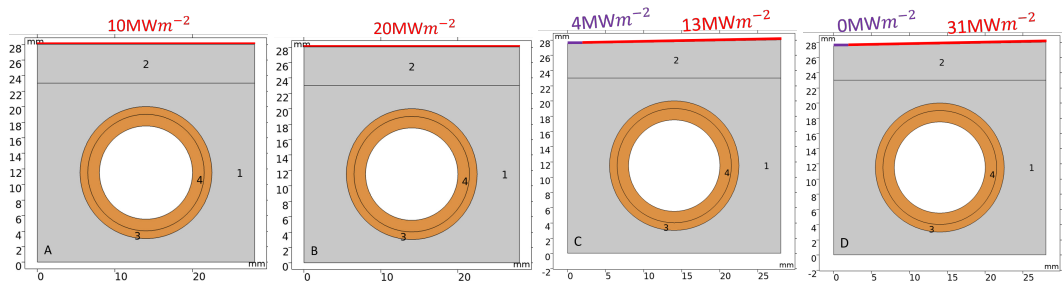


Figure 5.1. Schematic of 2D geometries for thermal conduction topology optimisation studies, showing flat monoblocks with steady-state (A) and transient (B) heat loads and bevelled monoblocks with steady-state (C) and transient (D) heat loads. The schematic includes (1): The design domain (initially W), used for the topology optimisation. (2) W minimum armour thickness of 5mm. (3) Cu interlayer. (4) CuCrZr cooling pipe described by an internal forced convection heat flux boundary representing 423.15K water at 10m s^{-1} .

5.2.1 Modelling setup

A 2D finite element heat conduction problem is solved for a flat monoblock design with a steady state heat flux of 10MW m^{-2} and 20s transients of 20MW m^{-2} . The same approach is then applied to a bevelled monoblock, designed to reduce the prominence of leading edges due to misalignment, as shown in Fig. 5.1. The heat flux profiles and a detailed account of monoblock shaping can be found in (R. A. Pitts *et al.* 2017) where 8% of the top surface receives a reduced load of 4MW m^{-2} in steady state and no load during transient fluxes. The other 92% of the top surface experiences 13MW m^{-2} in steady state operation and 31MW m^{-2} during 20s transients. These heat fluxes are higher than those in the flat geometry, as they take into account global tilting of the divertor plates, which results in a

different plasma interaction. The Fourier law for heat conduction, Eq. 5.1, forms the basis for the topology optimisation objective functions.

$$\mathbf{q} = -k\nabla T \quad (5.1)$$

where \mathbf{q} is the conductive heat flux, k is the thermal conductivity and ∇T is the gradient of the temperature field. The objectives include:

- i The minimisation of average temperature T ,
- ii The minimisation of average thermal gradient magnitude $|\nabla T|$,
- iii The maximisation of conductive flux magnitude $|\mathbf{q}|$.

Changes in the values of these objectives are made through the iterative modification of the material properties in the design domain. The topology optimisation relies on the density-based SIMP implementation found in COMSOL Multiphysics which involves penalisation of intermediate material values, resulting in distinct high conductivity and low conductivity domains in optimised designs.

The algorithm is based on the Globally Convergent Method of Moving Asymptotes (GCMMA) (Svanberg 2002). The transition in thermal conductivity, density, and heat capacity between W and Cu is handled by linear interpolation of material properties. Average values for the objectives rather than maxima or minima were found to be more robust in the software. Both filtering and projection were used in the topology optimisation in order to produce designs with smoother more manufacturable domains and to reduce the mesh dependency.

5.3 Results

The images in Fig. 5.2 show the optimised geometries with discrete high and low conductivity regions in the design domain. The flat monoblocks and bevelled cases have similar resulting optimised geometries however minor differences are observable. This is particularly apparent on the right side of the coolant pipe where there is a greater armour thickness. It is possible that more significant differences would be visible if the optimisation design domain included the sacrificial armour layer. It is clear that the different objectives result in distinct geometries, with the heat flux objective in particular (Figs. 5.2c and 5.2f) showing deviation from the others. The Cu ‘arms’ appear to redirect heat flux to the sides of the pipe. Figs. 5.2b, 5.2a, 5.2d, 5.2e display more minor differences, however, with the main result being increased thermal conduction to the top of the pipe.

Fig. 5.3 displays temperature profiles as measured between the top of the topology optimisation design domain and the sacrificial armour layer (labelled as 1 and 2 in Fig. 5.1) for the optimised geometries shown in Fig. 5.2. Fig. 5.3 shows that the temperature and thermal gradient minimised designs have similar performance characteristics as outlined in Table

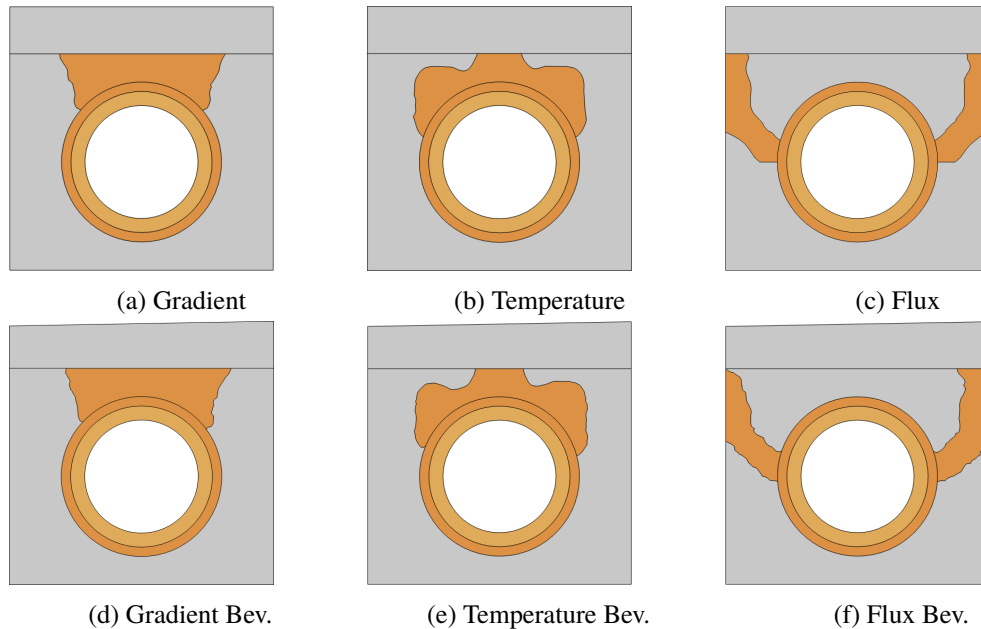


Figure 5.2. Optimised geometries for the flat (top row) and bevelled (lower row) monoblock objectives.

5.1. The same is true for the thermal gradient minimised designs in steady-state operation. More significant reductions are seen in the transient loading scenarios, lowering temperature profiles at the top of the design domain by approximately 200K in the flat monoblock and 300K in the bevelled monoblock, as shown in Fig. 5.3.

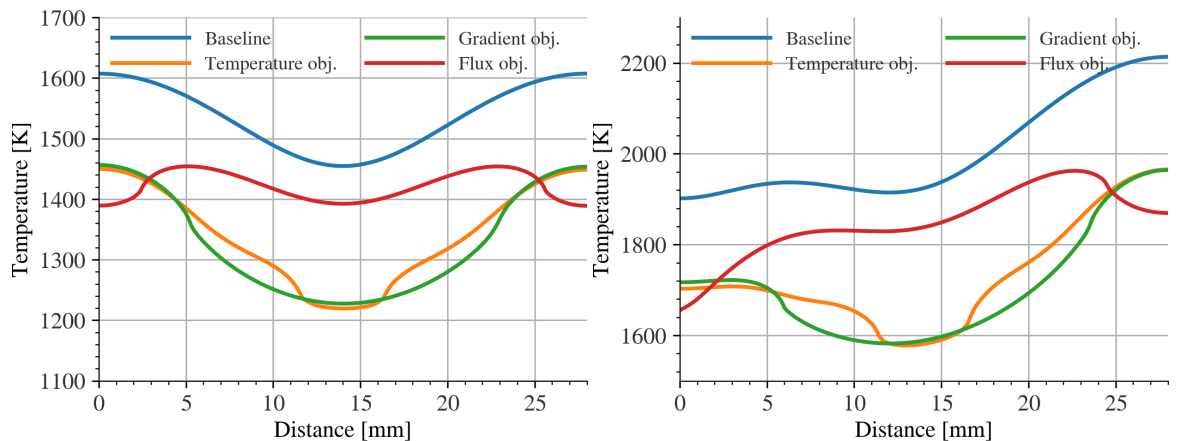


Figure 5.3. Temperature profiles during transient loading conditions along the upper boundary of the design domain for baseline and optimised geometries. Left: flat monoblocks. Right: bevelled monoblocks.

Fig.5.4 shows a strong reduction in thermal gradient magnitude in the regions occupied by the topology-optimised heat transfer promoters above the cooling pipes for the temperature and thermal gradient minimised designs. The geometry resulting from conductive heat flux maximisation does not result in significant average reductions in design domain temperature or thermal gradient and only produces a slight increase in average conductive heat flux, but does produce a more even temperature profile across the top of the design domain (see Fig. 5.3), which may lead to reductions in thermally induced stress. The placement of Cu at the sides of the monoblock counteracts the flux concentration associated with using a circular pipe to cool a square cross-sectioned monoblock.

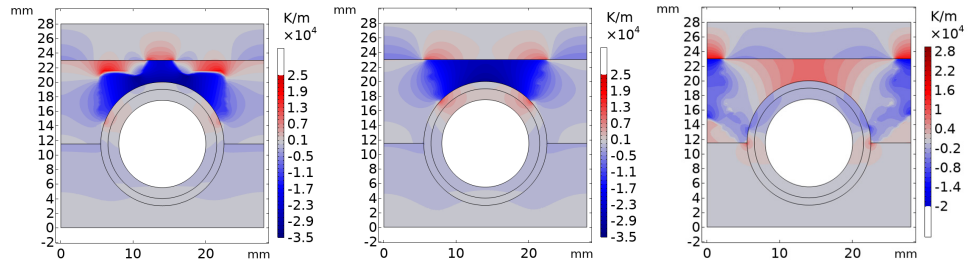


Figure 5.4. Contours showing the change in thermal gradient magnitude with respect to the conventional ITER baseline design, for temperature (left), thermal gradient (middle) and conductive heat flux (right) optimised flat monoblocks in 10MW m^{-2} steady state heat fluxes.

Table 5.1. Design domain average values for temperature and thermal gradient for all geometries. The values are displayed as percentages of the baseline design steady-state performance.

	Objective	Flat monoblock		Bevelled monoblock	
Heat flux [MW m^{-2}]		10	20	(4,13)	(0,31)
Temperature	Baseline	100%	136%	100%	153%
	Temperature	97%	120%	97%	143%
	Gradient	98%	128%	98%	144%
	Flux	100%	133%	100%	154%
Thermal gradient	Baseline	100%	226%	100%	262%
	Temperature	87%	168%	87%	195%
	Gradient	83%	164%	83%	188%
	Flux	101%	198%	102%	262%

5.4 Conclusions

Whilst this optimisation setup only provides a limited encapsulation of the challenges facing the fusion reactor divertor, it has been demonstrated that the addition of high conductivity features in the monoblock armour domain has the potential to cause a significant reduction in thermal gradient and to reduce the temperature at the top of the design domain by over 200K for temperature and thermal gradient minimised designs during high heat flux transient events. The application of topology optimisation to an asymmetric design shows the potential of the technique to generate novel geometries targeted to specific applications. There may be merit to considering this approach in future reactor designs, as the application of topology optimisation to thermal problems becomes more mature and the material considerations evolve. The addition of high conductivity heat transfer elements in the design creates thermally induced stress concentrations not accounted for in this study, however, the use of a secondary topology optimisation step such as that used in (Curzadd *et al.* 2019) is suggested as a potential solution. Simultaneous multi-objective optimisation of temperature or thermal gradient and stress was found to produce unsatisfactory results with the available software tools and was therefore not pursued in this study but may be the subject of future work.

Acknowledgements

Oliver Marshall was supported by EPSRC [EP/L01663X/1]. Lee Margetts was supported by EPSRC grants EP/N026136/1 and EP/T026136/1. Llion Evans was supported by EPSRC grant EP/R012091/1.

Chapter 6

Paper 4 - Multi-Objective Topology Optimisation of a Tungsten Divertor Monoblock, With Consideration of Toroidal Bevelling and Multiple Attachment Scenarios

**Multi-objective topology optimisation of a tungsten divertor monoblock,
with consideration of toroidal bevelling and multiple attachment
scenarios**

Oliver H.R. Marshall^{1*}, Lee Margetts¹, Llion M. Evans^{2,3} and Matthew J. Roy^{1,4}

¹ Department of Mechanical, Aerospace and Civil Engineering, George Begg Building, The University of Manchester, Manchester, United Kingdom, oliver.marshall@manchester.ac.uk, lee.margetts@manchester.ac.uk, matthew.roy@manchester.ac.uk

² College of Engineering, Swansea University, Swansea, United Kingdom, llion.evans@swansea.ac.uk

³ United Kingdom Atomic Energy Authority, Culham, United Kingdom

⁴ Henry Royce Institute, University of Manchester, United Kingdom

Abstract

The potential for topology optimisation to contribute to future fusion reactors is considered and applied to a W-Cu divertor monoblock, a component responsible for handling the most intense heat fluxes. A density-based topology optimisation method implemented in commercially available software has been applied to two different monoblock geometries in order to investigate the impact of an asymmetric bevel on the top surface. Additionally, two different attachment methods are considered: suspension of the monoblock on a structural

cooling pipe and bonding of the bottom edge to a support. Multi-objective optimisation, with terms linked to both thermally induced stress and heat transfer characteristics, employing a 2D plane stress approximation has been investigated, alongside the impact of reducing the maximum allowable Cu content of designs. Minimising thermally induced stress was found to reduce the maximum stress in the design domain to 35% of the reference value in one case. Thermal performance improvements include a temperature reduction of 270°C in the upper portion of the monoblock and a 20% transfer of heat flux from the top of the cooling pipe to the sides. Four design concepts are presented which could inform future development and manufacture of monoblocks aided by functional grading manufacturing techniques. Realistic structure-property relationships in Cu-W alloys are beyond the scope of this study, but further research in this area would enable better interpretation of topology-optimised designs for manufacture. The results presented are provided within the context of long-term application to fusion design and demonstrate the ability of topology optimisation both to provide novel geometries and to illustrate the impact even minor changes to geometry and operating conditions can have on the search for an optimal design.

6.1 Introduction

The planning, design and construction of new fusion reactors (tokamaks) is a time-intensive process. ITER will be the world's largest tokamak when it is completed, however, in the 47 years between the beginning of Conceptual Design Activities (1988) (Tomabechi 1991) and planned full power operation (2035) (Bigot 2019), the power of design tools and the capabilities of novel manufacturing techniques available to engineers and designers have advanced dramatically. The ITER plasma-facing components (PFCs) which line the reactor first-wall and divertor face unique operational conditions including high steady-state heat loads, damaging transient events, neutron and gamma radiation, sputtering, arcing and a number of other processes which challenge engineering design. The divertor, which is responsible for handling the most intense heat loads in ITER, consists of 54 cassettes containing thousands of monoblocks: W armour blocks with a CuCrZr water-cooled heat pipe in the centre, separated by a stress-relieving Cu interlayer. Divertor components in ITER may receive heat fluxes of $\geq 10 \text{ MW m}^{-2}$ in steady state with transients of up to 20 MW m^{-2} , leading to extremes of temperature and a thermally induced stress which can induce component failure (R. A. Pitts *et al.* 2017).

Divertor operation is a crucial design-driving factor that plays a major part in the conceptualisation of future devices (D. Maisonnier *et al.* 2007) and hence it is chosen here as the subject for a topology optimisation study with the goal of minimising a set of stress and temperature based objectives whilst maintaining compatibility with the monoblock concept. The technique is subsequently applied to asymmetric, bevelled monoblocks, designed to limit heat flux concentration by reducing the prominence of monoblock leading edges exposed to the plasma. This paper aims to contribute to the development of divertor components which exploit developments in functional grading enabled by additive manufacturing (Loh *et al.*

2018). This is done in order to improve component performance whilst remaining resilient to the uncertainty that is present in future reactor operating conditions, which may see increases to heat loads (Zohm *et al.* 2013). A selection of baseline divertor components which are then tailored to specific devices using techniques like topology optimisation may reduce the current risk associated with designing components for future reactors such as DEMO, which have significant uncertainty in design requirements (G. Federici, Bachmann, Barucca, Biel, *et al.* 2018).

6.2 Concept and methodology

The divertor monoblock optimisation process involves using finite element analysis and topology optimisation to obtain design concepts which minimise stress and improve thermal performance. Beveling of the top surface of the monoblocks was a recent introduction to the component design which has been found to protect leading edges from high steady state heat fluxes and offer some protection from plasma disruptions such as Edge-Localised Modes (ELMs) (J. Gunn, T. Hirai, *et al.* 2019). As beveling is a novel design modification, topology optimisation is used to explore the design space both in regard to behaviour under load and influence on optimum geometry. It is thought that topology optimisation is particularly appropriate for the generation of optimum designs where there is asymmetry (introduced by the monoblock beveling) due to the possibility of specifying a generic design domain. This reduces the need for detailed parameterisation and initial concept development associated with other optimisation techniques. Furthermore, whilst topology optimisation could be applied to any property of monoblock design, to constrain the scope of the work, this study focuses on elements already established in the literature as part of the design.

6.2.1 Finite element analysis

The modelling is formulated using linear elastic material models. Whilst some recent work investigates modelling of a non-structural interlayer which undergoes inelastic deformation by design (M. Fursdon, J. H. You, *et al.* 2018), this approach is outside the scope of the present study. The results from the linear elastic analysis are likely to be somewhat unrealistic, however, as inelasticity is common for the subject application and therefore the stresses presented in the optimised geometries should be interpreted relative to the reference cases primarily and not as absolute or ‘design’ values. The finite element analysis is composed of a thermal conduction problem and a linear elastic stress analysis. The divertor monoblock problem is simplified to 2D, where the plane stress approximation of a thin plate stretched in its own plane (the monoblock cross-section) is employed. The geometries and boundary conditions used are shown in Fig. 6.1.

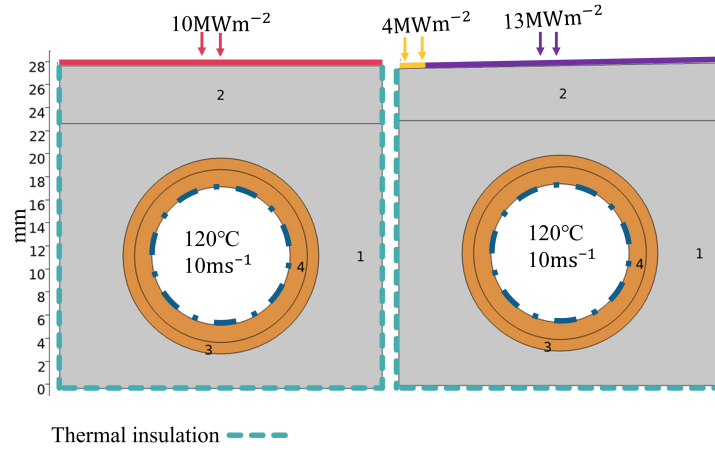


Figure 6.1. Sketch of 2D geometries for topology optimisation studies showing flat monoblock (left) and bevelled monoblock (right) with a 0.5mm bevel resulting in a higher heat flux over 92% of the top surface and a shadowed area on the left-most 8%. (1): The design domain (initially W), used for the topology optimisation. (2) W minimum armour thickness of 5mm. (3) Cu interlayer. (4) CuCrZr cooling pipe described by an internal forced convection heat flux boundary representing 120°C water at 10m s⁻¹ and a 4MPa load on the internal boundary of the pipe representing water pressure.

6.2.2 Geometries and loading conditions

The geometries shown in Fig. 6.1 are based on the ITER monoblock design, and were chosen in order to facilitate comparison to current design performance. The case for shaping the upper edge of divertor monoblock components is presented in (R. A. Pitts *et al.* 2017), where a bevel with a height of 0.5mm and an angle of 1° was evaluated for its ability to reduce the likelihood of concentrated heat fluxes and melting occurring on leading edges. The resulting difference in plasma exposure gives rise to the different heat fluxes incident on the top edges of the two monoblock geometries. The minimum armour thickness of 5mm shown in Fig. 6.1 is also referred to as the ‘sacrificial armour’ region and is designed to account for erosion during the component’s life. This is visualised as a separate domain for the purposes of identifying the design domain for topology optimisation however it is designed to be part of a continuous armour plate and not a separate entity requiring joining. The monoblocks are assumed to be operating in a vacuum, preventing heat transfer to the environment by conduction or convection. Radiative heat transfer is assumed to be negligible and so a thermal insulation condition is imposed (Fig. 6.1), described by $-\mathbf{n}\cdot\mathbf{q} = 0$, where \mathbf{n} is the normal vector on the boundary and \mathbf{q} is the heat flux. In the ITER design, every fifth monoblock is fixed at its base to a support structure, with the remaining 80% suspended on the structural CuCrZr pipe (Ezato *et al.* 2016). To reflect this, results are presented for both a geometry with minimal mechanical constraints, where the bottom left corner is constrained in the y -direction and the bottom right corner in both the x and y directions and for a monoblock with a fixed constraint on its bottom edge. To avoid excessive repetition, the minimally constrained case referred to as ‘suspended’ and the fixed constraint case is referred to simply as ‘fixed’. This results in four cases: a suspended flat monoblock, a fixed flat monoblock, a suspended bevelled monoblock and a fixed bevelled monoblock.

The water-cooled pipe is modelled with a convective heat flux (q_0) of $\mathbf{n}\cdot\mathbf{q} = q_0$ where

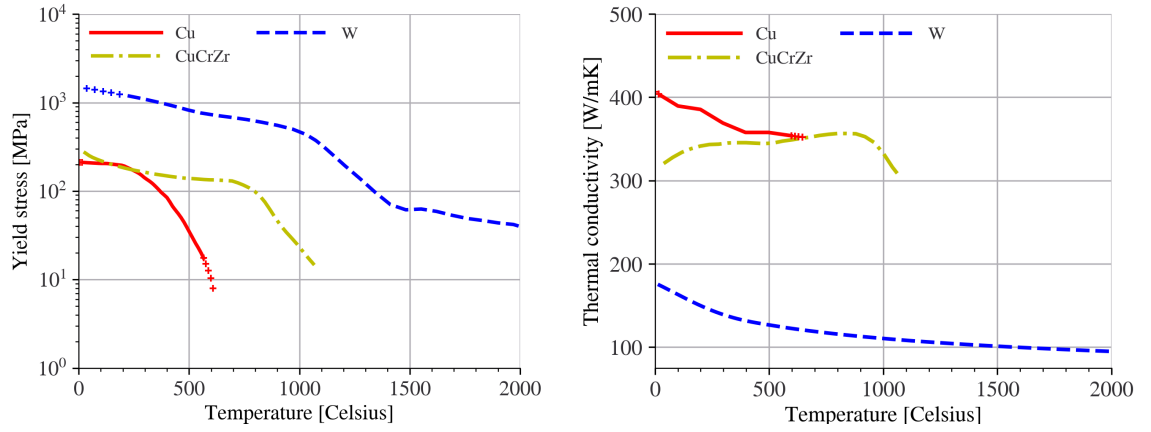


Figure 6.2. Left: Variation in yield stress and conductivity with temperature for the monoblock constituent materials: tungsten (W (*Tungsten as a Structural Divertor Material* 2018)), pure copper (Cu (Karditsas and Baptiste 1995)) and copper-chrome-zirconium alloy (CuCrZr (Gonzalez *et al.* 2018)) Right: Conductivity variation with temperature for W, Cu (krishna *et al.* 2012), and CuCrZr (Gonzalez *et al.* 2018). Where material properties were not available in the built-in material library, representative properties were found in the literature and extrapolated linearly (in regions indicated with the ‘+’ symbol) when not available for the appropriate temperature range.

$q_0 = h \cdot (T_{ext} - T)$. The temperature-dependent heat transfer coefficient h is calculated for a 12mm diameter pipe with a coolant temperature (T_{ext}) of 120°C and a velocity of 10m s⁻¹. A force of 4MPa is applied to the inner surface of the pipe to represent water pressure, but the pipe is not mechanically constrained, allowing for inward thermal expansion.

6.2.3 Topology optimisation

The topology optimisation approach relies on a density-based technique implemented in commercial software (COMSOL Multiphysics 5.6[®]) that utilises the Globally Convergent Method of Moving Asymptotes (GCMMA). The (GC)MMA method divides the optimisation problem into solvable convex sub-problems in a manner that ensures global convergence (GC). The reader is directed to background on the density-based method (M. Bendsøe and Ole Sigmund 1999) and the globally convergent MMA method (Svanberg 1987, 2002). The material properties of W, Cu and CuCrZr exhibit significant spatial variation in the monoblock due to the high temperature difference between the top and bottom of the design. The variation of conductivity and yield stress is highlighted in Fig. 6.2. The stress-free reference temperature (indicating the temperature at which there is no residual stress) is kept constant at 26.85°C. Its influence on the design of topology optimised monoblocks is investigated in Ref. (Curzadd *et al.* 2019; Kerkhof *et al.* 2021). Furthermore, it is indicated in Ref. (M. Fursdon, J. H. You, *et al.* 2018) that attempts to incorporate the impact of residual stress in elastic modelling are not recommended.

6.2.4 Temperature constraints

The influence of temperature-based constraints (summarised in Table 6.1) on the constituent materials is investigated. These include a constraint designed to limit the presence of W

below the Ductile to Brittle Transition Temperature (DBTT), set at a value of 200°C. The W operational temperature range continues up to the recrystallisation limit, set at 1200°C. A limit of 500°C (T_{cu}) is used for pure Cu. This is a ‘soft’ limit, however, as Cu may be placed in regions that will exceed this temperature in a linearly diminishing fraction up to the recrystallisation limit. In practice, however, the placement of Cu becomes undesirable to the optimisation algorithm at higher temperatures due to the reduction in yield stress. The recrystallisation temperature limit (T_w) can be imposed on the temperature variable for individual elements of varying material content: $T_{lim} = (T_{cu} - T_w)\theta + T_w$, where θ is the topology optimisation density variable used for the interpolation of material properties. This variable θ varies in the design domain as $0 \leq \theta \leq 1$, where $\theta = 0$ indicates a region of pure W and $\theta = 1$ indicates a region of pure Cu. The design domain is initialised with $\theta = 0.5$.

Table 6.1. Summary of material-based temperature limits. *These limits are ‘soft’ limits which are linearly interpolated in topology optimisation problems in order to account for the local mixing of materials.

Material	Upper/Lower	Temperature limit [°C]
W (DBTT)*	Lower	200
W	Upper	1200
Cu	Lower	26.85
Cu*	Upper	500
CuCrZr	Upper	350

The lower DBTT limit (also a ‘soft’ limit) is imposed on the topology optimisation density variable θ , with $(T_{DBTT} - T)/T_{DBTT}$ acting as a constraint on the lower bound of θ . The limit is not physics-based, but formulated such that the W fraction is limited to $< 100\%$ if the temperature is below the DBTT. The DBTT limit was investigated in preparatory work but not applied to the results presented due to its impact on the optimisation, but is described here to add context to the discussion in Section 6.3.4. The upper limits for W and Cu were combined in an interpolated constraint to reflect the local material content at all points during the optimisation. It is surmised that the structural CuCrZr is unsuitable for operation above 350°C (K. Zhang, Gaganidze, and M. Gorley 2019) due to thermal creep exacerbated by neutron radiation (Jeong-Ha You 2015). The CuCrZr is outside the present design domain and so a limit is not imposed, however, visualisation of the temperature results relative to the local temperature limit makes reference to this value. A volume fraction constraint (surface-area fraction in 2D) is investigated in Section 6.3.5 as a means of reducing the Cu content of optimised designs.

6.2.5 Materials and manufacturing

The variation in the yield strengths of the materials considered with temperature is presented in Fig. 6.2. As the mismatch of coefficients of thermal expansion (CTE) is one of the primary drivers of thermally induced stress in the design (Linke *et al.* 2019), intermediate density elements are not penalised, to reflect the capability of functional grading to produce transitions in material properties not anticipated in early topology optimisation works where penalisation was established to accommodate traditional manufacturing techniques (see Ref.

(G. I. N. Rozvany *et al.* 1993)). A filter based on the Helmholtz partial differential Eq. with a radius of 1mm (see Ref. (B. S. Lazarov and O. Sigmund 2011)) is used to reduce mesh dependence and the occurrence of fine structures which would further hinder manufacture. The relevant material properties are linearly interpolated between the two materials. These include thermal conductivity, coefficient of thermal expansion, density, Poisson’s ratio, elastic modulus and yield strength. Research into the material properties of W-Cu composite materials is ongoing but incomplete. For example, there is some indication that Cu-infiltrated W has a lower DBTT (Hiraoka *et al.* 2005). The linear interpolation of material properties in the present work should be interpreted as representing ‘target material properties’ which do not correspond to exact proportions of functionally graded Cu-W and are a guide to future design work. Ongoing development in the fields of additive manufacturing and functional grading are identified as methods for the construction of topology-optimised designs, however, it is likely that a substantial amount of interpretation and post-processing will be required before any topology-optimised design is suitable for manufacture.

6.2.6 Consideration of cost functions

It is likely that partial monoblock melting due to intense transient loads resulting from plasma disruptions including Edge Localised Modes (ELMs) (R. A. Pitts *et al.* 2017) will occur in ITER and future devices. Furthermore, there is a high degree of uncertainty regarding the operating conditions of future divertors (DEMO), with some suggesting a heat flux limit of 5MW m^{-2} (Zohm *et al.* 2013) and others expecting heat fluxes between $10 - 20\text{MW m}^{-2}$ (Bachmann *et al.* 2018), which may mean that future divertor components may be manufactured from different, often lower conductivity materials such as Eurofer (Li-Puma *et al.* 2013). For these reasons, whilst the problem considered in this paper is framed in terms of the ITER reference design for ease of comparison, thermal objectives are considered worthy of investigation in addition to the more conventional minimisation of thermally induced stress. The thermal objective problem can be thought of as the distribution of a limited quantity of high-conductivity material in the armour domain. The Fourier law for heat conduction, Eq. 6.1, forms the basis for the thermal topology optimisation objective functions:

$$\mathbf{q} = -k\nabla T \quad (6.1)$$

where \mathbf{q} is the conductive heat flux, k is the thermal conductivity and ∇T is the gradient of the temperature field. All of these quantities can be used as thermal objectives to be minimised or maximised. The thermal conductivity is related to the density ρ , specific heat c_p through the thermal diffusivity α .

$$\alpha = \frac{k}{\rho c_p} \quad (6.2)$$

Therefore, temperature ($\frac{T}{T_i}$) and the inverse of conductive heat flux magnitude ($\frac{q_i}{|q|}$) have been minimised. The domain selection for the minimisation of the thermal objectives changes and is specified with individual results. Normalisation constants q_i and T_i are equivalent to

the average reference design conductive heat flux and temperature, respectively. The stress minimisation is performed using the von Mises stress σ_V and the yield stress σ_y as a cost function $\frac{\sigma_V}{\sigma_i \sigma_y}$, where σ_i is a normalisation constant equal to the average von Mises stress in the reference design.

6.2.7 Reducing the Cu-content of designs

The European Fusion Development Agreement (EFDA) in (Romanelli *et al.* 2012, pp. 5) sets out the goal that ‘at around 100 years after the reactor shutdown all the materials can be recycled in a new reactor’. Whilst the ITER monoblock design uses Cu, its presence is considered unfavourable as the time taken for activity to decay such that it is suitable for disposal or recycling exceeds 100 years (Okada, Noda, and Abe 1989). For this reason, there is a strong motivation for reducing the Cu content of the designs generated in this study. This is approached by placing a limit on the maximum Cu content in the design domain.

The ‘surface-area’ fraction θ_{avg} (commonly referred to as volume fraction in 3D) is defined in Eq. 6.3, where Ω is the design domain. Here, θ_{avg} represents the maximum allowable fraction of the design domain which can be occupied with Cu:

$$\theta_{avg} = \int_{\Omega} \theta d\Omega / \int_{\Omega} d\Omega \quad (6.3)$$

Eq. 6.3 implies that in the case of intermediate material density material ($0 < \theta < 1$), the surface-area fraction constraint can be met equally by a small high Cu content region or a larger, more diffuse area. Minimising the amount of Cu in topology-optimised designs may also be important to comply with performance-related requirements placed on the divertor, as the physical and mechanical properties of pure Cu degrade with neutron irradiation (Richou, Li-Puma, and Visca 2014).

Goals for successful optimisation

The topology optimisation of the monoblock may be considered a success only if the results do not interfere with the component’s other functions and requirements. In this study, the following factors may be considered desirable:

- i The use of a minimum amount of Cu.
- ii The placement of Cu as far away from the extreme operating conditions of the plasma-facing surface as possible.
- iii Any contribution to relieving other monoblock challenges such as uneven heat dissipation or cooling limitations.

Points (i) and (ii) are important to reduce the impact of excess material activation in the monoblock (Li-Puma *et al.* 2013) and (iii) aims to ensure that the flexibility presented by the

topology optimisation process is exploited. Ease of manufacture is arguably as important as any of these points, but as mentioned previously, is beyond the scope of this study.

6.3 Flat monoblock results

The results of the reference design analysis for a suspended flat monoblock are presented in Fig. 6.3. The temperature in Celsius and relative to the operational limits: $(\frac{T}{T_{lim}})$, presented in Fig. 6.3a and 6.3b show that the top of both the W armour and the CuCrZr pipe exceed the operational temperature limits, specified in Table 6.1. Von Mises stress and relative stress $(\frac{\sigma_V}{\sigma_{yield}})$ are shown in Fig. 6.3c and 6.3d respectively, including maximum values for σ_{rel} . Whilst the absolute values of the von Mises stress may not be fully reliable, it is clear that the thermally induced stress in the monoblock is significant, with particular stress concentrations in and around the top of the coolant pipe. As previously mentioned, there is very high stress in the interlayer relative to the yield strength, however as this is not the focus of the present study, interlayer stress is not discussed further.

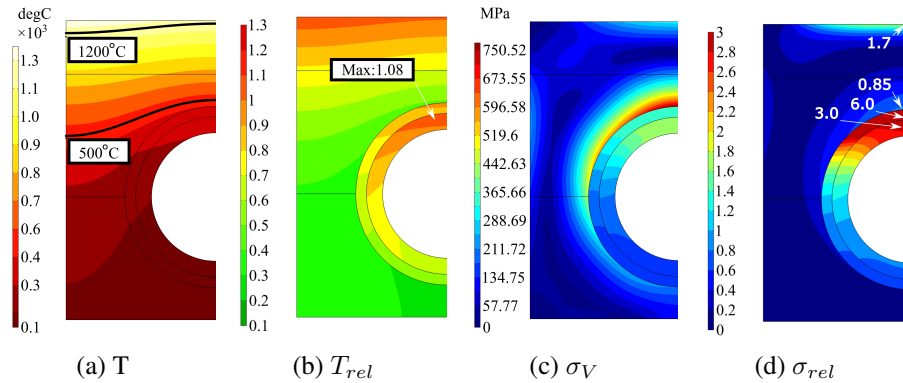


Figure 6.3. Results for the suspended flat monoblock reference design. a) Temperature distribution with contours highlighting Cu 500°C and W 1200°C temperature limits. b) Temperature relative to respective material limits. c) von Mises Stress. d) von Mises stress relative to yield stress. The maximum values of σ_{rel} are highlighted in each domain.

6.3.1 Suspended flat monoblock optimisation results

Fig. 6.4 shows the topology optimisation results for the suspended flat geometry, for: stress σ_V (Fig. 6.4a); stress and conductive heat flux $\sigma_V + q$ (Fig. 6.4b); stress and temperature $\sigma_V + T$ (Fig. 6.4c). The results for temperature, flux and stress difference with respect to the suspended flat reference design are also displayed.

For all of the optimisation cases in Fig. 6.4, the Cu fraction plots show that Cu is placed around the bottom of the pipe and transitions to an intermediate density region around the sides of the pipe, enabling a gradual transition of CTEs. The temperature difference plots (δT) show a reduced temperature in the top half of the monoblock with large regions experiencing a $\delta T > 100^\circ\text{C}$ (highlighted) and maximum δT values of 167°C, 181°C and 183°C. The flux difference plots (δq) show transfer of conductive heat flux from the top of the coolant pipe to the sides. Contours representing changes of $\geq 1\text{MW m}^{-2}$ are highlighted.

Table 6.2 shows significant reduction of stress relative to the interpolated material dependent elastic limits is seen in the pipe, where the σ_V case is best at reducing stress in the design domain and the sacrificial armour layer (labelled as ‘Top’), but the multi-objective cases produce better stress reduction in the interlayer and pipe. The multi-objective cases in Fig. 6.4 in general feature more Cu placement, and consequently better cooling capability (with peak δT approximately 20°C greater) and more extensive regions where the increase in heat flux to the sides of the monoblock is greater than 1MW m⁻². The $\sigma_V + q$ case uses more Cu and involves a significantly different geometry whereas the $\sigma_V + T$ result increases the density of structures already observable in the single objective case. The enhancement of features found in the σ_V case and the use of less Cu than the $\sigma_V + q$ design indicate that the $\sigma_V + T$ case may be considered the most compatible with the objectives set out in Section 6.2.6 for a desirable topology optimisation result.

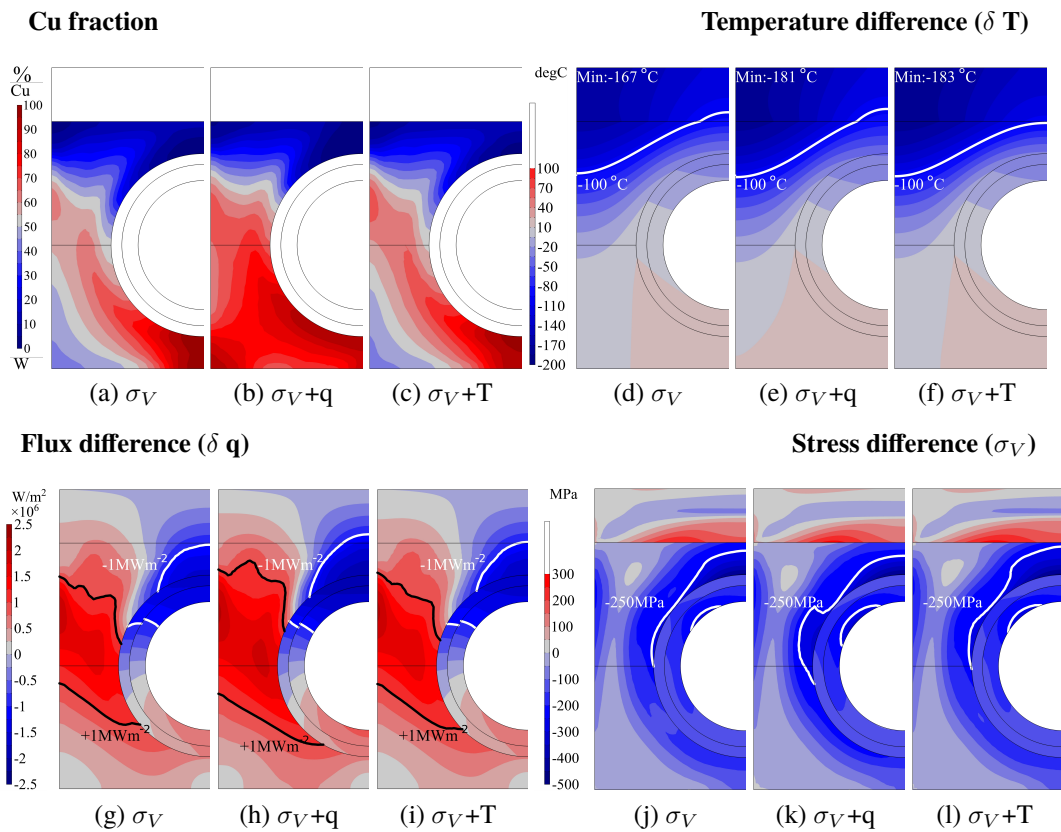


Figure 6.4. Results presented for suspended flat monoblock designs, identified by the objective function listed below the sub-plot. The difference plots are calculated by subtracting the data for the corresponding reference design.

Table 6.2. Maximum relative stresses σ_{rel} for suspended flat monoblock sub-components

	Top	Design domain	Interlayer	Pipe
Reference	1.7	0.85	6.9	3
σ_V	1	0.38	3.2	1.8
$\sigma_V + q$	1.1	0.46	2.8	1.7
$\sigma_V + T$	0.96	0.4	3.1	1.8

In all the optimised cases, the stress in the design domain is significantly decreased, with large regions exhibiting $\delta\sigma_V \geq 250\text{MPa}$ reduction in von Mises stress. There is, however, an increase in stress of around 200MPa where the design domain meets the lower edge of the sacrificial armour layer. Whilst this is not desirable, this region was not near its yield

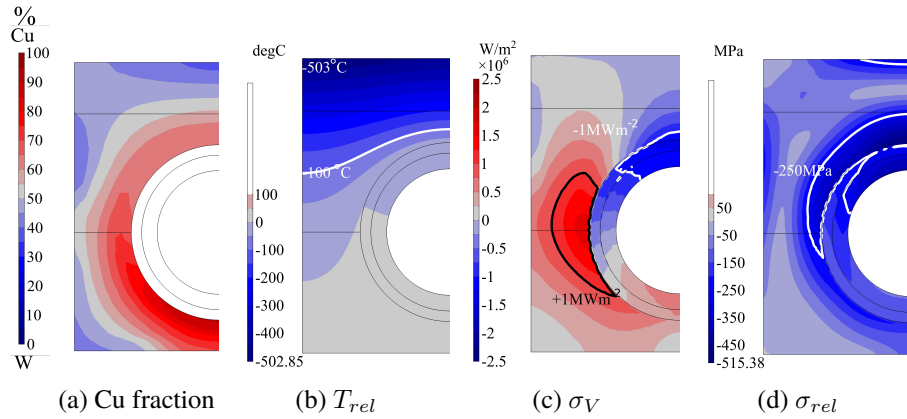


Figure 6.5. Designs without a constrained sacrificial armour layer. (a) Cu fraction [%]. (b) Temperature difference with respect to the reference design, with contours highlighting -100°C . (c) Flux difference. (d) Difference in von Mises stress.

stress in the reference design and or after optimisation (where it is between 40 – 60% of σ_y). This stress increase is present for two primary reasons. Firstly, during the optimisation, Cu is placed at the sides of the monoblock to minimise stress in the design domain on the basis that lateral expansion is largely unrestricted. Secondly, the material composition approaching the upper boundary of the design domain is not 100% W and hence there is a difference in CTE that does not exist in the reference design.

6.3.2 Extension of the design domain

Fig. 6.5a shows the distribution of material obtained when the sacrificial armour layer is included in the design domain. The plots in Fig. 6.5 feature greater reductions in stress and temperature, distribution of Cu less dependent on placement at the sides of the domain and no increase in stress at the sacrificial armour domain boundary. As the goal of this study is to produce designs compatible with the geometric requirements for the ITER monoblock, this approach is not pursued further, but again highlights the importance of boundary conditions in the topology optimisation process. It is likely that a managed transition to 0% Cu at this boundary would result in a compromise between the two approaches, however, this was not possible to implement in the available software. It is emphasised that the sacrificial armour layer is not intended as a separate sub-component and exists in the monoblock model solely for the purpose of defining the boundary of the design domain.

6.3.3 Fixed flat monoblock optimisation results

Results for the fixed flat monoblock case are presented in Fig. 6.6, which follows the layout established in Fig. 6.4. The conductivity distribution is very different to the suspended case, and Cu is added to the sides of the pipe rather than below it. The tops (or top corners in the case of the σ_V objective) of the monoblocks display negative δT of $\geq 100^{\circ}\text{C}$. Again, there are regions at the sides of the pipe where the difference in flux exceeds $\pm 1\text{MW}/\text{m}^2$. The fixed boundary condition selection results in stress singularities around the lower corners of

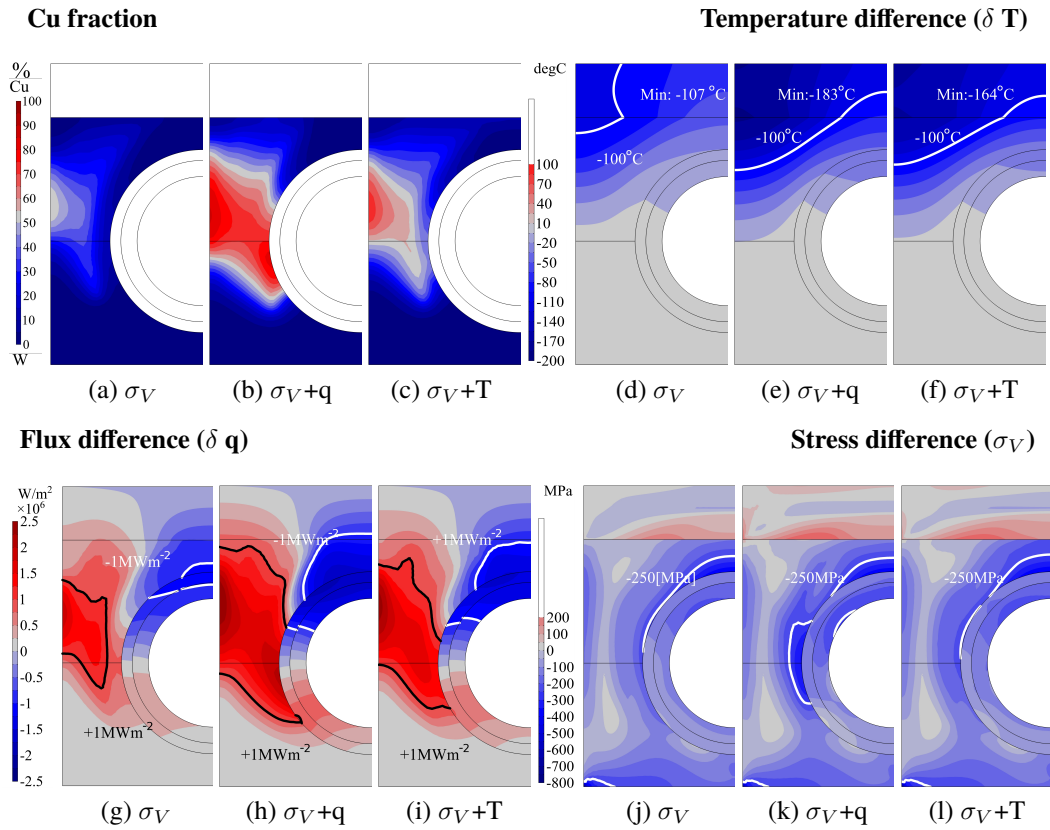


Figure 6.6. Results presented for fixed flat monoblock designs, identified by the objective function listed below the sub-plot. The difference plots are calculated by subtracting the data for the corresponding reference design.

the fixed flat reference design, the topology optimisation reduces the magnitudes of these concentrations, and hence in Fig. 6.6, the monoblock lower corners display high levels of stress reduction. The reductions in maximum relative stresses (σ_{rel}) are presented in Table 6.3. The increased stress on the lower edge of the sacrificial armour layer is again seen in all the designs presented. The geometries for multi-objective results in Fig. 6.6 follow a different pattern to those in the suspended flat monoblock cases, and remain closer to the stress-only objective result in topology but with more Cu placement. The $\sigma_V + q$ and $\sigma_V + T$ cases both result in significant temperature reductions and transfer of conductive heat flux away from the top of the pipe, however, the $\sigma_V + q$ case utilises more Cu and so may be considered less favourable according to the goals established in Section 6.2.7.

Table 6.3. Fixed flat monoblock maximum relative stresses σ_{rel} for reference and optimised designs.

	Top	Design domain	Interlayer	Pipe
Reference	1.46	1.26	6.34	3.19
σ	1.00	0.52	3.70	2.00
$\sigma + q$	1.02	0.59	2.89	1.81
$\sigma + T$	0.90	0.57	3.37	1.96

6.3.4 The ductile to brittle transition temperature (DBTT) constraint

The regions above the re-crystallisation limit and below the DBTT limit for flat and bevelled geometries are shown in Fig. 6.7. Both designs feature a region under the pipe where the temperature falls below the DBTT. Whilst in the case of results for the suspended flat

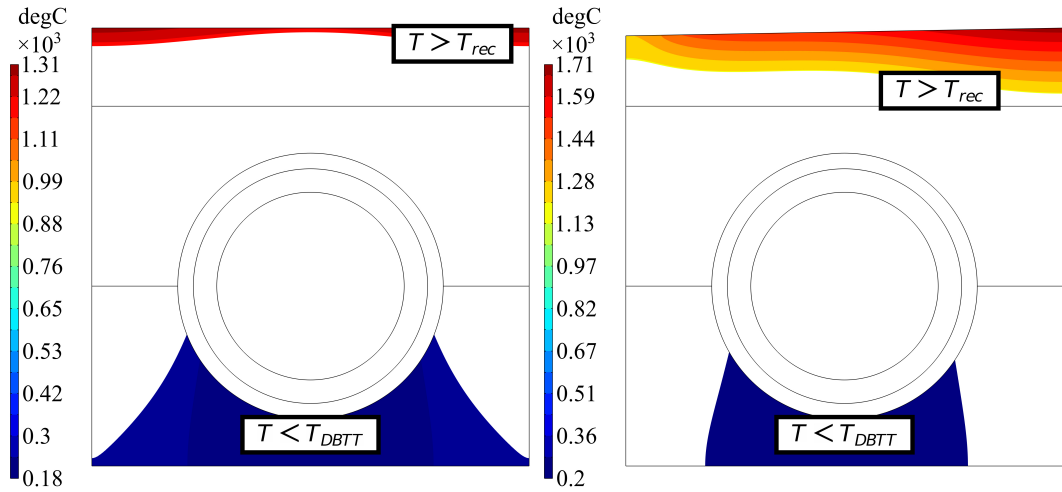


Figure 6.7. Regions where the temperature falls outside the W operational range for flat (left), and bevelled (right) reference geometries.

monoblock, presented in Fig. 6.4, a significant proportion of the Cu is placed in this region without a DBTT constraint enabled, this is not true for the fixed flat case shown in Fig. 6.6. When applied, the DBTT constraint results in the addition of a large quantity of Cu below the pipe at the start of the optimisation. This Cu is not directly tied to meeting the objectives and significantly changes the optimisation problem, reducing the design sensitivity of elements around the pipe, and leading to faster convergence to a local minimum. This is because the convergence method relies on the variation of the optimisation variable in successive iterations. If it is below a specified value (1×10^{-4}), the optimisation terminates. Consequently, the DBTT constraint was not enforced for any of the results presented, as it was decided that the topology optimisation technique employed was most useful as an early-stage design tool to explore the design space. The right side of Fig. 6.7 shows a smaller region of material below the DBTT due to the overall higher average armour temperature. However, there is a much larger region of material above the recrystallisation temperature. The impact of this region is clear in Fig. 6.9d, where the stress reaches almost $7 \times$ yield. For the purposes of this optimisation, the focus is on reducing the region experiencing the highest temperature - and therefore stress relative to yield - rather than on ensuring it operates above its DBTT.

6.3.5 Reduced Cu content designs

This section explores the consequences of constraining the maximum allowable Cu content in the design domain, in line with the optimisation goals presented in Section 6.2.7. Fig. 6.8 shows that reducing θ_{avg} from 50% to 5% counter-intuitively results in a reduction of peak stress in the design domain (DD) and in the sacrificial armour layer (Top). Whilst due to the limitations of the material models, the material properties at intermediate Cu fractions are not fully reliable, a dramatic reduction in peak stress can be observed with only 5% Cu. Although low Cu content designs maintain low maximum stresses (see Table 6.4), these stresses are spread over a larger area. Furthermore, Table 6.4 shows that the cooling capability and flux changes brought about by the addition of the Cu dramatically decrease. Whilst relative stress decreases in the design domain, it increases in the sacrificial armour

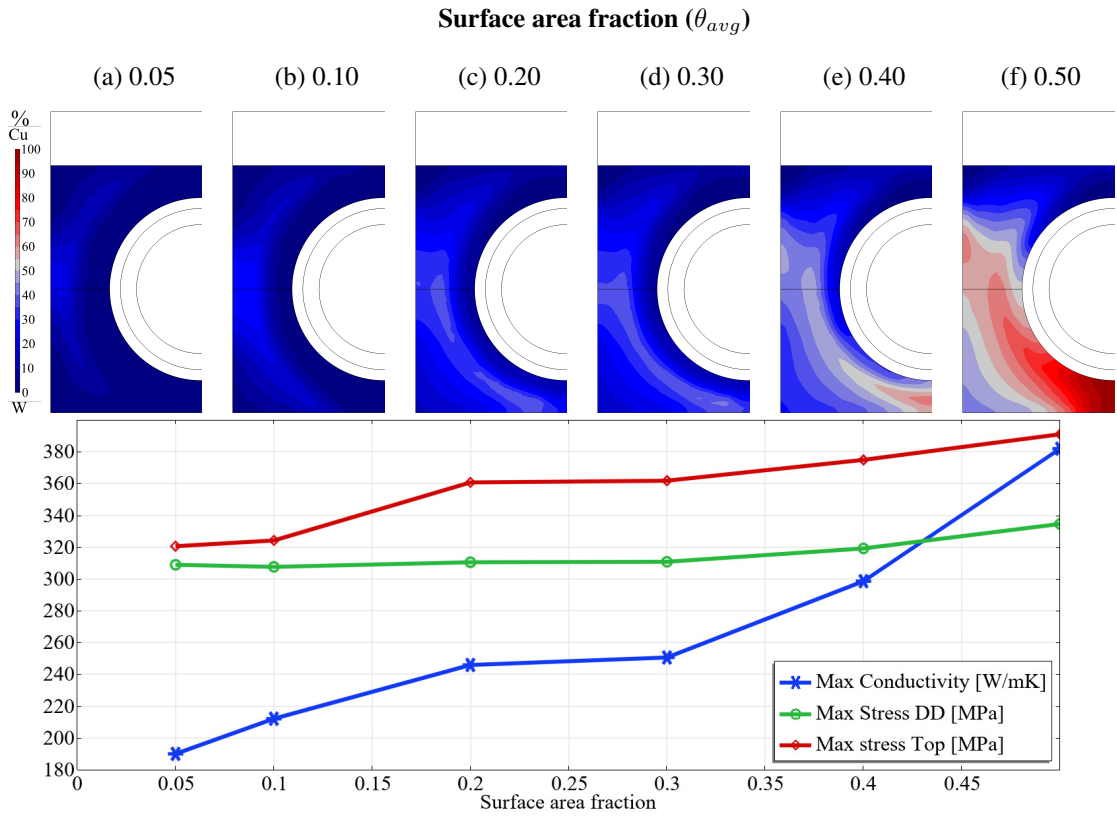


Figure 6.8. Upper: Topologies for reduced surface area fraction designs for a range of average surface area fractions from 5-50%. Lower: Corresponding maximum stress and conductivity data. DD= design domain.

Table 6.4. Relative stress with surface area fraction, presented to summarise the performance of reduced Cu content designs.

θ_{avg}	Max. σ_{rel} (DD)	Max. σ_{rel} (Top)	Min. δT [K]	Max. δT [K]	Max. δq [MW m^{-2}]	Min δq [MW m^{-2}]
0.5	0.39	1	166	14.9	1.98	1.61
0.4	0.34	1	130	10.6	1.55	1.15
0.3	0.34	1.1	98.8	8.31	1.22	0.836
0.2	0.34	1.1	95.7	8.15	1.19	0.812
0.1	0.34	1.1	61.7	7.96	1.03	0.596
0.05	0.34	1.2	44.8	7.08	0.796	0.44

layer due to the higher operating temperature. Higher Cu content designs, therefore, enable a reduction in temperature in the sacrificial armour layer, increasing its yield strength under 10MW m^{-2} operating conditions.

6.4 Bevelled monoblock results

The results for the reference design for the bevelled monoblock are presented in Fig. 6.9. The temperature distribution reflects the asymmetry of the geometry and heat load (see Fig. 6.9a). The upper right-hand corner of Fig. 6.9b includes a point where the temperature is $1.35\times$ the W re-crystallisation limit. The influence of temperature on the yield strength of the component is made clear by observing the differences between Figs. 6.9c and 6.9d. The significantly reduced yield strength at the hottest part of the monoblock results in very high relative stresses, with a maximum of 6.9 in the sacrificial armour layer (see Fig. 6.9d). Asymmetry is visible in Fig. 6.9b) and to a lesser extent than relative stress (Fig. 6.9d), but

not significantly in the von Mises contours (Fig. 6.9c) indicating that the main driver of any asymmetry observable in topology optimisation results is the temperature dependence of yield strength. Whilst the suspended bevelled monoblock optimisation results are presented in Section 6.4.1, the fixed bevelled monoblock results are not presented as they contain a combination of features already observed in the fixed flat and suspended bevelled monoblock cases, but are pursued further in Section 6.4.2.

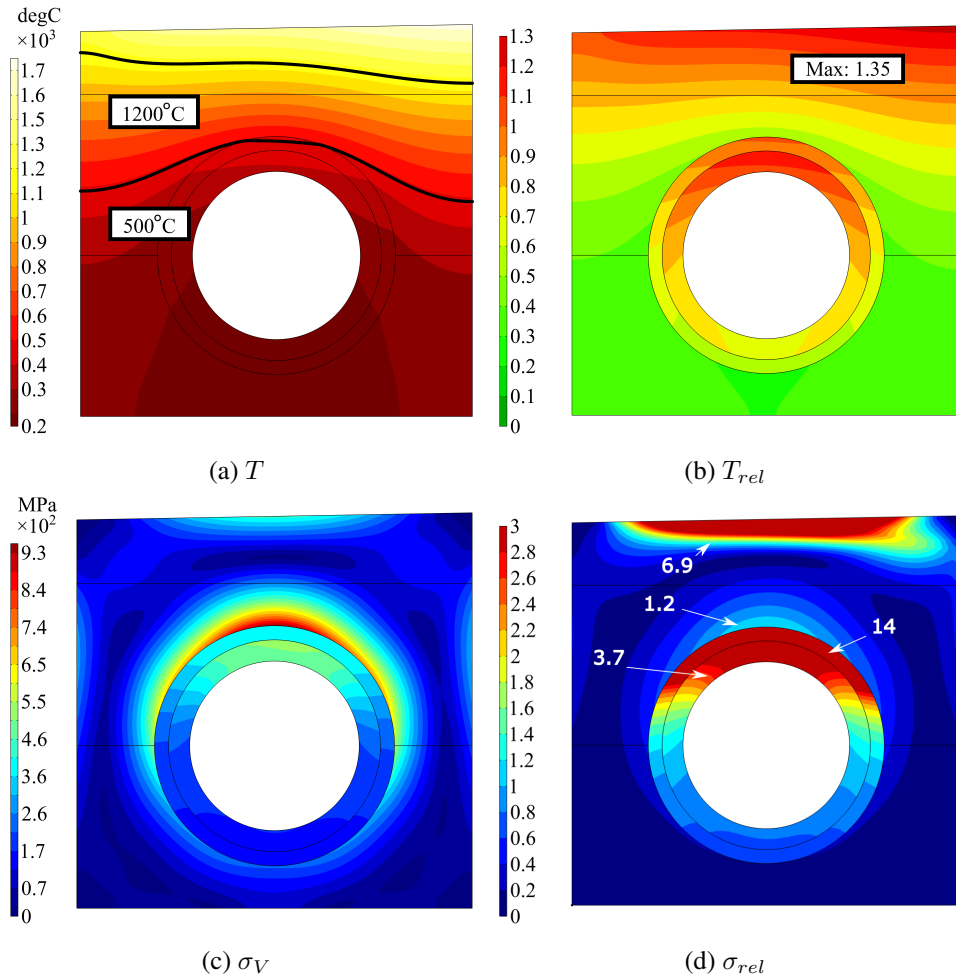


Figure 6.9. Temperature and stress results for the bevelled reference design.

6.4.1 Suspended bevelled monoblock optimisation results

The results for suspended bevelled monoblock optimisation are presented in Fig. 6.10. The Cu fraction plots show large regions of between 55-60% Cu extending from below the pipe to the sides of the monoblock, promoting the transfer of conductive heat flux away from the top of the pipe. These regions are surrounded by a layer of material that is 50% Cu, 50% W. The geometries show some similarity with optimisation results for the flat monoblocks in Fig. 6.4 but with a more diffuse placement of Cu. The placement of Cu is however constrained by the higher temperature (shown in Fig. 6.9b) in the upper half of the monoblock compared to the suspended and fixed flat monoblock cases. The multi-objective geometries display a small amount of asymmetry in Cu placement, with marginally more Cu placed on the left side, away from the highest temperature regions. The thermal objectives were calculated over the entire design domain due to the diffuse nature of Cu placement in the σ -only case. Fig. 6.10h

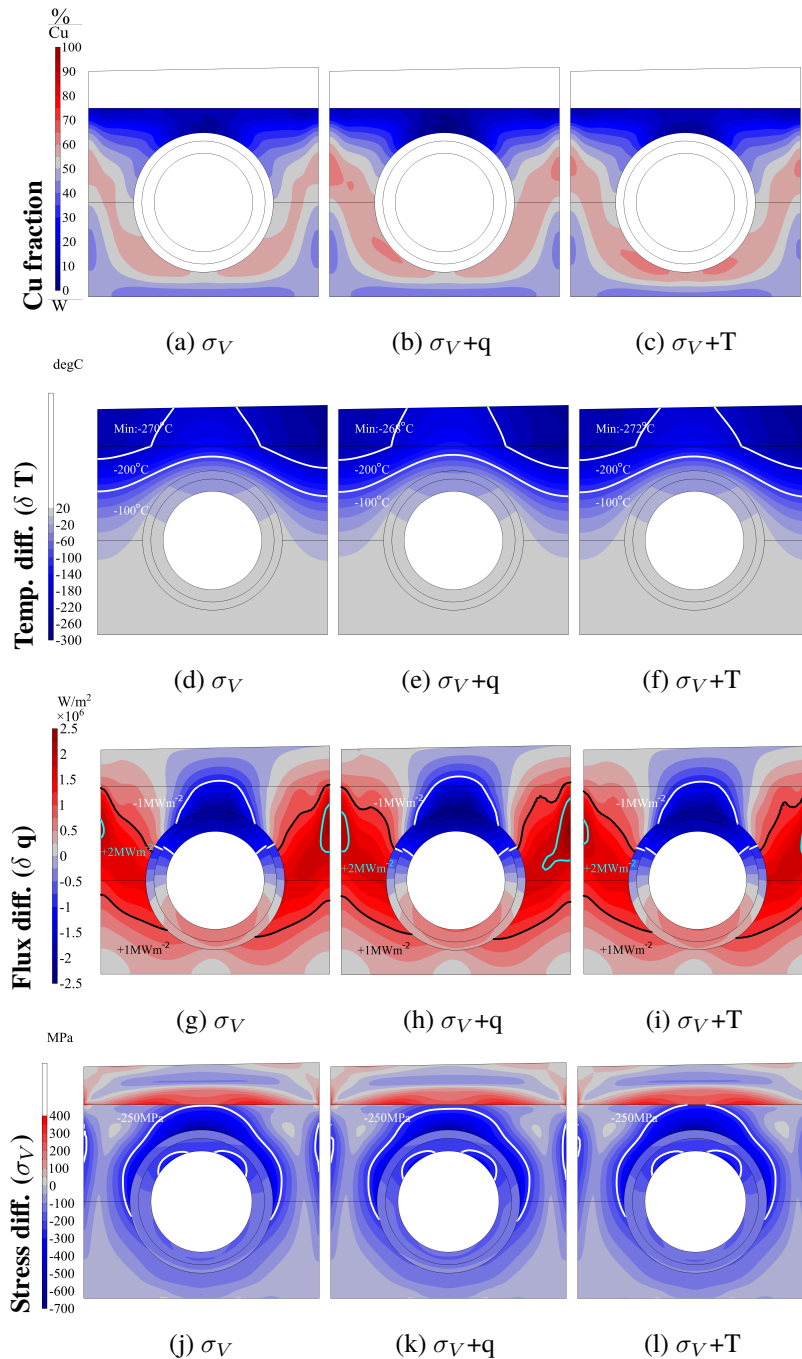


Figure 6.10. Results presented for suspended bevelled monoblock designs, identified by the objective function listed below the sub-plot. The difference plots are calculated by subtracting the data for the corresponding reference design.

shows that a small difference in the Cu fraction on the right side of the monoblock (Shown in Fig. 6.10b) has a significant impact on conductive heat flux transfer, with the $+2\text{MW m}^{-2}$ contour enclosing a significantly larger area on the right side of the pipe. In other respects, there are only minor differences between the temperature, flux and stress results for the multi-objective designs compared to the single-objective stress-minimised geometry shown in Fig. 6.10a. The higher stresses also limit the placement of Cu, which has a lower yield strength than W. The reductions in relative stress are presented in Table 6.5. The maximum relative stresses in the design domain are reduced below unity in all optimisation cases, with the $\sigma + T$ case resulting in the most significant reduction. The temperature difference plots show significant temperature reduction in the top corners, with δT peaking at around 270°C .

Table 6.5. Maximum relative stresses σ_{rel} for suspended bevelled sub-components

	Top	Design domain	Interlayer	Pipe
Reference	6.9	1.2	14	3.7
σ	4.8	0.72	6.5	2.3
$\sigma + q$	5.2	0.74	5.9	2.2
$\sigma + T$	4.8	0.64	6.4	2.3

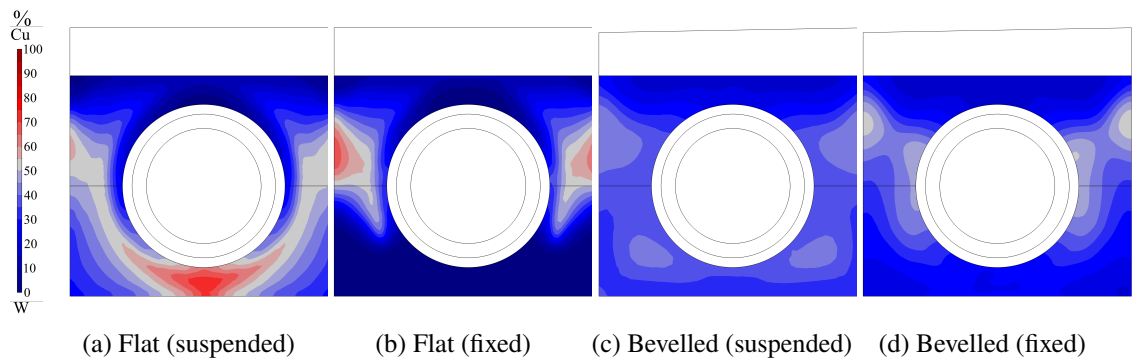


Figure 6.11. Design concepts for the four different monoblock scenarios, obtained with $\sigma_V + T$ optimisation and a surface area fraction constraint of 0.40.

6.4.2 Identifying a design compromise

The optimisation objectives stated in Section 6.2.6 provide a route to navigating the many competing optimisation parameters in order to suggest more specific design concepts. In all the cases considered, the $\sigma_V + T$ results seem to meet the criteria best, with the multi-objective optimisation subtly improving the thermal performance, resulting in a further reduction of von Mises stress relative to yield. Furthermore, in Section 6.3.5, it was found that for the suspended flat monoblock, the surface area fraction could be reduced whilst maintaining significant stress reduction, albeit at a cost to the thermal objectives. The combination of multi-objective $\sigma_V + T$ optimisation with a 0.4 surface-area fraction constraint was therefore chosen as a compromise. The resulting topologies from this suggestion at a design compromise are presented in Fig. 6.11 and their performance is summarised in Table 6.6. The suspended flat design (Fig. 6.11a) performs similarly to the 0.4 surface area fraction case presented in Fig. 6.3 but with a higher maximum design domain conductivity and better thermal performance, including a temperature reduction of $\delta T \approx 156^\circ\text{C}$ (compared to 130°C in Fig. 6.3), and greater flux transfer away from the top of the pipe. The fixed flat (Fig. 6.11b) and suspended bevelled (Fig. 6.11c) designs also perform similarly to their previously presented equivalents but with less Cu in the design domain. The fixed bevelled design resembles a combination of the fixed flat $\sigma_V + T$ (Fig. 6.6c) and the suspended bevelled (Fig. 6.10c) cases with regions of higher Cu fraction around the sides of the pipe that promote heat flux redistribution.

Table 6.6. Summary of results from the chosen four design concepts. The maximum value for the specified parameter is displayed in each case, as evaluated in the location given in the row below. Design domain is abbreviated to ‘DD’ and ‘Top’ and refers to the sacrificial armour layer.

Concept	λ [W/mK]	% σ_{Rel} of ref. design		$-ve \delta T$ [°C]	$-ve \delta q$ [MW m ⁻²]
	DD	DD	Top	Top	Above pipe
Flat suspended	325.21	42.35%	57.65%	-155.63	-1.36
Flat fixed	294.11	75.64%	60.00%	-157.54	-1.52
Bevelled suspended	246.8	73.33%	68.12%	-268.84	-2.75
Bevelled fixed	252.4	94.55%	71.67%	-266.8	-1.64

6.5 Discussion and conclusions

6.5.1 Multi-objective optimisation

The suspended and fixed monoblock geometries respond very differently under multi-objective optimisation. There are many ways to approach multi-objective optimisation and potential for a wide range of ‘optimal’ topologies which may perform similarly. The results presented here aim at enhancing a topology already present in the stress-only case. Multi-objective optimisation was found to work best when the modification of element density contributes to meeting both objectives. As the objectives are summed, elements which contribute to meeting both represent a steeper gradient, which is more attractive to the GCMMA algorithm. In the suspended flat monoblock stress-only minimisation case, Cu is placed below the pipe with a transition region that stretches up the sides of the monoblock. For this reason, the entirety of the design domain (labelled as ‘1’ in Fig. 6.1) was chosen as the domain for multi-objective optimisation. In the fixed case, stress-minimisation presents a geometry with a more well-defined region of Cu placed in the upper half of the domain and so the thermal objectives were evaluated in the top half of the design domain only. This was done to ensure that the multi-objective optimisation enhanced the features already present in the stress-only optimisation case and that the highest temperature regions of the monoblock were targeted.

6.5.2 Material temperature constraints

It could be argued that the upper temperature limit considered on the Cu is not severe enough, with the lack of penalisation of intermediate material properties making Cu-W composites artificially desirable to the optimiser. However, whilst the material models in this study are simplistic, they are intended to serve as a guide to further design and development with conductivities that represent target material properties rather than exact material fractions. This may mean that some of the material properties are difficult to achieve with current materials science and manufacturing, but this was considered preferable to an attempt to fully encapsulate material properties for functional grading techniques which are not yet well defined (Loh *et al.* 2018). The impact of operating the W monoblock below the DBTT is thought to be more severe if that material has undergone re-crystallisation (M. Fursdon, J.-H. You, and M. Li 2019). In (S. Wang *et al.* 2020) it is suggested that cracking is likely to

occur in W-rich areas below the DBTT if the stress is above a maximum principal stress of 700 – 900MPa. The DBTT, therefore, is likely to be more of a problem for the upper portion of the monoblock during shutdown or startup rather than the section below the pipe, and hence whilst testing was performed with this constraint enabled, it wasn't used for the results presented in this study. It is likely that the loads on monoblocks in future devices will differ from those used as boundary conditions in this study, however, the design process utilised in this study could be applied to tailor standardised tokamak components to individual reactor specifications once their operating conditions are well defined whilst maintaining some compatibility with the engineering design. The differences between the results for flat and bevelled monoblocks and between fixed and suspended monoblocks indicate that the impact of minor changes to monoblock geometry or attachment scenario can have consequences for design optimisation. This is perhaps particularly important in the divertor, where the extreme heat loads push designs close to their operating limits.

6.5.3 The case for an increased thermal conductance monoblock

The designs presented in this paper follow a different approach to several previous monoblock design optimisation studies, where the focus is primarily on interlayer engineering. In (T.R. Barrett *et al.* 2015) a reduced conductance approach to monoblock stress minimisation is presented, based on a idea proposed in (Li-Puma *et al.* 2013). Whilst these studies aim to increase heat flux tolerance, this comes at the expense of higher armour temperatures. The dangers associated with stress in the monoblock are highly temperature dependent, with a decreased yield strength in the upper portion of the component potentially facilitating failure. Whilst the designs presented in this study represent early concepts, the prospect of being able to cool a region at the top of the monoblock by 100 – 300°C, allowing for a higher yield strength to be maintained at the top of the component and a reduction in material that exceeds recrystallisation temperature warrants further study. The redistribution of heat flux may also aid in overcoming limitations associated with exceeding the critical heat flux of water at the internal edge of the coolant pipe. It is suggested that future work focuses on adding accurate manufacturing and materials constraints to the topology optimisation process and further development of an increased conductance monoblock design.

6.5.4 Conclusions

Multi-objective topology optimisation combining both stress and thermal terms was performed on an ITER-like divertor monoblock resulting in four different design concepts, featuring maximum stress reductions of up to 65%, a peak reduction in temperature of approximately 270°C and a 20% transfer of heat flux from the top of the cooling pipe to the sides. The results can be interpreted for manufacture via functional grading with conductivities representing target material properties rather than explicit Cu-W fractions, and are presented in the context of evolving design and manufacturing technology which may enable high-performance PFCs to be targeted to future tokamaks. This study demonstrates that even

minor changes to the geometry and loading conditions of the components can drastically affect optimisation results. Beyond the bounds of topology optimisation, the differences in behaviour observed in this study may warrant further investigation, particularly if monoblocks with different fixing mechanisms are found to have different rates of failure. Whilst the geometries presented in this study are not intended for direct manufacture, it is suggested that topology optimisation of the monoblock may help to inform PFC design as the technology grows in maturity and the operating conditions expected in future reactors become better defined.

Acknowledgements

Oliver Marshall was supported by EPSRC [EP/L01663X/1]. Lee Margetts was supported by EPSRC grants EP/N026136/1 and EP/T026136/1. Llion Evans was supported by EPSRC grant EP/R012091/1.

6.6 Additional commentary on Chapters 5 and 6

The methodology employed in Chapter 5 is a proof of concept that is later developed further in Chapter 6. Alongside this, testing was performed for a number of different objective functions and problem setups. The problem was extended to 3D, however, this proved to be trivial as no bending forces are modelled, and the 2D implementation was pursued. The decision to focus on the bevelling of the monoblock was made as it represents a comparatively recent design modification to the divertor monoblock. Topology optimisation can be used to explore the impact of this geometry modification on optimum design. Secondly, bevelling adds asymmetry to the monoblock design. Due to the use of a generic design domain, topology optimisation is ideally suited to finding a novel solution to asymmetric problems without the need for initial guesses or seed features. In addition, the ability to combine mechanical and thermal objectives is considered by the author to represent one of the technique's most significant advantages. This is not, however, explored in the other fusion topology optimisation works that were published during the course of this project (Curzadd *et al.* 2019) and (Kerkhof *et al.* 2021). The use of temperature-based objectives provided a pathway for the reduction of the thermally induced stress through the minimisation of material CTE mismatch, in combination with a reduction in operating temperature and a corresponding increase in yield strength.

Chapter 7

Paper 5 - Conjugate Topology

Optimisation of Turbulent Flow for the Design of Novel Plasma Facing Component Geometries

Conjugate topology optimisation of turbulent flow for the design of novel plasma-facing component geometries

Oliver H.R. Marshall^{1*}, Lee Margetts¹, Llion M. Evans^{2,3} and Matthew J. Roy^{1,4}

¹ Department of Mechanical, Aerospace and Civil Engineering, George Begg Building, The University of Manchester, Manchester, United Kingdom, oliver.marshall@manchester.ac.uk, lee.margetts@manchester.ac.uk, matthew.roy@manchester.ac.uk

² College of Engineering, Swansea University, Swansea, United Kingdom, llion.evans@swansea.ac.uk

³ United Kingdom Atomic Energy Authority, Culham, United Kingdom

⁴ Henry Royce Institute, University of Manchester, United Kingdom

Abstract

Topology optimisation is applied to the design of internal features in a recently proposed monoblock concept in order to improve cooling performance. The problem is formulated as a forced convection conjugate heat transfer problem where the fluid flow is modelled using the $k - \epsilon$ turbulence model. The topology optimisation includes Brinkman penalisation of the fluid flow with additional terms included to account for the turbulent kinetic energy k and dissipation rate ϵ . The thermal conductivity and specific heat capacity are interpolated using the SIMP method. The divertor monoblock geometry considered consists of a water-cooled rectangular CuCrZr pipe surrounded by a stress-relieving Cu interlayer and a W armour domain. The fluid forms the design domain for topology optimisation, where three objectives

relating to thermal performance are tested: thermal compliance and solid domain temperature are minimised, and fluid temperature is maximised. All cases are subject to a pressure drop constraint. The resulting geometries are post-processed and found to promote convective heat transfer in a verification study. This study demonstrates the application of topology optimisation to the extreme conditions experienced by the plasma-facing components and represents an initial step in the conceptual design of new internal geometries designed to improve cooling performance. The work is performed using commercial software on a standard quad-core workstation PC.

Key words: *Topology optimisation, Conjugate heat transfer, Turbulence*

7.1 Introduction

The tokamak divertor is responsible for handling approximately 18 % of the total thermal power emitted from the plasma that the reactor uses as fuel (Li Puma *et al.* 2002). The divertor design for the upcoming ITER tokamak is made up of 54 cassettes containing thousands of water-cooled plasma-facing components known as monoblocks. The divertor monoblocks are exposed to extreme, one-sided heat loads on their upper surface. The challenges faced in divertor monoblock design are compounded due to their exposure to damaging 14.1MeV neutron fluences, the inaccessibility of the components for maintenance and the desire to use materials designed to reduce activation (Romanelli *et al.* 2012). The current ITER monoblock design employs W armour, separated from a CuCrZr water-cooled pipe by a Cu interlayer designed to relieve thermally induced stress. The monoblocks need to effectively transfer heat to the coolant to prevent damage to the armour surface. In the ITER design, there is a 10MW m^{-2} engineering limit for heat flux on the divertor, however, it is thought that occasionally, higher heat fluxes will be experienced, with 20MW m^{-2} specified as the maximum allowable limit (J. Gunn, T. Hirai, *et al.* 2019), without exceeding the margin to Critical Heat Flux (CHF) (F. Escourbiac *et al.* 2019).

This paper investigates the application of topology optimisation to the design of the divertor monoblock coolant channel. Topology optimisation allows for the use of a generic design domain to investigate geometries which may improve performance whilst maintaining a level of compatibility with the reference design. The resulting structures often involve complex internal geometries and are often associated with additive manufacturing techniques. The motivation for considering introducing additional complexity to the divertor is related to ongoing design challenges. Whilst the results from ITER will be used to inform future reactor designs, heat flux to the divertor is currently both subject to significant uncertainty, with ‘major progress needed’ to the understanding of power exhaust in order to enable predictive capability (Zohm *et al.* 2013) and likely to increase with future devices (Prachai Norajitra, Said I. Abdel-Khalik, *et al.* 2008). The tolerable heat load to the divertor is also considered design-driving with regards to the size and cost of reactors (Marbach, Cook, and Maisonnier 2002). The results of this study are ultimately proposed as initial steps in the conceptual design of components that may improve divertor heat-transfer performance.

7.1.1 Plasma-Facing Component (PFC) design

There are three main ways that single-phase heat transfer from a solid to a fluid may be enhanced (without material changes). Firstly, a smaller free-flow cross-sectional area increases fluid velocity and reduces the thickness of the laminar sub-layer. Secondly, the internal pipe surfaces can be designed to enhance turbulence. Thirdly, the use of mechanical inserts can promote local turbulence (L. Castro Gómez 2019). The utilisation of any of these methods, however, can result in increases to pressure drop. As the ultimate goal of tokamaks is efficient electricity production, any enhancements to the cooling performance must be weighed against any additional pumping power required to combat an increased pressure drop.

In water-cooled PFC design, the use of mechanical inserts is commonplace, with twist tapes used in the ITER divertor monoblock concept (Wiggins, Cabral, and Carasik 2021). The use of a circular cross-section coolant pipe in the ITER monoblock design, however, results in a geometrically concentrated heat flux, which is 1.5-1.8 times the surface value at the top of the pipe (Greuner *et al.* 2019). Local turbulence enhancement has been pursued with the development of the hypervapotron (Cattadori *et al.* 1993) but has not been used in the highest heat flux regions of the divertor due to the consequences of the detachment of the associated flat-tile armour design. (Merola and Vieider 1998) details the temperature rise on the leading edge of the adjacent tile in the case of tile detachment and the potential for a cascade failure. (Oh *et al.* 2021) aims to combine the monoblock design with a hypervapotron internal geometry that incorporates a wider, flatter coolant channel somewhat similar to the resulting shape-optimised cross-section proposed in (Lim *et al.* 2018). The geometry used in this study is inspired by the armour and pipe design used in (Oh *et al.* 2021), with the internal volume of the pipe used as the design domain for topology optimisation. The larger pipe cross-sectional area (compared to the ITER monoblock design) provides a greater design domain volume, and therefore a larger parameter space, increasing design freedom.

7.2 Methodology

The monoblock can be described as a forced convection conjugate heat transfer system, where the heat transfer is dependent on the quantity and distribution of conductive material, the contact surface area between the solid and fluid, the velocity distribution of the fluid, the temperature and heat capacity (S. B. Dilgen *et al.* 2018). The finite element implementation used in this study involves a solid conduction problem coupled to a CFD simulation describing the flow of the coolant.

7.2.1 Boundary conditions

The monoblock is set up with ‘ITER relevant’ boundary conditions, similar to those adopted in (Lim *et al.* 2018) which include a heat flux on the plasma-facing armour surface of 10MW m^{-2} and a water temperature of 120°C . A visual representation of the model is shown

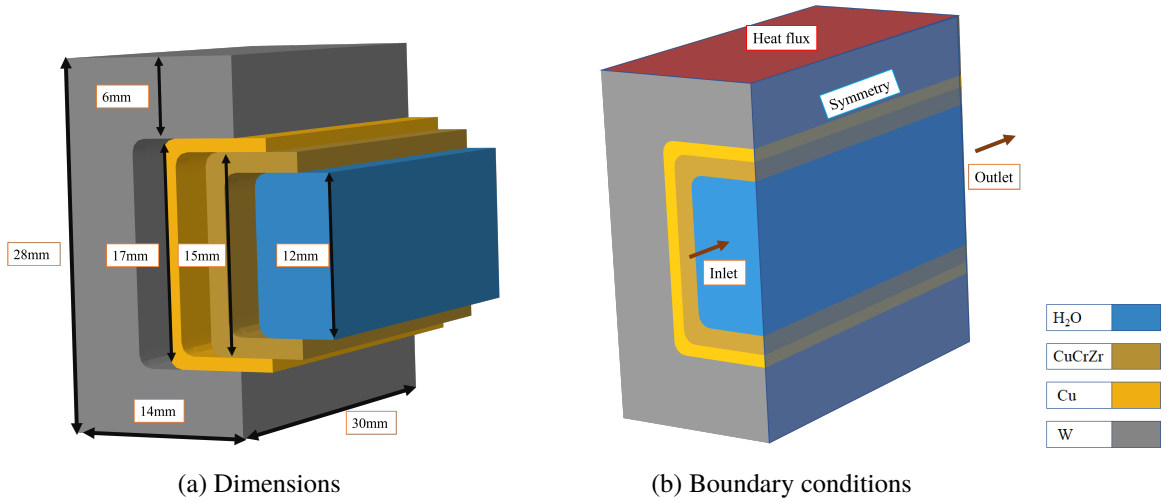


Figure 7.1. Exploded view of the monoblock geometry inspired by a component developed in (Oh *et al.* 2021). The water coolant channel is used as the design domain for topology optimisation. A depth of 30mm, equivalent to 3 monoblocks, was chosen as a compromise between increasing the volume of the design domain, computational expense, and the need for any optimised geometry to be periodic.

in Fig. 7.1. A coolant channel with a length of 30mm is used as the design domain for topology optimisation, equivalent to the depth of three monoblocks. This represents only a small fraction of an ITER-scale divertor, where rows of armour tiles extend over the scale of a metre (C. B. Baxi 1995), and so the effects of modifying a small fraction of the geometry are necessarily minor. Symmetry conditions are specified for the plane which intersects the plasma-facing surface and the longitudinal axis of the coolant pipe, meaning that half of the monoblock is simulated in order to reduce computational expense. The fluid inlet is modelled with a 10m s^{-1} velocity and the outlet with a 4MPa pressure. The coolant domain is used as the design domain for topology optimisation.

7.2.2 Turbulence modelling

The flow is described using the Reynolds Averages Navier Stokes (RANS) realisable $k - \epsilon$ turbulence model, which includes transport equations for the turbulent properties including turbulent kinetic energy (k) and turbulent dissipation rate (ϵ), that allow for the description of the convection and diffusion of turbulent energy. The $k - \epsilon$ realisable turbulence model has previously been applied to the divertor monoblock in Refs. (Kwon, Kim, *et al.* 2021; Lim *et al.* 2018) and is commonly applied to industrial problems in which computational resources are limited.

7.2.3 Computational cost

In the topology optimisation literature, many industrial problems are either treated in 2D or feature a 3D implementation which is simply an extruded version of the 2D problem (for example (Lundgren *et al.* 2019)). The coolant pipe in the monoblock geometry, however, is completely surrounded by the W armour, which combined with the one-sided heat load, forces a 3D treatment of the problem. This increases computational time significantly and

therefore requires a coarser finite element mesh than would be possible in a 2D model, in order to enable computation on a quad-core workstation PC. The PC used for the study had a 3.4GHz maximum processor speed and 16GB of RAM.

7.2.4 Topology optimisation formulation

The topology optimisation of the coolant channel relies on a Globally Convergent Method of Moving Asymptotes (GCMMA) technique, originally developed in Refs. (Svanberg 2002, 2007) and implemented in COMSOL Multiphysics 5.6 (COMSOL 2021). The goal of the optimisation is to improve the thermal performance of the monoblock at an acceptable pressure drop. The end goal is a system which can be described in terms of discrete domains, with an optimal design consisting of elements which either belong to the coolant fluid or internal Cu features. Topology optimisation techniques allow the relaxation of the problem to one in which the material density is allowed to vary continuously between that of a solid and a void (M. P. Bendsøe and O. Sigmund 2003), or in this case, a fluid and a solid. This allows for the use of efficient, gradient-based methods for calculating element sensitivities, greatly reducing the computational cost of the technique, but requires continuous interpolation of relevant material properties to describe intermediate densities.

7.2.5 Fluid optimisation

The topology optimisation domain is conceptualised as a porous medium, in a similar manner to the fluid topology optimisation methodology for Stokes flow, presented in (Borrvall and Petersson 2003). The technique used in this paper however is based primarily on an extension of the method to treat full incompressible Navier-Stokes flow in steady state (Olesen, Okkels, and Bruus 2006). This approach is further modified for application to several turbulence models in (C. B. Dilgen *et al.* 2018) and the $k - \epsilon$ model in (Yoon 2020) through the penalisation of k and ϵ such that they reduce to zero in solid regions. This is in addition to the modification of the Navier-Stokes momentum equation, known as Brinkman penalisation, which introduces a friction force which impedes fluid velocity in solid regions.

The friction force \mathbf{f} is proportional to the fluid velocity (\mathbf{v}), and defined as: $\mathbf{f} = -\alpha\mathbf{v}$, where $\alpha(\mathbf{r})$ is the inverse of the local permeability in the medium at position \mathbf{r} . As inverse permeability increases, the flow is restricted, with velocity tending to zero in ‘solid’ regions. The porous medium is described by the Darcy law $q = -\frac{k}{\mu}\Delta p$ where q is the instantaneous flow rate, k is the permeability, μ is the dynamic viscosity of the fluid and Δp is the pressure drop. The Darcy number (Da) represents the relative impact of the permeability of a medium over its cross-sectional area and is defined as $Da = \frac{k}{d^2}$ where d is the characteristic length.

A design variable field which controls the local permeability of the medium $\gamma(\mathbf{r})$ is then introduced, where $0 \geq \gamma \leq 1$. Solid material is obtained when $\gamma = 0$ and a fluid corresponds to $\gamma = 1$. The method used in both (Borrvall and Petersson 2003) and (Olesen, Okkels, and Bruus 2006) is followed, where an interpolation scheme is formed by relating the local

inverse permeability $\alpha(r)$ to the design variable field through the Darcy number. The Darcy number can be reformulated as in Eq. 7.1.

$$Da = \frac{\eta}{\alpha_{max} L^2} \quad (7.1)$$

η is the dynamic viscosity, L is the characteristic length scale in the system and α_{max} controls the maximum value of the friction force \mathbf{f} . The variation of $\alpha(\gamma)$ is described in Eq. 7.2.

$$\alpha(\gamma) \equiv \alpha_{min} + (\alpha_{max} - \alpha_{min}) \frac{q[1 - \gamma]}{q + \gamma} \quad (7.2)$$

Where q is used to control the strength of the penalisation in the interpolation function, as indicated in Fig. 7.2. α_{min} is chosen as zero, to ensure free flow in fluid regions. In theory, solid walls are obtained when $\alpha_{max} = \infty$, however, the numerical implementation requires a finite value, which is calculated by rearranging Eq. 7.1, giving Eqs. 7.3 and 7.4.

$$\alpha(\gamma) = \alpha_{max} \frac{q[1 - \gamma]}{q + \gamma} \quad (7.3)$$

$$\alpha(\gamma) = \frac{\eta}{Da L^2} \frac{q[1 - \gamma]}{q + \gamma} \quad (7.4)$$

It is suggested in (Olesen, Okkels, and Bruus 2006) that Darcy numbers on the order of $Da \lesssim 10^{-5}$ are required in order to represent material approaching impermeability. The high fluid velocities in the divertor monoblock however mean that lower Darcy numbers are required in order to ensure the impermeability of solid regions. More detail on the impact the Darcy number has on the resulting topologies is available in (Olesen, Okkels, and Bruus 2006).

In a similar manner to the Brinkman method for modification of the Navier-Stokes momentum equation, penalty terms shown in Eqs. 7.5 and 7.6 are added to the k and ϵ transport equations respectively, following the method established in (Yoon 2020). The use of the $\kappa - \epsilon$ turbulence model requires the introduction of values for the turbulent kinetic energy k_0 and the turbulent energy dissipation ϵ_0 in solid domains, which are set equal to zero for the purposes of this study.

$$-\alpha^k(\gamma)(k - k_0) \quad (7.5)$$

$$-\alpha^\epsilon(\gamma)(\epsilon - \epsilon_0) \quad (7.6)$$

Where α^k and α^ϵ are defined in Eqs. 7.7 and 7.8 respectively.

$$\alpha^k = (\alpha_{max}^k - \alpha_{min}^k) \frac{q[1 - \gamma]}{q + \gamma} \quad (7.7)$$

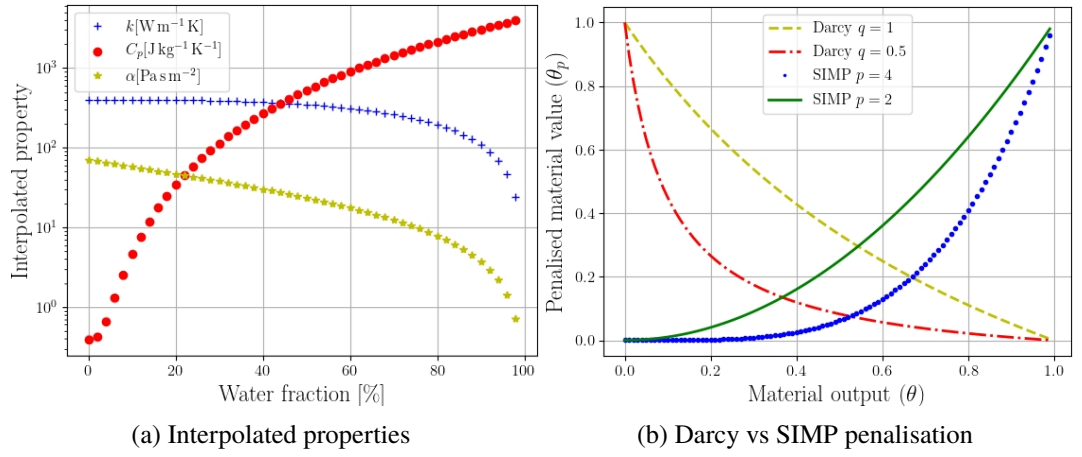


Figure 7.2. Left: Interpolated thermal material properties using SIMP penalisation and inverse permeability α , which forms part of the Darcy interpolation scheme. Right: comparison between Darcy and SIMP material interpolation schemes for different values of penalisation parameters q and p .

$$\alpha^\epsilon = (\alpha_{max}^\epsilon - \alpha_{min}^\epsilon) \frac{q[1 - \gamma]}{q + \gamma} \quad (7.8)$$

Where α_{max}^k and α_{max}^ϵ are chosen to be large enough to significantly reduce k in solid regions and $-\alpha_{min}^k = \alpha_{min}^\epsilon = 0$.

Heat transfer across the internal surfaces of the pipe is treated with wall functions during optimisation and fluid velocity at the interface with the topology optimised structures is reduced such that a no-slip boundary condition is approximated (as discussed in (S. B. Dilgen *et al.* 2018)). As discussed in (Yoon 2020), challenges in the implementation of a no-slip boundary condition regarding this technique for the penalisation of $k - \epsilon$ turbulence, mean that a slip condition is used between the internal walls and fluid during the optimisation process. Whilst imposing standard no-slip boundary conditions would result in a more accurate simulation of the thermal boundary layer and heat transfer to the coolant, there are ongoing problems facing the accurate description of thermal boundary layers for topology optimisation studies, as discussed in (Alexandersen and Andreasen 2020). The local mesh refinement and high aspect ratio elements often used to simulate boundary layer behaviour in CFD can also cause problems for topology optimisation. Initial testing found that these elements often become Cu early in the optimisation, with no mechanism for adjusting the refinement of elements to describe a newly formed boundary layer. The study was also limited by computational expense. The simulations therefore only constitute an approximation of heat transfer in the main fluid bulk as a first step in applying the technique to the divertor coolant channel. Furthermore, accounting for the CHF and multi-phase modelling is beyond the scope of this study and the optimisation involves improving the single-phase performance only.

7.2.6 Material property interpolation

The fluid viscosity and density are not interpolated. This allows the fluid simulation to remain more realistic and numerically stable during the formation of solid regions. The

heat capacity and thermal conductivity are interpolated using the design variable γ defined previously, as shown in Eqs. 7.10 and 7.11 and visualised in Fig. 7.2. This is done using the SIMP interpolation scheme described in Eq. 7.9.

$$\gamma_p = \gamma_{min} + (1 - \gamma_{min})\gamma^p \quad (7.9)$$

$$Cp_{interp} = (Cp_{(Cu)} - Cp_{(H_2O)})\gamma_p + Cp_{(Cu)} \quad (7.10)$$

$$k_{interp} = (k_{(Cu)} - k_{(H_2O)})\gamma_p + k_{(Cu)} \quad (7.11)$$

γ_p is the local value of the design penalisation, γ_{min} is the minimum penalised volume fraction, and p is an exponent usually chosen to be between 1 and 3. SIMP interpolation is used for the thermal properties due to its established status in solid domain topology optimisation, and initial testing, which found that the ability to alter the penalisation independently resulted in improved convergence. As previously, $\gamma = 0$ represents the solid domain (CuCrZr), with $\gamma = 1$ corresponding to fluid (H_2O), however, as shown in Fig. 7.2, when changing from Darcy to SIMP interpolation, the variables relating to Cu and H_2O in Eqs. 7.10 and 7.11 are switched.

7.2.7 Consideration of objective functions

The choice of objective function can have a significant impact on the geometries obtained from the optimisation, even if the properties involved share a similar physical basis. Whilst the goal of the study may be to improve heat transfer, there are many ways of formulating objectives to achieve this. Furthermore, the domain over which the objective function is evaluated is also likely to affect the results.

7.2.8 Thermal objectives in conjugate heat transfer topology optimisation

The literature on topology optimisation of conjugate heat transfer systems contains a broad range of objective functions. The following survey is presented as an equivalent was not found in the literature and is based on the forced convection section of an in-depth review of fluid topology optimisation presented in (Alexandersen and Andreasen 2020). Typically these papers employ multi-objective optimisation with a function composed of a term to improve thermal performance and another designed to minimise pressure drop. The pressure drop minimisation is typically approached either through an explicit formulation of pressure drop or through a power dissipation function (as in (Hao Li *et al.* 2019)). Not all studies provide a full description of the objective functions used, however, those which contained objectives based on standard thermal properties are categorised in Table 7.1. There are some studies which choose a different combination of thermal properties, such as thermal power in (V. Subramaniam, T. Dbouk, and J. L. Harion 2019), the integral product of heat transfer coefficient and temperature in (Kobayashi *et al.* 2019) and conductance in (Jan H. K. Haertel

Table 7.1. Objectives used in the literature for topology optimisation of forced convection conjugate heat transfer systems. The first column divides studies with respect to whether the relevant property was minimised or maximised.

Min/Max	Objective	Reference
Min	Thermal compliance	(Alexandersen, Aage, <i>et al.</i> 2014; Alexandersen, Ole Sigmund, and Aage 2016; Alexandersen, Ole Sigmund, K. E. Meyer, <i>et al.</i> 2018; Jahan <i>et al.</i> 2019; Lv and Sheng Liu 2018; Santhanakrishnan, Tilford, and Bailey 2018; Yoon 2010; Yu <i>et al.</i> 2019)
Max	Recoverable thermal power	(Marck, Nemer, and J.-L. Harion 2013; Ramalingom, Cocquet, and Bastide 2018; Ramalingom, Cocquet, Maleck, <i>et al.</i> 2018)
Min	Thermal resistance	(Dong and X. Liu 2020; Jan H. K. Haertel, Engelbrecht, <i>et al.</i> 2018)
Max	Max temp.	(Lundgren <i>et al.</i> 2019; Yan <i>et al.</i> 2019)
Max	Outlet temp.	(Pietropaoli <i>et al.</i> 2017)
Min	Mean temp.	(Ercan M Dede 2009, 2012; S. B. Dilgen <i>et al.</i> 2018; Hu, Z. Zhang, and Q. Li 2020; K. Lee 2012; Hao Li <i>et al.</i> 2019; Makhija and Beran 2019; Matsumori <i>et al.</i> 2013; Qian and Ercan M. Dede 2016; S. Sun, Liebersbach, and Qian 2019; Zhao <i>et al.</i> 2018)
Min	Temp. difference	(Kontoleonos <i>et al.</i> 2013; Pizzolato <i>et al.</i> 2017b)
Max	Heat generation	(Sato <i>et al.</i> 2018; Yaji, Ogino, <i>et al.</i> 2018; Yaji, Yamada, Kubo, <i>et al.</i> 2015; Yaji, Yamada, Yoshino, <i>et al.</i> 2016; B. Zhang and L. Gao 2019)
Min	Heat flux	(McConnell and Georg Pingen 2012)
Max	Heat flux	(Laniewski-Wollk and Rokicki 2016; Lundgaard, Engelbrecht, and Ole Sigmund 2019)

and Nellis 2017). Multiple case studies are featured in (Yaji, Yamasaki, and Fujita 2020), with the second maximising the ratio of thermal conductance to pressure drop. Some studies focus on minimising energy dissipation for a given thermal performance, such as (Ghasemi and Elham 2019) where drag force is minimised, and (S. Zeng, Kanargi, and P. S. Lee 2018; S. Zeng and P. S. Lee 2019) where pressure drop is minimised, subject to a temperature constraint. There does not, however, seem to be a consistent agreed-upon approach for the determination of objective functions in the literature.

Preparatory work included the investigation of a range of objective functions. Multi-objective optimisation including a heat transfer objective and a pressure drop minimisation objective was not found to be effective and resulted in pressure drop minimisation only despite attempts at weighting the objectives appropriately. It was observed that multi-objective optimisation works best when the consequences of changing the density of an individual element contribute to meeting both (or all) objectives. After consideration of the literature and preparatory testing, three separate objectives were selected. The first is the solid domain thermal compliance (ϕ), defined through the product of heat flux and temperature, as shown in Eq. 7.12. The other objectives are based on domain temperature and defined in Eqs. 7.13 and 7.14. The objectives are defined as averages, with respect to Γ which represents a domain composed of the pipe, interlayer and armour, and Ω which is the fluid domain (and the design domain for the topology optimisation). The average pressure drop constraint is defined in Eq. 7.15, relative to inlet (and outlet) area A .

$$\text{Min. } \bar{\phi} = \frac{1}{V_{\Gamma}} \int_{\Gamma} T q_{in} d\Gamma \quad (7.12)$$

Table 7.2. Values of topology optimisation parameters

Scheme	Parameter	Value
Constraint	Δp_{av}	0.2MPa
Darcy	q	0.5
Darcy	Da	10^{-6}
Darcy	U	10m s^{-1}
Darcy	L	12mm
$k - \epsilon$	α_{max}^k	2500
$k - \epsilon$	α_{max}^ϵ	2500
SIMP	γ_{min}	1e-3
SIMP	γ^p	γ^3

$$Min. \quad \bar{T}_S = \frac{1}{V_\Gamma} \int T_S d\Gamma \quad (7.13)$$

$$Max. \quad \bar{T}_F = \frac{1}{V_\Omega} \int T_F d\Omega \quad (7.14)$$

$$\Delta p = \frac{1}{A} \left[\int_{inlet} p dS - \int_{outlet} p dS \right] \quad (7.15)$$

7.3 Results

Parameters common to all optimisation studies are listed in Table 7.2, where the level of penalisation was established based on a continuation method which involved gradually increasing penalisation strength until solid domains that rejected fluid flow sufficiently were observed. A similar approach was used to define the average pressure drop constraint, where the value of $\delta p_{av} = 0.2\text{MPa}$ allows for the formation of solid internal features given the size and mesh resolution of the fluid domain.

7.3.1 Laminar flow results

An initial investigation was made using laminar flow conditions for thermal compliance (ϕ), solid domain temperature (T_S), and fluid temperature (T_F) objectives. This was performed with otherwise the same boundary conditions and loads as the turbulent flow simulations discussed in Section 7.3.2. The resulting geometries, thresholded at $\gamma \leq 0.3$ are presented in Fig. 7.3 and show three distinct geometries, despite the coarse mesh used. The greatest similarity is seen in the ϕ and T_S geometries (Figs. 7.3a and 7.3b), reflecting the similarity in the composition of the objectives. The decision to threshold the results at $\gamma \leq 0.3$ is made for consistency with results presented in Section 7.3.2, where it is discussed further. In this implementation of topology optimisation, with no clear material interpretation of intermediate density elements, the range where $0 < \gamma < 1$, can be thought of as uncertainty regarding whether an element is optimally placed in either domain, with 0.5 representing the highest uncertainty. In this study, intermediate-density elements form a thin band between the solid and fluid domains and so thresholding the results is necessary to obtain well-defined geometries.

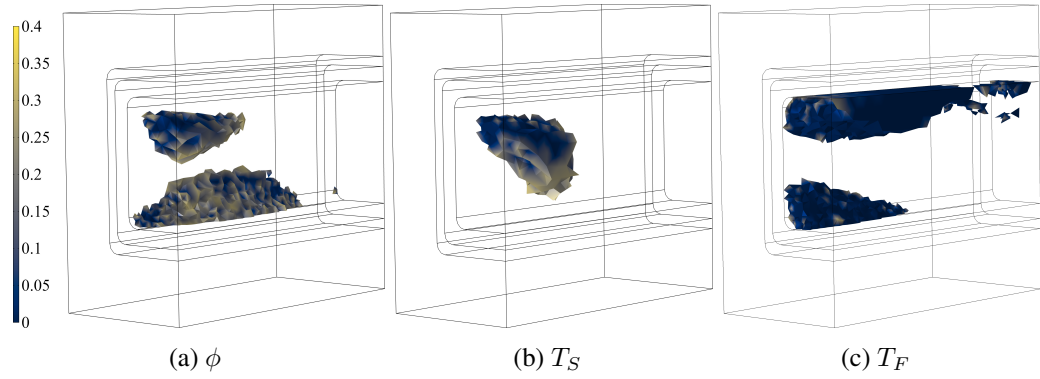


Figure 7.3. Optimised geometries thresholded at $\gamma \leq 0.3$ performed as initial tests of thermal compliance minimisation (7.3a), solid temperature minimisation (7.3b) and fluid temperature maximisation (7.3c) for laminar flow conditions and a coarse mesh which enabled faster evaluation.

Table 7.3. Completion times for turbulent flow topology optimisation simulations.

Geom.	Completion time
ϕ	39 h 14 min 34 s
T_S	21 h 58 min 55 s
T_F	61 h 56 min 2 s

7.3.2 Turbulent flow results

The turbulent flow simulations were completed in the times specified in Table 7.3. These studies were all performed with identical meshes (consisting of 271497 elements) and problem setups (using the parameters listed in Table 7.2).

The optimisation was performed with a termination condition based on either a change in the relative change in control variables of $(1e-6)$ or a maximum number of model iterations (250). All results terminated after exceeding the maximum number of model evaluations, however, in all cases, the objectives stabilised after only a few iterations, as indicated in Fig. 7.4. The ϕ and T_S objectives result in reductions of 4% and 2% respectively. The T_F case shows an increase in the objective of 18% relative to the initial value. Furthermore, the plots of maximum turbulent kinetic energy and turbulent dissipation rate for the ϕ minimisation study (Figs. 7.5a and 7.5b) show that these properties increase significantly from their initial values (0.8145J kg^{-1} and $15.86\text{J kg}^{-1} \text{s}$ respectively) as a result of the formation of internal features. The low level of turbulence in the initial conditions combined with the quick convergence of the objectives likely contributes to the similarity between the optimised geometries for laminar flow designs presented in Fig. 7.3 and those obtained using the $k - \epsilon$ model, presented in Fig. 7.6.

The geometries resulting from the three objectives are thresholded at $\gamma \leq 0.1$ and $\gamma \leq 0.3$ are visualised in Fig. 7.6, where it can be seen that despite the penalisation techniques employed, there remains a thin layer of intermediate density elements at the solid-fluid interface. This is not particularly surprising considering the computational limitations of the optimisation, and a better definition of the fluid-solid boundary might be obtained with a finer mesh, the use of filtering and projection techniques, and more model evaluations. The ϕ minimised design thresholded at $\gamma \leq 0.1$ (Fig. 7.6a) shows two large features near the

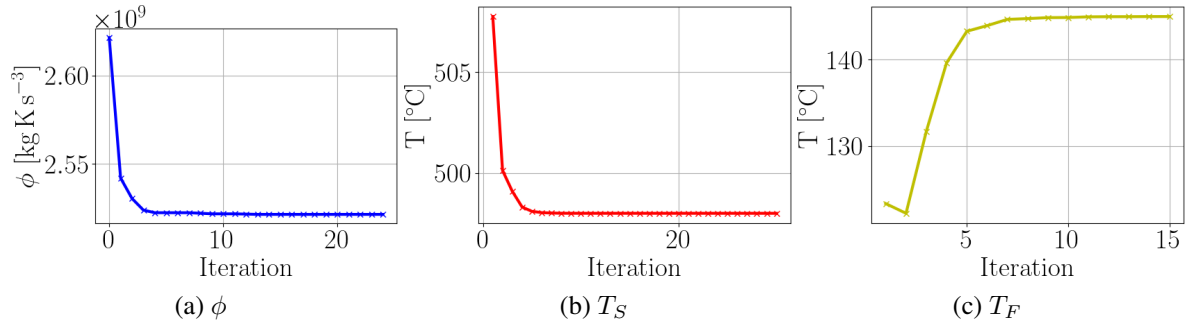


Figure 7.4. Variation in the mean thermal compliance (ϕ): 7.4a, solid domain temperature T_S : 7.4b and fluid temperature T_F : 7.4c objectives objectives during the optimisation process.

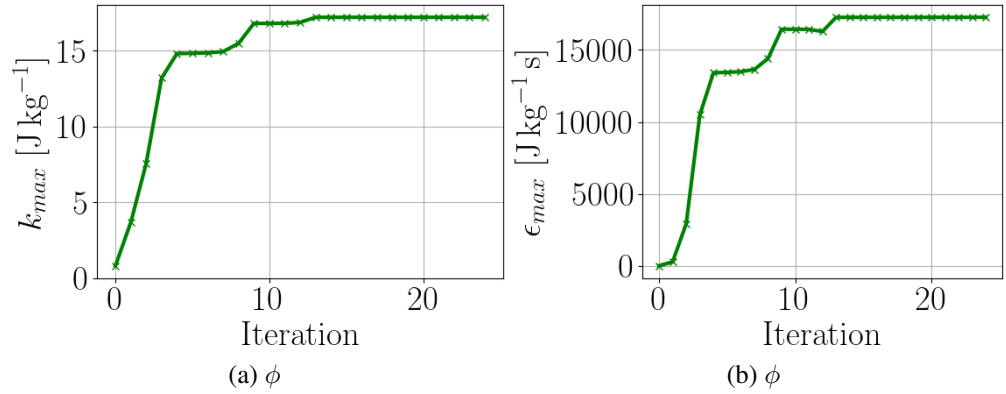


Figure 7.5. The evolution of turbulent kinetic energy and turbulent dissipation rate for ϕ minimisation.

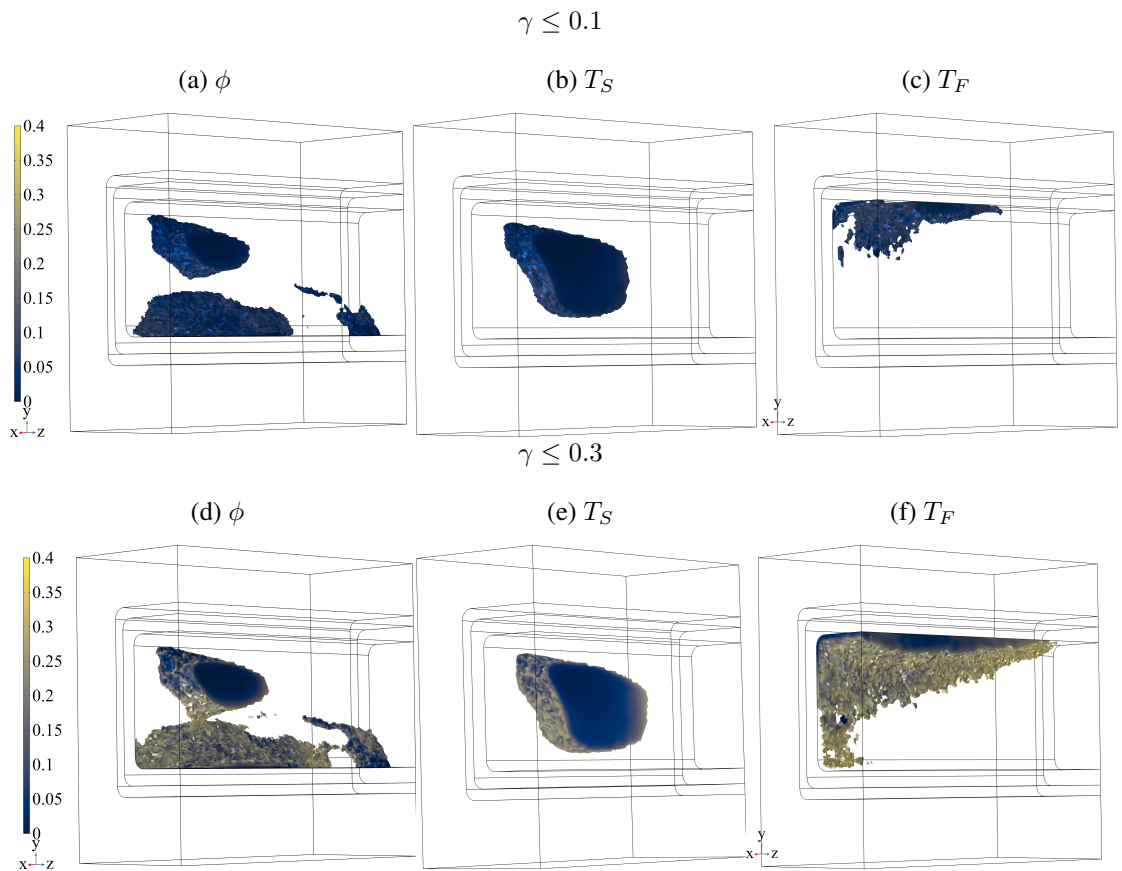


Figure 7.6. Optimised geometries thresholded at $\gamma \leq 0.1$ (upper row) and $\gamma \leq 0.3$ (lower row). The difference between the two rows is a thin layer of intermediate-density elements surrounding the optimised geometries. The decision was made to progress with the $\gamma \leq 0.3$ thresholded designs due to the potential for interpretation of the ϕ case as a continuous pipe insert.

inlet and a smaller separated entity near the outlet. The $\gamma \leq 0.3$ thresholded design (Fig. 7.6d) indicates a manner in which the large features near the inlet might be connected if the geometry was interpreted for manufacture and use as a pipe insert. The T_S minimised geometry contains a single large feature (see Figs. 7.6b,7.6e), with no indication of how it might be fixed to the internal pipe surface. The T_F maximisation result (Figs. 7.6c,7.6f) resembles conventional methods for improving heat transfer in pipes where internal fins or grooves are added in order to increase the surface area at the fluid-solid interface. The fluid temperature maximisation result (seen in Figs. 7.6c and 7.6f) differs more significantly from the laminar flow design (Fig. 7.3c) than the other two objective results. It is thought that this is because the objective function is evaluated in the design domain, allowing for a closer coupling of the local values of the objective and the iterative optimisation result, enabling turbulent heat transfer to have a greater impact on the resulting geometry.

Comparing optimisation results

A comparison between outlet velocities and local Reynolds numbers for the optimised geometries is presented in Fig. 7.7 where higher velocities and Reynolds numbers can be seen in upper region of the outlet of the ϕ optimised results (7.7a,7.7d) compared to those for T_S (7.7b,7.7e), and T_F (7.7c,7.7f).

The ϕ and T_F designs both have features near the outlets. The impact of these features can be seen in the low fluid velocities in the lower right corner of Fig. 7.7a and the upper right corner of Fig. 7.7c. The friction force implementation appears to create a shadowing of velocity behind features, indicating that the fluid is not realistically deflected by solid regions. This may be linked both to the computational limitations of the study (including the small domain size) and the fusion-specific conditions, such as the high inlet velocity. Whilst this shadowing of fluid velocity undoubtedly impacts heat transfer downstream of features, the outlet temperature distribution is provided for comparative purposes. Fig. 7.8 shows the region of the fluid which exceeds the inlet temperature of 120°C penetrates further into the domain in the ϕ minimised design (7.8a), suggesting enhanced heat transfer. However, the temperature maximisation geometry results in significantly higher temperatures than seen in the other two results, reaching 150°C in Fig. 7.8c. Fig. 7.8c includes an additional colour legend, to resolve the extended range whilst preserving colour levels consistent with Figs. 7.8a and 7.8b for the rest of the domain. The outlet turbulent kinetic energy, however, is higher in the T_S minimised result (Fig. 7.8e) than either the ϕ or T_F results, shown in Figs. 7.8d and 7.8f respectively.

The regions containing the highest convective heat fluxes (where the magnitude of the y-component is $\geq 5\text{MW m}^{-2}$) are shown in Fig. 7.9. The T_F result clearly has larger volumes and higher maximum heat fluxes (note the different colour bar limit). These figures show that in all cases, the regions of greatest convective heat flux surround the internal features, indicating a direct promotion of convective heat transfer.

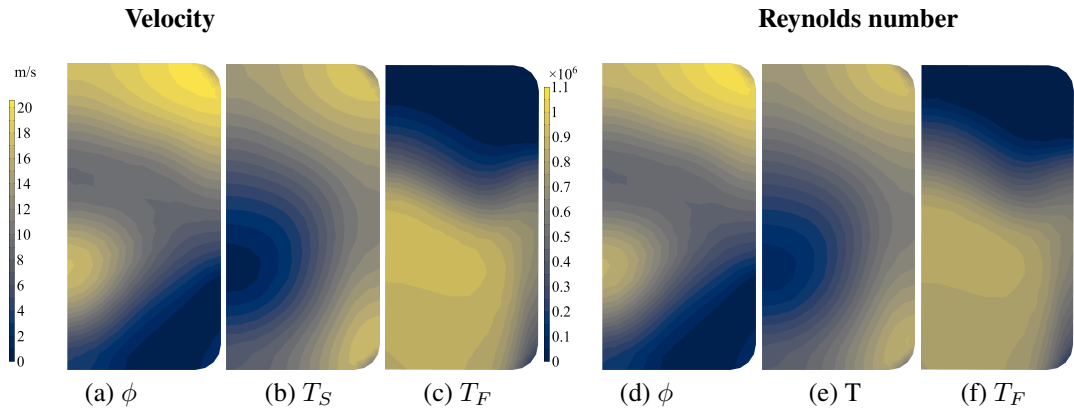


Figure 7.7. Left: comparison of velocity contours at the outlets of the ϕ , T_S and T_F studies: 7.7a, 7.7b and 7.7c respectively. Right: comparison of Reynolds number contours at the outlets of the ϕ , T_S and T_F studies: 7.7d, 7.7e and 7.7f respectively, showing a maximum of above $> 10^6$, indicating the evolution of more turbulent flow downstream of the internal features.

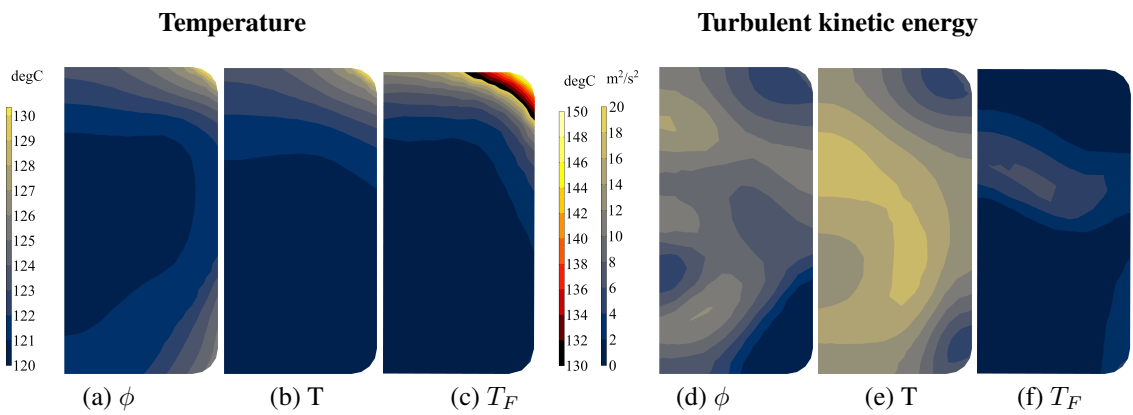


Figure 7.8. Left: Temperature distribution at the outlet of the ϕ (7.8a), T_S (7.8b) and T_F (7.8c) designs. 7.8c includes an additional colour legend to display the extended temperature range in the upper right corner. Right: Outlet turbulent kinetic energy for the ϕ (7.8d), T_S (7.8e), and T_F (7.8f) results.

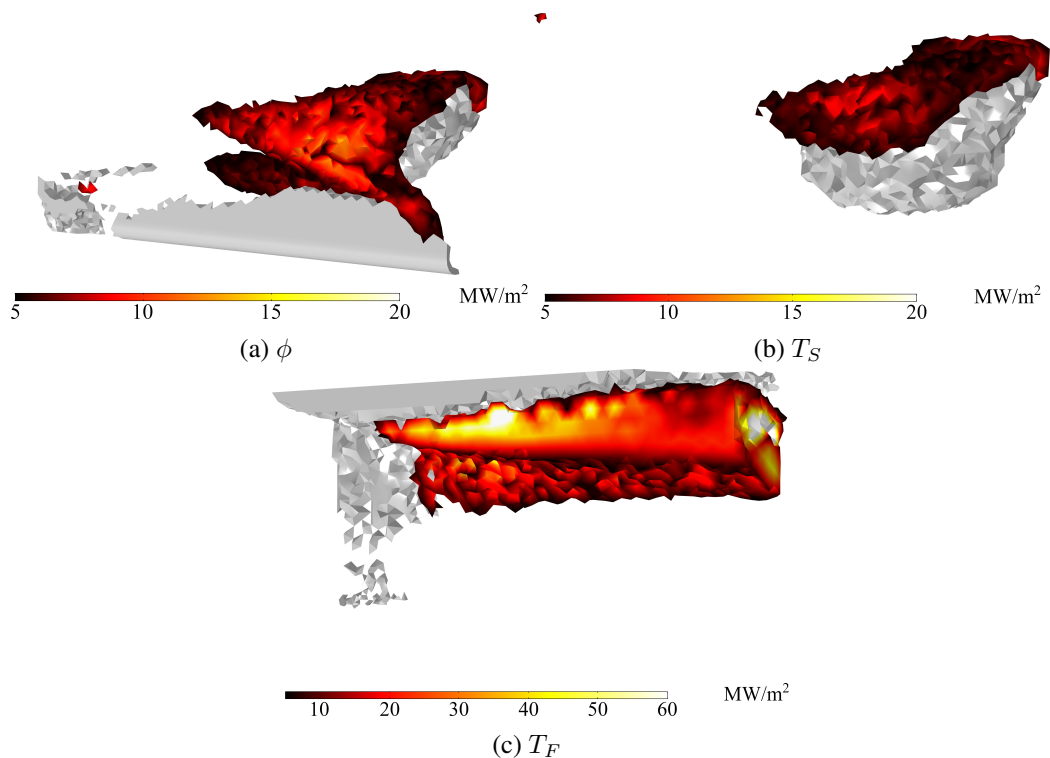


Figure 7.9. Regions of highest convective heat fluxes ($\geq 5 \text{ MW m}^{-2}$) in the ϕ , T_S and T_F geometries.

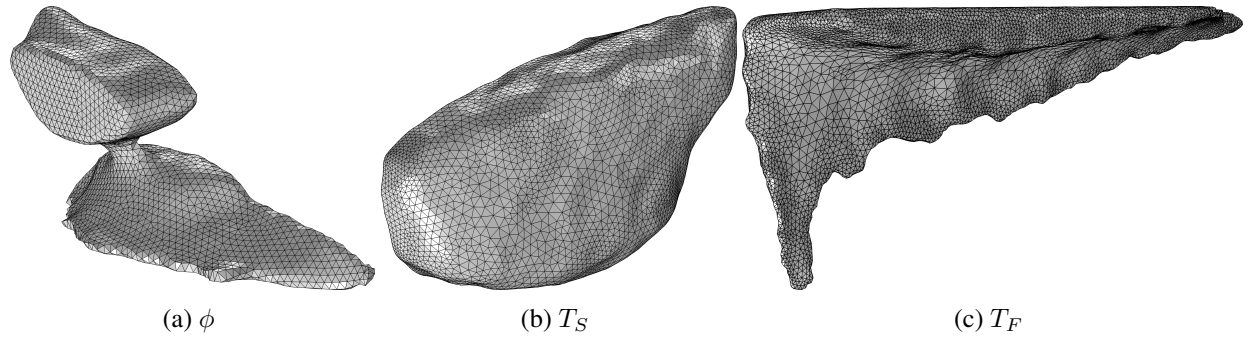


Figure 7.10. Post-processed and meshed inserts for the ϕ (7.10a), T_S (7.10b) and T_F (7.10c) results, which are then assembled for performance testing in elongated versions of the original geometries. Only the T_S and T_F designs make contact with the inside of the pipe, whereas 7.10b remains ‘suspended’ in the fluid.

Post-processing the results

The central locations of the features in the ϕ and T_S results seem to promote the mixing of hot and cold regions of fluid, whereas the T_F result seems to rely on enhancing heat transfer at the solid-fluid interface. In order to investigate this further, the optimised geometries, thresholded at $\gamma \leq 0.3$ are then exported as ‘.stl’ files, smoothed, and re-meshed as shown in Fig. 7.10 for further testing as prototype inserts. The smaller disconnected feature near the outlet in the ϕ minimised geometries presented in Fig. 7.6 is discarded to enable easier post-processing. It should be noted that the process of exporting the results, simplifying the geometry re-assembling with the reference design and re-meshing (as shown in Fig. 7.10) was not trivial and required careful manual adjustment. The T_F optimisation result is almost fully continuous with the internal pipe walls. The element-scale roughness might improve heat transfer in a manufactured component, however, the same smoothing process is applied for consistency.

Testing the re-assembled optimised geometries

The topology optimisation creates geometries which lead to increased turbulence and adds additional boundaries in the fluid domain which are likely to lead to more complex heat transfer processes than in the original problem. Therefore, whilst the aim of testing the assembled designs is to provide a more accurate representation of flow, the full quantitative treatment of their performance is therefore outside the scope of the paper. Fig. 7.11 presents a comparison of the flow around features in the re-assembled geometries following simulation under steady state weakly-compressible conditions with the $k - \epsilon$ turbulence model and no-slip boundary conditions imposed on the inner pipe surfaces and internal geometries. Whilst only the optimised features are shown, the testing was performed on a fully assembled monoblock, similar to that shown in Fig. 7.1 but extruded to a length of 80mm to better visualise the impact on flow downstream and improve convergence. The average pressure drops are presented in Table 7.4, evaluated over the 80mm test domains. These values are presented as rough estimates only, however, in order to aid comparison with other PFCs. The study makes no account for the periodicity of the inserts, however, and it is likely that topology optimisation studies performed over different lengths of pipe would produce different resulting geometries.

Table 7.4. Average pressure drops for post-processed geometries. These results were obtained in 80mm long domains, however pressure drop per metre estimates are presented to facilitate comparison with other PFCs.

Geometry	ΔP [MPa]	$\Delta P/L$ ($L = 80\text{mm}$) [MPa m^{-1}]
ϕ	0.049	0.61
T_S	0.028	0.35
T_F	0.014	0.175

Table 7.5. Average temperature differences between the outlet and inlet for the three geometries, evaluated over the 80mm design domain.

Geometry	ΔT $^{\circ}\text{C}$
ϕ	3.84
T_S	5.49
T_F	3.99

Whilst the optimisation was attempted using a periodic flow condition, this was found to cause convergence issues. The average temperature rises associated with each geometry, calculated as a difference between the outlet and inlet, are presented in Table 7.5. To put the pressure drops into context, any topology optimised designs would have to out-match pressure drops on the order of 0.5MPa m^{-1} for swirl tubes and around 0.1MPa m^{-1} for hypervaportrons (Schlosser, F. Escourbiac, *et al.* 2005). The T_F minimisation case presents the lowest pressure drop at 0.175MPa m^{-1} , and as shown in Table 7.5, it has the second highest average temperature rise (approx. 4°C) over 80mm.

Figs. 7.11a, 7.11c, and 7.11e show velocity streamlines coloured by pressure, and clarify the higher average pressure drop observed in the ϕ design, which is caused by the obstruction of the fluid by the two large features. Figs. 7.11b, 7.11d, and 7.11f show that whilst fluid is accelerated around the inserts in all cases, the fluid velocity is highest in the region between the two large connected features in the ϕ design. The T_S and T_F cases appear to cause lower pressure drops than the ϕ case but result in higher average temperature rises, as shown in Table 7.5. The ϕ geometry does appear to promote significant fluid mixing, which should promote heat transfer due to the one-sided heat load, however, further work would be required to investigate this.

7.4 Discussion

In a review of thermal topology optimisation (T. Dbouk 2017, pp. 852), the author concludes that the process is not yet a ‘robust numerical design technique for finding the optimal designs of thermal systems’. The implication of this statement is not that topology optimisation cannot be used, but rather that the problems require careful treatment to ensure they function as desired. That sentiment is supported by this study, where obtaining meaningful designs required a trial and error balancing of the various optimisation parameters. Further work extending the capability of the optimisation implementation is required before the application could be considered mature, however, the topology optimisation implementation was able to successfully minimise performance-related cost functions, producing features reminiscent of mechanical inserts in the thermal compliance (ϕ) and solid domain temperature (T_S) cases.

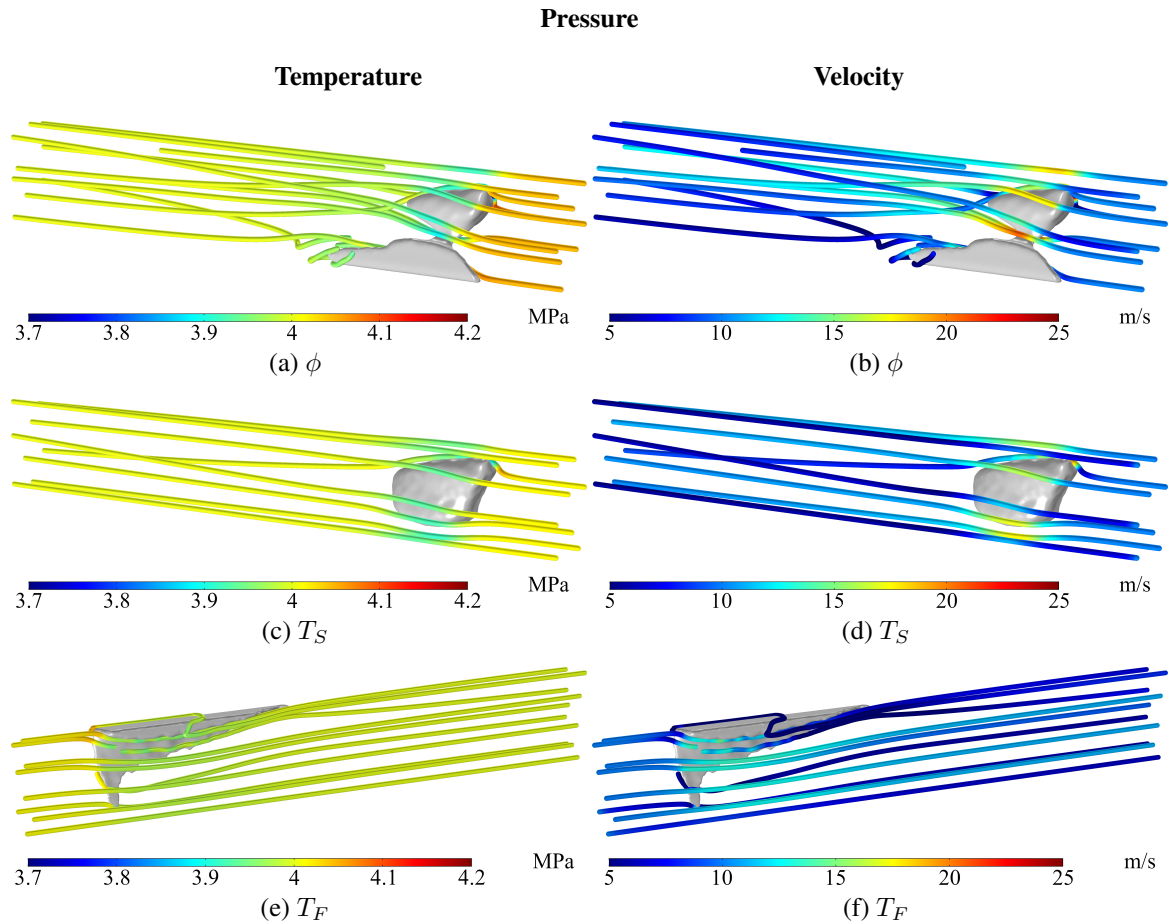


Figure 7.11. Velocity streamlines around optimised geometries coloured by absolute temperature and velocity magnitude.

The fluid temperature (T_F) maximisation case resulted in a geometry that improves heat transfer at the solid-fluid interface. These results are intended as first steps towards the exploration of non-intuitive fluid-domain PFC design concepts which may enable performance improvements.

7.4.1 Topology optimisation challenges and limitations

There are several factors which contribute to the numerical challenge and computational cost of the problem. These include the extreme, one-sided heat load, and the required 3D treatment of the problem. The relative scale of the fluid velocity compared to the scale of the monoblock model requires the application of large friction forces to ensure the creation of impermeable features in the topology optimisation design domain. The computational resource limitations require the use of a coarser mesh than might otherwise be desirable, and therefore a larger pressure drop per solid element formed in the design domain. It is thought that this contributed to large pressure drops in the topology-optimised designs compared to those typically associated with PFCs, as discussed in (Schlosser, F. Escourbiac, *et al.* 2005). A finer mesh would allow for the creation of smaller features. Furthermore, the Brinkman penalisation term and the associated regions of porosity were found to create unrealistic pressure losses due to friction forces present in intermediate-density regions

and unrealistic reductions in fluid velocity after solid features. This is likely partly due to the computational limitations in the implementation, however, rather than an unavoidable consequence of the technique. Traditional PFC heat transfer enhancement techniques rely on turbulence promotion. Despite the introduction of a RANS turbulence model, density-based topology optimisation requires further development to capture the effects of heat transfer in turbulent boundary layers following their creation in the design domain, as discussed briefly in (Alexandersen and Andreasen 2020). Finally, in-depth testing of the optimised results was found to be challenging due to the time and complexity associated with post-processing and re-assembly of the results. The re-simulation of topology optimised results is made more challenging due to the need to configure boundary conditions and meshes for geometrically complex and uneven features.

7.5 Conclusion

Forced convection heat transfer topology optimisation was performed for a recently proposed PFC where the flow was described using the $k - \epsilon$ turbulence model for steady-state incompressible Navier-Stokes flow. The gradient-based optimisation relied on the GCMMA implementation in COMSOL Multiphysics. Three objective cases are treated: mean solid domain thermal compliance and temperature were minimised, whereas coolant fluid temperature was maximised. All optimisation cases were performed with a constraint on average pressure drop and resulted in geometries that promote convective heat transfer. The minimisation cases produced geometries with internal features that resemble mechanical inserts and promote downstream turbulence. The fluid temperature maximisation result was found to enhance heat transfer near the solid-fluid interface. The resulting geometries were exported and re-assembled with the original monoblocks in order to perform a verification study to better visualise the behaviour of fluid flow around the optimised designs. The results are presented as a first step in the application of a topology optimisation workflow to the design of coolant pipe internal geometry in a novel PFC. Future work should include, when it is possible given computing power and software implementation, more realistic no-slip boundary conditions, the treatment of periodic flow (which suffered from convergence issues when implemented in COMSOL Multiphysics) and the use of finer meshing. Currently, the workflow for testing optimised components is challenging due to the requirements associated with re-assembling and meshing geometries with small irregular features. Improvements to this workflow would greatly improve the efficiency with which designs can be tested, allowing for quicker design iteration.

Chapter 8

Conclusions and commentary

The following section presents overall conclusions to the work based on the outcomes of the individual chapters, excluding Chapter 1, which contains an introduction to the project.

8.1 Chapter 2 conclusions

Chapter 2 discussed divertor design at a number of different levels, from the performance of individual components to the impact divertor choice has on the operation of a power plant and potential influences on the safety case of a reactor.

- It was found that much of the world's fusion research capability is tied to the development of ITER, delaying progress and increasing the risk for the development of alternate technological pathways.
- Top-down constraints such as the low activation criterion can artificially constrain material selection, as several recent studies suggest that operating within the required limits may be unfeasible, acting only to slow the development of commercially viable fusion reactors.
- Divertor design is further constrained due to systems integration issues, such as the desire to use a single coolant to simplify design (or safety case) or to use divertor heat to generate electricity.
- The discussion of reactor systems codes established that some codes, such as PROCESS are seen as not conducive to significant deviation from baseline design due to the long associated implementation time.
- Systems code modelling suggests that divertor heat flux handling capability strongly drives design complexity size and cost.
- The heat flux handling requirements for future divertor targets have significant levels of uncertainty which challenge efficient design and make progress hard to assess.
- Significant risks to future divertor operation include poorly characterised transient events which may result in heat loads several times the engineering limit, cyclic loading and heat concentration on leading edges.

- As the design of fusion reactor components is device led and there are large gaps between devices, research tends to be conducted sporadically, resulting in non-linear progress.
- Advanced divertor configurations with extended legs or additional strike points may lower the heat flux handling requirements of the target plates, however, their operation is not fully understood and therefore cannot be relied upon.
- The long time scales associated with tokamaks and the lack of representative test facilities to develop operational confidence hinder the transition to more advanced divertor technologies including liquid metal.
- This is compounded by the difficulty in modelling complex behaviour such as turbulent heat transfer in hypervapourators or MHD effects in liquid metal concepts.
- Fusion-specific design codes such as the MEAP are starting to accelerate progress towards design by analysis for divertor components, and many advanced monoblock concepts have been proposed, however many reactor design codes are still based on fission pressure-vessel codes that are of limited applicability.

8.1.1 Commentary and further work

This work suggested that some of the challenges to divertor design could be mitigated through a combination of novel optimisation techniques that encourage design space exploration, in combination with novel manufacturing techniques which may enable the construction of complex geometries.

8.2 Chapter 3 conclusions

In Chapter 3, a set of AM CuCrZr samples produced by 3T Additive Manufacturing were subjected to thermal testing using dilatometry and laser flash analysis. The samples were built with a range of laser powers (370-900W) with the aim of establishing the impact on thermal performance, and the ultimate goal of decreasing manufacture time. Results were obtained for thermal expansion and diffusivity for a temperature range of 30 – 700°C.

- The samples manufactured with the highest laser power (900W) and greatest layer thickness (60µm) were found to have the highest thermal diffusivity and the lowest coefficients of thermal expansion.
- Low coefficients of thermal expansion are desirable for use in multi-material divertor components designed to operate over a wide temperature range as constrained expansion results in stresses which may lead to part failure.
- The results indicate that a reduction of the associated build time by increasing laser power is possible without compromising thermal performance.

- Samples manufactured using the lowest laser power (370W) and layer thickness (30 μ m) representing the most conservative build process, performed the worst.

8.2.1 Commentary and further work

Further testing would be required to fully optimise the process parameters, however, the results in this study indicate that the aforementioned changes to the build parameters produce observable differences in the thermal properties which could impact the performance and lifetime of manufactured parts. This is of particular importance when considering the application of the material to high-temperature environments such as a fusion reactor cooling system. Experimental challenges encountered during the work included the difficulty in spot welding thermo-couples to highly conductive material and unexpected phase changes for the temperature range considered.

Further investigation is required in order to establish the cause of the observed sample phase change at temperatures well below the given melting point for CuCrZr. This paper demonstrated the potential viability of additive manufacturing as a route to developing advanced divertor components. Whilst significantly more work would be required to fully qualify the material for use in a fusion reactor, this was not the goal of the study. As discussed throughout this thesis, the other components of this project - fusion and topology optimisation - are not fully commercially mature. The demonstration of promising thermal properties with the potential for process optimisation indicates that at the present time, additive manufacturing should not be ruled out for future fusion component manufacture, particularly as the technique will likely evolve in parallel to developments in the other fields.

8.3 Chapter 4 conclusions

Chapter 4 investigated the development of thermal topology optimisation for solids and fluids including the theory, methods and software implementation.

- The literature shows a progression from 2D proof of concept studies (such as the widely used fluid methodology presented in (Borrvall and Petersson 2003) and attempts to increase computational efficiency, to more advanced descriptions of physical phenomena such as turbulence (Deng *et al.* 2011), convective heat transfer (Yoon 2010) and high resolution problems in 3D (Pizzolato *et al.* 2017a).
- As the field matures, it is finding more application to engineering problems, where manufacturing constraints are being considered (Lei *et al.* 2018).
- Whilst a review on thermal topology optimisation (T. Dbouk 2017) concluded that the technique is not a robust approach to finding the optimal designs of thermal systems, it is clear that in the years since that review was published, advances continue to be made and thermal topology optimisation is becoming sufficiently mature that it is of interest to a broad range of industrial applications.

8.3.1 Commentary and further work

The field appears to be lacking a comprehensive investigation into the impact of material property variation and the exploration of different multi-term design objectives. The influence of these parameters on topology-optimised geometries warrants further investigation, as they have the potential to change the designs in ways not fully accounted for in the present literature.

There is a large variety of topology optimisation codes being developed in the research community, based on a range of different algorithms. However, some of these are developed exclusively for the use of individual research groups and are either not made available to external researchers or are provided in a rudimentary form with varying levels of documentation. The prevalence of lots of codes with small user bases can make it difficult for newcomers to the field and those interested in using topology optimisation in an engineering context. It is recommended that future development of topology optimisation codes focuses on improving accessibility, as this would likely allow for more rapid development and implementation of a broad, consistent feature set which could be better exploited in industrially relevant applications.

8.4 Chapter 5 conclusions

Chapter 5 presented an initial step towards divertor monoblock optimisation, demonstrating the addition of high conductivity features in the monoblock armour domain.

- Thermal topology optimisation has the potential to cause a significant reduction in armour thermal gradients and temperature during high heat flux transient events.
- The application of topology optimisation to an asymmetric design demonstrates the potential of the technique to generate novel geometries targeted to specific applications.

8.4.1 Commentary and further work

The addition of high conductivity heat transfer elements in the design creates thermally induced stress concentrations not accounted for in this study. The use of a secondary topology optimisation step was suggested as a potential solution, however, in subsequent work, this was implemented as simultaneous multi-objective optimisation.

8.5 Chapter 6 conclusions

Multi-objective topology optimisation of an ITER-like divertor monoblock combining both stress and thermal terms was implemented in Chapter 6. Four different design concepts

were considered, based on standard and bevelled geometries with two different attachment scenarios.

- Maximum stress was reduced by up to 65%, with a peak reduction in temperature of approximately 270°C.
- The conductive heat flux optimised designs displayed a 20% transfer of heat flux from the top of the cooling pipe to the sides, countering the issue of heat flux concentration associated with the monoblock.
- The changes in load due to the addition of a bevel to the top surface of the monoblock were found to have a significant impact on optimum designs, making the addition of Cu to the upper half of the armour domain less favourable.
- Monoblocks fixed to the underlying cassette structure were found to exhibit different optimal geometries due to reduced potential for unrestrained thermal expansion.

8.5.1 Commentary and further work

The results can be interpreted for manufacture via functional grading with conductivities representing target material properties rather than Cu-W fractions, and are presented in the context of evolving design and manufacturing technology that may enable PFC performance improvements in future tokamaks. There exists significant uncertainty in the operating conditions expected in the divertor in tokamaks beyond ITER. The study demonstrates that even minor changes to the geometry and loading conditions of the components can drastically affect optimisation results. Beyond the bounds of topology optimisation, the differences in behaviour observed in this study may warrant further investigation, particularly if monoblocks with different fixing mechanisms are found to have different rates of failure. Further work should focus on the development of more detailed constraints and boundary conditions that more realistically reflect component requirements and loading conditions.

8.6 Chapter 7 conclusions

The extension of the topology optimisation methodology to a conjugate heat transfer problem was presented in Chapter 7. Forced convection heat transfer topology optimisation was performed for a recently proposed plasma-facing component where flow was described using the $k - \epsilon$ turbulence model for steady-state incompressible Navier-Stokes flow. The gradient-based optimisation relied on the GCMMA implementation in COMSOL Multiphysics. Three objective cases are treated: mean solid domain thermal compliance and temperature were minimised, whereas coolant fluid temperature was maximised.

- All optimisation cases were performed with a constraint on average pressure drop and result in geometries that promote convective heat transfer.

- The minimisation cases produced geometries with internal features that resemble mechanical inserts and promote downstream turbulence.
- The fluid temperature maximisation result enhances heat transfer near the solid-fluid interface.
- The resulting geometries were exported and re-assembled into the original components in order to perform a verification study to better visualise the behaviour of fluid flow in the novel geometries.
- The pressure drops in the optimised components were found to be larger than for existing plasma-facing components, suggesting further development of the technique is required.

8.6.1 Commentary and future work

The results are presented as a first step in the application of a topology optimisation workflow suitable for the design of coolant pipe internal geometry in a novel plasma-facing component. Future work should include, when it is possible given computing power and software implementation, more realistic no-slip boundary conditions, the treatment of periodic flow (which suffered from convergence issues when implemented in COMSOL Multiphysics) and the use of finer meshing. Currently, the workflow for testing optimised components is challenging due to the requirements associated with re-assembling and meshing geometries with small irregular features. Improvements to this workflow would greatly improve the efficiency with which designs can be tested, allowing for faster design iteration.

Chapter 9

Overall discussion

9.1 Overall project summary

The project has reviewed the design of the divertor and identified challenges concerning the difficulty of matching top-down design requirements and performance-related constraints. The combination of novel optimisation and manufacturing techniques was identified as a route to mitigating some of the challenges identified. The limitations targeted consisted principally of the difficulties in meeting performance requirements and in exploring the design space whilst maintaining a level of compatibility with existing concepts.

A collaboration was undertaken in order to assess the performance of contemporary additively manufactured fusion-relevant materials, finding thermal performance comparable with literature data for conventionally manufactured alloys. Next, a topology optimisation methodology was developed and applied to the ITER divertor monoblock armour domain, enabling significant reductions in thermal and stress-based objectives and exploration of a variety of design concepts. The methodology was subsequently applied to a conjugate heat transfer problem related to the active cooling channel of a novel plasma-facing component geometry. This resulted in the identification of internal pipe features which promoted convective heat transfer, however, the application was limited by available software and hardware capability.

9.2 Evolution of the project

As is common to many PhD projects, the premise that prompted this work was initially broad. Metal AM techniques were highlighted as possibly enabling the creation of specialised components with complex internal geometries. The divertor was considered early on as a candidate for investigation, primarily due to the substantial level of progress still thought to be required in order for mature divertor designs to emerge. At this point some major decisions needed to be made regarding definition of the design methodology and the specific operating conditions and geometry to be targeted. The author's background in Physics led him to favour design-by-analysis approaches, leading to the identification of generative design processes and ultimately topology optimisation. The specification of the modelling setup is complicated by the relative immaturity of the three components of the project so far: nuclear fusion, additive manufacturing and topology optimisation are all to some extent

considered emerging techniques about which there is uncertainty regarding the operating conditions, quality and effectiveness respectively. In order to reduce this uncertainty, ITER was chosen as the basis for the design work, as components and operating conditions are well documented in the literature. However, as the designs of ITER components have already been finalised, the motivation behind the topology optimisation turned towards design exploration, and investigation of the impact different choices have on the performance of components. This approach sees topology optimisation as an extension of sensitivity analysis, where changes to the design are in some sense more important than the final design.

9.3 The body of work

Chapter 2 is a review which aims to illustrate the considerations required in the digital engineering design of plasma-facing components for the divertor. This paper is set in the context of development difficulties that the fusion community is presently facing. New reactors are hugely complex and expensive to build, and ever-larger devices are required to improve performance. This ultimately slows progress towards to goal of commercially viable power generation as devices become delayed due to scale and complexity, alongside political and logistical issues (such as the provision of components by ITER members around the world). This encourages an approach whereby significant leaps in performance and technological capability are required between subsequent devices, meaning that in the case of components like the divertor, the next reactor might require a completely different geometry. This creates problems for an iterative design approach, instead requiring revolutionary design in each reactor. This problem is compounded by the uncertainty in the operating conditions of future reactors, leading to problems of design credibility when proposing new devices. For the divertor, significant uncertainties exist in the incident heat loads, required tolerance of plasma disruptions and material properties. Additionally, uncertainties in the performance of components in reactor-relevant conditions, and systems integration aspects, such as whether the same coolant as the breeder blanket will have to be used, or whether the heat extracted will be part of the power plant cycle, make efficient design hard to achieve. Integrated development environments for fusion are an attractive prospect, however, the complexity of modelling involved, alongside a lack of comprehensive experimental data means that these concepts remain unrealised. A different approach to digital twinning and the use of systems codes is suggested, whereby digital twins of tokamaks are maintained with different design choices made in key areas such as the divertor. These could then be updated with experimental data and developments in emerging technologies that may have influenced the choice if known beforehand, in an attempt to better enable continuous assessment of designs part way through a reactor's life cycle. The challenges associated with the development of this modelling system and a proper assessment of the viability of the concept is however outside the scope of this thesis.

The industrial collaboration detailed in Chapter 3 fulfilled a mandatory component of the Fusion CDT programme and was sought in order to establish a grounding for the suggestion

of AM for fusion-relevant manufacturing. Despite experimental difficulties, the study indicated that AM CuCrZr may be able to achieve thermal properties that do not significantly disadvantage it when compared to conventionally manufactured material.

The principle behind the topology optimisation performed in Chapters 5, 6 and 7 was to incrementally build on the implementation to treat more complex processes. This led to a focus on thermal objectives in the armour domain not considered by other authors, whose work on topology optimisation of the divertor monoblock was published during the course of this project. Whilst there is some discrepancy in the literature over the ideal operating temperature ranges for the materials used in the monoblock, Chapter 6 concludes that using topology-optimised geometries to reduce the operating temperature on the monoblock plasma facing surface could lead to desirable increases in yield strength. Furthermore, changes to the design including a bevelled top surface (and associated heat loads) and different attachment techniques resulted in drastically different design results. Whilst this is sometimes presented as a criticism of topology optimisation techniques, it is potentially important to divertor design where the consequences of component failure are high and the operating conditions present a severe barrier to producing adequately performant designs. A study was also performed to investigate the consequences of reducing the Cu content of optimised designs. The results indicate that lower Cu-content designs maintain significant stress reductions without the associated lower operating temperatures under load. This may be beneficial where low Cu-content designs are sought to avoid activation, or where higher W operating temperatures are sought. The designs are interpreted for manufacture through the use of functionally graded AM.

The extension of these techniques to application in the monoblock coolant channel challenged the topology optimisation methodology and the computational resources available. Chapter 7 is presented as an initial step towards the application of the technique to the design of internal coolant pipe geometry for plasma-facing components. It is thought that there is significant potential for the technique to change divertor component design, however, this will likely require more flexible software suitable for use on high-performance computing facilities.

9.4 Further work and research impact

In retrospect, there are some aspects of the work presented which could have been done differently if it were to be repeated, and some areas that would remain outside of the scope of the project. For future application of topology optimisation to fusion design, the following steps are recommended.

- I Efforts should be made to coordinate the development of design optimisation codes for fusion in a similar manner to the collaboration and bench-marking associated with systems code development.
- II The basis should be an existing open-source high-performance topology optimisation

code, such as one of the ones investigated in Chapter 4. This will also allow for more flexibility in the specification of constraints in topology optimisation, such as those relevant to manufacturing.

- III This could be integrated with parallel finite element and computational fluid dynamics codes to enable use on high-performance computing facilities, required to perform the optimisation in sufficient detail to capture complex behaviour.
- IV Further effort should be made to integrate the requirements of codes such as the MEAP, which focuses on monoblock design.
- V Further investigation is recommended into the impact of uncertainties in material properties (implemented through Monte Carlo simulation perhaps) and loading conditions.
- VI In general, developments in topology optimisation methodology, such as those recommended for thermal and fluid problems in (Alexandersen and Andreasen 2020), are broadly applicable to fusion as a subject area, particularly where they refer to improving the characterisation of physical processes and incorporation of numerical and experimental verification.
- VII Incorporation of deep learning techniques may enable the acceleration of topology optimisation convergence, as discussed in (Lin, Hong, *et al.* 2018).

It is the author's belief that many of the problems that face divertor design will be resolved by technologies that are beginning to emerge in other industries but are as yet not sufficiently mature for serious application to reactors. This thesis has explored topology optimisation and additive manufacturing as ways of changing design methodology, either as a route for the exploration of a wider design space through rapid prototyping or through the tailoring of standardised components to specific devices and loading conditions in order to best meet operational challenges.

References

- Aage, Niels, Erik Andreassen, and Boyan Stefanov Lazarov (Mar. 1, 2015). “Topology Optimization Using PETSc: An Easy-to-Use, Fully Parallel, Open Source Topology Optimization Framework”. In: *Struct Multidisc Optim* 51.3, pp. 565–572. ISSN: 1615-1488. DOI: 10.1007/s00158-014-1157-0. URL: <https://doi.org/10.1007/s00158-014-1157-0> (visited on 01/22/2019).
- Aage, Niels and Boyan S. Lazarov (Apr. 1, 2013). “Parallel Framework for Topology Optimization Using the Method of Moving Asymptotes”. In: *Struct Multidisc Optim* 47.4, pp. 493–505. ISSN: 1615-1488. DOI: 10.1007/s00158-012-0869-2. URL: <https://doi.org/10.1007/s00158-012-0869-2> (visited on 03/05/2019).
- Aage, Niels, Thomas H. Poulsen, *et al.* (Feb. 2008). “Topology Optimization of Large Scale Stokes Flow Problems”. In: *Structural and Multidisciplinary Optimization* 35.2, pp. 175–180. ISSN: 1615-147X, 1615-1488. DOI: 10.1007/s00158-007-0128-0. URL: <http://link.springer.com/10.1007/s00158-007-0128-0> (visited on 04/01/2019).
- Abdelwahed, M., M. Hassine, and M. Masmoudi (Aug. 2009). “Optimal Shape Design for Fluid Flow Using Topological Perturbation Technique”. In: *Journal of Mathematical Analysis and Applications* 356.2, pp. 548–563. ISSN: 0022247X. DOI: 10.1016/j.jmaa.2009.02.045. URL: <https://linkinghub.elsevier.com/retrieve/pii/S0022247X09001863> (visited on 04/11/2019).
- Abdelwahed, Mohamed and Maatoug Hassine (2014). *Topology Optimization of Time Dependent Viscous Incompressible Flows*. Abstract and Applied Analysis. DOI: 10.1155/2014/923016. URL: <https://www.hindawi.com/journals/aaa/2014/923016/abs/> (visited on 04/11/2019).
- Abdou, Mohamed *et al.* (Nov. 2015). “Blanket/First Wall Challenges and Required R&D on the Pathway to DEMO”. In: *Fusion Engineering and Design* 100, pp. 2–43. ISSN: 09203796. DOI: 10.1016/j.fusengdes.2015.07.021. URL: <https://linkinghub.elsevier.com/retrieve/pii/S0920379615302465> (visited on 10/08/2022).
- Abernethy, R.G. (Mar. 4, 2017). “Predicting the Performance of Tungsten in a Fusion Environment: A Literature Review”. In: *Materials Science and Technology* 33.4, pp. 388–399. ISSN: 0267-0836, 1743-2847. DOI: 10.1080/02670836.2016.1185260. URL: <https://www.tandfonline.com/doi/full/10.1080/02670836.2016.1185260> (visited on 04/15/2019).

- The Blender Foundation (2019). *About*. blender.org. URL: <https://www.blender.org/about/> (visited on 05/10/2019).
- Ahrens, James, Geveci, Berk, Law, Charles (n.d.). *ParaView: An End-User Tool for Large Data Visualization, Visualization Handbook*.
- Alatrash, Yazan *et al.* (June 2022). “Investigation of Subcooled Boiling Wall Closures at High Pressure Using a Two-Phase CFD Code”. In: *Nuclear Engineering and Technology* 54.6, pp. 2276–2296. ISSN: 17385733. DOI: 10.1016/j.net.2021.12.012. URL: <https://linkinghub.elsevier.com/retrieve/pii/S1738573321006811> (visited on 09/11/2022).
- Alexandersen, Joe, Niels Aage, *et al.* (Dec. 10, 2014). “Topology Optimisation for Natural Convection Problems: TOPOLOGY OPTIMISATION FOR NATURAL CONVECTION PROBLEMS”. In: *International Journal for Numerical Methods in Fluids* 76.10, pp. 699–721. ISSN: 02712091. DOI: 10.1002/flid.3954. URL: <http://doi.wiley.com/10.1002/flid.3954> (visited on 09/21/2018).
- Alexandersen, Joe and Casper Andreasen (Mar. 4, 2020). “A Review of Topology Optimisation for Fluid-Based Problems”. In: *Fluids* 5. DOI: 10.3390/fluids5010029.
- Alexandersen, Joe and Boyan Stefanov Lazarov (2015). “Tailoring Macroscale Response of Mechanical and Heat Transfer Systems by Topology Optimization of Microstructural Details”. In: *Engineering and Applied Sciences Optimization: Dedicated to the Memory of Professor M.G. Karlaftis*. Ed. by Nikos D. Lagaros and Manolis Papadrakakis. Computational Methods in Applied Sciences. Cham: Springer International Publishing, pp. 267–288. ISBN: 978-3-319-18320-6. DOI: 10.1007/978-3-319-18320-6_15. URL: https://doi.org/10.1007/978-3-319-18320-6_15 (visited on 03/07/2019).
- Alexandersen, Joe, Ole Sigmund, and Niels Aage (Sept. 2016). “Large Scale Three-Dimensional Topology Optimisation of Heat Sinks Cooled by Natural Convection”. In: *International Journal of Heat and Mass Transfer* 100, pp. 876–891. ISSN: 00179310. DOI: 10.1016/j.ijheatmasstransfer.2016.05.013. URL: <https://linkinghub.elsevier.com/retrieve/pii/S0017931015307365> (visited on 02/15/2019).
- Alexandersen, Joe, Ole Sigmund, Knud Erik Meyer, *et al.* (July 2018). “Design of Passive Coolers for Light-Emitting Diode Lamps Using Topology Optimisation”. In: *International Journal of Heat and Mass Transfer* 122, pp. 138–149. ISSN: 00179310. DOI: 10.1016/j.ijheatmasstransfer.2018.01.103. URL: <https://linkinghub.elsevier.com/retrieve/pii/S0017931017336190> (visited on 10/28/2021).
- Amir, Oded, Niels Aage, and Boyan S. Lazarov (May 1, 2014). “On Multigrid-CG for Efficient Topology Optimization”. In: *Struct Multidisc Optim* 49.5, pp. 815–829. ISSN: 1615-

1488. DOI: 10.1007/s00158-013-1015-5. URL: <https://doi.org/10.1007/s00158-013-1015-5> (visited on 02/15/2019).
- Andreassen, Erik *et al.* (Jan. 2011). “Efficient Topology Optimization in MATLAB Using 88 Lines of Code”. In: *Structural and Multidisciplinary Optimization* 43.1, pp. 1–16. ISSN: 1615-147X, 1615-1488. DOI: 10.1007/s00158-010-0594-7. URL: <http://link.springer.com/10.1007/s00158-010-0594-7> (visited on 04/10/2019).
- Anflor, Carla T.M. and Rogério J. Marczak (Sept. 2009). “A Boundary Element Approach for Topology Design in Diffusive Problems Containing Heat Sources”. In: *International Journal of Heat and Mass Transfer* 52.19-20, pp. 4604–4611. ISSN: 00179310. DOI: 10.1016/j.ijheatmasstransfer.2009.02.048. URL: <https://linkinghub.elsevier.com/retrieve/pii/S0017931009002580> (visited on 04/11/2019).
- Araki, Masanori, Masato Akiba, *et al.* (Sept. 1992). “Thermal Response of Bonded CFC/OFHC Divertor Mock-Ups for Fusion Experimental Reactors under Large Numbers of Cyclic High Heat Loads”. In: *Journal of Nuclear Science and Technology* 29.9, pp. 901–908. ISSN: 0022-3131, 1881-1248. DOI: 10.1080/18811248.1992.9731610. URL: <http://www.tandfonline.com/doi/abs/10.1080/18811248.1992.9731610> (visited on 07/01/2020).
- Araki, Masanori, Masuro Ogawa, *et al.* (Sept. 1996). “Experiments on Heat Transfer of Smooth and Swirl Tubes under One-Sided Heating Conditions”. In: *International Journal of Heat and Mass Transfer* 39.14, pp. 3045–3055. ISSN: 00179310. DOI: 10.1016/0017-9310(95)00344-4. URL: <https://linkinghub.elsevier.com/retrieve/pii/0017931095003444> (visited on 07/01/2020).
- Arquis, E and J.P. Caltagirone (1984). “Sur Les Conditions Hydrodynamiques Au Voisinage d’une Interface Milieu Fluide-Milieu Poreux: Application a’ La Convection Naturelle”. In: *CR Acad. Sci. Paris II* 299.
- Arrizubieta, Jon Iñaki *et al.* (Jan. 2020). “Thermal Diffusivity Measurement of Laser-Deposited AISI H13 Tool Steel and Impact on Cooling Performance of Hot Stamping Tools”. In: *Metals* 10.1 (1), p. 154. ISSN: 2075-4701. DOI: 10.3390/met10010154. URL: <https://www.mdpi.com/2075-4701/10/1/154> (visited on 10/10/2022).
- ASTM-E1461-13 (Oct. 2013). *Test Method for Thermal Diffusivity by the Flash Method*. ASTM-E1461-13. ASTM International. DOI: 10.1520/E1461-13. URL: <http://www.astm.org/cgi-bin/resolver.cgi?E1461-13> (visited on 06/12/2019).
- ASTM-E228-17 (2017). *Test Method for Linear Thermal Expansion of Solid Materials With a Push-Rod Dilatometer*. ASTM-E228-17. ASTM International. DOI: 10.1520/E0228-17. URL: <http://www.astm.org/cgi-bin/resolver.cgi?E228-17> (visited on 09/19/2019).

- Bacellar, Daniel *et al.* (2016). “Novel Airside Heat Transfer Surface Designs Using an Integrated Multi-Scale Analysis with Topology and Shape Optimization”. In: URL: /paper/Novel-Airside-Heat-Transfer-Surface-Designs-Using-BACELLAR-Aute/b308f3e4bff0ddc0416f787521935118210147a1 (visited on 08/15/2018).
- Bachmann, C. *et al.* (Nov. 2018). “Overview over DEMO Design Integration Challenges and Their Impact on Component Design Concepts”. In: *Fusion Engineering and Design* 136, pp. 87–95. ISSN: 09203796. DOI: 10.1016/j.fusengdes.2017.12.040. URL: <https://linkinghub.elsevier.com/retrieve/pii/S0920379617309997> (visited on 07/22/2020).
- Barabash, V.R. *et al.* (Oct. 2011). “Specification of CuCrZr Alloy Properties after Various Thermo-Mechanical Treatments and Design Allowables Including Neutron Irradiation Effects”. In: *Journal of Nuclear Materials* 417.1-3, pp. 904–907. ISSN: 00223115. DOI: 10.1016/j.jnucmat.2010.12.158. URL: <https://linkinghub.elsevier.com/retrieve/pii/S0022311510009803> (visited on 08/20/2022).
- Barash, M. (July 1962). “Electric Spark Machining”. In: *International Journal of Machine Tool Design and Research* 2.3, pp. 281–295. ISSN: 00207357. DOI: 10.1016/0020-7357(62)90016-1. URL: <https://linkinghub.elsevier.com/retrieve/pii/0020735762900161> (visited on 06/26/2019).
- Barrett, T. R. *et al.* (Jan. 2019). “Virtual Engineering of a Fusion Reactor: Application to Divertor Design, Manufacture, and Testing”. In: *IEEE Transactions on Plasma Science* 47.1, pp. 889–896. ISSN: 0093-3813. DOI: 10.1109/TPS.2018.2856888.
- Barrett, T.R. *et al.* (Oct. 2015). “Enhancing the DEMO Divertor Target by Interlayer Engineering”. In: *Fusion Engineering and Design* 98–99, pp. 1216–1220. ISSN: 09203796. DOI: 10.1016/j.fusengdes.2015.03.031. URL: <https://linkinghub.elsevier.com/retrieve/pii/S0920379615001908> (visited on 12/14/2020).
- Barrett, Thomas R. *et al.* (Nov. 2016). “Progress in the Engineering Design and Assessment of the European DEMO First Wall and Divertor Plasma Facing Components”. In: *Fusion Engineering and Design* 109–111, pp. 917–924. ISSN: 09203796. DOI: 10.1016/j.fusengdes.2016.01.052. URL: <http://linkinghub.elsevier.com/retrieve/pii/S0920379616300540> (visited on 07/09/2018).
- Bastide, Alain, Pierre-Henri Cocquet, and Delphine Ramalingom (July 2018). “Penalization Model for Navier–Stokes–Darcy Equations with Application to Porosity-Oriented Topology Optimization”. In: *Mathematical Models and Methods in Applied Sciences* 28.08, pp. 1481–1512. ISSN: 0218-2025, 1793-6314. DOI: 10.1142/S0218202518500409. URL: <https://www.worldscientific.com/doi/abs/10.1142/S0218202518500409> (visited on 03/21/2019).

- Batet, L. *et al.* (Apr. 2014). “Modelling of a Supercritical CO₂ Power Cycle for Nuclear Fusion Reactors Using RELAP5–3D”. In: *Fusion Engineering and Design* 89.4, pp. 354–359. ISSN: 09203796. DOI: 10.1016/j.fusengdes.2014.03.018. URL: <https://linkinghub.elsevier.com/retrieve/pii/S0920379614001975> (visited on 07/16/2020).
- Baxi, C B and C P C Wong (2000). “Review of Helium Cooling for Fusion Reactor Applications”. In: *Fusion Engineering and Design*, p. 6.
- Baxi, C. B. (Sept. 1995). “Comparison of Swirl Tube and Hypervapotron for Cooling of ITER Divertor”. In: *Proceedings of 16th International Symposium on Fusion Engineering*. Proceedings of 16th International Symposium on Fusion Engineering. Vol. 1, 186–189 vol.1. DOI: 10.1109/FUSION.1995.534199.
- (Oct. 2001). “Thermal Hydraulics of Water Cooled Divertors”. In: *Fusion Engineering and Design* 56–57, pp. 195–198. ISSN: 09203796. DOI: 10.1016/S0920-3796(01)00258-7. URL: <https://linkinghub.elsevier.com/retrieve/pii/S0920379601002587> (visited on 01/20/2021).
- Bejan, Adrian (2000). “From Heat Transfer Principles to Shape and Structure in Nature: Constructal Theory”. In: *Journal of Heat Transfer* 122.3, p. 430. ISSN: 00221481. DOI: 10.1115/1.1288406. URL: <http://HeatTransfer.asmedigitalcollection.asme.org/article.aspx?articleid=1444332> (visited on 09/25/2018).
- (Mar. 25, 2003). “Constructal Tree-Shaped Paths for Conduction and Convection”. In: *International Journal of Energy Research* 27.4, pp. 283–299. ISSN: 1099-114X. DOI: 10.1002/er.875. URL: <https://onlinelibrary.wiley.com/doi/abs/10.1002/er.875> (visited on 09/25/2018).
- Bendsøe, Martin and Ole Sigmund (Nov. 1, 1999). “Material Interpolation Schemes in Topology Optimization”. In: *Archive of Applied Mechanics* 69, pp. 635–654. DOI: 10.1007/s004190050248.
- Bendsøe, Martin P. and O. Sigmund (2003). *Topology Optimization: Theory, Methods, and Applications*. Berlin ; New York: Springer. 370 pp. ISBN: 978-3-540-42992-0.
- United States General Accounting Office (1999). *Best Practices: Better Management of Technology Development Can Improve Weapon System Outcomes*. Washington D.C: United States General Accounting Office. URL: <https://digital.library.unt.edu/ark:/67531/metadc291025/> (visited on 12/22/2021).
- Bigot, Bernard (Sept. 1, 2019). “ITER Construction and Manufacturing Progress toward First Plasma”. In: *Fusion Engineering and Design*. SI:SOFT-30 146, pp. 124–129. ISSN: 0920-3796. DOI: 10.1016/j.fusengdes.2018.11.052. URL: <https://www.sciencedirect.com/science/article/pii/S0920379618307592> (visited on 03/29/2021).

- Blagoev, Alexander (May 20, 2020). “ARE THE HYBRID NUCLEAR REACTORS THE ANSWER FOR THE FUTURE ENERGY NEEDS?” In: *EEEP*, pp. 40–49. DOI: 10 . 32006/eeep . 2020 . 1 . 4049. URL: <http://ecoleng.org/archive/2020/1/40-49.pdf> (visited on 10/15/2022).
- Bloom, E E *et al.* (1984). “Low Activation Materials for Fusion Applications”. In: *Journal of Nuclear Materials* 122.1, pp. 17–26. DOI: 10 . 1016/0022-3115(84)90570-1. URL: <http://www.sciencedirect.com/science/article/pii/0022311584905701>.
- Bonnin, X. *et al.* (Aug. 2017). “ITER Divertor Plasma Response to Time-Dependent Impurity Injection”. In: *Nuclear Materials and Energy* 12, pp. 1100–1105. ISSN: 23521791. DOI: 10 . 1016/j . nme . 2017 . 03 . 010. URL: <https://linkinghub.elsevier.com/retrieve/pii/S2352179116302769> (visited on 02/18/2019).
- Borrvall, Thomas and Joakim Petersson (Jan. 10, 2003). “Topology Optimization of Fluids in Stokes Flow”. In: *International Journal for Numerical Methods in Fluids* 41.1, pp. 77–107. ISSN: 1097-0363. DOI: 10.1002/flid.426. URL: <https://onlinelibrary.wiley.com/doi/abs/10.1002/flid.426> (visited on 09/18/2018).
- Brotzu, A. *et al.* (2019). “Study of CuCrZr Alloy for the Production of a Passive Satellite”. In: *Procedia Structural Integrity* 18, pp. 742–748. ISSN: 24523216. DOI: 10 . 1016/j . prostr . 2019 . 08 . 222. URL: <https://linkinghub.elsevier.com/retrieve/pii/S2452321619304329> (visited on 08/07/2022).
- Bruns, T. E. (July 1, 2007). “Topology Optimization of Convection-Dominated, Steady-State Heat Transfer Problems”. In: *International Journal of Heat and Mass Transfer* 50.15, pp. 2859–2873. ISSN: 0017-9310. DOI: 10 . 1016/j . ijheatmasstransfer . 2007 . 01 . 039. URL: <http://www.sciencedirect.com/science/article/pii/S0017931007001330> (visited on 03/04/2019).
- (Dec. 2005). “A Reevaluation of the SIMP Method with Filtering and an Alternative Formulation for Solid–Void Topology Optimization”. In: *Structural and Multidisciplinary Optimization* 30.6, pp. 428–436. ISSN: 1615-147X, 1615-1488. DOI: 10 . 1007/s00158-005-0537-x. URL: <http://link.springer.com/10.1007/s00158-005-0537-x> (visited on 03/22/2019).
- Buchmayr, Bruno *et al.* (Apr. 2017). “Laser Powder Bed Fusion - Materials Issues and Optimized Processing Parameters for Tool Steels, AlSiMg- and CuCrZr-Alloys: Tool Steels, AlSiMg- and CuCrZr-Alloys”. In: *Adv. Eng. Mater.* 19.4, p. 1600667. ISSN: 14381656. DOI: 10 . 1002/adem . 201600667. URL: <http://doi.wiley.com/10.1002/adem.201600667> (visited on 04/30/2019).
- Burchell, T D *et al.* (1992). “A Carbon-Carbon Composite Materials Development Program For”. In: p. 63.

- Burger, Francois H., Jaco Dirker, and Josua P. Meyer (Dec. 2013). “Three-Dimensional Conductive Heat Transfer Topology Optimisation in a Cubic Domain for the Volume-to-Surface Problem”. In: *International Journal of Heat and Mass Transfer* 67, pp. 214–224. ISSN: 00179310. DOI: 10.1016/j.ijheatmasstransfer.2013.08.015. URL: <https://linkinghub.elsevier.com/retrieve/pii/S0017931013006753> (visited on 04/11/2019).
- Buttery, R. J. *et al.* (Feb. 2019). “DIII-D Research to Prepare for Steady State Advanced Tokamak Power Plants”. In: *J Fusion Energ* 38.1, pp. 72–111. ISSN: 0164-0313, 1572-9591. DOI: 10.1007/s10894-018-0185-y. URL: <http://link.springer.com/10.1007/s10894-018-0185-y> (visited on 07/22/2020).
- Campbell, David J. *et al.* (Feb. 2019). “Innovations in Technology and Science R&D for ITER”. In: *J Fusion Energ* 38.1, pp. 11–71. ISSN: 0164-0313, 1572-9591. DOI: 10.1007/s10894-018-0187-9. URL: <http://link.springer.com/10.1007/s10894-018-0187-9> (visited on 07/22/2020).
- Cardella, A. *et al.* (1993). “DESIGN MANUFACTURING AND TESTING OF THE MONOBLOCK DIVERTOR”. In: *Fusion Technology 1992*. Elsevier, pp. 211–215. ISBN: 978-0-444-89995-8. DOI: 10.1016/B978-0-444-89995-8.50033-3. URL: <https://linkinghub.elsevier.com/retrieve/pii/B9780444899958500333> (visited on 08/17/2021).
- Carlson, Lane *et al.* (June 2011). “ARIES Systems Code Development, Visualization and Application”. In: *2011 IEEE/NPSS 24th Symposium on Fusion Engineering*. 2011 IEEE/NPSS 24th Symposium on Fusion Engineering, pp. 1–6. DOI: 10.1109/S0FE.2011.6052294.
- Cattadori, G. *et al.* (Oct. 1993). “Hypervapotron Technique in Subcooled Flow Boiling CHF”. In: *Experimental Thermal and Fluid Science* 7.3, pp. 230–240. ISSN: 08941777. DOI: 10.1016/0894-1777(93)90006-5. URL: <https://linkinghub.elsevier.com/retrieve/pii/0894177793900065> (visited on 08/19/2021).
- Challis, Vivien J. (Apr. 2010). “A Discrete Level-Set Topology Optimization Code Written in Matlab”. In: *Structural and Multidisciplinary Optimization* 41.3, pp. 453–464. ISSN: 1615-147X, 1615-1488. DOI: 10.1007/s00158-009-0430-0. URL: <http://link.springer.com/10.1007/s00158-009-0430-0> (visited on 02/11/2019).
- Chapman, I. T. and A. W. Morris (Mar. 25, 2019). “UKAEA Capabilities to Address the Challenges on the Path to Delivering Fusion Power”. In: *Phil. Trans. R. Soc. A*. 377.2141, p. 20170436. ISSN: 1364-503X, 1471-2962. DOI: 10.1098/rsta.2017.0436. URL: <https://royalsocietypublishing.org/doi/10.1098/rsta.2017.0436> (visited on 07/22/2020).

- Chapman, I.T. *et al.* (July 19, 2015). “Overview of MAST Results”. In: *Nuclear Fusion* 55, p. 104008. DOI: 10.1088/0029-5515/55/10/104008.
- Chen, Huangxin *et al.* (Dec. 21, 2018). “An Efficient Threshold Dynamics Method for Topology Optimization for Fluids”. arXiv: 1812.09437 [math]. URL: <http://arxiv.org/abs/1812.09437> (visited on 03/21/2019).
- Cheng, Lin *et al.* (Apr. 15, 2018). “Coupling Lattice Structure Topology Optimization with Design-Dependent Feature Evolution for Additive Manufactured Heat Conduction Design”. In: *Computer Methods in Applied Mechanics and Engineering* 332, pp. 408–439. ISSN: 0045-7825. DOI: 10.1016/j.cma.2017.12.024. URL: <http://www.sciencedirect.com/science/article/pii/S0045782517307740> (visited on 03/21/2019).
- Chung, Hayoung *et al.* (Apr. 2019). “Topology Optimization in OpenMDAO”. In: *Struct Multidisc Optim* 59.4, pp. 1385–1400. ISSN: 1615-147X, 1615-1488. DOI: 10.1007/s00158-019-02209-7. URL: <http://link.springer.com/10.1007/s00158-019-02209-7> (visited on 05/10/2019).
- Ciattaglia, Sergio *et al.* (May 1, 2020). “Energy Analysis for the Connection of the Nuclear Reactor DEMO to the European Electrical Grid”. In: *Energies* 13.9, p. 2157. ISSN: 1996-1073. DOI: 10.3390/en13092157. URL: <https://www.mdpi.com/1996-1073/13/9/2157> (visited on 10/13/2022).
- Clark, Emily Buckman (May 2017). “Computational Thermal-Hydraulics Modeling of Twisted Tape Enabled High Heat Flux Components”. In: p. 197.
- Coffin, Peter and Kurt Maute (May 2016). “Level Set Topology Optimization of Cooling and Heating Devices Using a Simplified Convection Model”. In: *Structural and Multidisciplinary Optimization* 53.5, pp. 985–1003. ISSN: 1615-147X, 1615-1488. DOI: 10.1007/s00158-015-1343-8. URL: <http://link.springer.com/10.1007/s00158-015-1343-8> (visited on 09/18/2018).
- Coleman, M. and S. McIntosh (Feb. 2019). “BLUEPRINT: A Novel Approach to Fusion Reactor Design”. In: *Fusion Engineering and Design* 139, pp. 26–38. ISSN: 09203796. DOI: 10.1016/j.fusengdes.2018.12.036. URL: <https://linkinghub.elsevier.com/retrieve/pii/S0920379618308019> (visited on 07/22/2020).
- COMSOL (2021). *COMSOL: Multiphysics Software for Optimizing Designs*. Version 5.6. COMSOL AB, Stockholm, Sweden. URL: <https://uk.comsol.com/> (visited on 10/31/2021).
- Copper Institute, European (2021). *CuCrZr Datasheet*. URL: <http://conductivity-app.org/alloy-sheet/19> (visited on 05/06/2020).
- Costley, A. E. (Mar. 25, 2019). “Towards a Compact Spherical Tokamak Fusion Pilot Plant”. In: *Phil. Trans. R. Soc. A* 377.2141, p. 20170439. ISSN: 1364-503X, 1471-2962. DOI:

- 10.1098/rsta.2017.0439. URL: <https://royalsocietypublishing.org/doi/10.1098/rsta.2017.0439> (visited on 07/22/2020).
- Costley, A.E., J. Hugill, and P.F. Buxton (Mar. 1, 2015). “On the Power and Size of Tokamak Fusion Pilot Plants and Reactors”. In: *Nucl. Fusion* 55.3, p. 033001. ISSN: 0029-5515, 1741-4326. DOI: 10.1088/0029-5515/55/3/033001. URL: <https://iopscience.iop.org/article/10.1088/0029-5515/55/3/033001> (visited on 07/16/2020).
- Crescenzi, F. *et al.* (Nov. 1, 2017). “ITER-like Divertor Target for DEMO: Design Study and Fabrication Test”. In: *Fusion Engineering and Design*. Proceedings of the 29th Symposium on Fusion Technology (SOFT-29) Prague, Czech Republic, September 5-9, 2016 124, pp. 432–436. ISSN: 0920-3796. DOI: 10.1016/j.fusengdes.2017.02.014. URL: <http://www.sciencedirect.com/science/article/pii/S0920379617300972> (visited on 12/03/2018).
- Crisanti, F. *et al.* (Aug. 1, 2017). “The Divertor Tokamak Test Facility Proposal: Physical Requirements and Reference Design”. In: *Nuclear Materials and Energy*. Proceedings of the 22nd International Conference on Plasma Surface Interactions 2016, 22nd PSI 12, pp. 1330–1335. ISSN: 2352-1791. DOI: 10.1016/j.nme.2017.05.008. URL: <https://www.sciencedirect.com/science/article/pii/S2352179116300813> (visited on 09/06/2021).
- Curzadd, Bailey *et al.* (May 8, 2019). “Topology Optimization of Tungsten/Copper Structures for Plasma-Facing Component Applications”. In: *Nucl. Fusion*. ISSN: 0029-5515, 1741-4326. DOI: 10.1088/1741-4326/ab1ff5. URL: <http://iopscience.iop.org/article/10.1088/1741-4326/ab1ff5> (visited on 05/20/2019).
- D’Onorio, Matteo *et al.* (June 2020). “Preliminary Safety Analysis of an In-Vessel LOCA for the EU-DEMO WCLL Blanket Concept”. In: *Fusion Engineering and Design* 155, p. 111560. ISSN: 09203796. DOI: 10.1016/j.fusengdes.2020.111560. URL: <https://linkinghub.elsevier.com/retrieve/pii/S0920379620301083> (visited on 12/31/2021).
- Damiani, C. *et al.* (Nov. 1, 2018). “Overview of the ITER Remote Maintenance Design and of the Development Activities in Europe”. In: *Fusion Engineering and Design*. Special Issue: Proceedings of the 13th International Symposium on Fusion Nuclear Technology (ISFNT-13) 136, pp. 1117–1124. ISSN: 0920-3796. DOI: 10.1016/j.fusengdes.2018.04.085. URL: <https://www.sciencedirect.com/science/article/pii/S0920379618303739> (visited on 09/19/2022).
- Dbouk, T. (Feb. 5, 2017). “A Review about the Engineering Design of Optimal Heat Transfer Systems Using Topology Optimization”. In: *Applied Thermal Engineering* 112, pp. 841–854. ISSN: 1359-4311. DOI: 10.1016/j.applthermaleng.2016.10.134. URL: <http://>

- [//www.sciencedirect.com/science/article/pii/S135943111632645X](http://www.sciencedirect.com/science/article/pii/S135943111632645X) (visited on 08/17/2018).
- De Meis, Domenico (Dec. 1, 2015). *RCC-MRx Design Code for Nuclear Components*.
- Deaton, Joshua David (2009). “A Dissertation Submitted in Partial Fulfillment of the Requirements for the Degree of Doctor of Philosophy”. In: p. 232.
- Dede, Ercan M (2009). “Multiphysics Topology Optimization of Heat Transfer and Fluid Flow Systems”. In: 2009, p. 7.
- (Aug. 29, 2012). “Optimization and Design of a Multipass Branching Microchannel Heat Sink for Electronics Cooling”. In: *Journal of Electronic Packaging* 134.4, p. 041001. ISSN: 1043-7398. DOI: 10.1115/1.4007159. URL: <http://electronicpackaging.asmedigitalcollection.asme.org/article.aspx?doi=10.1115/1.4007159> (visited on 04/10/2019).
- Dede, Ercan M., Shailesh N. Joshi, and Feng Zhou (Oct. 12, 2015). “Topology Optimization, Additive Layer Manufacturing, and Experimental Testing of an Air-Cooled Heat Sink”. In: *J. Mech. Des* 137.11, pp. 111403-111403–9. ISSN: 1050-0472. DOI: 10.1115/1.4030989. URL: <http://dx.doi.org/10.1115/1.4030989> (visited on 08/17/2018).
- Dede, Ercan M. and Yan Liu (June 1, 2013). “Experimental and Numerical Investigation of a Multi-Pass Branching Microchannel Heat Sink”. In: *Applied Thermal Engineering* 55.1, pp. 51–60. ISSN: 1359-4311. DOI: 10.1016/j.applthermaleng.2013.02.038. URL: <http://www.sciencedirect.com/science/article/pii/S135943111300152X> (visited on 03/04/2019).
- Dedov, A. V. (Mar. 2010). “Critical Heat Flowrates in Subcooled Flow Boiling”. In: *Therm. Eng.* 57.3, pp. 185–192. ISSN: 0040-6015, 1555-6301. DOI: 10.1134/S0040601510030018. URL: <http://link.springer.com/10.1134/S0040601510030018> (visited on 07/01/2020).
- Delaporte-Mathurin, Rémi *et al.* (Oct. 20, 2020). “Parametric Study of Hydrogenic Inventory in the ITER Divertor Based on Machine Learning”. In: *Sci Rep* 10.1 (1), p. 17798. ISSN: 2045-2322. DOI: 10.1038/s41598-020-74844-w. URL: <https://www.nature.com/articles/s41598-020-74844-w> (visited on 08/16/2022).
- Deng, Yongbo *et al.* (July 2011). “Topology Optimization of Unsteady Incompressible Navier–Stokes Flows”. In: *Journal of Computational Physics* 230.17, pp. 6688–6708. ISSN: 00219991. DOI: 10.1016/j.jcp.2011.05.004. URL: <https://linkinghub.elsevier.com/retrieve/pii/S0021999111003019> (visited on 04/01/2019).
- Denkevits, A. (Dec. 2010). “Hydrogen/Dust Explosion Hazard in ITER: Effect of Nitrogen Dilution on Explosion Behavior of Hydrogen/Tungsten Dust/Air Mixtures”. In: *Fusion Engineering and Design* 85.7-9, pp. 1059–1063. ISSN: 09203796. DOI: 10.1016/j.

- fusengdes.2010.01.009. URL: <https://linkinghub.elsevier.com/retrieve/pii/S0920379610000104> (visited on 04/12/2019).
- Di Maio, P.A. *et al.* (Nov. 2018). “On the Thermal-Hydraulic Optimization of DEMO Divertor Plasma Facing Components Cooling Circuit”. In: *Fusion Engineering and Design* 136, pp. 1438–1443. ISSN: 09203796. DOI: 10.1016/j.fusengdes.2018.05.032. URL: <https://linkinghub.elsevier.com/retrieve/pii/S0920379618304599> (visited on 09/19/2022).
- Diaz, Alejandro and Ole Sigmund (Aug. 1, 1995). “Checkerboard Patterns in Layout Optimization”. In: *Structural Optimization* 10, pp. 40–45. DOI: 10.1007/BF01743693.
- Dietz, K J *et al.* (1995a). “Engineering and Design Aspects Related to the Development of the ITER Divertor”. In: *Fusion Engineering and Design*, p. 13.
- Dietz, K. J. *et al.* (Sept. 1995b). “The ITER Divertor”. In: *Proceedings of 16th International Symposium on Fusion Engineering*. Proceedings of 16th International Symposium on Fusion Engineering. Vol. 1, 144–149 vol.1. DOI: 10.1109/FUSION.1995.534191.
- Dilgen, Cetin B. *et al.* (Apr. 1, 2018). “Topology Optimization of Turbulent Flows”. In: *Computer Methods in Applied Mechanics and Engineering* 331, pp. 363–393. ISSN: 0045-7825. DOI: 10.1016/j.cma.2017.11.029. URL: <http://www.sciencedirect.com/science/article/pii/S0045782517307478> (visited on 03/07/2019).
- Dilgen, Sumer B. *et al.* (May 1, 2018). “Density Based Topology Optimization of Turbulent Flow Heat Transfer Systems”. In: *Struct Multidisc Optim* 57.5, pp. 1905–1918. ISSN: 1615-1488. DOI: 10.1007/s00158-018-1967-6. URL: <https://doi.org/10.1007/s00158-018-1967-6> (visited on 03/07/2019).
- Dirker, Jaco and Josua P. Meyer (Sept. 23, 2013). “Topology Optimization for an Internal Heat-Conduction Cooling Scheme in a Square Domain for High Heat Flux Applications”. In: *J. Heat Transfer* 135.11, pp. 111010–111010–10. ISSN: 0022-1481. DOI: 10.1115/1.4024615. URL: <http://dx.doi.org/10.1115/1.4024615> (visited on 04/11/2019).
- Dolan, Thomas J. (Feb. 10, 2014). *Magnetic Fusion Technology*. Springer Science & Business Media. 816 pp. ISBN: 978-1-4471-5556-0.
- Domalapally, Phani Kumar and Slavomir Entler (Apr. 30, 2015). “COMPARISON OF COOLING SCHEMES FOR HIGH HEAT FLUX COMPONENTS COOLING IN FUSION REACTORS”. In: *Acta Polytech* 55.2, pp. 86–95. ISSN: 1805-2363, 1210-2709. DOI: 10.14311/AP.2015.55.0086. URL: <https://ojs.cvut.cz/ojs/index.php/ap/article/view/2203> (visited on 09/02/2020).
- Domptail, F. *et al.* (May 1, 2020). “The Design and Optimisation of a Monoblock Divertor Target for DEMO Using Thermal Break Interlayer”. In: *Fusion Engineering and Design* 154, p. 111497. ISSN: 0920-3796. DOI: 10.1016/j.fusengdes.2020.111497. URL:

- <https://www.sciencedirect.com/science/article/pii/S0920379620300454> (visited on 05/28/2021).
- Dong, Xin and Xiaomin Liu (Jan. 2, 2020). “Multi-Objective Optimal Design of Microchannel Cooling Heat Sink Using Topology Optimization Method”. In: *Numerical Heat Transfer, Part A: Applications* 77.1, pp. 90–104. ISSN: 1040-7782, 1521-0634. DOI: 10.1080/10407782.2019.1682872. URL: <https://www.tandfonline.com/doi/full/10.1080/10407782.2019.1682872> (visited on 10/29/2021).
- Donné, A. J. H. (Mar. 25, 2019). “The European Roadmap towards Fusion Electricity”. In: *Phil. Trans. R. Soc. A* 377.2141, p. 20170432. ISSN: 1364-503X, 1471-2962. DOI: 10.1098/rsta.2017.0432. URL: <https://royalsocietypublishing.org/doi/10.1098/rsta.2017.0432> (visited on 07/22/2020).
- Donnelly, Russell J. (1985). *Advances in Heat Transfer [17]*. Advances in Heat Transfer vol. 17. Orlando: Academic Press. ISBN: 978-0-12-020017-7.
- Dragojlovic, Zoran, Charles Kessel, *et al.* (2009). “An Advanced Computational Approach to System Modeling of Tokamak Power Plants”. In: 56, p. 6.
- Dragojlovic, Zoran, A Rene Raffray, *et al.* (2010). “An Advanced Computational Algorithm for Systems Analysis of Tokamak Power Plants”. In: *Fusion Engineering and Design*, p. 23.
- Dubus, Grégory Dominique (Oct. 2014). “From Plain Visualisation to Vibration Sensing: Using a Camera to Control the Flexibilities in the ITER Remote Handling Equipment”. In: p. 217.
- Entler, Slavomir *et al.* (June 2018). “Approximation of the Economy of Fusion Energy”. In: *Energy* 152, pp. 489–497. ISSN: 03605442. DOI: 10.1016/j.energy.2018.03.130. URL: <https://linkinghub.elsevier.com/retrieve/pii/S0360544218305395> (visited on 11/05/2020).
- Eschenauer, Hans A and Niels Olhoff (July 1, 2001). “Topology Optimization of Continuum Structures: A Review*”. In: *Appl. Mech. Rev* 54.4, pp. 331–390. ISSN: 0003-6900. DOI: 10.1115/1.1388075. URL: <http://dx.doi.org/10.1115/1.1388075> (visited on 08/15/2018).
- Escourbiac, F *et al.* (2012). “Effort on Design of a Full Tungsten Divertor for ITER”. In: p. 8.
- Escourbiac, F. *et al.* (Sept. 2019). “Assessment of Critical Heat Flux Margins on Tungsten Monoblocks of the ITER Divertor Vertical Targets”. In: *Fusion Engineering and Design* 146, pp. 2036–2039. ISSN: 09203796. DOI: 10.1016/j.fusengdes.2019.03.094. URL: <https://linkinghub.elsevier.com/retrieve/pii/S0920379619304168> (visited on 03/18/2021).

- Evans, Llion M, Triestino Minniti, and Tom Barrett (2019). “Virtual Qualification of Novel Heat Exchanger Components with the Image-Based Finite Element Method”. In: p. 10.
- Evgrafov, Anton (Oct. 2005). “The Limits of Porous Materials in the Topology Optimization of Stokes Flows”. In: *Applied Mathematics and Optimization* 52.3, pp. 263–277. ISSN: 0095-4616, 1432-0606. DOI: 10.1007/s00245-005-0828-z. URL: <http://link.springer.com/10.1007/s00245-005-0828-z> (visited on 04/02/2019).
- (Apr. 2015). “On Chebyshev’s Method for Topology Optimization of Stokes Flows”. In: *Structural and Multidisciplinary Optimization* 51.4, pp. 801–811. ISSN: 1615-147X, 1615-1488. DOI: 10.1007/s00158-014-1176-x. URL: <http://link.springer.com/10.1007/s00158-014-1176-x> (visited on 04/01/2019).
- Ezato, Koichiro *et al.* (Nov. 1, 2016). “Progress of ITER Full Tungsten Divertor Technology Qualification in Japan: Manufacturing Full-Scale Plasma-Facing Unit Prototypes”. In: *Fusion Engineering and Design*. Proceedings of the 12th International Symposium on Fusion Nuclear Technology-12 (ISFNT-12) 109–111, pp. 1256–1260. ISSN: 0920-3796. DOI: 10.1016/j.fusengdes.2015.12.049. URL: <https://www.sciencedirect.com/science/article/pii/S0920379615304336> (visited on 07/14/2021).
- Federici, G., C. Bachmann, L. Barucca, C. Baylard, *et al.* (June 1, 2019). “Overview of the DEMO Staged Design Approach in Europe”. In: *Nucl. Fusion* 59.6, p. 066013. ISSN: 0029-5515, 1741-4326. DOI: 10.1088/1741-4326/ab1178. URL: <https://iopscience.iop.org/article/10.1088/1741-4326/ab1178> (visited on 07/22/2020).
- Federici, G., C. Bachmann, L. Barucca, W. Biel, *et al.* (Nov. 2018). “DEMO Design Activity in Europe: Progress and Updates”. In: *Fusion Engineering and Design* 136, pp. 729–741. ISSN: 09203796. DOI: 10.1016/j.fusengdes.2018.04.001. URL: <https://linkinghub.elsevier.com/retrieve/pii/S0920379618302898> (visited on 07/22/2020).
- Federici, G., W. Biel, *et al.* (Sept. 1, 2017). “European DEMO Design Strategy and Consequences for Materials”. In: *Nucl. Fusion* 57.9, p. 092002. ISSN: 0029-5515, 1741-4326. DOI: 10.1088/1741-4326/57/9/092002. URL: <https://iopscience.iop.org/article/10.1088/1741-4326/57/9/092002> (visited on 12/22/2021).
- Federici, G., G. Giruzzi, *et al.* (June 2013). “EU DEMO Design and R D Studies”. In: *2013 IEEE 25th Symposium on Fusion Engineering (SOFE)*. 2013 IEEE 25th Symposium on Fusion Engineering (SOFE), pp. 1–8. DOI: 10.1109/SOFE.2013.6635288.
- Fetton, F. *et al.* (Jan. 8, 2019). “Shape Optimization of a Coupled Thermal Fluid–Structure Problem in a Level Set Mesh Evolution Framework”. In: *SeMA Journal*. ISSN: 2254-3902, 2281-7875. DOI: 10.1007/s40324-018-00185-4. URL: <http://link.springer.com/10.1007/s40324-018-00185-4> (visited on 03/19/2019).

- Ferrari, M. *et al.* (Oct. 2001). “Evaluation of Divertor Conceptual Designs for a Fusion Power Plant”. In: *Fusion Engineering and Design* 56–57, pp. 255–259. ISSN: 09203796. DOI: 10.1016/S0920-3796(01)00296-4. URL: <https://linkinghub.elsevier.com/retrieve/pii/S0920379601002964> (visited on 02/01/2021).
- Flanagan, George *et al.* (Dec. 2010). “Safety Issues and Approach to Meet the Safety Requirements in the Tokamak Cooling Water System of ITER”. In: *Fusion Engineering and Design* 85.10-12, pp. 1847–1851. ISSN: 09203796. DOI: 10.1016/j.fusengdes.2010.06.011. URL: <https://linkinghub.elsevier.com/retrieve/pii/S092037961000267X> (visited on 08/27/2020).
- Fujieda, Hirobumi, Yoshiki Murakami, and Sugihara Masayoshi (1992). *Tokamak Plasma Power Balance Calculation Code*. URL: https://inis.iaea.org/collection/NCLCollectionStore/_Public/24/055/24055724.pdf?r=1 (visited on 12/01/2020).
- Funke, S. W. and P. E. Farrell (Feb. 15, 2013). “A Framework for Automated PDE-constrained Optimisation”. arXiv: 1302.3894 [cs]. URL: <http://arxiv.org/abs/1302.3894> (visited on 05/10/2019).
- Fursdon, M (2017). “The Development and Testing of the Thermal Break Divertor Monoblock Target Design Delivering 20 MW/M² Heat Load Capability”. In: *Phys. Scr. T*, p. 8.
- Fursdon, M., J. H. You, *et al.* (Oct. 1, 2018). “A Hybrid Analysis Procedure Enabling Elastic Design Rule Assessment of Monoblock-Type Divertor Components”. In: *Fusion Engineering and Design* 135, pp. 154–164. ISSN: 0920-3796. DOI: 10.1016/j.fusengdes.2018.07.014. URL: <http://www.sciencedirect.com/science/article/pii/S0920379618305696> (visited on 02/18/2019).
- Fursdon, M., J.-H. You, and M. Li (Oct. 2019). “Towards Reliable Design-by-Analysis for Divertor Plasma Facing Components – Guidelines for Inelastic Assessment (Part 1: Unirradiated)”. In: *Fusion Engineering and Design* 147, p. 111234. ISSN: 09203796. DOI: 10.1016/j.fusengdes.2019.06.007. URL: <https://linkinghub.elsevier.com/retrieve/pii/S0920379619307124> (visited on 02/04/2021).
- Galatanu, Magdalena *et al.* (Sept. 2019). “Development of W-monoblock Divertor Components with Embedded Thermal Barrier Interfaces”. In: *Fusion Engineering and Design* 146, pp. 1351–1354. ISSN: 09203796. DOI: 10.1016/j.fusengdes.2019.02.074. URL: <https://linkinghub.elsevier.com/retrieve/pii/S0920379619302480> (visited on 07/22/2020).
- Gao, T. *et al.* (Oct. 2008). “Topology Optimization of Heat Conduction Problem Involving Design-Dependent Heat Load Effect”. In: *Finite Elements in Analysis and Design* 44.14, pp. 805–813. ISSN: 0168874X. DOI: 10.1016/j.finel.2008.06.001. URL: <https://doi.org/10.1016/j.finel.2008.06.001>

- [//linkinghub.elsevier.com/retrieve/pii/S0168874X08000905](https://linkinghub.elsevier.com/retrieve/pii/S0168874X08000905) (visited on 04/11/2019).
- Garrett, Grant and Justin Watson (Apr. 2019). “Comparison of Water, Helium, and Carbon Dioxide as Coolants for next Generation Power Plants Using TRACE”. In: *Annals of Nuclear Energy* 126, pp. 292–302. ISSN: 03064549. DOI: 10.1016/j.anucene.2018.11.016. URL: <https://linkinghub.elsevier.com/retrieve/pii/S0306454918306157> (visited on 07/22/2020).
- Gersborg-Hansen, A., O. Sigmund, and R.B. Haber (Sept. 1, 2005). “Topology Optimization of Channel Flow Problems”. In: *Struct Multidisc Optim* 30.3, pp. 181–192. ISSN: 1615-1488. DOI: 10.1007/s00158-004-0508-7. URL: <https://doi.org/10.1007/s00158-004-0508-7> (visited on 01/17/2019).
- Gersborg-Hansen, Allan (2003). “Topology Optimization of Incompressible Newtonian Flows at Moderate Reynolds Numbers”. In: p. 123.
- Ghasemi, A and A Elham (2019). “FLOW TOPOLOGY OPTIMIZATION IN PERIODIC DOMAINS WITH APPLICATION TO MICRO HEAT EXCHANGER OPTIMIZATION”. In: *COUPLED PROBLEMS 2019*. VIII International Conference on Computational Methods for Coupled Problems in Science and Engineering, p. 12.
- Giancarli, L. *et al.* (Nov. 2005). “Conceptual Design of a High Temperature Water-Cooled Divertor for a Fusion Power Reactor”. In: *Fusion Engineering and Design* 75–79, pp. 383–386. ISSN: 09203796. DOI: 10.1016/j.fusengdes.2005.06.282. URL: <https://linkinghub.elsevier.com/retrieve/pii/S0920379605001110> (visited on 10/28/2020).
- Gilbert, M.R. *et al.* (Nov. 2018). “Waste Assessment of European DEMO Fusion Reactor Designs”. In: *Fusion Engineering and Design* 136, pp. 42–48. ISSN: 09203796. DOI: 10.1016/j.fusengdes.2017.12.019. URL: <https://linkinghub.elsevier.com/retrieve/pii/S0920379617309717> (visited on 07/22/2020).
- Girtan, Mihaela *et al.* (Apr. 7, 2021). “The Critical Raw Materials Issue between Scarcity, Supply Risk, and Unique Properties”. In: *Materials* 14, p. 1826. DOI: 10.3390/ma14081826.
- Giruzzi, G. *et al.* (July 1, 2015). “Modelling of Pulsed and Steady-State DEMO Scenarios”. In: *Nucl. Fusion* 55.7, p. 073002. ISSN: 0029-5515, 1741-4326. DOI: 10.1088/0029-5515/55/7/073002. URL: <https://iopscience.iop.org/article/10.1088/0029-5515/55/7/073002> (visited on 10/21/2020).
- Gliss, Curt *et al.* (Nov. 2018). “Initial Layout of DEMO Buildings and Configuration of the Main Plant Systems”. In: *Fusion Engineering and Design* 136, pp. 534–539. ISSN: 09203796. DOI: 10.1016/j.fusengdes.2018.02.101. URL: <https://linkinghub.elsevier.com/retrieve/pii/S0920379618302072> (visited on 07/22/2020).

- Gonzalez, J.M. *et al.* (Oct. 2018). “Numerical Analysis of the Manufacturing Processes of a Mock-up of the ITER NHF First Wall Panel”. In: *Fusion Engineering and Design* 135, pp. 65–73. ISSN: 09203796. DOI: 10.1016/j.fusengdes.2018.07.012. URL: <https://linkinghub.elsevier.com/retrieve/pii/S0920379618305672> (visited on 06/03/2019).
- Gorley, M. J. (June 2015). “Critical Assessment 12: Prospects for Reduced Activation Steel for Fusion Plant”. In: *Materials Science and Technology* 31.8, pp. 975–980. ISSN: 0267-0836, 1743-2847. DOI: 10.1179/1743284714Y.0000000732. URL: <http://www.tandfonline.com/doi/full/10.1179/1743284714Y.0000000732> (visited on 02/18/2019).
- Greuner, Henri *et al.* (Sept. 2019). “Progress in High Heat Flux Testing of European DEMO Divertor Mock-Ups”. In: *Fusion Engineering and Design* 146, pp. 216–219. ISSN: 09203796. DOI: 10.1016/j.fusengdes.2018.12.021. URL: <https://linkinghub.elsevier.com/retrieve/pii/S0920379618307865> (visited on 09/30/2021).
- El-Guebaly, L (July 2007). “Evaluation of Disposal, Recycling and Clearance Scenarios for Managing ARIES Radwaste after Plant Decommissioning”. In: *Nucl. Fusion* 47.7, S485–S488. ISSN: 0029-5515, 1741-4326. DOI: 10.1088/0029-5515/47/7/S13. URL: <https://iopscience.iop.org/article/10.1088/0029-5515/47/7/S13> (visited on 06/21/2021).
- Guest, James K. and Jean H. Prévost (Apr. 16, 2006). “Topology Optimization of Creeping Fluid Flows Using a Darcy–Stokes Finite Element”. In: *International Journal for Numerical Methods in Engineering* 66.3, pp. 461–484. ISSN: 0029-5981, 1097-0207. DOI: 10.1002/nme.1560. URL: <http://doi.wiley.com/10.1002/nme.1560> (visited on 04/02/2019).
- Guillaume, Ph. and K. Sid Idris (Jan. 2004). “Topological Sensitivity and Shape Optimization for the Stokes Equations”. In: *SIAM Journal on Control and Optimization* 43.1, pp. 1–31. ISSN: 0363-0129, 1095-7138. DOI: 10.1137/S0363012902411210. URL: <http://epubs.siam.org/doi/10.1137/S0363012902411210> (visited on 04/01/2019).
- Gulden, W, J Raeder, and I Cook (Nov. 1, 2000). “SEAFP and SEAL: Safety and Environmental Aspects”. In: *Fusion Engineering and Design* 51–52, pp. 429–434. ISSN: 0920-3796. DOI: 10.1016/S0920-3796(00)00291-X. URL: <https://www.sciencedirect.com/science/article/pii/S092037960000291X> (visited on 07/06/2021).
- Gunn, J. P. *et al.* (June 1, 2021). “Thermal Loads in Gaps between ITER Divertor Monoblocks: First Lessons Learnt from WEST”. In: *Nuclear Materials and Energy* 27, p. 100920. ISSN: 2352-1791. DOI: 10.1016/j.nme.2021.100920. URL: <https://www.sciencedirect.com/science/article/pii/S235217912100017X> (visited on 05/20/2021).

- Gunn, J.P., S. Carpentier-Chouchana, *et al.* (Apr. 1, 2017). “Surface Heat Loads on the ITER Divertor Vertical Targets”. In: *Nuclear Fusion* 57.4, p. 046025. ISSN: 0029-5515, 1741-4326. DOI: 10.1088/1741-4326/aa5e2a. URL: <http://stacks.iop.org/0029-5515/57/i=4/a=046025?key=crossref.7d2d648448285fd3240c9cb62a9d3834> (visited on 04/23/2019).
- Gunn, J.P., T. Hirai, *et al.* (Dec. 1, 2019). “A Study of Planar Toroidal–Poloidal Beveling of Monoblocks on the ITER Divertor Outer Vertical Target”. In: *Nucl. Fusion* 59.12, p. 126043. ISSN: 0029-5515, 1741-4326. DOI: 10.1088/1741-4326/ab4071. URL: <https://iopscience.iop.org/article/10.1088/1741-4326/ab4071> (visited on 05/11/2021).
- Haertel, J H K *et al.* (2015). “Topology Optimization of Thermal Heat Sinks”. In: p. 7.
- Haertel, Jan H. K., Kurt Engelbrecht, *et al.* (June 1, 2018). “Topology Optimization of a Pseudo 3D Thermofluid Heat Sink Model”. In: *International Journal of Heat and Mass Transfer* 121, pp. 1073–1088. ISSN: 0017-9310. DOI: 10.1016/j.ijheatmasstransfer.2018.01.078. URL: <http://www.sciencedirect.com/science/article/pii/S0017931017337146> (visited on 09/20/2018).
- Haertel, Jan H. K. and Gregory F. Nellis (June 5, 2017). “A Fully Developed Flow Thermofluid Model for Topology Optimization of 3D-printed Air-Cooled Heat Exchangers”. In: *Applied Thermal Engineering* 119, pp. 10–24. ISSN: 1359-4311. DOI: 10.1016/j.applthermaleng.2017.03.030. URL: <http://www.sciencedirect.com/science/article/pii/S1359431116320129> (visited on 09/18/2018).
- Hahn, T. A. *et al.* (1972). “Thermal Expansion of Platinum from 293 to 1900 K”. In: PROCEEDINGS OF THE 1971 THERMAL EXPANSION SYMPOSIUM. Corning, New York (USA), pp. 87–95. DOI: 10.1063/1.2948578. URL: <http://aip.scitation.org/doi/abs/10.1063/1.2948578> (visited on 04/24/2020).
- Hancock, David, Tom Barrett, *et al.* (Oct. 1, 2015). “Testing Candidate Interlayers for an Enhanced Water-Cooled Divertor Target”. In: *Fusion Engineering and Design*. Proceedings of the 28th Symposium On Fusion Technology (SOFT-28) 98–99, pp. 1323–1327. ISSN: 0920-3796. DOI: 10.1016/j.fusengdes.2014.12.026. URL: <http://www.sciencedirect.com/science/article/pii/S092037961400670X> (visited on 07/31/2018).
- Hancock, David, David Homfray, *et al.* (Mar. 2018). “Exploring Complex High Heat Flux Geometries for Fusion Applications Enabled by Additive Manufacturing”. In: *Fusion Engineering and Design*. ISSN: 09203796. DOI: 10.1016/j.fusengdes.2018.02.097. URL: <http://linkinghub.elsevier.com/retrieve/pii/S0920379618302060> (visited on 07/30/2018).

- Hartmann, Tobias (Apr. 4, 2013). “Development of a Modular Systems Code to Analyse the Implications of Physics Assumptions on the Design of a Demonstration Fusion Power Plant”.
- Hassanein, A. and V. Sizyuk (Dec. 2021). “Potential Design Problems for ITER Fusion Device”. In: *Sci Rep* 11.1, p. 2069. ISSN: 2045-2322. DOI: 10.1038/s41598-021-81510-2. URL: <http://www.nature.com/articles/s41598-021-81510-2> (visited on 09/01/2021).
- Hawryluk, R.J. *et al.* (June 2009). “Principal Physics Developments Evaluated in the ITER Design Review”. In: *Nucl. Fusion* 49.6, p. 065012. ISSN: 0029-5515, 1741-4326. DOI: 10.1088/0029-5515/49/6/065012. URL: <https://iopscience.iop.org/article/10.1088/0029-5515/49/6/065012> (visited on 11/26/2020).
- Hermesmeyer, S. and K. Kleefeldt (2001). *Review and Comparative Assessment of Helium-Cooled Divertor Concepts*. FZKA-6597. Forschungszentrum Karlsruhe GmbH Technik und Umwelt (Germany). Inst. fuer Kern- und Energietechnik, Forschungszentrum Karlsruhe GmbH Technik und Umwelt (Germany). Programm Kernfusion. URL: http://inis.iaea.org/Search/search.aspx?orig_q=RN:33022363 (visited on 07/10/2018).
- Herrero, D, J Martinez, and P Martı (2013). “An Implementation of Level Set Based Topology Optimization Using GPU”. In: p. 10.
- Herzog, Dirk *et al.* (Sept. 2016). “Additive Manufacturing of Metals”. In: *Acta Materialia* 117, pp. 371–392. ISSN: 13596454. DOI: 10.1016/j.actamat.2016.07.019. URL: <https://linkinghub.elsevier.com/retrieve/pii/S1359645416305158> (visited on 04/25/2019).
- Hirai, T, F Escourbiac, *et al.* (Apr. 1, 2014). “ITER Full Tungsten Divertor Qualification Program and Progress”. In: *Physica Scripta* T159, p. 014006. ISSN: 0031-8949, 1402-4896. DOI: 10.1088/0031-8949/2014/T159/014006. URL: <http://stacks.iop.org/1402-4896/2014/i=T159/a=014006?key=crossref.6f7d54d38161f36950e1ee1e84d0345b> (visited on 04/13/2019).
- Hirai, T, S Panayotis, *et al.* (2016). “Use of Tungsten Material for the ITER Divertor”. In: *Nuclear Materials and Energy* 9 (Supplement C), pp. 616–622. DOI: 10.1016/j.nme.2016.07.003. URL: <internal-pdf://0512817531/1-s2.0-S2352179115301046-main.pdf>.
- Hirai, T, G Pintsuk, *et al.* (2009). “Cracking Failure Study of ITER-reference Tungsten Grade under Single Pulse Thermal Shock Loads at Elevated Temperatures”. In: *Journal of Nuclear Materials* 390 (Supplement C), pp. 751–754. DOI: 10.1016/j.jnucmat.2009.

- 01.313. URL: internal-pdf://116.185.216.22/1-s2.0-S002231150900227X-main.pdf.
- Hiraoka, Yutaka *et al.* (2005). “Ductile-to-Brittle Transition Characteristics in W–Cu Composites with Increase of Cu Content”. In: *Mater. Trans.* 46.7, pp. 1663–1670. ISSN: 1345-9678, 1347-5320. DOI: 10.2320/matertrans.46.1663. URL: https://www.jstage.jst.go.jp/article/matertrans/46/7/46_7_1663/_article (visited on 05/13/2021).
- Hirooka, Y. *et al.* (Oct. 2015). “A Review of the Present Status and Future Prospects of the Application of Liquid Metals for Plasma-Facing Components in Magnetic Fusion Devices”. In: *Fusion Science and Technology* 68.3, pp. 477–483. ISSN: 1536-1055, 1943-7641. DOI: 10.13182/FST15-125. URL: <https://www.tandfonline.com/doi/full/10.13182/FST15-125> (visited on 12/14/2021).
- Hiwatari, R *et al.* (Jan. 2004). “Generation of Net Electric Power with a Tokamak Reactor under Foreseeable Physical and Engineering Conditions”. In: *Nucl. Fusion* 44.1, pp. 106–116. ISSN: 0029-5515, 1741-4326. DOI: 10.1088/0029-5515/44/1/013. URL: <https://iopscience.iop.org/article/10.1088/0029-5515/44/1/013> (visited on 07/01/2021).
- Hu, DingHua, ZhiWei Zhang, and Qiang Li (Jan. 2020). “Numerical Study on Flow and Heat Transfer Characteristics of Microchannel Designed Using Topological Optimizations Method”. In: *Sci. China Technol. Sci.* 63.1, pp. 105–115. ISSN: 1674-7321, 1869-1900. DOI: 10.1007/s11431-019-1438-8. URL: <http://link.springer.com/10.1007/s11431-019-1438-8> (visited on 10/29/2021).
- IAEA Selects Winner of Net Zero Challenge on Policies for Clean Energy Transition (Sept. 20, 2021). URL: <https://www.iaea.org/newscenter/news/iaea-selects-winner-of-net-zero-challenge-on-policies-for-clean-energy-transition> (visited on 01/06/2022).
- Ihli, T. *et al.* (Nov. 2005). “An Advanced He-cooled Divertor Concept: Design, Cooling Technology, and Thermohydraulic Analyses with CFD”. In: *Fusion Engineering and Design* 75–79, pp. 371–375. ISSN: 09203796. DOI: 10.1016/j.fusengdes.2005.06.069. URL: <https://linkinghub.elsevier.com/retrieve/pii/S0920379605001808> (visited on 07/16/2020).
- Ikeda, Kaname (Jan. 2010). “ITER on the Road to Fusion Energy”. In: *Nucl. Fusion* 50.1, p. 014002. ISSN: 0029-5515, 1741-4326. DOI: 10.1088/0029-5515/50/1/014002. URL: <https://iopscience.iop.org/article/10.1088/0029-5515/50/1/014002> (visited on 08/15/2022).

- Ikonen, Teemu J. *et al.* (Nov. 2018). “Topology Optimization of Conductive Heat Transfer Problems Using Parametric L-systems”. In: *Structural and Multidisciplinary Optimization* 58.5, pp. 1899–1916. ISSN: 1615-147X, 1615-1488. DOI: 10.1007/s00158-018-2055-7. URL: <http://link.springer.com/10.1007/s00158-018-2055-7> (visited on 03/21/2019).
- Im, Kihak, Sungjin Kwon, and Jong Sung Park (Oct. 2016). “A Preliminary Development of the K-DEMO Divertor Concept”. In: *IEEE Transactions on Plasma Science* 44.10, pp. 2493–2501. ISSN: 1939-9375. DOI: 10.1109/TPS.2016.2604408.
- ITER (2021). *ITER Members*. ITER. URL: <http://www.iter.org/proj/countries> (visited on 09/06/2021).
- Ivanov, A.D. *et al.* (Dec. 2002). “Effect of Heat Treatments on the Properties of CuCrZr Alloys”. In: *Journal of Nuclear Materials* 307–311, pp. 673–676. ISSN: 00223115. DOI: 10.1016/S0022-3115(02)01110-8. URL: <https://linkinghub.elsevier.com/retrieve/pii/S0022311502011108> (visited on 06/07/2019).
- Jahan, Suchana *et al.* (2019). “Thermo-Fluid Topology Optimization and Experimental Study of Conformal Cooling Channels for 3D Printed Plastic Injection Molds”. In: *Procedia Manufacturing* 34, pp. 631–639. ISSN: 23519789. DOI: 10.1016/j.promfg.2019.06.120. URL: <https://linkinghub.elsevier.com/retrieve/pii/S2351978919308480> (visited on 10/28/2021).
- Janeschitz, G. (Mar. 25, 2019). “An Economical Viable Tokamak Fusion Reactor Based on the ITER Experience”. In: *Phil. Trans. R. Soc. A* 377.2141, p. 20170433. ISSN: 1364-503X, 1471-2962. DOI: 10.1098/rsta.2017.0433. URL: <https://royalsocietypublishing.org/doi/10.1098/rsta.2017.0433> (visited on 07/22/2020).
- Jean, Johner (Feb. 2011). “HELIOS: A Zero-Dimensional Tool for Next Step and Reactor Studies”. In: *Fusion Science and Technology* 59.2, pp. 308–349. ISSN: 1536-1055, 1943-7641. DOI: 10.13182/FST11-A11650. URL: <https://www.tandfonline.com/doi/full/10.13182/FST11-A11650> (visited on 11/24/2020).
- Jenkins, Nicholas and Kurt Maute (July 2015). “Level Set Topology Optimization of Stationary Fluid-Structure Interaction Problems”. In: *Structural and Multidisciplinary Optimization* 52.1, pp. 179–195. ISSN: 1615-147X, 1615-1488. DOI: 10.1007/s00158-015-1229-9. URL: <http://link.springer.com/10.1007/s00158-015-1229-9> (visited on 04/11/2019).
- Jensen, Kristian Ejlebjerg (2018). “Solving 2D/3D Heat Conduction Problems by Combining Topology Optimization and Anisotropic Mesh Adaptation”. In: *Advances in Structural and Multidisciplinary Optimization*. Ed. by Axel Schumacher *et al.* Springer International Publishing, pp. 1224–1238. ISBN: 978-3-319-67988-4.

- K, Sai Nithin Reddy *et al.* (Aug. 21, 2016). “Topology Optimization Software for Additive Manufacturing: A Review of Current Capabilities and a Real-World Example”. In: ASME 2016 International Design Engineering Technical Conferences and Computers and Information in Engineering Conference. American Society of Mechanical Engineers, V02AT03A029–V02AT03A029. DOI: 10.1115/DETC2016-59718. URL: <https://proceedings.asmedigitalcollection.asme.org/proceeding.aspx?articleid=2591597> (visited on 03/07/2019).
- Kalsey, M. and M. Porton (July 7, 2014). “Developing Structural Design Criteria for Fusion Reactor In-Vessel Components”. In: *Volume 6: Nuclear Education, Public Acceptance and Related Issues; Instrumentation and Controls (I&C); Fusion Engineering; Beyond Design Basis Events*. 2014 22nd International Conference on Nuclear Engineering. Prague, Czech Republic: American Society of Mechanical Engineers, V006T14A008. ISBN: 978-0-7918-4596-7. DOI: 10.1115/ICONE22-31216. URL: <https://asmedigitalcollection.asme.org/ICONE/proceedings/ICONE22/45967/Prague,%20Czech%20Republic/250772> (visited on 01/05/2021).
- Kang, Ziliang and Kai A. James (Mar. 9, 2019). “Multimaterial Topology Design for Optimal Elastic and Thermal Response with Material-specific Temperature Constraints”. In: *International Journal for Numerical Methods in Engineering* 117.10, pp. 1019–1037. ISSN: 0029-5981, 1097-0207. DOI: 10.1002/nme.5989. URL: <https://onlinelibrary.wiley.com/doi/abs/10.1002/nme.5989> (visited on 03/21/2019).
- Karditsas, P. J. and M.-J. Baptiste (1995). *Thermal and Structural Properties of Fusion Related Materials*. UKAEA-FUS-294. UKAEA Government Division. URL: http://inis.iaea.org/Search/search.aspx?orig_q=RN:26078864 (visited on 06/02/2021).
- Katoh, Y *et al.* (2018). *Advanced Manufacturing for Fusion PFC and Blanket Materials*. URL: https://www.burningplasma.org/activities/uploads_tec/FESAC_TEC_White_Paper_AM-Rev20170614.pdf (visited on 07/27/2018).
- Kembleton, R., G. Federici, *et al.* (Sept. 2019). “Engineering and Integration Risks Arising from Advanced Magnetic Divertor Configurations”. In: *Fusion Engineering and Design* 146, pp. 2281–2284. ISSN: 09203796. DOI: 10.1016/j.fusengdes.2019.03.172. URL: <https://linkinghub.elsevier.com/retrieve/pii/S0920379619305058> (visited on 07/22/2020).
- Kembleton, R., A. W. Morris, *et al.* (June 2020). “Design Issues for Fusion Commercialization”. In: *IEEE Transactions on Plasma Science* 48.6, pp. 1703–1707. ISSN: 1939-9375. DOI: 10.1109/TPS.2020.2967889.

- Kemp, R, M Nakamura, *et al.* (2012). “Benchmarking Reactor Systems Studies by Comparison of EU and Japanese System Code Results for Different DEMO Concepts”. In: p. 8.
- Kemp, R, D J Ward, *et al.* (2014). “DEMO Design Point Studies”. In: p. 8.
- Kerkhof, S. Van den *et al.* (Mar. 2021). “Optimized Design of a Tungsten–Copper Functionally Graded Material Monoblock for Minimal von Mises Stress Meeting the Material Operational Temperature Window”. In: *Nucl. Fusion* 61.4, p. 046050. ISSN: 0029-5515. DOI: 10.1088/1741-4326/abe7bb. URL: <https://doi.org/10.1088/1741-4326/abe7bb> (visited on 05/12/2021).
- Kikuchi, Mitsuru (Nov. 10, 2010). “A Review of Fusion and Tokamak Research Towards Steady-State Operation: A JAEA Contribution”. In: *Energies* 3.11, pp. 1741–1789. ISSN: 1996-1073. DOI: 10.3390/en3111741. URL: <http://www.mdpi.com/1996-1073/3/11/1741> (visited on 07/20/2018).
- Kirby, R K (1991). “Platinum, a Thermal Expansion Reference Material”. In: p. 7.
- Knaster, J. *et al.* (Oct. 1, 2017). “Overview of the IFMIF/EVEDA Project”. In: *Nucl. Fusion* 57.10, p. 102016. ISSN: 0029-5515, 1741-4326. DOI: 10.1088/1741-4326/aa6a6a. URL: <https://iopscience.iop.org/article/10.1088/1741-4326/aa6a6a> (visited on 09/07/2021).
- Kobayashi, Hiroki *et al.* (Oct. 2019). “Freeform Winglet Design of Fin-and-Tube Heat Exchangers Guided by Topology Optimization”. In: *Applied Thermal Engineering* 161, p. 114020. ISSN: 13594311. DOI: 10.1016/j.applthermaleng.2019.114020. URL: <https://linkinghub.elsevier.com/retrieve/pii/S1359431118377135> (visited on 10/28/2021).
- Koga, Adriano A. *et al.* (Sept. 2013). “Development of Heat Sink Device by Using Topology Optimization”. In: *International Journal of Heat and Mass Transfer* 64, pp. 759–772. ISSN: 00179310. DOI: 10.1016/j.ijheatmasstransfer.2013.05.007. URL: <https://linkinghub.elsevier.com/retrieve/pii/S0017931013003979> (visited on 02/11/2019).
- Kontoleonos, E. A. *et al.* (Aug. 1, 2013). “Adjoint-Based Constrained Topology Optimization for Viscous Flows, Including Heat Transfer”. In: *Engineering Optimization* 45.8, pp. 941–961. ISSN: 0305-215X. DOI: 10.1080/0305215X.2012.717074. URL: <https://doi.org/10.1080/0305215X.2012.717074> (visited on 10/28/2021).
- Kovari, M., F. Fox, *et al.* (Mar. 2016). ““PROCESS”: A Systems Code for Fusion Power Plants – Part 2: Engineering”. In: *Fusion Engineering and Design* 104, pp. 9–20. ISSN: 09203796. DOI: 10.1016/j.fusengdes.2016.01.007. URL: <https://linkinghub.elsevier.com/retrieve/pii/S0920379616300072> (visited on 09/23/2020).

- Kovari, M., R. Kemp, *et al.* (Dec. 1, 2014). ““PROCESS”: A Systems Code for Fusion Power Plants—Part 1: Physics”. In: *Fusion Engineering and Design* 89.12, pp. 3054–3069. ISSN: 0920-3796. DOI: 10 . 1016 / j . fusengdes . 2014 . 09 . 018. URL: <http://www.sciencedirect.com/science/article/pii/S0920379614005961> (visited on 09/22/2020).
- Kreissl, S., G. Pingen, and K. Maute (2011). “Topology Optimization for Unsteady Flow”. In: *International Journal for Numerical Methods in Engineering* 87.13, pp. 1229–1253. DOI: 10 . 1002/nme . 3151.
- krishna, S. Chenna *et al.* (Dec. 30, 2012). “Thermal Conductivity of Cu-Cr-Zr-Ti Alloy in the Temperature Range of 300–873 K”. In: *ISRN Metallurgy* 2012. DOI: 10 . 5402/2012/580659.
- Kurihara, Ryoichi (Nov. 2002). “Thermofluid Analysis of Free Surface Liquid Divertor in Tokamak Fusion Reactor”. In: *Fusion Engineering and Design* 61–62, pp. 209–216. ISSN: 09203796. DOI: 10 . 1016 / S0920 - 3796 (02) 00171 - 0. URL: <https://linkinghub.elsevier.com/retrieve/pii/S0920379602001710> (visited on 08/26/2021).
- Kwon, Sungjin, Kihak Im, and Jong Sung Park (Nov. 17, 2017). “Thermohydraulic Assessment for the Modified Concept of the K-DEMO Divertor Target”. In: *Fusion Science and Technology* 72.4, pp. 737–746. ISSN: 1536-1055, 1943-7641. DOI: 10 . 1080 / 15361055 . 2017 . 1350479. URL: <https://www.tandfonline.com/doi/full/10.1080/15361055.2017.1350479> (visited on 09/06/2021).
- (Sept. 2018). “Thermo-Hydraulic Optimization Study for a High Heat Flux Unit of the K-DEMO Divertor Target”. In: *Fusion Engineering and Design* 134, pp. 68–73. ISSN: 09203796. DOI: 10 . 1016 / j . fusengdes . 2018 . 06 . 012. URL: <https://linkinghub.elsevier.com/retrieve/pii/S0920379618305325> (visited on 06/03/2019).
- Kwon, Sungjin, Hong-Tack Kim, *et al.* (Aug. 9, 2021). “CFD Analyses for the Upgrade Divertor System of KSTAR”. In: *Fusion Science and Technology*, pp. 1–11. ISSN: 1536-1055, 1943-7641. DOI: 10 . 1080 / 15361055 . 2021 . 1918960. URL: <https://www.tandfonline.com/doi/full/10.1080/15361055.2021.1918960> (visited on 10/30/2021).
- L. Castro Gómez, Laura (Feb. 20, 2019). “Introductory Chapter: Heat Exchangers”. In: *Advances in Heat Exchangers*. Ed. by Laura Castro Gómez and Víctor Manuel Velázquez Flores. IntechOpen. ISBN: 978-1-78985-073-4. DOI: 10 . 5772 / intechopen . 83376. URL: <https://www.intechopen.com/books/advances-in-heat-exchangers/introductory-chapter-heat-exchangers> (visited on 10/04/2021).
- Lange, F *et al.* (Nov. 2018). “Numerical Optimization of Active Heat Sinks Considering Restrictions of Selective Laser Melting”. In: p. 8.

- Laniewski-Wollk, L. and J. Rokicki (Feb. 2016). “Adjoint Lattice Boltzmann for Topology Optimization on Multi-GPU Architecture”. In: *Computers & Mathematics with Applications* 71.3, pp. 833–848. ISSN: 08981221. DOI: 10.1016/j.camwa.2015.12.043. URL: <https://linkinghub.elsevier.com/retrieve/pii/S0898122115006215> (visited on 10/28/2021).
- Larsson, Robin (2016). “Methodology for Topology and Shape Optimization: Application to a Rear Lower Control Arm”. In: p. 53.
- Lawson, J. D. (1955). *Some Criteria for a Useful Thermonuclear Reactor*. Technical report. Harwell, Berkshire, UK: Atomic Energy Research Establishment. URL: https://www.euro-fusion.org/fileadmin/user_upload/Archive/wp-content/uploads/2012/10/dec05-aere-gpr1807.pdf (visited on 12/22/2021).
- Lazarov, B. S. and O. Sigmund (2011). “Filters in Topology Optimization Based on Helmholtz-type Differential Equations”. In: *International Journal for Numerical Methods in Engineering* 86.6, pp. 765–781. ISSN: 1097-0207. DOI: 10.1002/nme.3072. URL: <https://onlinelibrary.wiley.com/doi/abs/10.1002/nme.3072> (visited on 07/01/2021).
- Lee, D. S. *et al.* (Nov. 17, 2019). “Thermal Hydraulics of Helium-Cooled Finger-Type Divertors at Higher Incident Heat Fluxes”. In: *Fusion Science and Technology* 75.8, pp. 873–878. ISSN: 1536-1055, 1943-7641. DOI: 10.1080/15361055.2019.1593008. URL: <https://www.tandfonline.com/doi/full/10.1080/15361055.2019.1593008> (visited on 02/01/2021).
- Lee, D. Y. and K. Vafai (May 1, 1999). “Comparative Analysis of Jet Impingement and Microchannel Cooling for High Heat Flux Applications”. In: *International Journal of Heat and Mass Transfer* 42.9, pp. 1555–1568. ISSN: 0017-9310. DOI: 10.1016/S0017-9310(98)00265-8. URL: <http://www.sciencedirect.com/science/article/pii/S0017931098002658> (visited on 02/01/2021).
- Lee, Kyungjun (2012). “Topology Optimization of Convective Cooling System Designs”. In: p. 171.
- Lehnert, B (1999). “Fusion Plasma Physics During Half a Century”. In: p. 58.
- Lei, Tian *et al.* (Dec. 2018). “Investment Casting and Experimental Testing of Heat Sinks Designed by Topology Optimization”. In: *International Journal of Heat and Mass Transfer* 127, pp. 396–412. ISSN: 00179310. DOI: 10.1016/j.ijheatmasstransfer.2018.07.060. URL: <https://linkinghub.elsevier.com/retrieve/pii/S001793101830454X> (visited on 02/05/2019).
- Leonard, Fabien *et al.* (Sept. 1, 2012). *Assessment by X-ray CT of the Effects of Geometry and Build Direction on Defects in Titanium ALM Parts*, p. 93. 85 pp.

- Li, Hao *et al.* (Dec. 1, 2019). “Optimal Design and Thermal Modelling for Liquid-Cooled Heat Sink Based on Multi-Objective Topology Optimization: An Experimental and Numerical Study”. In: *International Journal of Heat and Mass Transfer* 144, p. 118638. ISSN: 0017-9310. DOI: 10.1016/j.ijheatmasstransfer.2019.118638. URL: <https://www.sciencedirect.com/science/article/pii/S0017931019320289> (visited on 10/29/2021).
- Li, Hui *et al.* (July 2022). “A Review of the Latest Developments in the Field of Additive Manufacturing Techniques for Nuclear Reactors”. In: *Crystals* 12.7 (7), p. 918. ISSN: 2073-4352. DOI: 10.3390/cryst12070918. URL: <https://www.mdpi.com/2073-4352/12/7/918> (visited on 08/29/2022).
- Li, Muyuan, Ewald Werner, and Jeong-Ha You (Jan. 2015). “Low Cycle Fatigue Behavior of ITER-like Divertor Target under DEMO-relevant Operation Conditions”. In: *Fusion Engineering and Design* 90, pp. 88–96. ISSN: 09203796. DOI: 10.1016/j.fusengdes.2014.11.017. URL: <https://linkinghub.elsevier.com/retrieve/pii/S0920379614006401> (visited on 01/06/2021).
- Li, Muyuan and Jeong-Ha You (Dec. 2015). “Interpretation of the Deep Cracking Phenomenon of Tungsten Monoblock Targets Observed in High-Heat-Flux Fatigue Tests at 20 MW/m²”. In: *Fusion Engineering and Design* 101, pp. 1–8. ISSN: 09203796. DOI: 10.1016/j.fusengdes.2015.09.008. URL: <https://linkinghub.elsevier.com/retrieve/pii/S0920379615302775> (visited on 01/06/2021).
- (2017). “Design Options to Mitigate Deep Cracking of Tungsten Armor”. In: *Fusion Engineering and Design*. DOI: 10.1016/j.fusengdes.2017.01.015. URL: <internal-pdf://199.252.93.247/1-s2.0-S092037961730025X-main.pdf>.
- Li, Qiang *et al.* (Oct. 2019). “Optimization of W/Cu Monoblock Mock-up with FGM Interlayer for CFETR Divertor Targets”. In: *Fusion Engineering and Design* 147, p. 111262. ISSN: 09203796. DOI: 10.1016/j.fusengdes.2019.111262. URL: <https://linkinghub.elsevier.com/retrieve/pii/S0920379619307409> (visited on 07/09/2020).
- Li Puma, A *et al.* (Nov. 1, 2002). “Optimization of a Water-Cooled Divertor for the European Power Plant Conceptual Study”. In: *Fusion Engineering and Design* 61–62, pp. 177–183. ISSN: 0920-3796. DOI: 10.1016/S0920-3796(02)00116-3. URL: <http://www.sciencedirect.com/science/article/pii/S0920379602001163> (visited on 04/10/2020).
- Li Puma, A. *et al.* (Sept. 2003). “Potential Performances of a Divertor Concept Based on Liquid Metal Cooled SiCf/SiC Structures”. In: *Fusion Engineering and Design* 66–68, pp. 401–405. ISSN: 09203796. DOI: 10.1016/S0920-3796(03)00167-4. URL: <https://www.sciencedirect.com/science/article/pii/S0920379603001674>

- [//linkinghub.elsevier.com/retrieve/pii/S0920379603001674](https://linkinghub.elsevier.com/retrieve/pii/S0920379603001674) (visited on 12/30/2021).
- Libeyre, P. *et al.* (June 2009). “Detailed Design of the ITER Central Solenoid”. In: *Fusion Engineering and Design* 84.7-11, pp. 1188–1191. ISSN: 09203796. DOI: 10.1016/j.fusengdes.2009.01.090. URL: <https://linkinghub.elsevier.com/retrieve/pii/S0920379609001215> (visited on 10/15/2022).
- Lim, Do Kyun *et al.* (Nov. 2018). “CFD-based Shape Optimization on Cross-Section of Monoblock Fusion Divertor Cooling Channel for Minimizing Local Heat Flux”. In: *Fusion Engineering and Design* 136, pp. 1100–1105. ISSN: 09203796. DOI: 10.1016/j.fusengdes.2018.04.077. URL: <https://linkinghub.elsevier.com/retrieve/pii/S092037961830365X> (visited on 08/15/2019).
- Lin, Qiyin, Jun Hong, *et al.* (Oct. 1, 2018). “Investigation into the Topology Optimization for Conductive Heat Transfer Based on Deep Learning Approach”. In: *International Communications in Heat and Mass Transfer* 97, pp. 103–109. ISSN: 0735-1933. DOI: 10.1016/j.icheatmasstransfer.2018.07.001. URL: <http://www.sciencedirect.com/science/article/pii/S0735193318301593> (visited on 03/21/2019).
- Lin, Qiyin, Jihong Wang, *et al.* (Jan. 1, 2019). “A Biomimetic Generative Optimization Design for Conductive Heat Transfer Based on Element-Free Galerkin Method”. In: *International Communications in Heat and Mass Transfer* 100, pp. 67–72. ISSN: 0735-1933. DOI: 10.1016/j.icheatmasstransfer.2018.12.001. URL: <http://www.sciencedirect.com/science/article/pii/S0735193318302604> (visited on 03/21/2019).
- Linke, Jochen *et al.* (Sept. 2019). “Challenges for Plasma-Facing Components in Nuclear Fusion”. In: *Matter and Radiation at Extremes* 4.5, p. 056201. ISSN: 2468-2047, 2468-080X. DOI: 10.1063/1.5090100. URL: <http://aip.scitation.org/doi/10.1063/1.5090100> (visited on 05/28/2021).
- Liu, Hui *et al.* (Oct. 2018). “Efficient Structure Topology Optimization by Using the Multiscale Finite Element Method”. In: *Structural and Multidisciplinary Optimization* 58.4, pp. 1411–1430. ISSN: 1615-147X, 1615-1488. DOI: 10.1007/s00158-018-1972-9. URL: <http://link.springer.com/10.1007/s00158-018-1972-9> (visited on 03/07/2019).
- Liu, Peng *et al.* (June 2018). “Conceptual Design Study for CFETR Divertor Target Using CLAM Steel as Structural Material”. In: *Fusion Engineering and Design* 131, pp. 90–95. ISSN: 09203796. DOI: 10.1016/j.fusengdes.2018.04.057. URL: <https://linkinghub.elsevier.com/retrieve/pii/S0920379618303454> (visited on 07/09/2020).
- Liu, Ping *et al.* (Jan. 2021). “Critical Heat Flux (CHF) Correlations for Subcooled Water Flow Boiling at High Pressure and High Heat Flux”. In: *J. Therm. Sci.* 30.1, pp. 279–

293. ISSN: 1003-2169, 1993-033X. DOI: 10.1007/s11630-021-1394-7. URL: <http://link.springer.com/10.1007/s11630-021-1394-7> (visited on 03/17/2021).
- Loarte, A. and R. Neu (Nov. 2017). “Power Exhaust in Tokamaks and Scenario Integration Issues”. In: *Fusion Engineering and Design* 122, pp. 256–273. ISSN: 09203796. DOI: 10.1016/j.fusengdes.2017.06.024. URL: <https://linkinghub.elsevier.com/retrieve/pii/S092037961730724X> (visited on 12/07/2021).
- Loarte, Alberto (June 1, 2001). “Effects of Divertor Geometry on Tokamak Plasmas”. In: *Plasma Phys. Control. Fusion* 43.6, R183–R224. ISSN: 0741-3335, 1361-6587. DOI: 10.1088/0741-3335/43/6/201. URL: <https://iopscience.iop.org/article/10.1088/0741-3335/43/6/201> (visited on 12/07/2021).
- Loh, Giselle Hsiang *et al.* (Oct. 1, 2018). “An Overview of Functionally Graded Additive Manufacturing”. In: *Additive Manufacturing* 23, pp. 34–44. ISSN: 2214-8604. DOI: 10.1016/j.addma.2018.06.023. URL: <https://www.sciencedirect.com/science/article/pii/S221486041730564X> (visited on 09/19/2021).
- Lu, Biwang *et al.* (Feb. 2019). “Heat Transfer Optimization of a Fully Solid State Micro-Unit Regeneration Magnetic Refrigerator”. In: *International Journal of Refrigeration* 98, pp. 42–50. ISSN: 01407007. DOI: 10.1016/j.ijrefrig.2018.11.004. URL: <https://linkinghub.elsevier.com/retrieve/pii/S0140700718304377> (visited on 03/21/2019).
- Lundgaard, Christian, Kurt Engelbrecht, and Ole Sigmund (Dec. 2019). “A Density-Based Topology Optimization Methodology for Thermal Energy Storage Systems”. In: *Struct Multidisc Optim* 60.6, pp. 2189–2204. ISSN: 1615-147X, 1615-1488. DOI: 10.1007/s00158-019-02375-8. URL: <http://link.springer.com/10.1007/s00158-019-02375-8> (visited on 10/29/2021).
- Lundgren, Jonas *et al.* (Dec. 1, 2019). “Topology Optimization of Periodic 3D Heat Transfer Problems with 2D Design”. In: *Struct Multidisc Optim* 60.6, pp. 2295–2303. ISSN: 1615-1488. DOI: 10.1007/s00158-019-02319-2. URL: <https://doi.org/10.1007/s00158-019-02319-2> (visited on 10/13/2021).
- Lurie, S. A., L. N. Rabinskiy, and Y. O. Solyaev (Jan. 1, 2019). “Topology Optimization of the Wick Geometry in a Flat Plate Heat Pipe”. In: *International Journal of Heat and Mass Transfer* 128, pp. 239–247. ISSN: 0017-9310. DOI: 10.1016/j.ijheatmasstransfer.2018.08.125. URL: <http://www.sciencedirect.com/science/article/pii/S0017931018338018> (visited on 03/21/2019).
- Lux, H. *et al.* (Nov. 2017). “Uncertainties in Power Plant Design Point Evaluations”. In: *Fusion Engineering and Design* 123, pp. 63–66. ISSN: 09203796. DOI: 10.1016/j.fusengdes.2017.06.024.

- fusengdes.2017.01.029. URL: <https://linkinghub.elsevier.com/retrieve/pii/S092037961730039X> (visited on 10/19/2020).
- Lv, Yi and Sheng Liu (Dec. 2018). “Topology Optimization and Heat Dissipation Performance Analysis of a Micro-Channel Heat Sink”. In: *Meccanica* 53.15, pp. 3693–3708. ISSN: 0025-6455, 1572-9648. DOI: 10.1007/s11012-018-0918-z. URL: <http://link.springer.com/10.1007/s11012-018-0918-z> (visited on 10/28/2021).
- M2DOLab (Mar. 30, 2019). *Contribute to M2DOLab/OpenLSTO Development by Creating an Account on GitHub*. URL: <https://github.com/M2DOLab/OpenLSTO> (visited on 05/10/2019).
- Maisonnier, D. *et al.* (2007). “Power Plant Conceptual Studies in Europe”. In: *Nucl. Fusion* 47.11, p. 1524. ISSN: 0029-5515. DOI: 10.1088/0029-5515/47/11/014. URL: <http://stacks.iop.org/0029-5515/47/i=11/a=014> (visited on 07/18/2018).
- Makhija, David S. and Philip S. Beran (Mar. 2019). “Concurrent Shape and Topology Optimization for Steady Conjugate Heat Transfer”. In: *Struct Multidisc Optim* 59.3, pp. 919–940. ISSN: 1615-147X, 1615-1488. DOI: 10.1007/s00158-018-2110-4. URL: <http://link.springer.com/10.1007/s00158-018-2110-4> (visited on 10/28/2021).
- Malizia, A. *et al.* (2014). “Safety Analysis in Large Volume Vacuum Systems Like Tokamak: Experiments and Numerical Simulation to Analyze Vacuum Ruptures Consequences”. In: *Advances in Materials Science and Engineering 2014*, pp. 1–29. ISSN: 1687-8434, 1687-8442. DOI: 10.1155/2014/201831. URL: <http://www.hindawi.com/journals/amse/2014/201831/> (visited on 08/27/2020).
- Mao, X. *et al.* (2018). “Exploring the Engineering Limit of Heat Flux of a W/RAFM Divertor Target for Fusion Reactors”. In: *Nucl. Fusion* 58.6, p. 066014. ISSN: 0029-5515. DOI: 10.1088/1741-4326/aabb64. URL: <http://stacks.iop.org/0029-5515/58/i=6/a=066014> (visited on 07/09/2018).
- Marbach, G, I Cook, and D Maisonnier (2002). “The EU Power Plant Conceptual Study”. In: *Fusion Engineering and Design*, p. 9.
- Marck, Gilles, Maroun Nemer, and Jean-Luc Harion (June 1, 2013). “Topology Optimization of Heat and Mass Transfer Problems: Laminar Flow”. In: *Numerical Heat Transfer, Part B: Fundamentals* 63.6, pp. 508–539. ISSN: 1040-7790. DOI: 10.1080/10407790.2013.772001. URL: <https://doi.org/10.1080/10407790.2013.772001> (visited on 03/04/2019).
- Marshall, Oliver H. R. *et al.* (May 14, 2021). “Thermal Topology Optimisation of a Plasma Facing Component for Use in Next-Generation Fusion Reactors”. In: DOI: 10.17028/rd.lboro.14595681.v1. URL: /articles/conference_contribution/Thermal_

- topology_optimisation_of_a_plasma_facing_component_for_use_in_next-generation_fusion_reactors/14595681/1 (visited on 05/20/2021).
- Marshall, Theron D (Feb. 1, 2001). *FILM-30: A Heat Transfer Properties Code for Water Coolant*. SAND2001-0626, 780297, SAND2001-0626, 780297. DOI: 10.2172/780297. URL: <http://www.osti.gov/servlets/purl/780297/> (visited on 07/02/2020).
- Martin, Denk (Apr. 30, 2019). *ToOptix Is Used for Multiphysical Topology Optimization. There Are Different Methods for Combining Structural, Thermal, ... Load Cases.: DMST1990/ToOptiX*. URL: <https://github.com/DMST1990/ToOptiX> (visited on 05/10/2019).
- Martinez, Victor J *et al.* (2011). “Development of Codes & Standards for ITER In-Vessel Components”. In: p. 10.
- Martínez-Frutos, Jesús and David Herrero-Pérez (Nov. 2016). “Large-Scale Robust Topology Optimization Using Multi-GPU Systems”. In: *Computer Methods in Applied Mechanics and Engineering* 311, pp. 393–414. ISSN: 00457825. DOI: 10.1016/j.cma.2016.08.016. URL: <https://linkinghub.elsevier.com/retrieve/pii/S0045782516309574> (visited on 02/07/2019).
- CuCrZr Tube Procurement Specification for Divertor* (2014). *Material Specification for the Supply of CuCrZr - IG Alloy Seamless Tubes for the ITER Divertor*. ITER_D_2A9VEN v2.1. The ITER Organisation. URL: https://industryportal.f4e.europa.eu/Lists/News/Attachments/316/CuCrZr-IG_Tube_Specification_2A9VEN_v2_1_published.pdf (visited on 10/10/2022).
- Matsumori, Tadayoshi *et al.* (Apr. 2013). “Topology Optimization for Fluid–Thermal Interaction Problems under Constant Input Power”. In: *Structural and Multidisciplinary Optimization* 47.4, pp. 571–581. ISSN: 1615-147X, 1615-1488. DOI: 10.1007/s00158-013-0887-8. URL: <http://link.springer.com/10.1007/s00158-013-0887-8> (visited on 02/11/2019).
- Maviglia, F. *et al.* (Nov. 2016). “Limitations of Transient Power Loads on DEMO and Analysis of Mitigation Techniques”. In: *Fusion Engineering and Design* 109–111, pp. 1067–1071. ISSN: 09203796. DOI: 10.1016/j.fusengdes.2016.01.023. URL: <https://linkinghub.elsevier.com/retrieve/pii/S0920379616300230> (visited on 10/13/2020).
- Mazul, I.V. (Dec. 1, 2016). “Alternative Divertor Target Concepts for next Step Fusion Devices”. In: *Nucl. Fusion* 56.12, p. 126009. ISSN: 0029-5515, 1741-4326. DOI: 10.1088/0029-5515/56/12/126009. URL: <https://iopscience.iop.org/article/10.1088/0029-5515/56/12/126009> (visited on 09/15/2020).
- Mazzini, Guido, Tadas Kaliatka, and Maria Teresa Porfiri (July 1, 2019). “Estimation of Tritium and Dust Source Term in European DEMONstration Fusion Reactor During

- Accident Scenarios”. In: *Journal of Nuclear Engineering and Radiation Science* 5.3, p. 030916. ISSN: 2332-8983, 2332-8975. DOI: 10 . 1115 / 1 . 4043379. URL: <https://asmedigitalcollection.asme.org/nuclearengineering/article/doi/10.1115/1.4043379/725860/Estimation-of-Tritium-and-Dust-Source-Term-in> (visited on 07/22/2020).
- McConnell, Caroline and Georg Pinggen (Nov. 9, 2012). “Multi-Layer, Pseudo 3D Thermal Topology Optimization of Heat Sinks”. In: *Volume 7: Fluids and Heat Transfer, Parts A, B, C, and D*. ASME 2012 International Mechanical Engineering Congress and Exposition. Houston, Texas, USA: American Society of Mechanical Engineers, pp. 2381–2392. ISBN: 978-0-7918-4523-3. DOI: 10 . 1115 / IMECE2012 – 93093. URL: <https://asmedigitalcollection.asme.org/IMECE/proceedings/IMECE2012/45233/2381/364960> (visited on 10/28/2021).
- Merola, M and G Vieider (1998). “On the Use of Flat Tile Armour in High Heat Flux Components”. In: *Journal of Nuclear Materials*, p. 5.
- Migliorini, F.L. (Sept. 2009). “Calculated Uncertainty of the Thermal Diffusivity Measurement Based on Flash Laser Method”. In: World Congress Fundamental and Applied Metrology. Lisbon, Portugal. URL: https://www.researchgate.net/publication/242254151_Calculated_uncertainty_of_the_thermal_diffusivity_measurement_based_on_flash_laser_method (visited on 05/06/2020).
- Milnes, Joseph, Alan Burns, and Dimitris Drikakis (Sept. 1, 2012). “Computational Modelling of the HyperVapotron Cooling Technique”. In: *Fusion Engineering and Design* 87.9, pp. 1647–1661. ISSN: 0920-3796. DOI: 10 . 1016 / j . fusengdes . 2012 . 06 . 014. URL: <http://www.sciencedirect.com/science/article/pii/S0920379612003171> (visited on 07/26/2018).
- Morris, J. *et al.* (June 2020). “Comparison of the Process Systems Code With the SONIC Divertor Code”. In: *IEEE Transactions on Plasma Science* 48.6, pp. 1799–1803. ISSN: 1939-9375. DOI: 10.1109/TPS.2020.2967859.
- El-Morshedy, Salah El-Din (Sept. 1, 2021). “Thermal-Hydraulic Modelling and Analysis of ITER Tungsten Divertor Monoblock”. In: *Nuclear Materials and Energy* 28, p. 101035. ISSN: 2352-1791. DOI: 10 . 1016 / j . nme . 2021 . 101035. URL: <https://www.sciencedirect.com/science/article/pii/S2352179121001083> (visited on 10/05/2021).
- Muldrew, Stuart I. *et al.* (May 2020). ““PROCESS”: Systems Studies of Spherical Tokamaks”. In: *Fusion Engineering and Design* 154, p. 111530. ISSN: 09203796. DOI: 10 . 1016 / j . fusengdes . 2020 . 111530. URL: <https://linkinghub.elsevier.com/retrieve/pii/S0920379620300788> (visited on 07/22/2020).

- Muraviev, E (1995). “Liquid Metal Cooled Divertor for ARIES”. In: p. 135.
- NAKAMURA, Makoto *et al.* (2009). “Development of the Integrated System Design Code for Fusion Power Plants”. In: URL: http://www.jspf.or.jp/JPFRS/PDF/Vo19/jpfrs2010_09-186.pdf (visited on 11/11/2020).
- Newton, Thomas R. *et al.* (July 2009). “Investigation of the Effect of Process Parameters on the Formation and Characteristics of Recast Layer in Wire-EDM of Inconel 718”. In: *Materials Science and Engineering: A* 513–514, pp. 208–215. ISSN: 09215093. DOI: 10.1016/j.msea.2009.01.061. URL: <https://linkinghub.elsevier.com/retrieve/pii/S0921509309000987> (visited on 06/20/2019).
- Nicholas, T. E. G. *et al.* (Feb. 1, 2021). “Re-Examining the Role of Nuclear Fusion in a Renewables-Based Energy Mix”. In: *Energy Policy* 149, p. 112043. ISSN: 0301-4215. DOI: 10.1016/j.enpol.2020.112043. URL: <https://www.sciencedirect.com/science/article/pii/S0301421520307540> (visited on 12/07/2021).
- Norajitra, Prachai, Said I. Abdel-Khalik, *et al.* (Dec. 1, 2008). “Divertor Conceptual Designs for a Fusion Power Plant”. In: *Fusion Engineering and Design*. Proceedings of the Eight International Symposium of Fusion Nuclear Technology 83.7, pp. 893–902. ISSN: 0920-3796. DOI: 10.1016/j.fusengdes.2008.05.022. URL: <http://www.sciencedirect.com/science/article/pii/S0920379608001129> (visited on 07/26/2018).
- Norajitra, Prachai, R. Giniyatulin, *et al.* (Jan. 1, 2008). “Status of Development of the EU He-cooled Divertor for DEMO”. In.
- Nordlund, K (2018). *European Research Roadmap to the Realisation of Fusion Energy*. URL: https://helda.helsinki.fi/bitstream/handle/10138/293624/2018_Research_roadmap_long_version_01.pdf?sequence=1 (visited on 11/20/2021).
- Nørgaard, Sebastian, Ole Sigmund, and Boyan Lazarov (Feb. 15, 2016). “Topology Optimization of Unsteady Flow Problems Using the Lattice Boltzmann Method”. In: *Journal of Computational Physics* 307, pp. 291–307. ISSN: 0021-9991. DOI: 10.1016/j.jcp.2015.12.023. URL: <http://www.sciencedirect.com/science/article/pii/S0021999115008426> (visited on 01/17/2019).
- Nuttall, William J. (Dec. 31, 2004). *Nuclear Renaissance: Technologies and Policies for the Future of Nuclear Power*. CRC Press. 346 pp. ISBN: 978-1-4200-3377-9. Google Books: [qi_wlX2WuHgC](https://books.google.com/books?id=qi_wlX2WuHgC).
- Nygren, R.E. and F.L. Tabarés (Dec. 2016). “Liquid Surfaces for Fusion Plasma Facing Components—A Critical Review. Part I: Physics and PSI”. In: *Nuclear Materials and Energy* 9, pp. 6–21. ISSN: 23521791. DOI: 10.1016/j.nme.2016.08.008. URL: <https://linkinghub.elsevier.com/retrieve/pii/S2352179115301307> (visited on 12/14/2021).

- Nygren, Richard E. *et al.* (Nov. 1, 2016). “A New Vision of Plasma Facing Components”. In: *Fusion Engineering and Design*. Proceedings of the 12th International Symposium on Fusion Nuclear Technology-12 (ISFNT-12) 109–111, pp. 192–200. ISSN: 0920-3796. DOI: 10.1016/j.fusengdes.2016.03.031. URL: <http://www.sciencedirect.com/science/article/pii/S0920379616302277> (visited on 07/04/2018).
- Oh, Hoongyo *et al.* (Jan. 2021). “Design and Assessment of a New Divertor Plasma Facing Component Containing the Hypervapotron Cooling Channel and Monoblock-Type Armor”. In: *Fusion Engineering and Design* 162, p. 112101. ISSN: 09203796. DOI: 10.1016/j.fusengdes.2020.112101. URL: <https://linkinghub.elsevier.com/retrieve/pii/S0920379620306499> (visited on 02/08/2021).
- Okada, Masatoshi, Tetsuji Noda, and Fujio Abe (Dec. 1989). “On the Development of Low-Activation Materials for Fusion Reactors”. In: *Journal of Nuclear Materials* 169, pp. 249–256. ISSN: 00223115. DOI: 10.1016/0022-3115(89)90541-2. URL: <https://linkinghub.elsevier.com/retrieve/pii/0022311589905412> (visited on 10/11/2022).
- Okano, Kunihiko, Gianfranco Federici, and Kenji Tobita (Oct. 2014). “DEMO Design Activities in the Broader Approach under Japan/EU Collaboration”. In: *Fusion Engineering and Design* 89.9-10, pp. 2008–2012. ISSN: 09203796. DOI: 10.1016/j.fusengdes.2014.04.005. URL: <https://linkinghub.elsevier.com/retrieve/pii/S0920379614002725> (visited on 12/03/2020).
- Olesen, Laurits Højgaard, Fridolin Okkels, and Henrik Bruus (Feb. 12, 2006). “A High-Level Programming-Language Implementation of Topology Optimization Applied to Steady-State Navier-Stokes Flow”. In: *International Journal for Numerical Methods in Engineering* 65.7, pp. 975–1001. ISSN: 0029-5981, 1097-0207. DOI: 10.1002/nme.1468. URL: <http://doi.wiley.com/10.1002/nme.1468> (visited on 04/07/2019).
- Ono, M. *et al.* (Oct. 2013). “Recent Progress in the NSTX/NSTX-U Lithium Programme and Prospects for Reactor-Relevant Liquid-Lithium Based Divertor Development”. In: *Nucl. Fusion* 53.11, p. 113030. ISSN: 0029-5515. DOI: 10.1088/0029-5515/53/11/113030. URL: <https://doi.org/10.1088/0029-5515/53/11/113030> (visited on 12/14/2021).
- Osher, Stanley and James A Sethian (Nov. 1, 1988). “Fronts Propagating with Curvature-Dependent Speed: Algorithms Based on Hamilton-Jacobi Formulations”. In: *Journal of Computational Physics* 79.1, pp. 12–49. ISSN: 0021-9991. DOI: 10.1016/0021-9991(88)90002-2. URL: <http://www.sciencedirect.com/science/article/pii/0021999188900022> (visited on 02/11/2019).
- Othmer, C. (Nov. 20, 2008). “A Continuous Adjoint Formulation for the Computation of Topological and Surface Sensitivities of Ducted Flows”. In: *International Journal for*

- Numerical Methods in Fluids* 58.8, pp. 861–877. ISSN: 02712091, 10970363. DOI: 10.1002/fld.1770. URL: <http://doi.wiley.com/10.1002/fld.1770> (visited on 04/01/2019).
- Othmer, Carsten, Eugene de Villiers, and Henry Weller (June 25, 2007). “Implementation of a Continuous Adjoint for Topology Optimization of Ducted Flows”. In: *18th AIAA Computational Fluid Dynamics Conference*. 18th AIAA Computational Fluid Dynamics Conference. Miami, Florida: American Institute of Aeronautics and Astronautics. ISBN: 978-1-62410-129-8. DOI: 10.2514/6.2007-3947. URL: <http://arc.aiaa.org/doi/10.2514/6.2007-3947> (visited on 10/10/2019).
- Otomori, Masaki *et al.* (May 2015). “Matlab Code for a Level Set-Based Topology Optimization Method Using a Reaction Diffusion Equation”. In: *Structural and Multidisciplinary Optimization* 51.5, pp. 1159–1172. ISSN: 1615-147X, 1615-1488. DOI: 10.1007/s00158-014-1190-z. URL: <http://link.springer.com/10.1007/s00158-014-1190-z> (visited on 04/10/2019).
- Papoutsis-Kiachagias, E M *et al.* (2011). “Constrained Topology Optimization for Laminar and Turbulent Flows, Including Heat Transfer”. In: *topology optimization*, p. 11.
- Park, Jaejong *et al.* (May 4, 2019). “Conceptual Design of Efficient Heat Conductors Using Multi-Material Topology Optimization”. In: *Engineering Optimization* 51.5, pp. 796–814. ISSN: 0305-215X, 1029-0273. DOI: 10.1080/0305215X.2018.1497613. URL: <https://www.tandfonline.com/doi/full/10.1080/0305215X.2018.1497613> (visited on 03/21/2019).
- Pascal-Ribot, S. *et al.* (Oct. 2007). “3D Numerical Simulations of Hypervapotron Cooling Concept”. In: *Fusion Engineering and Design* 82.15-24, pp. 1781–1785. ISSN: 09203796. DOI: 10.1016/j.fusengdes.2006.12.011. URL: <https://linkinghub.elsevier.com/retrieve/pii/S0920379607000178> (visited on 11/10/2021).
- Patterson, Eann (May 1, 2015). “On the Credibility of Engineering Models and Meta-Models”. In: *The Journal of Strain Analysis for Engineering Design* 50.4, pp. 218–220. ISSN: 0309-3247. DOI: 10.1177/0309324715577930. URL: <https://doi.org/10.1177/0309324715577930> (visited on 12/22/2021).
- Patterson, Eann A. *et al.* (Oct. 2019). “An Integrated Digital Framework for the Design, Build and Operation of Fusion Power Plants”. In: *R. Soc. open sci.* 6.10, p. 181847. ISSN: 2054-5703, 2054-5703. DOI: 10.1098/rsos.181847. URL: <https://royalsocietypublishing.org/doi/10.1098/rsos.181847> (visited on 07/22/2020).
- Pearce, A J *et al.* (2019). “Systems Studies of Double Null Divertor Models”. In: p. 1.
- Pearson, R. J. *et al.* (Sept. 1, 2020). “Technology Roadmapping for Mission-Led Agile Hardware Development: A Case Study of a Commercial Fusion Energy Start-Up”. In:

- Technological Forecasting and Social Change* 158, p. 120064. ISSN: 0040-1625. DOI: 10.1016/j.techfore.2020.120064. URL: <https://www.sciencedirect.com/science/article/pii/S0040162519318281> (visited on 12/08/2021).
- Pietropaoli, M. *et al.* (Apr. 25, 2017). “Design for Additive Manufacturing: Internal Channel Optimization”. In: *Journal of Engineering for Gas Turbines and Power* 139.10, p. 102101. ISSN: 0742-4795. DOI: 10.1115/1.4036358. URL: <http://gasturbinespower.asmedigitalcollection.asme.org/article.aspx?doi=10.1115/1.4036358> (visited on 04/01/2019).
- Pingen, Georg, Anton Evgrafov, and Kurt Maute (Oct. 24, 2007). “Topology Optimization of Flow Domains Using the Lattice Boltzmann Method”. In: *Structural and Multidisciplinary Optimization* 34.6, pp. 507–524. ISSN: 1615-147X, 1615-1488. DOI: 10.1007/s00158-007-0105-7. URL: <http://link.springer.com/10.1007/s00158-007-0105-7> (visited on 04/01/2019).
- (Apr. 2009). “Adjoint Parameter Sensitivity Analysis for the Hydrodynamic Lattice Boltzmann Method with Applications to Design Optimization”. In: *Computers & Fluids* 38.4, pp. 910–923. ISSN: 00457930. DOI: 10.1016/j.compfluid.2008.10.002. URL: <https://linkinghub.elsevier.com/retrieve/pii/S0045793008001989> (visited on 04/01/2019).
- Pitts, R. A. *et al.* (Aug. 1, 2017). “Physics Conclusions in Support of ITER W Divertor Monoblock Shaping”. In: *Nuclear Materials and Energy*. Proceedings of the 22nd International Conference on Plasma Surface Interactions 2016, 22nd PSI 12, pp. 60–74. ISSN: 2352-1791. DOI: 10.1016/j.nme.2017.03.005. URL: <https://www.sciencedirect.com/science/article/pii/S2352179116302885> (visited on 03/19/2021).
- Pitts, R.A. *et al.* (July 2013). “A Full Tungsten Divertor for ITER: Physics Issues and Design Status”. In: *Journal of Nuclear Materials* 438, S48–S56. ISSN: 00223115. DOI: 10.1016/j.jnucmat.2013.01.008. URL: <https://linkinghub.elsevier.com/retrieve/pii/S0022311513000160> (visited on 11/29/2018).
- Pizzolato, Alberto *et al.* (Dec. 2017a). “Design of Effective Fins for Fast PCM Melting and Solidification in Shell-and-Tube Latent Heat Thermal Energy Storage through Topology Optimization”. In: *Applied Energy* 208, pp. 210–227. ISSN: 03062619. DOI: 10.1016/j.apenergy.2017.10.050. URL: <https://linkinghub.elsevier.com/retrieve/pii/S0306261917314642> (visited on 06/04/2019).
- (Oct. 1, 2017b). “Topology Optimization for Heat Transfer Enhancement in Latent Heat Thermal Energy Storage”. In: *International Journal of Heat and Mass Transfer* 113, pp. 875–888. ISSN: 0017-9310. DOI: 10.1016/j.ijheatmasstransfer.2017.05.098.

- URL: <http://www.sciencedirect.com/science/article/pii/S0017931017303034> (visited on 08/15/2018).
- Porfiri, Maria Teresa *et al.* (June 2020). “Safety Assessment for EU DEMO – Achievements and Open Issues in View of a Generic Site Safety Report”. In: *Fusion Engineering and Design* 155, p. 111541. ISSN: 09203796. DOI: 10.1016/j.fusengdes.2020.111541. URL: <https://linkinghub.elsevier.com/retrieve/pii/S0920379620300892> (visited on 07/22/2020).
- Pradel, Patrick *et al.* (2017). “Complexity Is Not for Free: The Impact of Component Complexity on Additive Manufacturing Build Time”. In: *Rapid Design, Prototyping & Manufacturing*. Newcastle.
- Li-Puma, Antonella *et al.* (Oct. 2013). “Potential and Limits of Water Cooled Divertor Concepts Based on Monoblock Design as Possible Candidates for a DEMO Reactor”. In: *Fusion Engineering and Design* 88.9-10, pp. 1836–1843. ISSN: 09203796. DOI: 10.1016/j.fusengdes.2013.05.114. URL: <https://linkinghub.elsevier.com/retrieve/pii/S0920379613005541> (visited on 01/06/2021).
- Qian, Xiaoping and Ercan M. Dede (Sept. 2016). “Topology Optimization of a Coupled Thermal-Fluid System under a Tangential Thermal Gradient Constraint”. In: *Struct Multi-disc Optim* 54.3, pp. 531–551. ISSN: 1615-147X, 1615-1488. DOI: 10.1007/s00158-016-1421-6. URL: <http://link.springer.com/10.1007/s00158-016-1421-6> (visited on 10/28/2021).
- Raeder, J. (Mar. 1995). “Report on the European Safety and Environmental Assessment of Fusion Power (SEAFP)”. In: *Fusion Engineering and Design* 29, pp. 121–140. ISSN: 09203796. DOI: 10.1016/0920-3796(95)80014-0. URL: <https://linkinghub.elsevier.com/retrieve/pii/0920379695800140> (visited on 10/27/2020).
- Raffray, A. R., S. Malang, and X. Wang (June 1, 2009). “Optimizing the Overall Configuration of a He-cooled W-alloy Divertor for a Power Plant”. In: *Fusion Engineering and Design*. Proceeding of the 25th Symposium on Fusion Technology 84.7, pp. 1553–1557. ISSN: 0920-3796. DOI: 10.1016/j.fusengdes.2008.12.069. URL: <https://www.sciencedirect.com/science/article/pii/S0920379608004614> (visited on 02/20/2021).
- Raffray, A. R., R. Nygren, *et al.* (Jan. 1, 2010). “High Heat Flux Components—Readiness to Proceed from near Term Fusion Systems to Power Plants”. In: *Fusion Engineering and Design* 85.1, pp. 93–108. ISSN: 0920-3796. DOI: 10.1016/j.fusengdes.2009.08.002. URL: <https://www.sciencedirect.com/science/article/pii/S092037960900252X> (visited on 08/15/2022).

- Raffray, A.R. *et al.* (Sept. 1998). “High Heat Flux Thermal–Hydraulic Analysis of ITER Divertor and Blanket Systems”. In: *Fusion Engineering and Design* 39–40, pp. 323–331. ISSN: 09203796. DOI: 10.1016/S0920-3796(98)00225-7. URL: <https://linkinghub.elsevier.com/retrieve/pii/S0920379698002257> (visited on 02/18/2021).
- Raffray, A.R. *et al.* (Aug. 1999). “Critical Heat Flux Analysis and R&D for the Design of the ITER Divertor”. In: *Fusion Engineering and Design* 45.4, pp. 377–407. ISSN: 09203796. DOI: 10.1016/S0920-3796(99)00053-8. URL: <https://linkinghub.elsevier.com/retrieve/pii/S0920379699000538> (visited on 07/14/2020).
- Ramalingom, Delphine, Pierre-Henri Cocquet, and Alain Bastide (May 2018). “A New Interpolation Technique to Deal with Fluid-Porous Media Interfaces for Topology Optimization of Heat Transfer”. In: *Computers & Fluids* 168, pp. 144–158. ISSN: 00457930. DOI: 10.1016/j.compfluid.2018.04.005. URL: <https://linkinghub.elsevier.com/retrieve/pii/S0045793018301932> (visited on 10/24/2021).
- Ramalingom, Delphine, Pierre-Henri Cocquet, Rezah Maleck, *et al.* (May 30, 2018). “A Multi-Objective Optimization Problem in Natural Convection for a Vertical Channel Asymmetrically Heated”. In: p. 43.
- Reimann, J. *et al.* (Oct. 2001). “Conceptual Design of an Evaporation-Cooled Liquid Metal Divertor for Fusion Power Plants”. In: *Fusion Engineering and Design* 56–57, pp. 369–373. ISSN: 09203796. DOI: 10.1016/S0920-3796(01)00326-X. URL: <https://linkinghub.elsevier.com/retrieve/pii/S092037960100326X> (visited on 09/02/2021).
- Reux, C., L. Di Gallo, *et al.* (July 1, 2015). “DEMO Reactor Design Using the New Modular System Code SYCOMORE”. In: *Nucl. Fusion* 55.7, p. 073011. ISSN: 0029-5515, 1741-4326. DOI: 10.1088/0029-5515/55/7/073011. URL: <https://iopscience.iop.org/article/10.1088/0029-5515/55/7/073011> (visited on 10/21/2020).
- Reux, C., S. Kahn, *et al.* (Nov. 2018). “DEMO Design Using the SYCOMORE System Code: Influence of Technological Constraints on the Reactor Performances”. In: *Fusion Engineering and Design* 136, pp. 1572–1576. ISSN: 09203796. DOI: 10.1016/j.fusengdes.2018.05.059. URL: <https://linkinghub.elsevier.com/retrieve/pii/S0920379618304927> (visited on 10/16/2020).
- Richou, Marianne, Antonella Li-Puma, and Eliseo Visca (Oct. 2014). “Design of a Water Cooled Monoblock Divertor for DEMO Using Eurofer as Structural Material”. In: *Fusion Engineering and Design* 89.7-8, pp. 975–980. ISSN: 09203796. DOI: 10.1016/j.fusengdes.2014.04.019. URL: <https://linkinghub.elsevier.com/retrieve/pii/S0920379614002968> (visited on 01/20/2021).
- Rivas, J.C. *et al.* (Nov. 2016). “Safety Studies of Plasma-Wall Events with AINA Code for Japanese DEMO”. In: *Fusion Engineering and Design* 109–111, pp. 1653–1657. ISSN:

09203796. DOI: 10.1016/j.fusengdes.2015.10.037. URL: <https://linkinghub.elsevier.com/retrieve/pii/S0920379615303240> (visited on 12/01/2020).
- Rocella, S. *et al.* (Dec. 2020). “CPS Based Liquid Metal Divertor Target for EU-DEMO”. In: *J Fusion Energ* 39.6, pp. 462–468. ISSN: 0164-0313, 1572-9591. DOI: 10.1007/s10894-020-00263-4. URL: <http://link.springer.com/10.1007/s10894-020-00263-4> (visited on 09/02/2021).
- Rohde, Magnus *et al.* (Jan. 1, 2014). “Intercomparison of Thermal Diffusivity Measurements on CuCrZr and PMMA”. In: *High Temperatures-High Pressures* 42.
- Romanelli, Francesco *et al.* (2012). *Fusion Electricity: A Roadmap to the Realisation of Fusion Energy*. Culham: EFDA. ISBN: 978-3-00-040720-8.
- Rosenfeld, J. and J. Lindemuth (Oct. 1993). “Evaluation of Porous Media Heat Exchangers for Plasma Facing Components”. In: *15th IEEE/NPSS Symposium. Fusion Engineering*. 15th IEEE/NPSS Symposium. Fusion Engineering. Vol. 2, 1210–1213 vol.2. DOI: 10.1109/FUSION.1993.518540.
- Rosenfeld, J.H. *et al.* (1997). “ADVANCES IN POROUS MEDIA HEAT EXCHANGERS FOR FUSION APPLICATIONS”. In: *Fusion Technology 1996*. Elsevier, pp. 487–490. ISBN: 978-0-444-82762-3. DOI: 10.1016/B978-0-444-82762-3.50092-6. URL: <https://linkinghub.elsevier.com/retrieve/pii/B9780444827623500926> (visited on 02/01/2021).
- Rozvany, G. I. N. (Jan. 1, 2009). “A Critical Review of Established Methods of Structural Topology Optimization”. In: *Struct Multidisc Optim* 37.3, pp. 217–237. ISSN: 1615-1488. DOI: 10.1007/s00158-007-0217-0. URL: <https://doi.org/10.1007/s00158-007-0217-0> (visited on 08/20/2018).
- Rozvany, G. I. N. *et al.* (1993). “Topology Optimization Using Iterative Continuum-Type Optimality Criteria (COC) Methods for Discretized Systems”. In: *Topology Design of Structures*. Ed. by Martin Philip Bendsøe and Carlos A. Mota Soares. Dordrecht: Springer Netherlands, pp. 273–286. ISBN: 978-94-010-4795-1. DOI: 10.1007/978-94-011-1804-0_18. URL: http://link.springer.com/10.1007/978-94-011-1804-0_18 (visited on 03/19/2019).
- Rozvany, G.I.N. (Apr. 2001). “Aims, Scope, Methods, History and Unified Terminology of Computer-Aided Topology Optimization in Structural Mechanics”. In: *Structural and Multidisciplinary Optimization* 21.2, pp. 90–108. ISSN: 1615-147X, 1615-1488. DOI: 10.1007/s001580050174. URL: <http://link.springer.com/10.1007/s001580050174> (visited on 03/20/2019).
- Sannazzaro, G. *et al.* (Oct. 2013). “Development of Design Criteria for ITER In-vessel Components”. In: *Fusion Engineering and Design* 88.9-10, pp. 2138–2141. ISSN: 09203796.

- DOI: 10.1016/j.fusengdes.2013.01.019. URL: <https://linkinghub.elsevier.com/retrieve/pii/S0920379613000203> (visited on 01/08/2021).
- Santhanakrishnan, Mani Sekaran, Timothy Tilford, and Christopher Bailey (Sept. 1, 2018). “Performance Assessment of Density and Level-Set Topology Optimisation Methods for Three Dimensional Heat Sink Design”. In: *Journal of Algorithms & Computational Technology* 12.3, pp. 273–287. ISSN: 1748-3026. DOI: 10.1177/1748301818779019. URL: <https://doi.org/10.1177/1748301818779019> (visited on 10/28/2021).
- Sardain, P. *et al.* (Sept. 2003). “Power Plant Conceptual Study—WCLL Concept”. In: *Fusion Engineering and Design* 69.1-4, pp. 769–774. ISSN: 09203796. DOI: 10.1016/S0920-3796(03)00146-7. URL: <https://linkinghub.elsevier.com/retrieve/pii/S0920379603001467> (visited on 11/19/2020).
- Sato, Yuki *et al.* (Mar. 1, 2018). “An Optimum Design Method for a Thermal-Fluid Device Incorporating Multiobjective Topology Optimization With an Adaptive Weighting Scheme”. In: *Journal of Mechanical Design* 140.3, p. 031402. ISSN: 1050-0472, 1528-9001. DOI: 10.1115/1.4038209. URL: <https://asmedigitalcollection.asme.org/mechanicaldesign/article/doi/10.1115/1.4038209/367672/An-Optimum-Design-Method-for-a-ThermalFluid-Device> (visited on 10/28/2021).
- Schlosser, J., P. Chappuis, and P. Deschamps (1993). “TECHNOLOGY DEVELOPMENTS FOR THE ITER DIVERTOR”. In: *Fusion Technology 1992*. Elsevier, pp. 367–371. ISBN: 978-0-444-89995-8. DOI: 10.1016/B978-0-444-89995-8.50066-7. URL: <https://linkinghub.elsevier.com/retrieve/pii/B9780444899958500667> (visited on 01/21/2021).
- Schlosser, J., F. Escourbiac, *et al.* (May 2005). “Technologies for ITER Divertor Vertical Target Plasma Facing Components”. In: *Nucl. Fusion* 45.6, pp. 512–518. ISSN: 0029-5515. DOI: 10.1088/0029-5515/45/6/013. URL: <https://doi.org/10.1088/0029-5515/45/6/013> (visited on 07/30/2019).
- Schmidt, Stephan and Volker Schulz (Aug. 1, 2011). “A 2589 Line Topology Optimization Code Written for the Graphics Card”. In: *Comput. Visual Sci.* 14.6, pp. 249–256. ISSN: 1433-0369. DOI: 10.1007/s00791-012-0180-1. URL: <https://doi.org/10.1007/s00791-012-0180-1> (visited on 09/28/2018).
- Secretary of State for Business, Energy and Industrial Strategy (Oct. 2021). *Towards Fusion Energy: Proposals for a Regulatory Framework*. GOV.UK. URL: <https://www.gov.uk/government/consultations/towards-fusion-energy-proposals-for-a-regulatory-framework> (visited on 11/30/2021).
- Segantin, S. *et al.* (Jan. 2, 2020). “Exploration of a Fast Pathway to Nuclear Fusion: Thermal Analysis and Cooling Design Considerations for the ARC Reactor”. In: *Fusion Science and*

- Technology* 76.1, pp. 45–52. ISSN: 1536-1055, 1943-7641. DOI: 10.1080/15361055.2019.1629252. URL: <https://www.tandfonline.com/doi/full/10.1080/15361055.2019.1629252> (visited on 07/22/2020).
- Siccino, M., W. Biel, *et al.* (July 2020). “DEMO Physics Challenges beyond ITER”. In: *Fusion Engineering and Design* 156, p. 111603. ISSN: 09203796. DOI: 10.1016/j.fusengdes.2020.111603. URL: <https://linkinghub.elsevier.com/retrieve/pii/S0920379620301514> (visited on 07/22/2020).
- Siccino, M., G. Federici, *et al.* (Oct. 1, 2019). “Figure of Merit for Divertor Protection in the Preliminary Design of the EU-DEMO Reactor”. In: *Nucl. Fusion* 59.10, p. 106026. ISSN: 0029-5515, 1741-4326. DOI: 10.1088/1741-4326/ab3153. URL: <https://iopscience.iop.org/article/10.1088/1741-4326/ab3153> (visited on 10/13/2020).
- Sigmund, O. (Apr. 2001). “A 99 Line Topology Optimization Code Written in Matlab”. In: *Structural and Multidisciplinary Optimization* 21.2, pp. 120–127. ISSN: 1615-147X, 1615-1488. DOI: 10.1007/s001580050176. URL: <http://link.springer.com/10.1007/s001580050176> (visited on 08/22/2018).
- Sigmund, Ole and Kurt Maute (2013). “Topology Optimization Approaches”. In: *Structural and Multidisciplinary Optimization* 48.6, pp. 1031–1055. ISSN: 1615-147X. DOI: 10.1007/s00158-013-0978-6.
- SIMULIA™ Support Documentation - Dassault Systèmes®* (2019). URL: <https://www.3ds.com/products-services/simulia/support/documentation/> (visited on 05/10/2019).
- Sizyuk, V. and A. Hassanein (June 1, 2018). “Comprehensive 3-D Simulation and Performance of ITER Plasma Facing and Nearby Components during Transient Events - Serious Design Issues”. In: *Physics of Plasmas* 25.6, p. 062508. ISSN: 1070-664X. DOI: 10.1063/1.5026597. URL: <https://aip.scitation.org/doi/10.1063/1.5026597> (visited on 07/14/2020).
- Smid, I. *et al.* (1997). “Comparison between Various Thermal Hydraulic Tube Concepts for the ITER Divertor”. In: *Fusion Technology* 1996. Elsevier, pp. 263–266. ISBN: 978-0-444-82762-3. DOI: 10.1016/B978-0-444-82762-3.50036-7. URL: <https://linkinghub.elsevier.com/retrieve/pii/B9780444827623500367> (visited on 07/30/2019).
- Song, Miao *et al.* (Jan. 2019). “Radiation Damage and Irradiation-Assisted Stress Corrosion Cracking of Additively Manufactured 316L Stainless Steels”. In: *Journal of Nuclear Materials* 513, pp. 33–44. ISSN: 00223115. DOI: 10.1016/j.jnucmat.2018.10.044. URL: <https://linkinghub.elsevier.com/retrieve/pii/S0022311518309061> (visited on 08/28/2022).

- Soprani, S *et al.* (2015). “Topology Optimization of an Actively Cooled Electronics Section for Downhole Tools”. In: CCOMSOL CONFERENCE, p. 8.
- Srinivas, V.S.S. (2006). *(PDF) Analysis and Topology Optimization of Heat Sinks with a Phase- Change Material on COMSOL Multiphysics™ Platform*. ResearchGate. URL: https://www.researchgate.net/publication/267679913_Analysis_and_Topology_Optimization_of_Heat_Sinks_with_a_Phase-Change_Material_on_COMSOL_Multiphysics_Platform (visited on 01/17/2019).
- Subramaniam, V., T. Dbouk, and J. L. Harion (Feb. 1, 2019). “Topology Optimization of Conjugate Heat Transfer Systems: A Competition between Heat Transfer Enhancement and Pressure Drop Reduction”. In: *International Journal of Heat and Fluid Flow* 75, pp. 165–184. ISSN: 0142-727X. DOI: 10.1016/j.ijheatfluidflow.2019.01.002. URL: <http://www.sciencedirect.com/science/article/pii/S0142727X18311342> (visited on 03/21/2019).
- Subramaniam, Vignaesh, Talib Dbouk, and Jean-Luc Harion (Apr. 2018). “Thermal Measurements in Conductive Heat Transfer Tree-Like Structures Obtained by Topology Optimization”. In: The 3rd World Congress on Momentum, Heat and Mass Transfer. DOI: 10.11159/enfht18.113. URL: http://avestia.com/MHMT2018_Proceedings/files/paper/ENFHT/ENFHT_113.pdf (visited on 03/21/2019).
- Sun, Fujia *et al.* (Nov. 7, 2020). “Mechanical Properties of High-Strength Cu–Cr–Zr Alloy Fabricated by Selective Laser Melting”. In: *Materials* 13.21, p. 5028. ISSN: 1996-1944. DOI: 10.3390/ma13215028. URL: <https://www.mdpi.com/1996-1944/13/21/5028> (visited on 08/19/2022).
- Sun, Sicheng, Piotr Liebersbach, and Xiaoping Qian (May 2019). “Large Scale 3D Topology Optimization of Conjugate Heat Transfer”. In: *2019 18th IEEE Intersociety Conference on Thermal and Thermomechanical Phenomena in Electronic Systems (ITherm)*. 2019 18th IEEE Intersociety Conference on Thermal and Thermomechanical Phenomena in Electronic Systems (ITherm), pp. 1–6. DOI: 10.1109/ITHERM.2019.8757230.
- Suresh, Krishnan (Nov. 2010). “A 199-Line Matlab Code for Pareto-optimal Tracing in Topology Optimization”. In: *Structural and Multidisciplinary Optimization* 42.5, pp. 665–679. ISSN: 1615-147X, 1615-1488. DOI: 10.1007/s00158-010-0534-6. URL: <http://link.springer.com/10.1007/s00158-010-0534-6> (visited on 04/10/2019).
- Svanberg, Krister (Feb. 1987). “The Method of Moving Asymptotes—a New Method for Structural Optimization”. In: *International Journal for Numerical Methods in Engineering* 24.2, pp. 359–373. ISSN: 0029-5981, 1097-0207. DOI: 10.1002/nme.1620240207. URL: <http://doi.wiley.com/10.1002/nme.1620240207> (visited on 02/11/2019).

- Svanberg, Krister (Jan. 2002). “A Class of Globally Convergent Optimization Methods Based on Conservative Convex Separable Approximations”. In: *SIAM Journal on Optimization* 12.2, pp. 555–573. ISSN: 1052-6234, 1095-7189. DOI: 10.1137/S1052623499362822. URL: <http://epubs.siam.org/doi/10.1137/S1052623499362822> (visited on 04/17/2019).
- (2007). “MMA and GCMMA – Two Methods for Nonlinear Optimization”. In: p. 15.
- Sykes, A. *et al.* (Jan. 1, 2018). “Compact Fusion Energy Based on the Spherical Tokamak”. In: *Nucl. Fusion* 58.1, p. 016039. ISSN: 0029-5515, 1741-4326. DOI: 10.1088/1741-4326/aa8c8d. URL: <https://iopscience.iop.org/article/10.1088/1741-4326/aa8c8d> (visited on 11/11/2020).
- Takeda, Shutaro, Shigeki Sakurai, and Satoshi Konishi (Apr. 2020). “Economic Performance of Fusion Power Plant on Deregulated Electricity Markets”. In: *J Fusion Energ* 39.1-2, pp. 31–39. ISSN: 0164-0313, 1572-9591. DOI: 10.1007/s10894-020-00230-z. URL: <http://link.springer.com/10.1007/s10894-020-00230-z> (visited on 07/22/2020).
- Talisch, Cameron *et al.* (Mar. 2012). “PolyTop: A Matlab Implementation of a General Topology Optimization Framework Using Unstructured Polygonal Finite Element Meshes”. In: *Structural and Multidisciplinary Optimization* 45.3, pp. 329–357. ISSN: 1615-147X, 1615-1488. DOI: 10.1007/s00158-011-0696-x. URL: <http://link.springer.com/10.1007/s00158-011-0696-x> (visited on 04/10/2019).
- Tavakoli, Rouhollah and Seyyed Mohammad Mohseni (Apr. 2014). “Alternating Active-Phase Algorithm for Multimaterial Topology Optimization Problems: A 115-Line MATLAB Implementation”. In: *Structural and Multidisciplinary Optimization* 49.4, pp. 621–642. ISSN: 1615-147X, 1615-1488. DOI: 10.1007/s00158-013-0999-1. URL: <http://link.springer.com/10.1007/s00158-013-0999-1> (visited on 04/10/2019).
- Taylor, Neill, Sergio Ciattaglia, Helen Boyer, *et al.* (Nov. 2017). “Resolving Safety Issues for a Demonstration Fusion Power Plant”. In: *Fusion Engineering and Design* 124, pp. 1177–1180. ISSN: 09203796. DOI: 10.1016/j.fusengdes.2017.02.018. URL: <https://linkinghub.elsevier.com/retrieve/pii/S0920379617301011> (visited on 04/15/2019).
- Taylor, Neill, Sergio Ciattaglia, Dave Coombs, *et al.* (Sept. 2019). “Safety and Environment Studies for a European DEMO Design Concept”. In: *Fusion Engineering and Design* 146, pp. 111–114. ISSN: 09203796. DOI: 10.1016/j.fusengdes.2018.11.049. URL: <https://linkinghub.elsevier.com/retrieve/pii/S0920379618307567> (visited on 07/22/2020).

- The Balance of Power* (2022). ITER. URL: <http://www.iter.org/newsline/-/2589> (visited on 01/07/2022).
- Thomas, Douglas S. and Stanley W. Gilbert (Dec. 2014). *Costs and Cost Effectiveness of Additive Manufacturing*. NIST SP 1176. National Institute of Standards and Technology. DOI: 10.6028/NIST.SP.1176. URL: <https://nvlpubs.nist.gov/nistpubs/SpecialPublications/NIST.SP.1176.pdf> (visited on 06/27/2018).
- Tillack, M. S. *et al.* (Jan. 1, 2011). “Recent US Activities on Advanced He-cooled W-alloy Divertor Concepts for Fusion Power Plants”. In: *Fusion Engineering and Design* 86.1, pp. 71–98. ISSN: 0920-3796. DOI: 10.1016/j.fusengdes.2010.08.015. URL: <https://www.sciencedirect.com/science/article/pii/S0920379610003637> (visited on 08/22/2021).
- Tillack, Mark (2009). “An Evaluation of Fusion Energy R&D Gaps Using Technology Readiness Levels”. In: 56, p. 9.
- Tobita, Kenji, Nobuyuki Asakura, *et al.* (Nov. 17, 2017). “Design Strategy and Recent Design Activity on Japan’s DEMO”. In: *Fusion Science and Technology* 72.4, pp. 537–545. ISSN: 1536-1055, 1943-7641. DOI: 10.1080/15361055.2017.1364112. URL: <https://www.tandfonline.com/doi/full/10.1080/15361055.2017.1364112> (visited on 08/25/2020).
- Tobita, Kenji, Gianfranco Federici, and Kunihiro Okano (Oct. 2014). “Research and Development Status on Fusion DEMO Reactor Design under the Broader Approach”. In: *Fusion Engineering and Design* 89.9-10, pp. 1870–1874. ISSN: 09203796. DOI: 10.1016/j.fusengdes.2014.02.077. URL: <https://linkinghub.elsevier.com/retrieve/pii/S0920379614001847> (visited on 12/01/2020).
- Tobita, Kenji, Ryoji Hiwatari, *et al.* (2019). “Japan’s Efforts to Develop the Concept of JA DEMO During the Past Decade”. In: *FUSION SCIENCE AND TECHNOLOGY* 75, p. 13.
- Tofail, Syed A.M. *et al.* (Jan. 2018). “Additive Manufacturing: Scientific and Technological Challenges, Market Uptake and Opportunities”. In: *Materials Today* 21.1, pp. 22–37. ISSN: 13697021. DOI: 10.1016/j.mattod.2017.07.001. URL: <https://linkinghub.elsevier.com/retrieve/pii/S1369702117301773> (visited on 08/17/2022).
- Tokimatsu, K *et al.* (June 1998). “Study of Design Parameters for Minimizing the Cost of Electricity of Tokamak Fusion Power Reactors”. In: *Nucl. Fusion* 38.6, pp. 885–902. ISSN: 0029-5515. DOI: 10.1088/0029-5515/38/6/307. URL: <https://iopscience.iop.org/article/10.1088/0029-5515/38/6/307> (visited on 11/05/2020).
- Tomabechei, K. (Dec. 1, 1991). “Overview of the ITER Conceptual Design Activities”. In: *Fusion Engineering and Design* 16, pp. 3–10. ISSN: 0920-3796. DOI: 10.1016/0920-

- 3796(91)90178-S. URL: <https://www.sciencedirect.com/science/article/pii/S092037969190178S> (visited on 03/29/2021).
- Tungsten as a Structural Divertor Material* (2018). ResearchGate. URL: https://www.researchgate.net/publication/233846142_Tungsten_as_a_Structural_Divertor_Material (visited on 07/24/2018).
- Van Oevelen, Tijs and Martine Baelmans (2014). “Numerical Topology Optimization of Heat Sinks”. In: *Proceedings of the 15th International Heat Transfer Conference*. The 15th International Heat Transfer Conference. Kyoto, Japan: Begellhouse. ISBN: 978-1-56700-421-2. DOI: 10.1615/IHTC15.opt.009168. URL: <http://www.ihtcdigitallibrary.com/conferences/ihtc15,26f2d44a76eafc57,6f9aca2c7ed0584b.html> (visited on 09/28/2018).
- Van Dijk, N. P. *et al.* (Sept. 1, 2013). “Level-Set Methods for Structural Topology Optimization: A Review”. In: *Struct Multidisc Optim* 48.3, pp. 437–472. ISSN: 1615-1488. DOI: 10.1007/s00158-013-0912-y. URL: <https://doi.org/10.1007/s00158-013-0912-y> (visited on 08/20/2018).
- Voss, G.M. *et al.* (Nov. 2000). “A Conceptual Design of a Spherical Tokamak Power Plant”. In: *Fusion Engineering and Design* 51–52, pp. 309–318. ISSN: 09203796. DOI: 10.1016/S0920-3796(00)00298-2. URL: <http://linkinghub.elsevier.com/retrieve/pii/S0920379600002982> (visited on 07/20/2018).
- Vozár, L. and W. Hohenauer (Nov. 2005). “Uncertainty of Thermal Diffusivity Measurements Using the Laser Flash Method”. In: *Int J Thermophys* 26.6, pp. 1899–1915. ISSN: 0195-928X, 1572-9567. DOI: 10.1007/s10765-005-8604-5. URL: <http://link.springer.com/10.1007/s10765-005-8604-5> (visited on 07/01/2019).
- Wadbro, Eddie and Martin Berggren (Nov. 4, 2009). “Megapixel Topology Optimization on a Graphics Processing Unit”. In: *SIAM Review* 51.4, pp. 707–721. ISSN: 0036-1445, 1095-7200. DOI: 10.1137/070699822. URL: <http://epubs.siam.org/doi/10.1137/070699822> (visited on 01/24/2019).
- Wallis, Christopher and Bruno Buchmayr (Jan. 2019). “Effect of Heat Treatments on Microstructure and Properties of CuCrZr Produced by Laser-Powder Bed Fusion”. In: *Materials Science and Engineering: A* 744, pp. 215–223. ISSN: 09215093. DOI: 10.1016/j.msea.2018.12.017. URL: <https://linkinghub.elsevier.com/retrieve/pii/S0921509318316964> (visited on 04/30/2019).
- Wan, Yuanxi *et al.* (Oct. 1, 2017). “Overview of the Present Progress and Activities on the CFETR”. In: *Nucl. Fusion* 57.10, p. 102009. ISSN: 0029-5515, 1741-4326. DOI: 10.1088/1741-4326/aa686a. URL: <https://iopscience.iop.org/article/10.1088/1741-4326/aa686a> (visited on 08/25/2020).

- Wang, Fengwen, Boyan Stefanov Lazarov, and Ole Sigmund (June 2011). “On Projection Methods, Convergence and Robust Formulations in Topology Optimization”. In: *Struct Multidisc Optim* 43.6, pp. 767–784. ISSN: 1615-147X, 1615-1488. DOI: 10.1007/s00158-010-0602-y. URL: <http://link.springer.com/10.1007/s00158-010-0602-y> (visited on 10/31/2021).
- Wang, Shuming *et al.* (Dec. 2020). “Thermal Damage of Tungsten-Armored Plasma-Facing Components under High Heat Flux Loads”. In: *Sci Rep* 10.1, p. 1359. ISSN: 2045-2322. DOI: 10.1038/s41598-020-57852-8. URL: <http://www.nature.com/articles/s41598-020-57852-8> (visited on 05/20/2021).
- Wang, X. R., A. R. Raffray, and S. Malang (June 2009). “Transient Thermal and Stress Response of a Helium-Cooled Tungsten Plate-Type Divertor”. In: *2009 23rd IEEE/NPSS Symposium on Fusion Engineering*. 2009 23rd IEEE/NPSS Symposium on Fusion Engineering, pp. 1–4. DOI: 10.1109/FUSION.2009.5226430.
- Wegener, Tobias *et al.* (Nov. 1, 2017). “Development and Analyses of Self-Passivating Tungsten Alloys for DEMO Accidental Conditions”. In: *Fusion Engineering and Design*. Proceedings of the 29th Symposium on Fusion Technology (SOFT-29) Prague, Czech Republic, September 5-9, 2016 124, pp. 183–186. ISSN: 0920-3796. DOI: 10.1016/j.fusengdes.2017.03.072. URL: <http://www.sciencedirect.com/science/article/pii/S092037961730296X> (visited on 07/20/2018).
- Wenninger, R., F. Arbeiter, *et al.* (June 1, 2015). “Advances in the Physics Basis for the European DEMO Design”. In: *Nucl. Fusion* 55.6, p. 063003. ISSN: 0029-5515, 1741-4326. DOI: 10.1088/0029-5515/55/6/063003. URL: <https://iopscience.iop.org/article/10.1088/0029-5515/55/6/063003> (visited on 10/19/2020).
- Wenninger, R., R. Kembleton, *et al.* (Jan. 1, 2017). “The Physics and Technology Basis Entering European System Code Studies for DEMO”. In: *Nucl. Fusion* 57.1, p. 016011. ISSN: 0029-5515, 1741-4326. DOI: 10.1088/0029-5515/57/1/016011. URL: <https://iopscience.iop.org/article/10.1088/0029-5515/57/1/016011> (visited on 10/19/2020).
- Wesson, John (Oct. 13, 2011). *Tokamaks*. Fourth Edition. International Series of Monographs on Physics. Oxford, New York: Oxford University Press. 832 pp. ISBN: 978-0-19-959223-4.
- Widak, V. and P. Norajitra (June 1, 2009). “Optimization of He-cooled Divertor Cooling Fingers Using a CAD-FEM Method”. In: *Fusion Engineering and Design*. Proceeding of the 25th Symposium on Fusion Technology 84.7, pp. 1973–1978. ISSN: 0920-3796. DOI: 10.1016/j.fusengdes.2009.02.045. URL: <https://www.sciencedirect.com/science/article/pii/S0920379609001719> (visited on 09/02/2021).

- Wiggins, Cody S., Arturo Cabral, and Lane B. Carasik (Aug. 9, 2021). “Heat Transfer Performance of Cu-Cr-Zr Tube with Swirl Insert Under Cyclic Thermal Loading in Monoblock Divertor”. In: *Fusion Science and Technology*, pp. 1–6. ISSN: 1536-1055, 1943-7641. DOI: 10.1080/15361055.2021.1898304. URL: <https://www.tandfonline.com/doi/full/10.1080/15361055.2021.1898304> (visited on 10/11/2021).
- Wiker, Niclas, Anders Klarbring, and Thomas Borrvall (Feb. 12, 2007). “Topology Optimization of Regions of Darcy and Stokes Flow”. In: *International Journal for Numerical Methods in Engineering* 69.7, pp. 1374–1404. ISSN: 00295981, 10970207. DOI: 10.1002/nme.1811. URL: <http://doi.wiley.com/10.1002/nme.1811> (visited on 04/02/2019).
- Wilson, Howard (Mar. 25, 2019). “The Impact of Plasma Physics on the Timescale to a Tokamak Fusion Power Plant”. In: *Phil. Trans. R. Soc. A*. 377.2141, p. 20170435. ISSN: 1364-503X, 1471-2962. DOI: 10.1098/rsta.2017.0435. URL: <https://royalsocietypublishing.org/doi/10.1098/rsta.2017.0435> (visited on 07/22/2020).
- Windsor, Colin (Mar. 25, 2019). “Can the Development of Fusion Energy Be Accelerated? An Introduction to the Proceedings”. In: *Phil. Trans. R. Soc. A*. 377.2141, p. 20170446. ISSN: 1364-503X, 1471-2962. DOI: 10.1098/rsta.2017.0446. URL: <https://royalsocietypublishing.org/doi/10.1098/rsta.2017.0446> (visited on 07/22/2020).
- Wisconsin Univ, Madison (USA) Dept of Nuclear Engineering (Mar. 1974). *UWMAK-I: A Wisconsin Toroidal Fusion Reactor Design Volume I*. United States, p. 771.
- Wu, Shuhao, Yongcun Zhang, and Shutian Liu (Jan. 23, 2019). “Topology Optimization for Minimizing the Maximum Temperature of Transient Heat Conduction Structure”. In: *Structural and Multidisciplinary Optimization*. ISSN: 1615-147X, 1615-1488. DOI: 10.1007/s00158-019-02196-9. URL: <http://link.springer.com/10.1007/s00158-019-02196-9> (visited on 03/21/2019).
- Xia, Qi, Tielin Shi, and Liang Xia (Dec. 2018). “Topology Optimization for Heat Conduction by Combining Level Set Method and BESO Method”. In: *International Journal of Heat and Mass Transfer* 127, pp. 200–209. ISSN: 00179310. DOI: 10.1016/j.ijheatmasstransfer.2018.08.036. URL: <https://linkinghub.elsevier.com/retrieve/pii/S0017931018320052> (visited on 03/21/2019).
- Xu, Ling *et al.* (Aug. 2017). “Design of Microchannel Heat Sink Using Topology Optimization for High Power Modules Cooling”. In: *2017 18th International Conference on Electronic Packaging Technology (ICEPT)*. 2017 18th International Conference on Electronic Packaging Technology (ICEPT). Harbin, China: IEEE, pp. 1092–1097. ISBN: 978-1-5386-2972-7. DOI: 10.1109/ICEPT.2017.8046632. URL: <http://ieeexplore.ieee.org/document/8046632/> (visited on 09/28/2018).

- Yadroitsev, I. and I. Smurov (2010). “Selective Laser Melting Technology: From the Single Laser Melted Track Stability to 3D Parts of Complex Shape”. In: *Physics Procedia* 5, pp. 551–560. ISSN: 18753892. DOI: 10.1016/j.phpro.2010.08.083. URL: <https://linkinghub.elsevier.com/retrieve/pii/S1875389210005092> (visited on 08/29/2019).
- Yagov, V. V. and A. V. Dedov (Mar. 2009). “Heat Transfer under Conditions of Film Boiling in Turbulent Flow of Subcooled Liquid”. In: *Therm. Eng.* 56.3, pp. 201–209. ISSN: 0040-6015, 1555-6301. DOI: 10.1134/S0040601509030033. URL: <http://link.springer.com/10.1134/S0040601509030033> (visited on 07/01/2020).
- Yaji, Kentaro, Masao Ogino, *et al.* (Aug. 1, 2018). “Large-Scale Topology Optimization Incorporating Local-in-Time Adjoint-Based Method for Unsteady Thermal-Fluid Problem”. In: *Struct Multidisc Optim* 58.2, pp. 817–822. ISSN: 1615-1488. DOI: 10.1007/s00158-018-1922-6. URL: <https://doi.org/10.1007/s00158-018-1922-6> (visited on 03/07/2019).
- Yaji, Kentaro, Takayuki Yamada, Seiji Kubo, *et al.* (Feb. 1, 2015). “A Topology Optimization Method for a Coupled Thermal–Fluid Problem Using Level Set Boundary Expressions”. In: *International Journal of Heat and Mass Transfer* 81, pp. 878–888. ISSN: 0017-9310. DOI: 10.1016/j.ijheatmasstransfer.2014.11.005. URL: <http://www.sciencedirect.com/science/article/pii/S0017931014009776> (visited on 09/18/2018).
- Yaji, Kentaro, Takayuki Yamada, Masato Yoshino, *et al.* (Feb. 2016). “Topology Optimization in Thermal-Fluid Flow Using the Lattice Boltzmann Method”. In: *Journal of Computational Physics* 307, pp. 355–377. ISSN: 00219991. DOI: 10.1016/j.jcp.2015.12.008. URL: <https://linkinghub.elsevier.com/retrieve/pii/S0021999115008244> (visited on 10/28/2021).
- Yaji, Kentaro, Shintaro Yamasaki, and Kikuo Fujita (Mar. 2020). “Multifidelity Design Guided by Topology Optimization”. In: *Struct Multidisc Optim* 61.3, pp. 1071–1085. ISSN: 1615-147X, 1615-1488. DOI: 10.1007/s00158-019-02406-4. URL: <http://link.springer.com/10.1007/s00158-019-02406-4> (visited on 10/29/2021).
- Yamada, Takayuki, Kazuhiro Izui, and Shinji Nishiwaki (Mar. 15, 2011). “A Level Set-Based Topology Optimization Method for Maximizing Thermal Diffusivity in Problems Including Design-Dependent Effects”. In: *J. Mech. Des* 133.3, pp. 031011-031011–9. ISSN: 1050-0472. DOI: 10.1115/1.4003684. URL: <http://dx.doi.org/10.1115/1.4003684> (visited on 02/13/2019).
- Yamada, Takayuki, Kazuhiro Izui, Shinji Nishiwaki, and Akihiro Takezawa (Nov. 2010). “A Topology Optimization Method Based on the Level Set Method Incorporating a Fictitious Interface Energy”. In: *Computer Methods in Applied Mechanics and Engineering* 199.45-

- 48, pp. 2876–2891. ISSN: 00457825. DOI: 10.1016/j.cma.2010.05.013. URL: <https://linkinghub.elsevier.com/retrieve/pii/S0045782510001623> (visited on 02/13/2019).
- Yan, Suna *et al.* (Nov. 2019). “Topology Optimization of Microchannel Heat Sinks Using a Two-Layer Model”. In: *International Journal of Heat and Mass Transfer* 143, p. 118462. ISSN: 00179310. DOI: 10.1016/j.ijheatmasstransfer.2019.118462. URL: <https://linkinghub.elsevier.com/retrieve/pii/S0017931019316928> (visited on 10/28/2021).
- Yang, Qiang *et al.* (Mar. 5, 2019). “Topology Optimisations for Integrated Thermal Protection Systems Considering Thermo-Mechanical Constraints”. In: *Applied Thermal Engineering* 150, pp. 995–1001. ISSN: 1359-4311. DOI: 10.1016/j.applthermaleng.2019.01.067. URL: <http://www.sciencedirect.com/science/article/pii/S1359431118364317> (visited on 03/21/2019).
- Yoda, M. and S. I. Abdel-Khalik (Oct. 3, 2017). “Overview of Thermal Hydraulics of Helium-Cooled Solid Divertors”. In: *Fusion Science and Technology* 72.3, pp. 285–293. ISSN: 1536-1055. DOI: 10.1080/15361055.2017.1333825. URL: <https://doi.org/10.1080/15361055.2017.1333825> (visited on 07/10/2018).
- Yoon, Gil Ho (June 2010). “Topological Design of Heat Dissipating Structure with Forced Convective Heat Transfer”. In: *Journal of Mechanical Science and Technology* 24.6, pp. 1225–1233. ISSN: 1738-494X, 1976-3824. DOI: 10.1007/s12206-010-0328-1. URL: <http://link.springer.com/10.1007/s12206-010-0328-1> (visited on 09/21/2018).
- (Apr. 2020). “Topology Optimization Method with Finite Elements Based on the K-Epsilon Turbulence Model”. In: *Computer Methods in Applied Mechanics and Engineering* 361, p. 112784. ISSN: 00457825. DOI: 10.1016/j.cma.2019.112784. URL: <https://linkinghub.elsevier.com/retrieve/pii/S0045782519306760> (visited on 10/01/2021).
- You, J.-H. *et al.* (July 2013). “Thermal and Mechanical Properties of Infiltrated W/Cu-CrZr Composite Materials for Functionally Graded Heat Sink Application”. In: *Journal of Nuclear Materials* 438.1-3, pp. 1–6. ISSN: 00223115. DOI: 10.1016/j.jnucmat.2013.03.005. URL: <https://linkinghub.elsevier.com/retrieve/pii/S002231151300487X> (visited on 08/30/2022).
- You, Jeong-Ha (2015). “A Review on Two Previous Divertor Target Concepts for DEMO: Mutual Impact between Structural Design Requirements and Materials Performance”. In: *Nucl. Fusion* 55.11, p. 113026. ISSN: 0029-5515. DOI: 10.1088/0029-5515/55/11/

113026. URL: <http://stacks.iop.org/0029-5515/55/i=11/a=113026> (visited on 07/09/2018).
- Youchison, D.L. *et al.* (Oct. 2007). “High Heat Flux Testing of a Helium-Cooled Tungsten Tube with Porous Foam”. In: *Fusion Engineering and Design* 82.15-24, pp. 1854–1860. ISSN: 09203796. DOI: 10.1016/j.fusengdes.2007.04.004. URL: <http://linkinghub.elsevier.com/retrieve/pii/S0920379607001627> (visited on 07/09/2018).
- Youchison, Dennis L *et al.* (Nov. 2000). “Thermal Performance and Flow Instabilities in a Multi-Channel, Helium-Cooled, Porous Metal Divertor Module”. In: *Fusion Engineering and Design* 49–50, pp. 407–415. ISSN: 09203796. DOI: 10.1016/S0920-3796(00)00243-X. URL: <http://linkinghub.elsevier.com/retrieve/pii/S092037960000243X> (visited on 07/09/2018).
- Yu, Minghao *et al.* (July 2019). “Topology Optimization of Thermal–Fluid Problem Using the MMC-based Approach”. In: *Struct Multidisc Optim* 60.1, pp. 151–165. ISSN: 1615-147X, 1615-1488. DOI: 10.1007/s00158-019-02206-w. URL: <http://link.springer.com/10.1007/s00158-019-02206-w> (visited on 10/10/2019).
- Zargham, Sajjad *et al.* (June 2016). “Topology Optimization: A Review for Structural Designs under Vibration Problems”. In: *Structural and Multidisciplinary Optimization* 53.6, pp. 1157–1177. ISSN: 1615-147X, 1615-1488. DOI: 10.1007/s00158-015-1370-5. URL: <http://link.springer.com/10.1007/s00158-015-1370-5> (visited on 09/25/2018).
- Zeng, K.J. and M. Hämmäläinen (Apr. 1995). “A Theoretical Study of the Phase Equilibria in the CuCrZr System”. In: *Journal of Alloys and Compounds* 220.1-2, pp. 53–61. ISSN: 09258388. DOI: 10.1016/0925-8388(94)06029-0. URL: <https://linkinghub.elsevier.com/retrieve/pii/S0925838894060290> (visited on 08/19/2022).
- Zeng, Shi, Bugra Kanargi, and Poh Seng Lee (June 2018). “Experimental and Numerical Investigation of a Mini Channel Forced Air Heat Sink Designed by Topology Optimization”. In: *International Journal of Heat and Mass Transfer* 121, pp. 663–679. ISSN: 00179310. DOI: 10.1016/j.ijheatmasstransfer.2018.01.039. URL: <https://linkinghub.elsevier.com/retrieve/pii/S0017931017336414> (visited on 10/28/2021).
- Zeng, Shi and Poh Seng Lee (Oct. 1, 2019). “Topology Optimization of Liquid-Cooled Microchannel Heat Sinks: An Experimental and Numerical Study”. In: *International Journal of Heat and Mass Transfer* 142, p. 118401. ISSN: 0017-9310. DOI: 10.1016/j.ijheatmasstransfer.2019.07.051. URL: <https://www.sciencedirect.com/science/article/pii/S0017931019312190> (visited on 10/28/2021).
- Zhang, Bin and Limin Gao (Nov. 2019). “Topology Optimization of Convective Heat Transfer Problems for Non-Newtonian Fluids”. In: *Struct Multidisc Optim* 60.5, pp. 1821–1840.

- ISSN: 1615-147X, 1615-1488. DOI: 10.1007/s00158-019-02296-6. URL: <http://link.springer.com/10.1007/s00158-019-02296-6> (visited on 10/28/2021).
- Zhang, Kuo, Ermile Gaganidze, and Michael Gorley (July 2019). “Development of the Material Property Handbook and Database of CuCrZr”. In: *Fusion Engineering and Design* 144, pp. 148–153. ISSN: 09203796. DOI: 10.1016/j.fusengdes.2019.04.094. URL: <https://linkinghub.elsevier.com/retrieve/pii/S0920379619306349> (visited on 03/16/2021).
- Zhao, Xi *et al.* (Jan. 2018). “A “Poor Man’s Approach” to Topology Optimization of Cooling Channels Based on a Darcy Flow Model”. In: *International Journal of Heat and Mass Transfer* 116, pp. 1108–1123. ISSN: 00179310. DOI: 10.1016/j.ijheatmasstransfer.2017.09.090. URL: <https://linkinghub.elsevier.com/retrieve/pii/S0017931017310037> (visited on 10/28/2021).
- Zheng, S. *et al.* (Feb. 2016). “Fusion Reactor Start-up without an External Tritium Source”. In: *Fusion Engineering and Design* 103, pp. 13–20. ISSN: 09203796. DOI: 10.1016/j.fusengdes.2015.11.034. URL: <https://linkinghub.elsevier.com/retrieve/pii/S0920379615303598> (visited on 01/04/2022).
- Zhou, M. and G.I.N. Rozvany (Aug. 1991). “The COC Algorithm, Part II: Topological, Geometrical and Generalized Shape Optimization”. In: *Computer Methods in Applied Mechanics and Engineering* 89.1-3, pp. 309–336. ISSN: 00457825. DOI: 10.1016/0045-7825(91)90046-9. URL: <http://linkinghub.elsevier.com/retrieve/pii/S0045782591900469> (visited on 03/20/2019).
- Zhou, Mingdong *et al.* (Oct. 2016). “Industrial Application of Topology Optimization for Combined Conductive and Convective Heat Transfer Problems”. In: *Structural and Multidisciplinary Optimization* 54.4, pp. 1045–1060. ISSN: 1615-147X, 1615-1488. DOI: 10.1007/s00158-016-1433-2. URL: <http://link.springer.com/10.1007/s00158-016-1433-2> (visited on 02/15/2019).
- Zhuang, Chungang and Zhenhua Xiong (May 1, 2014). “A Global Heat Compliance Measure Based Topology Optimization for the Transient Heat Conduction Problem”. In: *Numerical Heat Transfer, Part B: Fundamentals* 65.5, pp. 445–471. ISSN: 1040-7790. DOI: 10.1080/10407790.2013.873309. URL: <https://doi.org/10.1080/10407790.2013.873309> (visited on 01/17/2019).
- Zhuang, ChunGang, ZhenHua Xiong, and Han Ding (Jan. 1, 2007). “A Level Set Method for Topology Optimization of Heat Conduction Problem under Multiple Load Cases”. In: *Computer Methods in Applied Mechanics and Engineering* 196.4, pp. 1074–1084. ISSN: 0045-7825. DOI: 10.1016/j.cma.2006.08.005. URL: <http://www.sciencedirect.com/science/article/pii/S0045782506002301> (visited on 02/11/2019).

Zhuang, Chungang, Zhenhua Xiong, and Han Ding (May 4, 2013). “Topology Optimization of the Transient Heat Conduction Problem on a Triangular Mesh”. In: *Numerical Heat Transfer, Part B: Fundamentals* 64.3, pp. 239–262. ISSN: 1040-7790. DOI: 10.1080/10407790.2013.791785. URL: <https://doi.org/10.1080/10407790.2013.791785> (visited on 01/17/2019).

Zohm, H. *et al.* (July 1, 2013). “On the Physics Guidelines for a Tokamak DEMO”. In: *Nucl. Fusion* 53.7, p. 073019. ISSN: 0029-5515, 1741-4326. DOI: 10.1088/0029-5515/53/7/073019. URL: <https://iopscience.iop.org/article/10.1088/0029-5515/53/7/073019> (visited on 11/16/2020).

Appendices

Appendix A

IAEA net zero policy proposal

A.1 Advanced Modular Forests

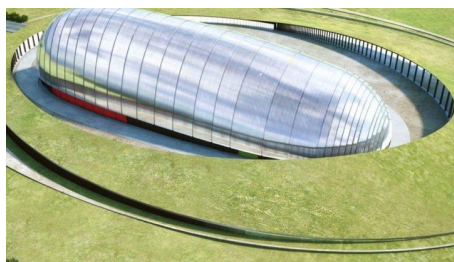


Figure 1 - Rendition of an SMR [Rolls Royce]

Advanced Modular Reactors (AMRs) have the potential to provide opportunities both for The UK nuclear sector and for meeting net zero emissions targets. Confronting the lack of public enthusiasm for nuclear builds is a necessary step toward their eventual viability in the UK. Afforestation packages present a unique opportunity to persuade the public that next generation nuclear can be done in a carbon negative and sustainable way. Additionally, re-forestation targets set by the UK government mesh well with concepts for the re-foresting of exclusion zones surrounding fission plants, which would otherwise remain empty.

Background

Of respondents in a YouGov poll, 62% would not like to live within 5 miles of a small modular reactor.^[1] Demographic concerns were found to be the primary issue when siting nuclear power plants in the UK.^[2] Furthermore, the UK is one of the least forested nations in Europe with 13% forest coverage compared to an EU average of 38%.^[3] Afforestation can contribute to meeting the net zero goal by long term carbon sequestration whilst also supporting wildlife, by providing crucial habitats for a number of species, including those with planned re-introduction schemes as part of re-wilding efforts. The current afforestation rate (2019-21) is c. 13,000ha per annum, however 30,000 ha of new trees are needed every year to 2050 to take woodland cover in the UK from 13-17%.^[4] Germany has a similar ratio of population to land area as the UK but is 33% forested.

Policy Statement

This report recommends the creation of a reactor forest partnership scheme. Companies wishing to build SMRs can benefit from a subsidy and improved chances of siting approval if they agree to environmental development of the surrounding area as a new sustainable forest habitat. This policy has several beneficial outcomes, chiefly to positively impact public opinion of nuclear power, enabling the creation of more future AMR sites.

The creation of new forest habitats tailored to restore and enhance the local environment around SMRs will demonstrate that nuclear power can be integrated into the environment and that the protected areas around the sites can be managed as semi-wild habitats for local species. Afforestation of AMR sites will act as nuclei for extension of the forests into larger regions. The forests must be protected throughout the life of the plant from use for timber.

This policy interacts with points 3, 8, 9 and 10 on the UK government 10-point plan for a green industrial revolution:^[5]

- 3) delivering new and advanced nuclear power;
- 8) investing in carbon capture usage and storage;
- 9) protecting our natural environment and
- 10) Green finance and innovation.

Siting

The zone required around new SMRs for emergency planning (EPZ) however is still under discussion and may vary between SMR design but is likely to be on the order of several kilometres. The designation of this area as forest would be tied to the approval of the site for its lifetime (on the order of 60 years)^[6] and so protecting the forest from removal for industrial or residential development, ensuring long term carbon sequestration (see box 1). The Strategic Siting Assessment (SSA) from Department for Energy and Climate Change in 2011 made a list of considerations for nuclear sites stemming from safety and environmental concerns. AMRs reduce dependency on water due to their reduced cooling requirements, while forest production may help alleviate the impact of power plants on sites of ecological importance.

Box 1: Afforestation carbon sink estimate

- **EPZ** of 5km yields a forest-ready area of 78.5 km², 26% of the UK's per annum afforestation goal.
- **New forest** captures 300-400 t of CO₂ per hectare per year at year 50 of existence.^[7]
- **CO₂** sequestered at year 50 by an AMR forest is 2.75 Mt per year.

Another point raised by siting considerations is the geographic location. Current nuclear sites in the UK are restricted mostly to locations on the coasts, where water is plentiful. Rising sea levels threaten much of the UK's coastal regions. In the interest of energy security, a future nuclear baseline energy production fleet should be positioned far from such threats. Reduced AMR dependence on water means new sites can be considered inland, requiring a new wave of local populations to be persuaded to accept fission power in their area.

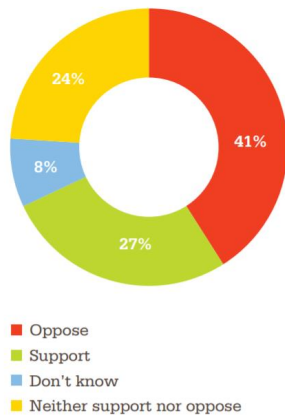


Figure 2 – UK attitudes toward nuclear plant construction in your local area.^[8]

Public Perception

Overcoming the attitude problem toward fission energy has no silver bullet solution. A recent report reveals that in the UK only 27% of people would support the building of a nuclear power plant in their local area, while 41% would oppose.^[8] Education must be at the heart of changing minds, but other efforts can factor into the discussion. Natural beauty has been shown to be the most widely accepted attraction in a local area,^[9] and exposure to nature has been shown

to reduce the risk of mental health problems by up to 55%.^[10] Leveraging these pre-established public attitudes will help to shift perception of nuclear power.

Box 2: Cost breakdown of Advanced Modular Forest

- **Cost** per hectare of forest is £5095, of which government already subsidises around 83%.^[11]
- **Small modular reactor (SMR)** cost estimated to be £1.8 billion for first reactors.^[12]
- **Cost of forest** estimated at £40 million, around 2% of total cost. Private cost is much less at £8 million, with the rest covered under subsidies.

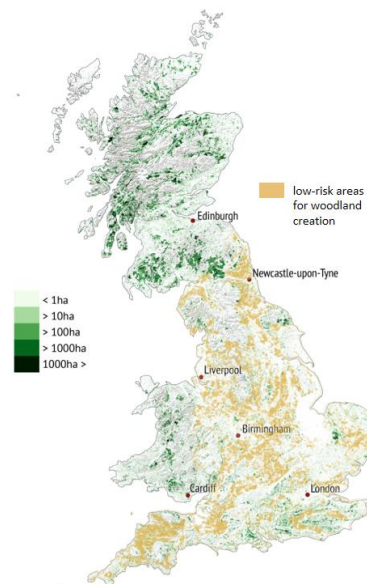


Figure 3 - Map of UK showing the "low risk" areas available for afforestation.^[13]

Summary

With a new era of nuclear power generation comes a unique opportunity to tackle multiple net-zero targets at once. At the same time a rare opportunity to positively impact public perception on fission energy presents itself. Advanced modular forests can accomplish much of this in a cheap and sustainable way.

References

- [1] Policy Exchange, "Small Modular Reactors: The Next Big Thing in Energy?", 2017.
- [2] Department for Energy and Climate Change, "National Policy Statement for Nuclear Power Generation", 2011.
- [4] House of Commons Library, "Tree Planting in the UK", 2021.
- [5] Department for Business, Energy and Industrial Strategy, "The Ten Point Plan for a Green Industrial Revolution", 2020.
- [6] Rolls Royce, "Small Modular Reactors: a Once in a Lifetime Opportunity for the UK", 2017.
- [7] Forestry Commission England, "Creating New Woodland: A Woodland Carbon Code", 2017.
- [8] Institution of Mechanical Engineers, "Public Perceptions of Nuclear Power", 2020.
- [9] Ipsos Mori, "People and Places: Public Attitudes to Beauty", 2010.
- [10] Engemann et al. "Residential green space in childhood is associated with lower risk of psychiatric disorders from adolescence into adulthood", *PNAS*, vol. 116, no. 11, pp. 5188-5193.
- [11] Forestry Commission, "Comparing the Cost-effectiveness of Forestry Options for Climate Change Mitigation," 2019.
- [12] World Nuclear Association, "Small Nuclear Power Reactors," 2021.
- [13] Josh Gabbatiss, "In Depth Q&A: How Will Tree Planting Help the UK Meet its Climate Goals", Carbon Brief. [Accessed 16/08/21: <https://www.carbonbrief.org/in-depth-qa-how-will-tree-planting-help-the-uk-meet-its-climate-goals>]